The dynamic kinetic resolution of azlactones towards amide formation and the hydrolysis of poly(ethylene terephthalate) by terephthalate-based ionic liquids

Trinity College Dublin
Coláiste na Tríonóide, Baile Átha Cliath
The University of Dublin

Trinity College Dublin, the University of Dublin

A thesis submitted to Trinity College Dublin, the University of Dublin for the degree of
Doctor of Philosophy

By
Ian Luke Martin

Under the supervision of Prof. Stephen J Connon

March 2025

Declaration

I declare that this thesis has not been submitted as an exercise for a degree at this or any other university and it is entirely my own work.

I agree to deposit this thesis in the University's open access institutional repository or allow the Library to do so on my behalf, subject to Irish Copyright Legislation and Trinity College Library conditions of use and acknowledgement.

Signed: Date: 31 Mar 2025

Abstract

Solid-liquid phase transfer catalysis was used in the enantioselective ring opening of tetrachlorophthalic anhydride-derived azlactones to provide *bis*-amide products using dynamic kinetic resolution. Using cinchona alkaloid-based phase-transfer catalysts, benzylation and alkylation of the quinuclidine unit afforded a considerable increase in the stereoselective formation of piperidine-amides and morpholine-amides in moderate enantiomeric excess (up to 64% *ee*).

However, this system proved to be restrictive with regards to catalyst scope, since complex cinchona alkaloid catalysts are relatively insoluble in toluene. A mode of homogenous catalysis using ion-pairs was also examined for the same process. These ion-pair catalysts had many potential benefits over phase-transfer catalysts, such as: higher rate of reaction, a wide variety of usable solvents and the certainty of a controlled amount of active catalyst in solution. Overall, this system gave a lower degree of stereocontrol (up to 50% *ee*) but the rate of catalytic formation of the *para*-nitrophenolate ester intermediate was higher.

A set of novel betaine catalysts were examined in the dynamic kinetic resolution of azlactones. This system allowed for the rapid introduction of novel nucleophiles without the necessity for isolation of intermediates. The addition of 1,1'-binaphthyl-2,2'-diol-derivatives in catalytic quantities along with the betaine catalyst increased the enantiocontrol facilitated by the system considerably (up to 77% *ee*, 83% *ee* at $-50\,^{\circ}\mathrm{C}$).

A series of alkyl phosphonium and ammonium phase-transfer catalysts were assayed in the neutral hydrolysis of poly(ethylene terephthalate) to form terephthalic acid. The best-performing phase-transfer catalysts were used in tandem with the conjugate base of the product (*i.e.* disodium terephthalate) to attain high yields of terephthalic acid (up to 71%). A later innovation to form phosphonium terephthalate ionic liquid catalysts proved to be worthwhile and the resulting yield

of terephthalic acid increased considerably in the presence of the catalyst at an extremely low loading (up to 97% yield at 0.5 mol% of catalyst loading). The relative yield of the product was relatively independent of the particle size associated with the starting material.

To expand on previously performed work by Dr. Lee Anderson, a set of experiments were conducted using half the concentration of sodium hydroxide in the alkaline hydrolysis of poly(ethylene terephthalate). Using the optimised conditions found by Dr. Anderson, tetrapentyl ammonium chloride facilitated the consumption of poly(ethylene terephthalate) to yield terephthalic acid (up to 81% yield)

Acknowledgements

First and foremost, I would like to thank my supervisor, Prof. Stephen Connon. Without a doubt, I found the trials and tribulations of the PhD to be incredibly daunting, and your endless encouragement and patience were greatly appreciated. Your words of wisdom will never be forgotten, and I will remember your advice fondly as I move forward in my career.

I would next like to thank Dr. John O'Brien, Dr. Manuel Ruether, Dr. Gary Hessman and Dr. Brendan Twamley for their world-class technical analysis in aiding me in my journey.

To my partners in crime, Lee and Lorenzo, your friendship and support have meant the world to me; I honestly could not have done it without you guys. A special thanks to Anshul for his incredible guidance and for introducing me to many Indian snacks. To Simon, Pierre and Danielle, thank you for being such amazing company.

I want to extend my gratitude to the friends in the chemistry post-graduate community. The seventh floor of TBSI is such a fun and inviting place, and I feel lucky to have met you all. Thank you all for the many memorable and enjoyable nights at silent disco. To Liam, I will miss our intricate discussions at lunch and our nonsensical jokes. To the members of the Dunne lab, thank you all for being so welcoming; I will miss the podcast sessions and chats immensely; they were a very fun part of my day towards the end of my PhD.

To my friends outside of Trinity, who have been with me through thick and thin, I am eternally grateful. To Jack, the Matts, Heather, Gareth, Daniil, Alex and Damien, your ceaseless belief in me is something I aspire to have; you are all the best friends I could possibly ask for.

I would also like to say thank you to my family for their undying faith in my abilities, love and support, without which, this journey would not have been possible.

Last but certainly not least, I want to thank my wonderful girlfriend Glenna for her unyielding kindness, love and support.

Published work

Effect of a phase transfer catalyst structure on the alkaline hydrolysis of poly(ethylene terephthalate).

L. B. Anderson, C. Molloy, L. Pedrini, I. L. Martin and S. J. Connon, *Green Chem.*, 2024, **26**, 11125–11131.

Neutral hydrolysis of poly(ethylene terephthalate) catalysed by highly active terephthalate-based ionic liquids at low loadings.

I. L. Martin, L. B. Anderson, D. A. McAdams, C. Molloy, P. W. Dunne and S. J. Connon, *Chem. Commun.*, 2025, **61**, 2750-2753.

Patent applications

Alkaline Hydrolysis of Polyethylene Terephthalate Using Phase Transfer Catalysis

Application date: 8th of July 2024

Application N°: 24187254.8

Neutral Hydrolysis of Polyethylene Terephthalate Using Phase Transfer Catalysis

Application date: 8th of July 2024

Application N°: 24187234.0

Contents

Abbreviations

AcOH	Acetic acid
app. d	Apparent doublet
app. t	Apparent triplet
ACN	Acetonitrile
BINOL	1,1'-Binaphthyl-2,2'-diol
BHET	*bis*(2-Hydroxyethyl) terephthalate
Bn	Benzyl
BnOH	Benzyl alcohol
BOC	*tert*-Butoxycarbonyl
br.s	Broad singlet
Bz	Benzoyl
BzOH	Benzoic acid
cat	Catalyst
conc.	Concentrated
conv.	Conversion
CSP	Chiral stationary phase
d	Doublet
DABCO	1,4-diazabicyclo[2.2.2]octane
DBU	1,8-Diazabicyclo[5.4.0]undec-7-ene
DCC	*N*,*N*'-dicyclohexylcarbodiimide
dd	Doublet of doublets
dec.	Decomposition
DIAC	Diisopropyl azodicarboxylate
DKR	Dynamic kinetic resolution
DMSO	Dimethyl sulfoxide
DMAP	*N*,*N*-4-dimethylaminopyridine
dr	Diastereomeric ratio
EDC·HCl	*N*-(3-dimethylaminopropyl)-*N*'-ethylcarbodiimide hydrochloride.

EDG	Electron donating group
EG	Ethylene glycol
ee	Enantiomeric excess
eq.	Equivalents
ESI	Electrospray ionization
Et	Ethyl
EtOH	Ethanol
EWG	Electron withdrawing group
h	Hours
HMBC	Heteronuclear multiple bond coherence
HPLC	High-performance liquid chromatography
HRMS	High-resolution mass spectroscopy
HSQC	Heteronuclear single quantum coherence
IR	Infrared
IL	Ionic liquid
i-PrOH	2-propanol
KR	Kinetic resolution
Me	Methyl
MeOH	Methanol
m-	*Meta*-
min	Minutes
mol	Moles
mp	Melting point
Mt	Million metric tonnes
MTBE	Methyl *tert*-butyl ether
m/z	Mass/charge
NaOH	Sodium hydroxide
NCS	*N*-chlorosuccinimide
NHS	*N*-Hydroxysuccinimide
NMR	Nuclear magnetic resonance

o-	*Ortho*-
p-	*Para*-
PET	Poly(ethylene terephthalate)
PEG	Poly(ethylene glycol)
PhCl	Chlorobenzene
PTC	Phase-transfer catalyst
p-TSA	*para*-Toluenesulfonic acid
q	Quartet
q	Quarternary
quint	Quintet
r.t.	Room temperature
SEM	Scanning electron microscopy
sept	Septet
t	Triplet
TCIC	Tetrachloroisopropoxycarbonyl
TCPI	Tetrachlorophthalamides
THF	Tetrahydrofuran
TFA	Trifluoroacetic acid
TFAA	Trifluoroacetic anhydride
TLC	Thin liquid chromatography
TPA	Terephthalic acid
UV	Ultraviolet

1 | Introduction

1.1 The demand for peptide-based therapeutics in the 21st century

Peptide-based therapeutics are chains of covalently bonded amino acids that are either synthesised[1] or isolated[2,3] for use in medicine. Although small-molecule drugs are ubiquitous in everyday life due to their potency, inexpensive cost of manufacture, and bioavailability, they are associated with more side effects and can be less selective than larger drug classes such as peptides and biologics. Protein therapeutics (biologics) have potent and selective biomimetic properties, but their discovery and manufacture are costly. Peptides occupy a niche where their properties correlate with the efficacy and selectivity of biologics and the cost-effective optimisation of small molecules.[4] There has been an increased demand for peptide-based drugs in the 21st century for the treatment of (*inter alia*) cancer[5] and diabetes.[6,7] In 2019, peptide drugs occupied a 5% market share of the pharmaceutical industry and generated around 50 billion US dollars in revenue.[8] In 2023, GLP-1 receptor agonist semaglutide[9] (Ozempic™) generated 18.5 billion US dollars in retail sales alone.[10] However, peptide synthesis is not trivial, and historically, the cost of manufacture was prohibitive.[11] Modern techniques have reduced this associated cost, however, peptide-based drugs still face several challenges, including poor *in vivo* stability and insolubility. A strategy to remedy these issues is the inclusion of unnatural amino acids in the peptide chain to change the peptide's lipophilicity/hydrophilicity.[12] Additionally, introducing unnatural amino acids can prevent cleavage by proteolytic enzymes, increasing metabolic stability.[13] Two examples of drugs containing unnatural amino acids are Carfilzomib (**1**) and Ganirelix (**2**) with the unnatural amino acids highlighted (Scheme 1.1).

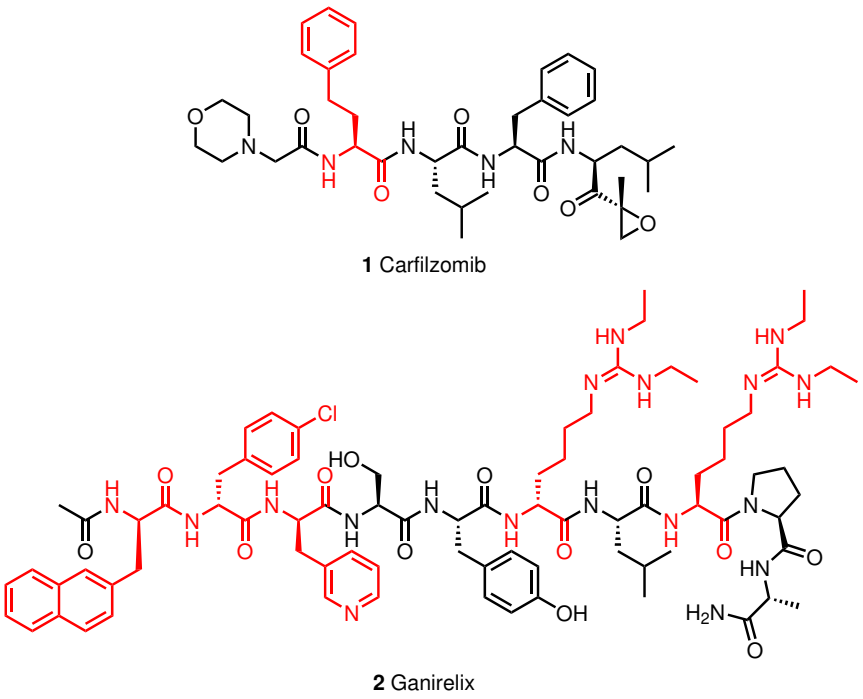

Scheme 1.1: Examples of approved drugs with the unnatural amino acids highlighted

1.1.1 A brief note on the challenges associated with peptide synthesis

There are many considerations to be made when making peptides. Protecting groups are a cornerstone of organic synthesis and are often necessary to achieve high regioselectivity.[14] A molecule with two or more protecting groups that can be selectively deprotected in the presence of the other(s) under different conditions is orthogonally protected.[15] The groups can be removed in any order, *i.e.* **3** can afford **3a** or **3b** depending on the conditions used (Scheme 1.2).[16]

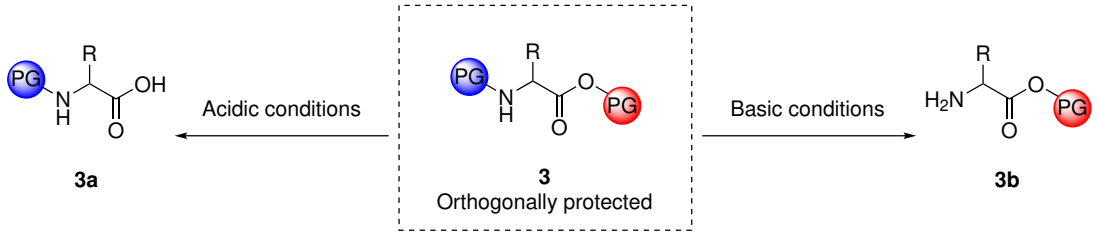

Scheme 1.2: An example of selective deprotections using a peptide equipped with orthogonal protecting groups

Another factor is the racemisation of stereocenters in the peptide chain.[17] For solution-phase synthesis, historically, this was a problem. Practitioners made peptides through acid halides of amino acids[18], leading to racemisation.[19] Modern solution-phase methods remedy this;

however, as the peptide chain lengthens, purification and isolation of clean material become increasingly challenging.[20]

1.1.2 The advent of solid-phase peptide synthesis

Solid-phase peptide synthesis was developed in 1963.[21] Synthesis starts with **4** an amino acid bound to a polymeric resin (Scheme 1.3). An *N*-protected activated amino acid, **5**, can then be coupled to **4** to yield resin-bound **6**. This sequence of deprotection and coupling can be repeated to achieve the desired peptide, which can be ultimately cleaved from the resin.[7,20,21]

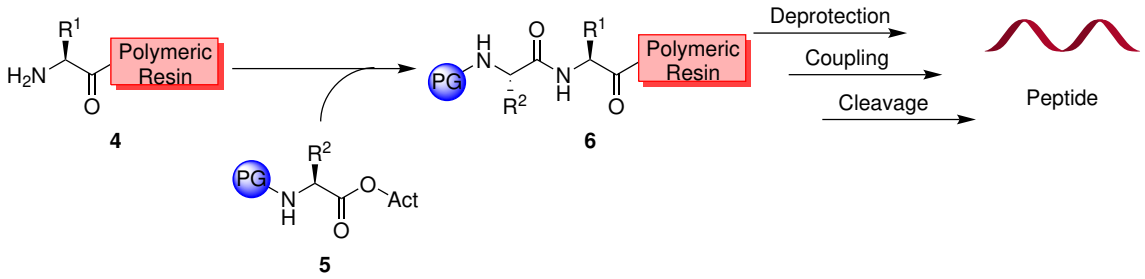

Scheme 1.3: A general example of solid-phase peptide synthesis

The invention of this technique revolutionised peptide chemistry. It provides both selective modification and usually a retention of amino acid stereochemistry.[20,22] It gives the practitioner the ability to synthesise complex polypeptide chains without the need to isolate each intermediate, vastly improving throughput.[20] However, this technique is not without its limitations; the process is wasteful and requires a large excess of solvent for washing the resin at each step.[23] Additionally, the superstoichiometric amounts of coupling reagents at each step is atom inefficient. These problems are compounded in cases where peptides require the synthesis of specific residues, such as unnatural amino acids.

1.1.3 General limitations of unnatural amino acid synthesis

The synthesis of unnatural amino acids for peptides is a wide field with a surfeit of ways to make them.[24,25] Traditionally, the synthesis of the unnatural amino acid, its chiral resolution[25] and peptide coupling occur in separate steps. Practitioners can reduce the number of steps by employing asymmetric synthesis, to either compound the steps of resolution and synthesis[26] or resolution and peptide coupling in one pot.[27] Azlactones are a reagent that has garnered interest

for the enantioselective synthesis of unnatural or modified amino acids due to their synthetic versatility.[28]

1.2 Azlactones: a synthetically useful substrate for the stereoselective synthesis of amino acid derivatives

Azlactones **7** are a heterocyclic scaffold synthesised through the dehydrative cyclisation of *N*-protected amino acids using either mixed anhydrides[29] or carbodiimide coupling reagents.[30] They have been of great interest to organic chemists for the past three decades due to the large numbers of possible transformations they participate in such as: ring-opening reactions[31] (Figure 1.1A); electrophilic additions[32] (Figure 1.1B, C) and hetero Diels-Alder chemistry[33] (Figure 1.1D) to name a few.

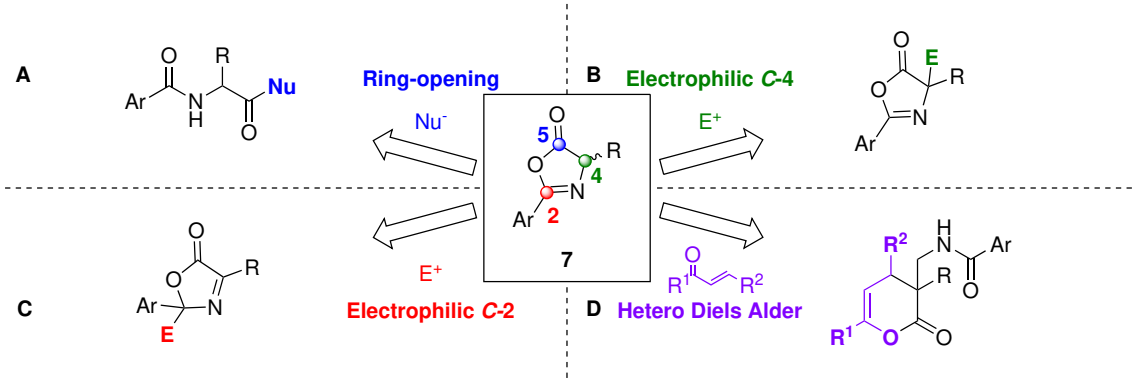

Figure 1.1: Transformations using azlactones as a substrate

Concerning nucleophilic ring-opening reactions, the goal of numerous studies has been to synthesise optically pure *N*-benzoyl protected amino acid,[34] thioesters[35] and amides[36] *via* dynamic kinetic resolution (DKR).

1.2.1 The dynamic kinetic resolution (DKR) of azlactones *via* ring-opening

Kinetic resolution (KR) is the separation of two enantiomers from an optically impure mixture using a chiral catalyst or reagent, due to the different enantiomers having unequal rates of reaction when in the presence of the chiral catalyst or reagent.[37–39] The rate of reaction of the fast-reacting enantiomer (k_{fast}, the reaction from **7a** to **8a**) must dwarf the rate of reaction of the slow-reacting enantiomer (k_{slow}, the reaction from **7b** to **8b**) (Scheme 1.4A) to achieve high

degrees of enantiomeric excess (*ee*). Reactions that undergo KR can yield an optically pure product, however, it can only achieve a maximum of 50% yield when using a racemic starting material.

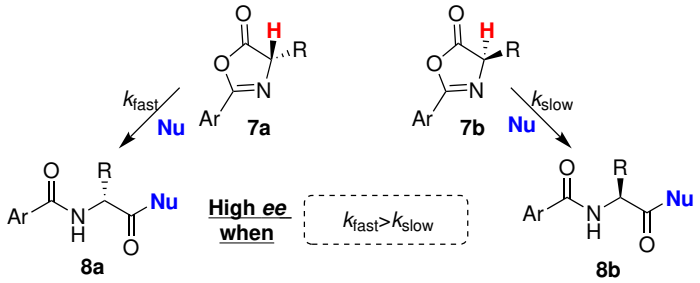

Scheme 1.4: **A**: A general depiction of azlactone KR

Part of what makes azlactones an interesting substrate class is the relatively acidic hydrogen atom at *C*-4 (pK_a *ca.* 9, H_2O, 25 °C) making racemisation *via* tautomerisation of **7** to the enol form **7c** relatively facile (Scheme 1.5A). In contrast to KR, DKR relies on the epimerisation of the racemic starting material.[40] This rate of epimersation (k_{rac}, racemisation between **7a** and **7b**), as well as k_{fast}, must both be substantially larger than k_{slow} to achieve enantiopure products in quantitative yield (Scheme 1.5B).[41] Azlactones, therefore, are an ideal substrate for DKR.[42,43] Theoretically, any nucleophile can be used for the enantioselective ring-opening of azlactones, however, alcoholysis is by far the most successful.

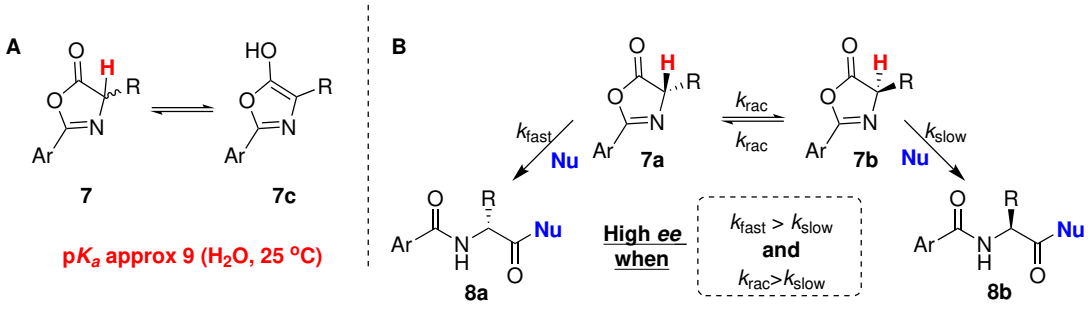

Scheme 1.5: **A**: Tautomerisation of azlactones, **B**: A general depiction of azlactone DKR

1.2.2 The dynamic kinetic resolution of azlactones *via* alcoholysis

Asymmetric catalytic methods to produce amino acid esters from azlactones is desirable as a synthetic tool to reduce waste from other more traditional processes.[28] Many different catalyst classes have found success towards this end and can be loosely defined into categories such as

enzymatic[44]; nucleophilic[45]; bifunctional[46] and phase-transfer catalysts.[47] It is worth noting that other catalyst classes have been used, but these have had limited success.[48]

1.2.2.1 Biocatalysis

Organisms have been used by humans to perform chemical reactions for millennia to produce alcohol and bread.[49] Enzymes were adopted for asymmetric catalysis in the 20th century. Bevinakatti *et al.* pioneered the alcoholysis of azlactones incorporating DKR using *Muco miehei* as a biocatalyst in 1990.[44] Initially, it was thought that this system would undergo a traditional KR and conversion from **9** to **10** was stopped at 45% and achieved moderate enantioselectivity (Scheme 1.6). However, the unreacted azlactone **9** was found to be racemic and therefore racemising in the reaction. They concluded the reaction must be undergoing a DKR. The study ended with an experiment in which conversion proceeded to 100% however, the enantioselectivity was reduced from 57% *ee* to 34% *ee*. While enantiomeric excess is poor, this study provided a much-needed precedent in the alcoholysis of azlactones.

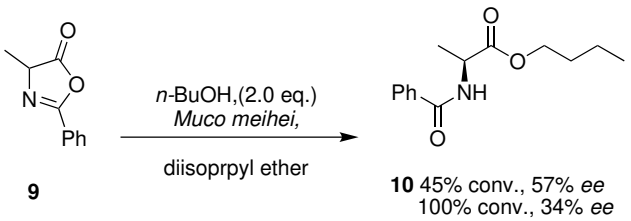

Scheme 1.6: Enzyme-catalysed DKR of azlactones by Bevinakatti *et al.*

Fox and co-workers later used enzymatic catalysis in the stereoselective ring-opening of dehydrocorononic acid derivative **11** (Scheme 1.7).[50] These *motifs* are found in drug candidates for the treatment of hepatitis C, such as **12** (dehydrocorononic acid *motif* highlighted).[51] What makes this work of particular note is that either the (*R*) **13** or (*S*) **14** products could be isolated in high yield, depending on the enzymatic catalyst used.

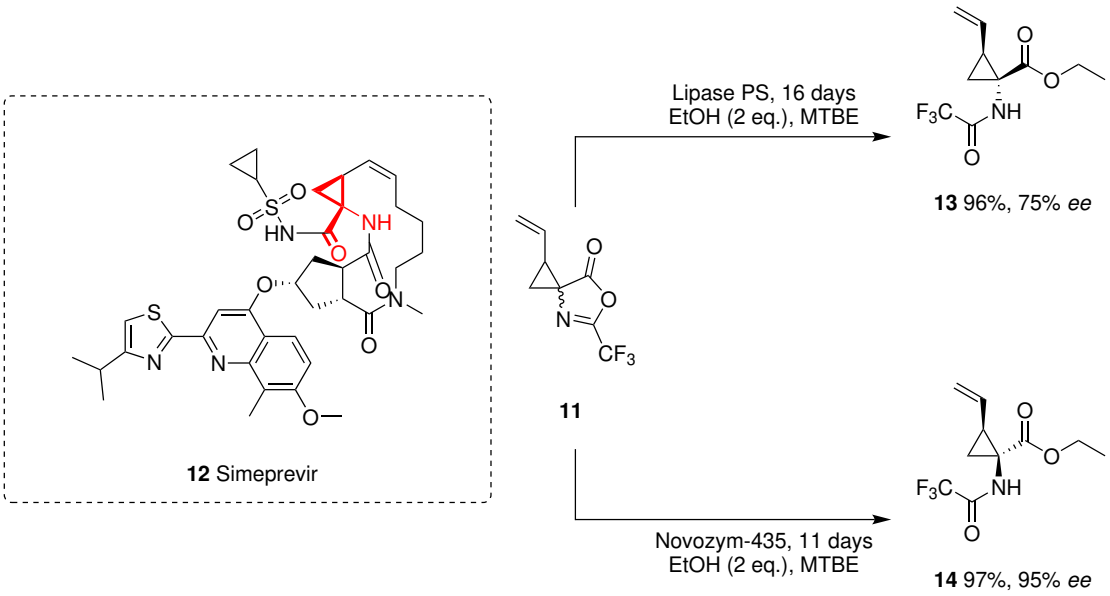

Scheme 1.7: Enzyme-catalyzed DKR of azlactones by Fox *et al.*

A core limitation associated with enzymatic alcoholysis is the often prohibitively long reaction times. For example, the synthesis of **13** took over two weeks to complete.[50] Additionally, the conditions required for enzymes to facilitate high selectivity are substrate-specific, making optimisation rather arduous. However, biocatalysis has found a niche in some industrial applications.[52,53]

1.2.2.2 Nucleophilic catalysis

Asymmetric catalysis using chiral nucleophilic bases has existed for around three decades.[54] In general the catalysts consist of an electron-rich chiral amine or phosphine that activates the electrophilic substrate. Chiral amine nucleophiles have been used as asymmetric acyl transfer agents for many different transformations,[41] yet only a few have been reported for the alcoholysis of azlactones.[30]

1.2.2.2.1 DMAP derivatives

Since its inception by Litvinenko *et al.*,[55] *N,N*-4-dimethylaminopyridine (DMAP) and its derivatives have been used in a breadth of catalytic transformations, including the eponymous Steglich reaction.[54,56] The first reported asymmetric alcoholysis of azlactones using a chiral nucleophilic catalyst was reported by Fu *et al.* using the chiral nucleophilic DMAP-fused-ferrocene **15** (Scheme 1.8).[57] Catalyst **15** had previously been used successfully in the enantioselective acy-

lation of secondary alcohols.[58]

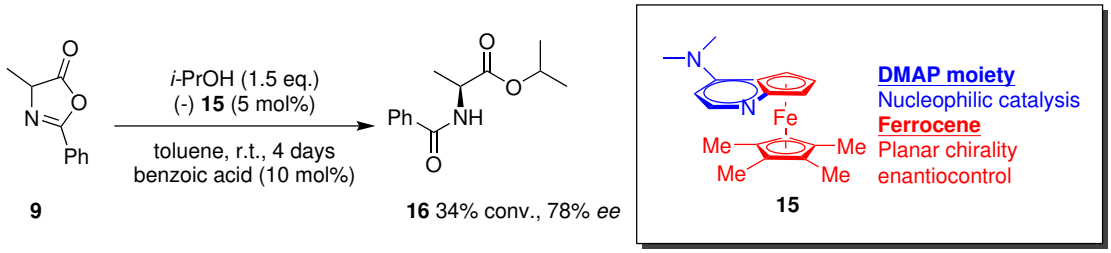

Scheme 1.8: Alcoholysis of azlactones by Fu using a DMAP-derived ferrocene

When azlactone **9** was reacted with propan-2-ol in the presence of **15**, amide **16** was obtained in a maximum of 78% *ee* with a slow rate of reaction. Simpler nucleophilic alcohols, such as methanol, were used to increase the rate of reaction, however, this came with a significant reduction in enantiocontrol. The steric bulk at the *C*-2 position of DMAP limits the rate of reaction due to the slow formation of the *N*-acyl pyridinium ion. This same large steric bulk also induces enantiocontrol. This work highlights an inherent limitation associated with this catalyst class, there is a trade-off between selectivity and activity.[59] Chiral information close to the nucleophilic nitrogen at the *C*-2 and *C*-3 positions[60,61] can hinder the rate of reaction but can lead to high enantioselectivity. Adding chiral information to the dialkylamino group does not lower the activity or stability of the pyridinium ion, however, it is often located too far away from the nucleophilic *N*-atom to control the stereochemical outcome of the reaction effectively. It is worth mentioning that there are many examples where practitioners have circumvented these general issues to great effect.[59,62]

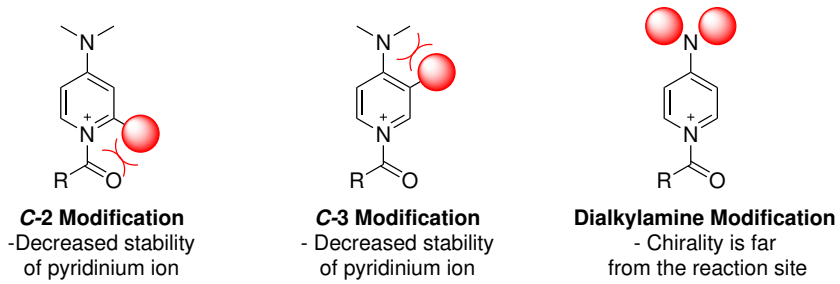

Figure 1.2: A diagrammatic representation of the general shortcomings associated with chiral DMAP catalysts

An example of dialkylamino modification in DMAP-derived alcoholysis was in 2018 when Suga *et al.* developed binaphthyl-based catalyst **17** (Scheme 1.9).[63] Similar catalysts from the same group had previously been used in asymmetric Steglich rearrangements.[62]

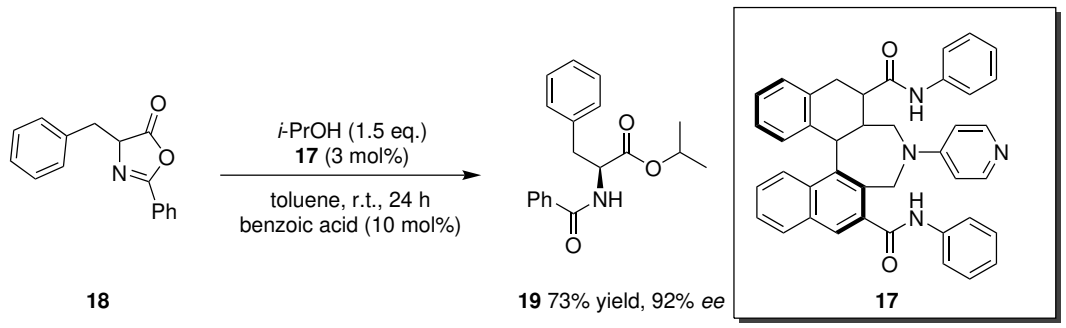

Scheme 1.9: Alcoholysis of azlactones by Suga *et al.*

Catalyst **17** was effective at low loading in the highly selective alcoholysis of **18** to **19** in moderate yield. Both activity and stereoinduction were contingent on the amides in the catalyst structure; removal of these was detrimental to both rate and enantiocontrol, yielding racemic **19**. Creative attempts have been made to bypass the selectivity/activity conundrum associated with chiral DMAP catalysts, however, the synthesis of chiral DMAP catalysts is inherently complex. Catalysts **15** and **17** require complicated multi-step syntheses with low overall yields.[62,64]

1.2.2.2.2 DMAP *N*-oxides

A contemporary solution in the field of chiral DMAP catalysis is to extend the reaction site away from the aryl-ring as seen in Scheme 1.10A using an ionic spacer. This modification minimises the activity deficit when chiral information is close to the nucleophilic nitrogen.[65,66]

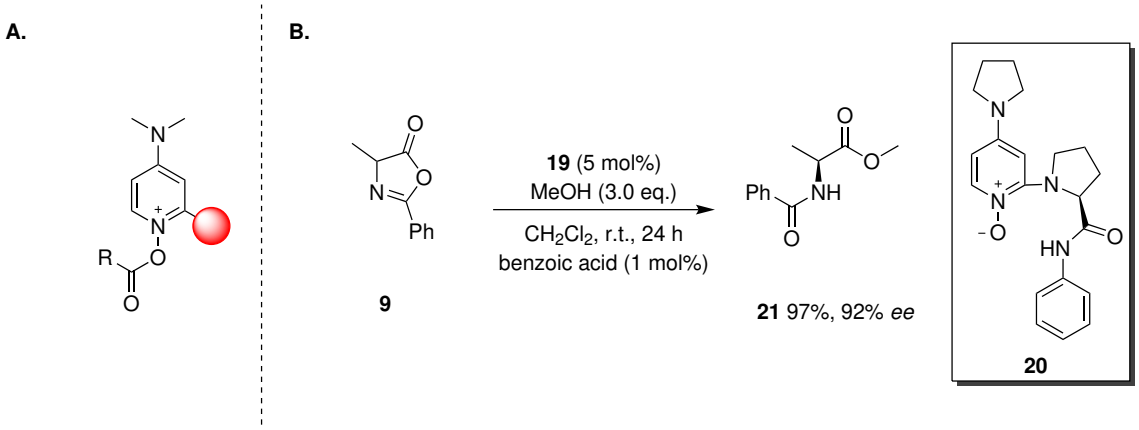

Scheme 1.10: **A**: A representation of a DMAP *N*-oxide derived acylating agent, **B**: Alcoholysis of azlactones using DMAP *N*-oxide **20**

In 2020 Guo *et al.* used **20** in the alcoholytic ring-opening of azlactone **9** to great effect (Scheme 1.10B).[67] This system was found to be highly selective with an expansive range of

azlactones. Catalyst **20** facilitated the highly enantioselective ring-opening of **9** with a wide range of alcohols in high yield. Reaction times ranged between 24 to 72 hours in all cases.

1.2.2.2.3 Benzotetramisole-derived catalysts

The use of amidine and tetramisole derivatives for acylative catalysis was pioneered by Birman *et al*. for the resolution of secondary alcohols.[68,69] Compared to other acyl-transfer catalysts, the synthesis is significantly less complex, requiring fewer overall steps. A derivative of tetramisole, benzotetramisole **22**, was found to be successful in the alcoholytic DKR of azlactones (Scheme 1.11).

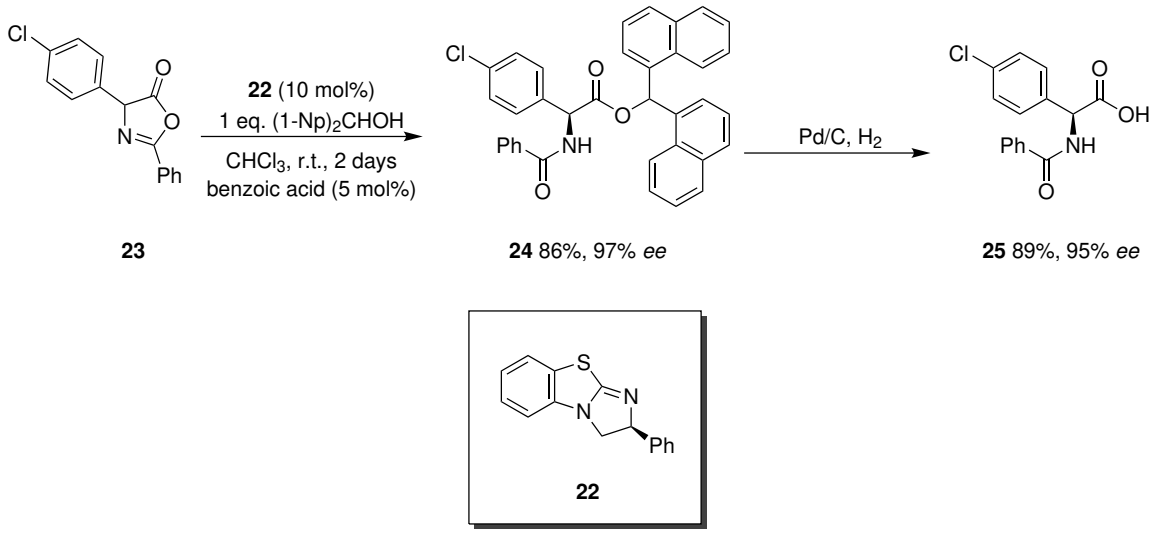

23 **24** 86%, 97% *ee* **25** 89%, 95% *ee*

22

Scheme 1.11: The asymmetric alcoholysis of azlactones by Birman *et al*.

This example is notable as **22** facilitates the enantioselective alcoholysis of aryl glycine analogues such as **23** in high yield. The only nucleophile compatible with high *ee* in the presence of **22** was di-1-naphthylmethanol, however, the resulting *N*-benzoyl amino acid ester, **24**, can be selectively deprotected at the *C*-terminus by hydrogenolysis to yield **25** with minimal change in enantiopurity. It was also shown that the synthesis of **23** can be performed *in situ* during the resolution.[45] Nucleophilic acyl-transfer catalysts have proven successful in the selective alcoholysis of azlactones. The overall method development for nucleophilic catalysis is an intricate balance of selectivity and reactivity, and catalyst synthesis can be challenging.

1.2.2.3 Bifunctional catalysis

An example of an asymmetric bifunctional organocatalyst is presented in Figure 1.3; a *H*-bond donor and a base covalently linked *via* a chiral spacer. This design simultaneously activates both electrophiles and nucleophiles to form enantioenriched products. Bifunctional catalysis allows for facile modification of an existing catalyst template to tune the catalytic sites easily.[70]

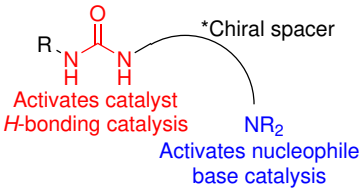

Figure 1.3: General structural features associated with urea-based bifunctional catalysts

1.2.2.3.1 *Trans*-1,2-diaminocyclohexane derivatives

Bifunctional catalysis was exploited in 2005 by Berkessel and coworkers in the alcoholytic DKR of azlactone **26**.[46] This work screened many different bifunctional catalyst cores, and the best-performing catalysts were urea **27** and thiourea **28** in the enantioselective synthesis of **29** (Scheme 1.12). Takemoto and coworkers had previously used these catalysts in a variety of enantioselective transformations to great effect.[71]

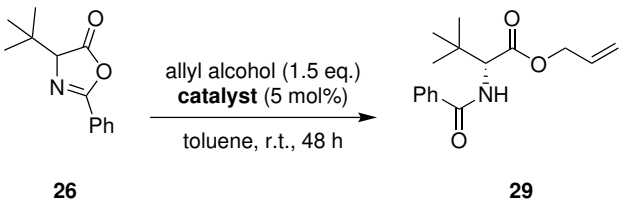

26 **29**

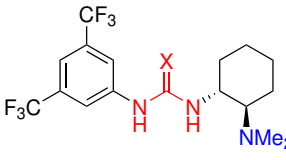

	X	conv.	*ee*
27	O	67%	87%
28	S	69%	83%

Scheme 1.12: Azlactone DKR by Berkeseel *et al.*

Both catalysts **27** and **28** catalysed the formation of **29** in moderate conversion (67-69%) and good enantioselectivity (83-87%). Berkessel *et al.* also reported a marked improvement in selectivity when using **28** at lower temperature with 91% *ee* for the synthesis of **29** at −20 °C.

The decrease in temperature significantly reduced activity, allowing only for 16% conversion in 2 days. A year later, Berkssel *et al.* aimed to improve this system using **28** as a template for modification. The L-*tert*-leucine derived catalysts **30**, **31** and **32** promoted the highly enantioselective synthesis of **29** (Scheme 1.13).[72]

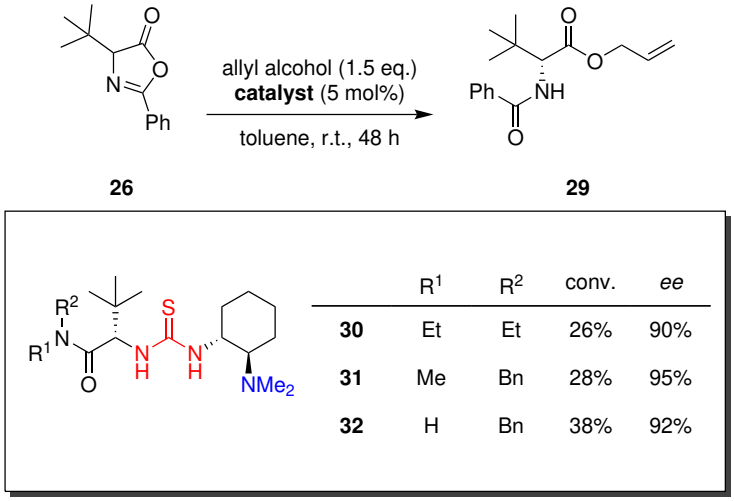

	R^1	R^2	conv.	*ee*
30	Et	Et	26%	90%
31	Me	Bn	28%	95%
32	H	Bn	38%	92%

Scheme 1.13: Azlactone DKR by Berkeseel *et al.* using second-generation thiourea catalysts

Compared to the first-generation bifunctional catalysts developed by Takemoto *et al.* (*vide supra*), these catalysts did not require low temperature to achieve >90% *ee*; however, the conversion was poor, peaking at 38%. Enantiopurity decreased when **30** was used with azlactones derived from amino acids with considerably less steric demand (<90% *ee* in all cases).

1.2.2.3.2 *Cinchona* alkaloid derivatives

There are naturally occurring compounds that can be modified to create effective asymmetric bifunctional catalysts. One of these families of natural products is the *cinchona* alkaloids, which are isolated from the bark of trees of the genus *cinchona*.[73] They are an attractive starting material since they are relatively inexpensive and commercially available in *pseudo*-enantiomeric forms and have been used in many enantioselective transformations for the last five decades.[74,75] It was not until 2008 that this catalyst core was applied to KR of azlacones by Connon *et al.*[35] Catalyst **33** was significantly more active but not as enantioselective in the stereoselective synthesis of **29**, relative to catalyst **32** (Scheme 1.14).

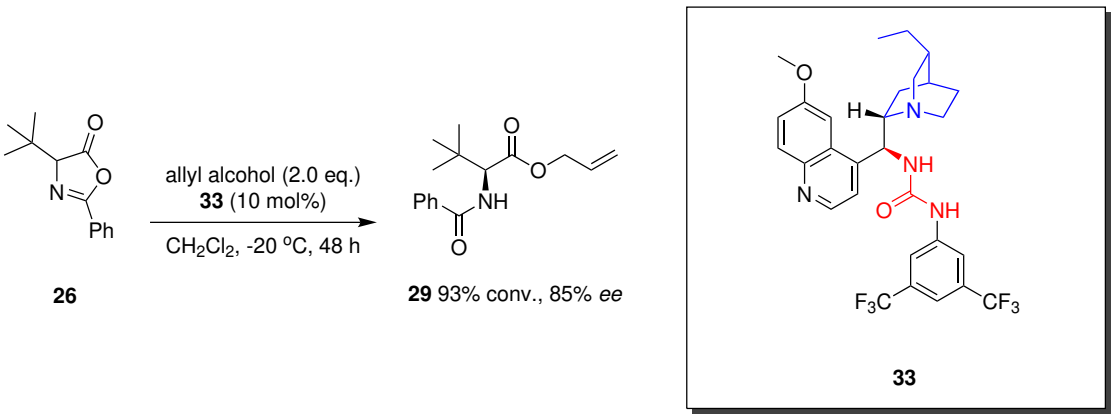

Scheme 1.14: Azlactone DKR by Connon *et al.* using *cinchona* alkaloid derived catalyst **33**

It was later reported that (thio)urea *H*-bond donors can aggregate in solution.[76,77] Aggregation of the catalyst can reduce both activity and enantioselectivity and can happen when the catalyst concentration in solution is too high. To circumvent this problem, Song *et al.* developed squaramide-derived catalyst **34**, which served as a benchmark for both high activity and high enantiocontrol in the alcoholysis of azlactones when using allyl alcohols as nucleophiles (Scheme 1.15).[78]

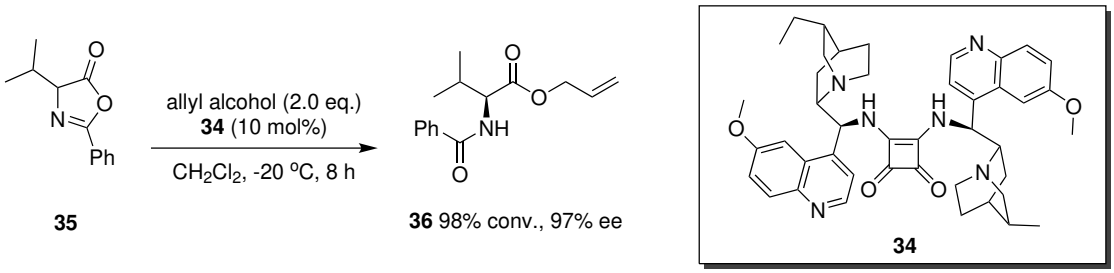

Scheme 1.15: Azlactone DKR by Song *et al.*

Many azlactones such as **35** were amenable to the stereoselective synthesis of *N*-benzyl amino acid allyl esters such as **36**. As seen in Scheme 1.16, a serious limitation associated with aryl-substituted azlactones, such as **37**, is that selective deprotection of the DKR product **38** is not possible and results in amino acid **39** (*i.e.* ester hydrolysis occurs under the conditions for *N*-benzoyl amide deprotection) due to the harsh conditions needed.[79]

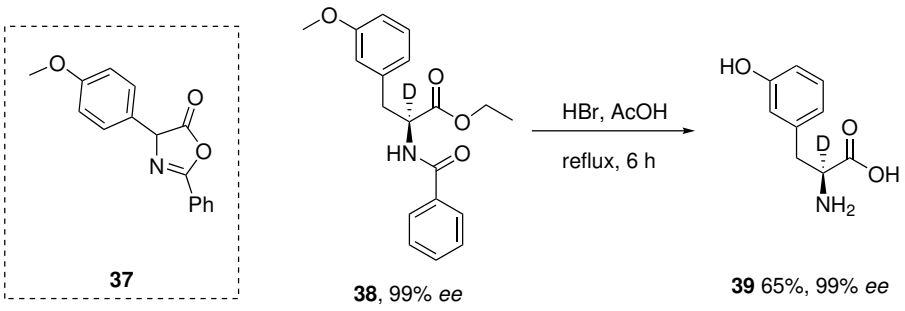

Scheme 1.16: Kinetic resolution and deprotection by Song *et al*.

In 2005, Connon and co-workers used a variant of Song's catalyst, catalyst **40**, on a broad range of *ad hoc*-designed tetrachloroisopropoxycarbonyl (TCIC)-protected azlactones such as **41**.[27] The significant advantage associated with this protecting group is that it leads to the formation of compounds such as **42**; orthogonally protected tetrachlorophthalimides (TCPI). The imide protecting group can be cleaved, producing **43**, thereby exposing the free amino acid ester. An alternative modification is to unmask the protected amino acid to give **44** through hydrogenolysis with palladium on carbon, retaining high *ee* and synthesising an orthogonally protected amino acid with excellent yield (Scheme 1.17).

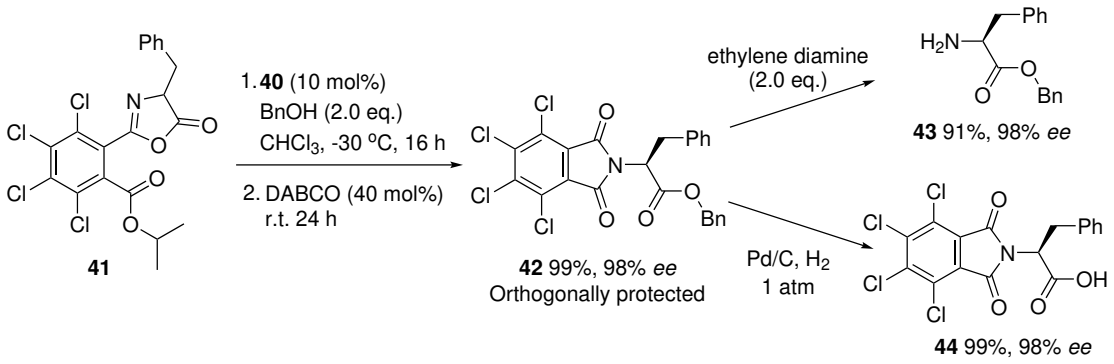

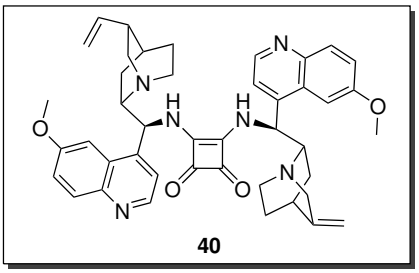

Scheme 1.17: Post DKR-modifications of TCIC-protected amino acid esters

This protocol utilised **45**, a *N*-protected serine-based nucleophile. This had the advantage that after the formation of the initial product from the reaction of **41** with **45**, the orthogonally protected **46** could undergo a trifluoroacetic acid (TFA)-mediated deprotection followed by a

DMAP mediated *O*→*N* acyl transfer reaction to form the diastereomerically pure dipeptide **47** (Scheme 1.18).

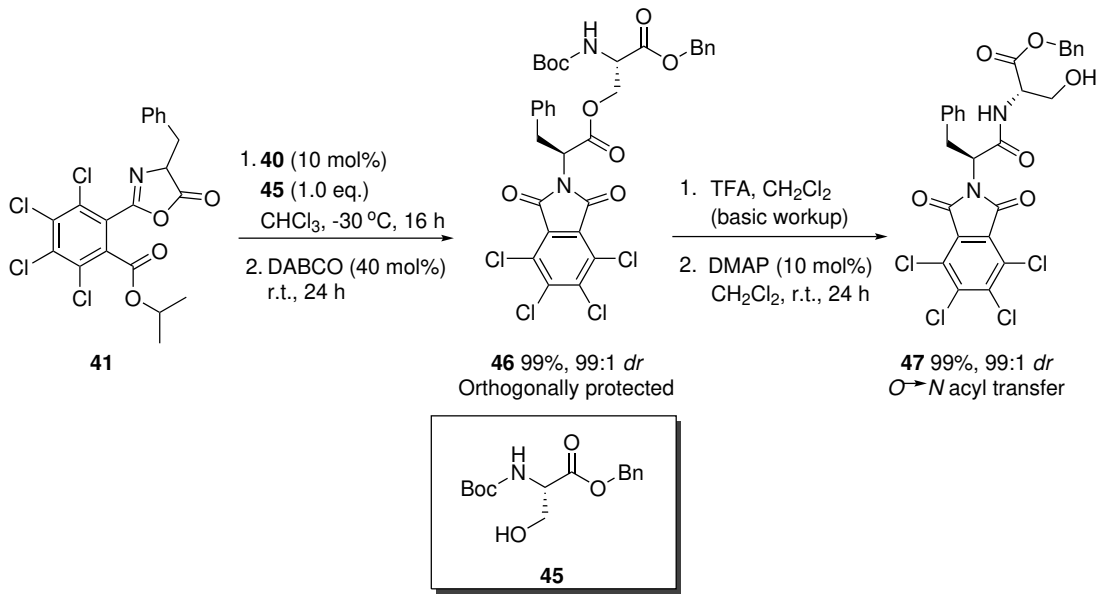

Scheme 1.18: Synthesis of orthogonally protected peptides using a modified variant of Song's catalyst.

This same research showed that it was possible to create a tripeptide using the same method; however, the number of available dipeptides that undergo this transformation is limited.

1.2.2.3.3 Bifunctional catalysis using chiral *bis*guanidine derivatives

A general disadvantage associated with azlactone alcoholysis is the limited number of transformations that ester groups can participate in. The direct transformation from amino acid esters to either amides or thioesters would be desirable, but is an ongoing challenge. In 2015 Feng *et al.* used bifunctional ionic catalyst **48** in the highly enantioselective transformation of azlactone **49** to *N*-aryl-amino acid-oxime-ester **50**, using oxime **51** as a nucleophile (Scheme 1.19).[80]

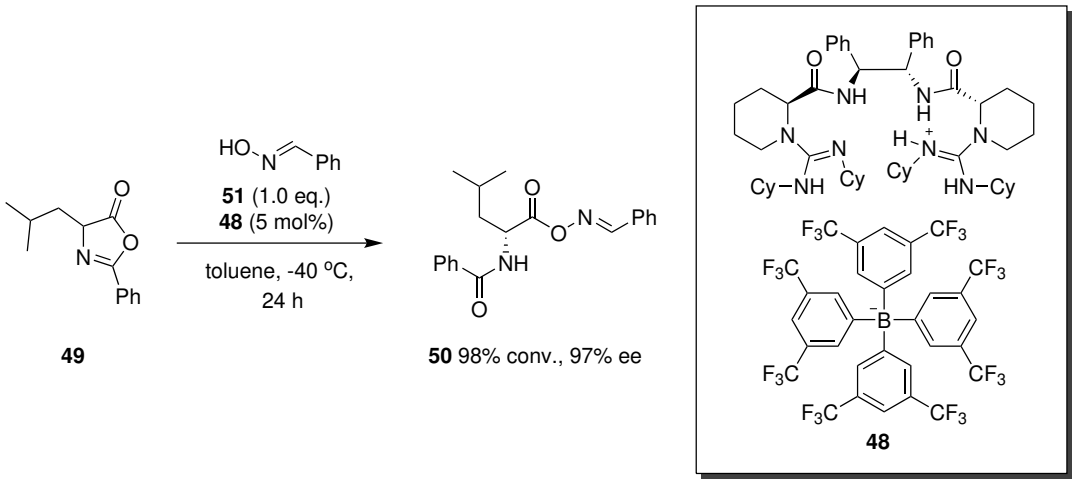

Scheme 1.19: DKR of azlactones using an oxime as a nucleophile

The resulting amino acid oxime ester **50** can then be displaced by either L-serine methyl-ester to form dipeptide **52** or by glycine methyl-ester to form dipeptide **53** (Scheme 1.20).

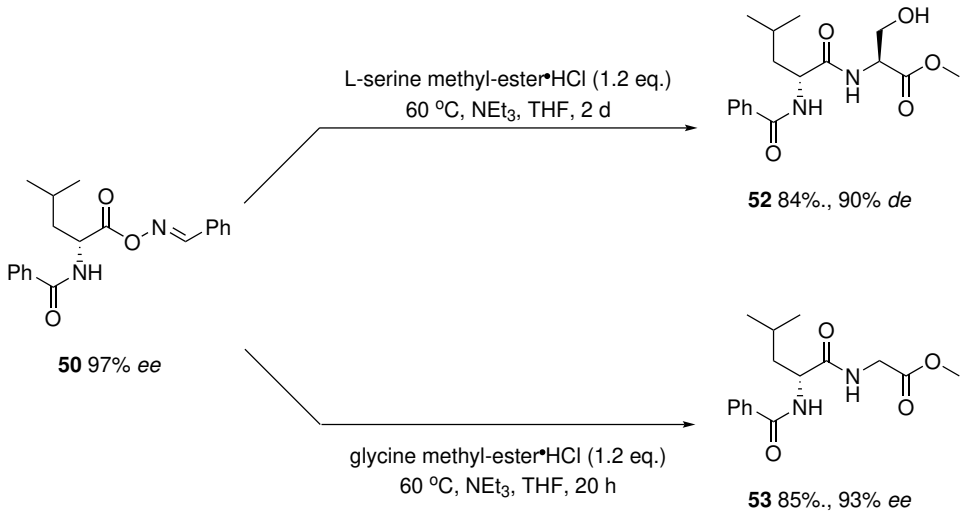

Scheme 1.20: Synthesis of dipeptides **52** and **53** from oxime ester **50**

The *N*-benzamide protection still poses a significant challenge since the removal of this group requires harsh conditions that can affect other functionalities.[79]

1.2.2.3.4 Bifunctional peptide-based catalysis

Peptide-based catalysts have been used in a wide variety of asymmetric transformations since their inception in 1980.[81] A significant benefit of using peptides as catalysts is that they can adopt complex secondary structures, which can aid in enantiocontrol.[82] In 2014 Miller *et al.* applied β-hairpin (*i.e.* with two intramolecular hydrogen bonds) tetrapeptide **54** in the selective

methanolysis of azlactone **18** to form **55** in 92% *ee* (Scheme 1.21).[83]

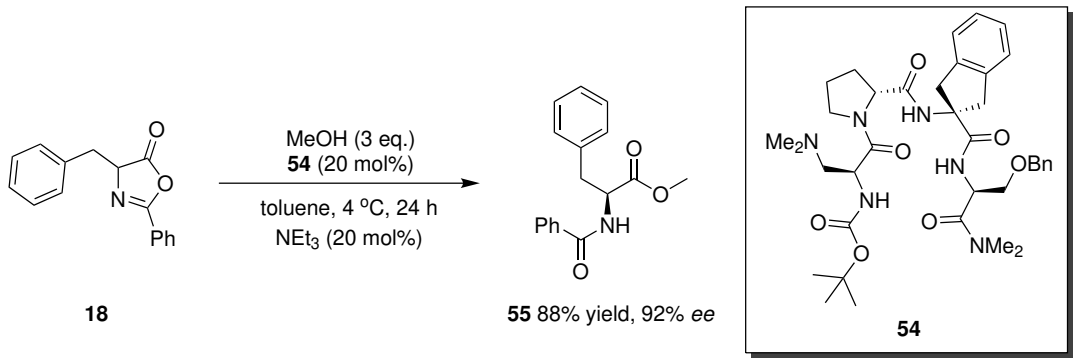

Scheme 1.21: Enantioselective methanolysis of azlactones using a peptide-based catalyst

Catalyst **54** was found to be highly selective (80-98%) in the formation of various amino acid methyl esters.

1.2.2.4 Phase-transfer catalysis

Phase-transfer catalysis is the use of a phase-transfer catalyst (PTC) to facilitate a reaction between reagents in different immiscible phases; the reaction between the reagents would normally be prohibited because they cannot interact. A PTC facilitates the reaction by undergoing ion metathesis, forming a reagent-catalyst ion-pair, which transports reagents between phases.[84] *Cinchona* alkaloid PTCs have historically been used for a variety of different transformations,[85] including asymmetric catalysis.[86]

The groups led by Tokunaga and Yamamoto performed the only enantioselective alcoholysis of azlactones *via* phase-transfer catalysis.[47] The pre-catalyst **56** forms the active catalyst **57** *via* ion exchange with **58** at the interface between phases; facilitated by sodium hydroxide, as seen in Scheme 1.22.

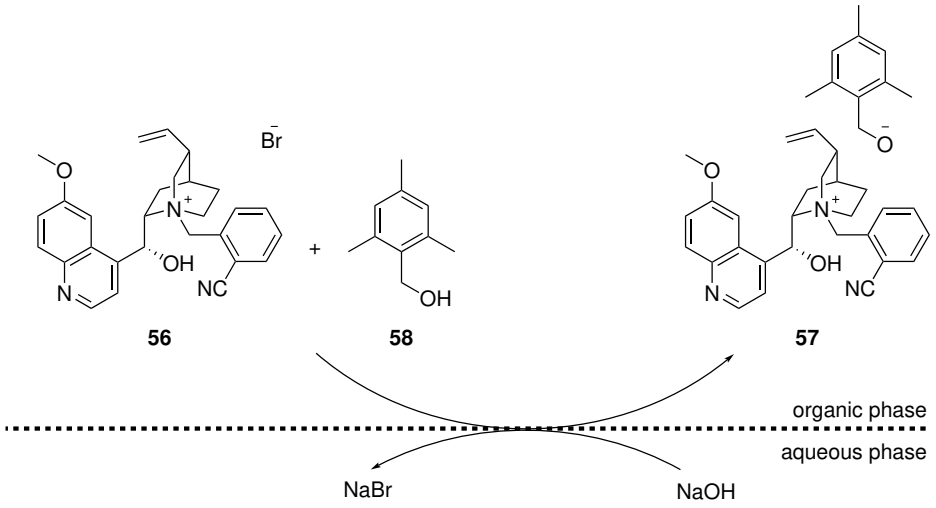

Scheme 1.22: Synthesis of active catalyst **57** through interaction at the organic/aqueous interface

Using azlactone **26** as a substrate and alcohol **58** as a nucleophile; catalyst **56** was used in liquid-liquid and solid-liquid phase-transfer systems giving rise to the highly enantioenriched **59** in moderate to low recovery (Scheme 1.23). The active catalyst is reformed through deprotonation of alcohol **58**, regenerating the benzyl alkoxide salt **57**.

Scheme 1.23: Alcoholysis of azlactones using phase-transfer catalysis

An array of azlactones was assessed, and only azlactones derived from amino acids with considerable steric demand were concordant with high enantioselectivity in moderate to low yields. Catalyst **56** was effective at catalyst loadings as low as 0.1 mol%, only marginally lowering yields and *ee*. This work also demonstrated that **59** can be selectively deprotected at either terminus without racemisation occurring (Scheme 1.24). The *N*-terminus can be deprotected using superstoichiometric amounts of Schwartz reagent, followed by acid hydrolysis to yield the primary amine **60** in moderate yield. While the *C*-terminus can undergo hydrogenolysis, affording *N*-benzoyl amino acid **61**.

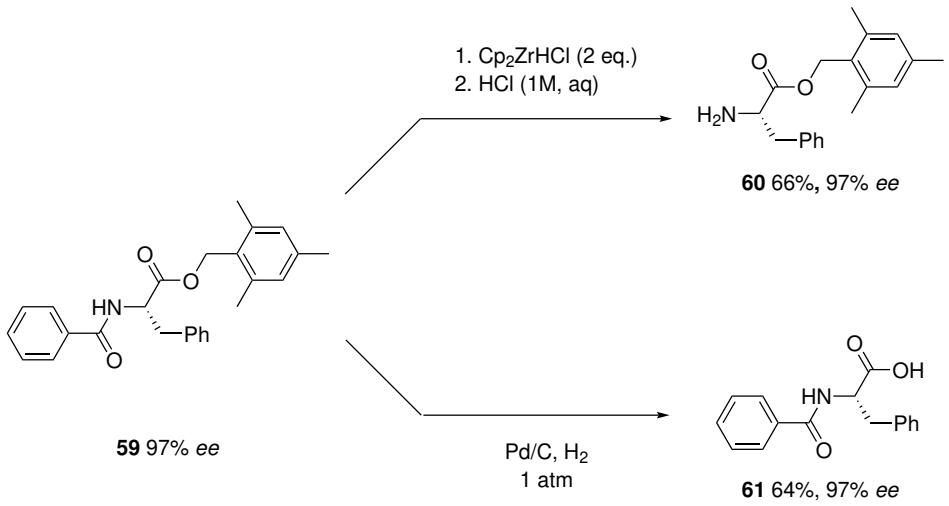

Scheme 1.24: Deprotection of orthogonally protected amino acid **59** by Tokunaga *et al.*

While the enantioselective alcoholysis of azlactones is well established, the highly selective ring-opening of azlactones with other nucleophiles remains a challenge.

1.2.3 Thiolysis of azlactones

Thiolysis of azlactones is desirable as it opens up new avenues for post-DKR modification, such as native chemical ligation (NCL). This is a coupling technique where a polypeptide can be made from two smaller peptides. An example of this is seen in Scheme 1.25, the transesterification between *N*-terminal cysteine **62** and *C*-terminal thioester **63** to form **64** ultimately results in an *S*→*N* acyl transfer to form peptide **65**.[87]

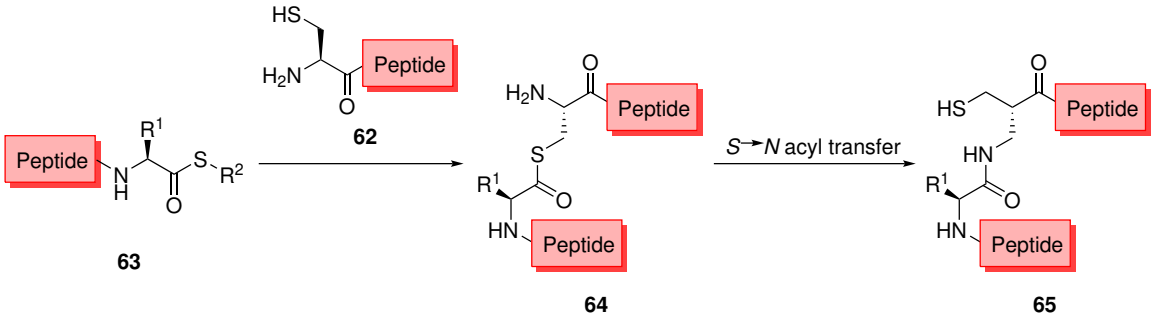

Scheme 1.25: An example of native chemical ligation using *N*-terminal cysteine **62** and *C*-terminal thioester **63**

Thiol-based nucleophiles are considerably more difficult to control in the ring-opening of azlactones due to their higher acidity and longer bond lengths relative to alcohols. In 2012, Connon *et al.* used benzylthiol nucleophile **66** in the selective thiolysis of azlactones (**67**); catalysed by *C*-9 arylated dihydroquinine catalyst **68** (Scheme 1.26).[88]

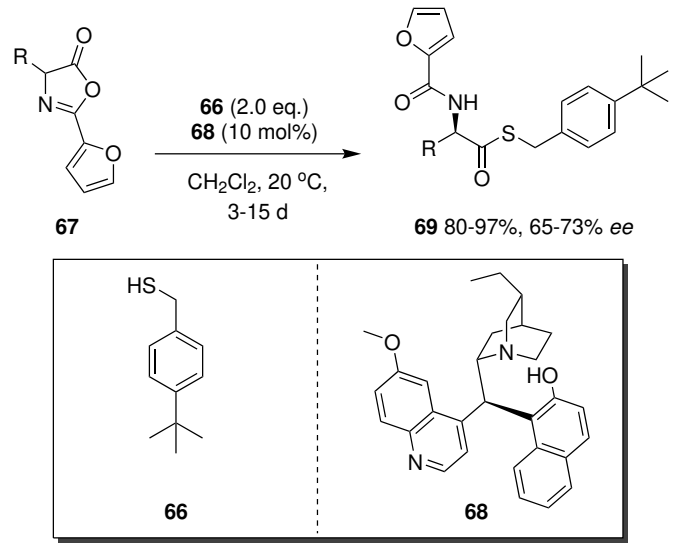

Scheme 1.26: Thiolysis of furyl-based azlactones using **68**

This study isolated thioesters (**69**), from a range of azlactones (**67**) in moderate enantioenrichment ranging from 65-73% *ee*. The rate of reaction was prohibitive, requiring days to achieve high isolated yields at room temperature. In 2013, Connon *et al.* developed dihydroquinine-derived azo-bifunctional catalyst **70**; which facilitated a high degree of stereocontrol in the low-yielding reaction between **66** and **71** to form **72** (Scheme 1.27).

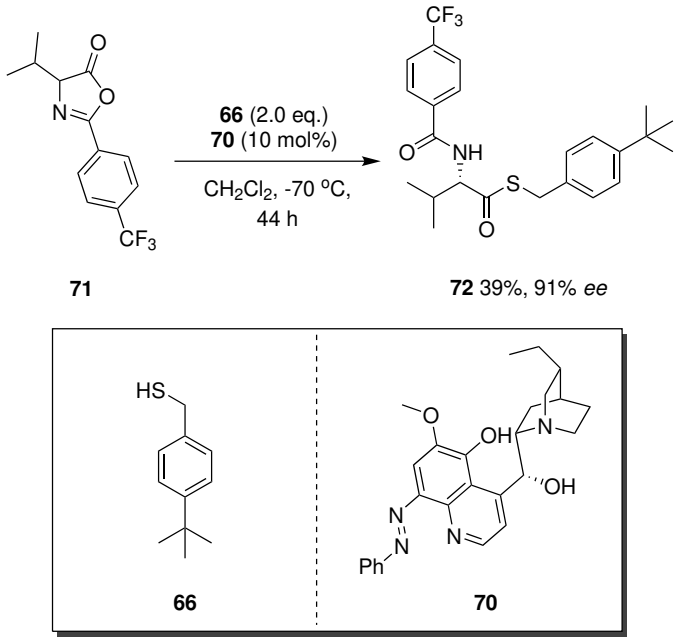

Scheme 1.27: Enantioselective thiolysis of azlactones *via* bifunctional catalysis

A wide range of azlactones were susceptible to the highly enantioselective synthesis of thioesters in the presence of **70**. While the thiolysis of azlactones using **66** as a nucleophile has been demonstrated, aminolysis still poses a significant challenge. Aminolysis of azlactones is a

desirable process for the stereoselective formation of peptides, yet there is only one example in the literature.[36]

1.2.4 Direct aminolysis of azlactones

Amines are difficult nucleophiles to control in the asymmetric ring-opening of azlactones, because they are significantly more nucleophilic than alcohols and can react with azlactones in the absence of a catalyst, making racemic addition far more likely. The first direct stereocontrolled aminolysis of azlactones was accomplished using chiral Brønsted acid catalyst **73**. Chiral phosphoric acid catalysts similar to catalyst **73** had previously been used by Birman *et al*. in the enantioselective alcoholysis of azlactones.[45] The catalyst activates the nucleophile **74** and azlactone **75** in a chiral environment through hydrogen bonding; this directs nucleophilic attack of **74** towards **75**, forming **76** in excellent yield and *ee* (Scheme 1.28).[36]

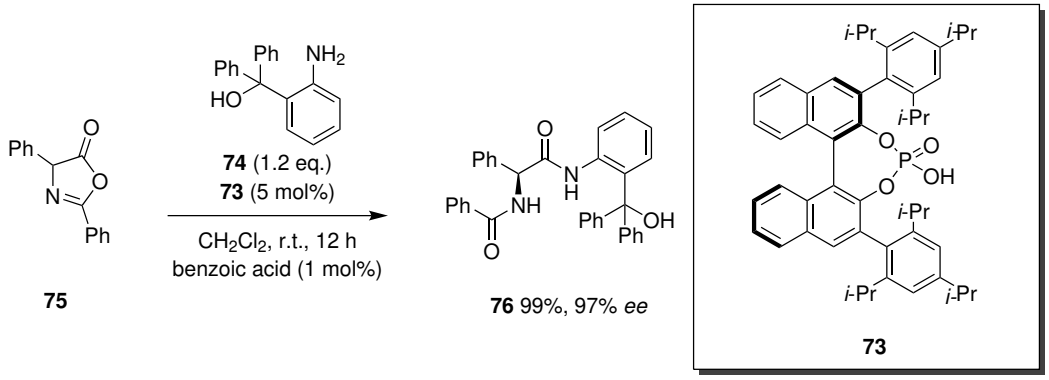

Scheme 1.28: DKR of azlactones to form enantioenriched amides using Brønsted acid chiral catalysts.

While Shi *et al*. succeeded in the enantioselective synthesis of diamides, the only nucleophile congruent with high *ee* is the relatively non-nucleophilic and bulky *ortho*-substituted aniline **74**, which greatly limits the scope of useful post-DKR transformations. Changing the nucleophile from **74** to aniline had a detrimental effect on enantiocontrol (37% *ee*).

1.2.5 Frontiers and remaining challenges in the catalytic asymmetric ring opening of azlactones

In summary, a vast amount of research has been done on the alcoholysis of azlactones with multiple systems, achieving high levels of enantiocontrol and generating high yields using nu-

merous nucleophiles and azlactones.[30,89] Azlactone research has expanded to the development of phthalimide protecting groups, making targeted post-DKR modifications relatively facile and high yielding[27] and enables indirect peptide formation through a DMAP catalysed *O*→*N* acyl transfer, if protected serine based nucleophiles are employed. Advances in azlactone DKR allowed for the use of oxime nucleophiles, which can be displaced post-DKR to form dipeptides from amino acid methyl esters.[80] Both the DKR of azlactones using thiols[90] and amines[36] as nucleophiles have appeared in only a few published examples, with non-negligible associated limitations. Therefore, the frontier of azlactone research lies in controlling these challenging nucleophiles to transform azlactones, which could have numerous potential applications, an example of which is peptide coupling. Thioesters have been used in peptide ligation *via* an *S*→*N* acyl shift for coupling small chain peptides involving terminal cysteine residues; while coupling *C*-protected amino acids could be used to directly form enantioenriched peptides from racemic azlactones *via* aminolysis.

1.3 *Cinchona* alkaloid-derived nucleophilic ion-pair catalysts, a new paradigm in nucleophilic catalysis

The first asymmetric process involving a fluoride ion as a nucleophilic catalyst was developed by Connon *et al*. using PTC **77** in the methanolytic desymmetrisation of *meso*-anhydrides.[91] In this system, **77** reacts with KF *via* ion metathesis to form the active catalyst salt, an ammonium fluoride ion pair, which attacks the anhydride **78** and enables methanolysis. The hemiester **79** was generated in excellent yield with moderate enantiocontrol (Scheme 1.29).[91]

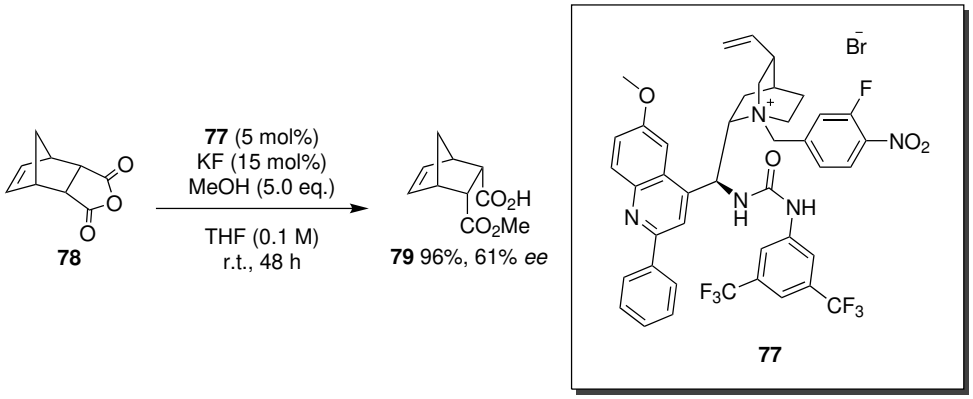

Scheme 1.29: Desymmetrisation of *meso*-anhydrides *via* phase-transfer-mediated alcoholysis

While the *ee* obtainable using catalyst **77** is not high, this process represents the first example of asymmetric catalysis by a nucleophilic fluoride ion and demonstrates that the mechanism at least partially involves nucleophilic catalysis. This work also presents a potential solution to the activity/selectivity compromise generally associated with nucleophilic catalysis, as seen in Section 1.2.2.2.1; *i.e.* having the chiral information and the nucleophile as separate ions in an ion pair. For example, in the active form of catalyst **77**, the small, unhindered fluoride anion is the nucleophile, while the *cinchona* alkaloid core is the larger chiral cation capable of hydrogen bonding through the urea *moeity* at *C*-9 (Figure 1.4).[92] The substitution of the *C*-9 alcohol in a quinine-based PTC to a functional group with more hydrogen bond donors (*i.e.* urea) can either increase the stability of the anion or activate the substrate.

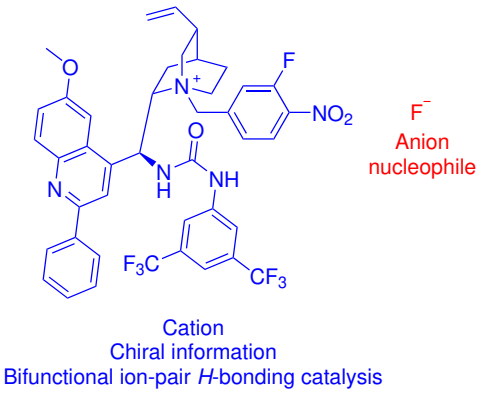

Figure 1.4: An example of a nucleophilic ion-pair catalyst using a fluoride nucleophile

The *cinchona* alkaloid backbone is ideal for creating novel and effective ionic catalysts because it can be readily transformed into a cationic salt through quaternisation of the tertiary amine.[73] Many modifications can be made to tune the catalytic and stereoselective properties of *cinchona* alkaloid cations (Figure 1.5).[70,73] Substitution of the anion is also relatively facile either through phase-transfer or *via* synthesis of a stable ion pair.[93,94]

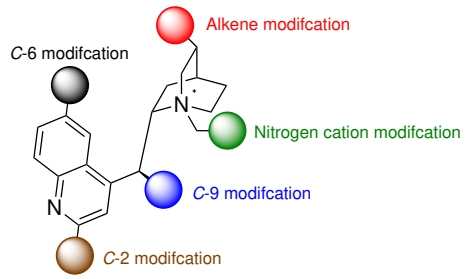

Figure 1.5: Common modifications of cinchona alkaloid PTCs and ion-pairs

A contemporary alternative to phase-transfer catalysis is ion-pair catalysis; a powerful method-

ology in which an *ad hoc* pre-synthesised ion-pair can catalyse reactions.[93] Unlike phase-transfer catalysis, ion-pair catalysis does not require a phase-transfer step to create the active catalyst, meaning the rate of reaction can be higher in cases where the phase-transfer step is rate-limiting.[93] Mukaiyama and co-workers used **80** to synthesise the stable ion-pair catalyst **81**, a chiral quaternary ammonium phenoxide salt, which can catalyse asymmetric Michael additions.[95] The technology to synthesise quaternary ammonium phenoxide salts was first developed by Reetz *et al.*[94] to create novel permanent ion-pairs; **81** was synthesised from **80** *via* ion metathesis using this methodology (Scheme 1.30).[85,96]

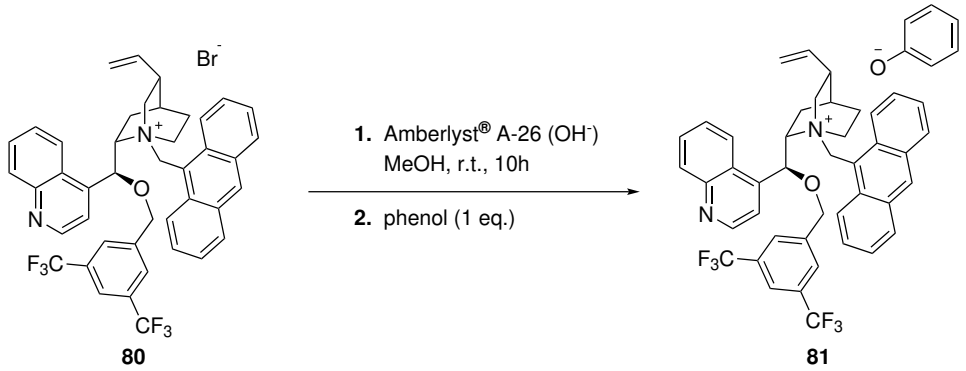

Scheme 1.30: Synthesis of ion-pair catalyst **81**

Mukaiyama and coworkers showed that **81** could be used to synthesise a variety of enantioenriched lactones; for example, the reaction of chalcone **82** and ketene silyl acetal **83** (activated by **81**) formed **84** in both excellent yield and *ee* with reaction times under an hour (Scheme 1.31). The active catalyst **81** is regenerated by phenoxide elimination after the intramolecular cyclisation of the lactone **84**. It is worth noting that reactions using phenols as nucleophiles can also be performed under phase-transfer conditions using both cinchona alkaloids[97] and 1,1'-binaphthyl-2,2'-diol (BINOL)[93] derived catalysts.

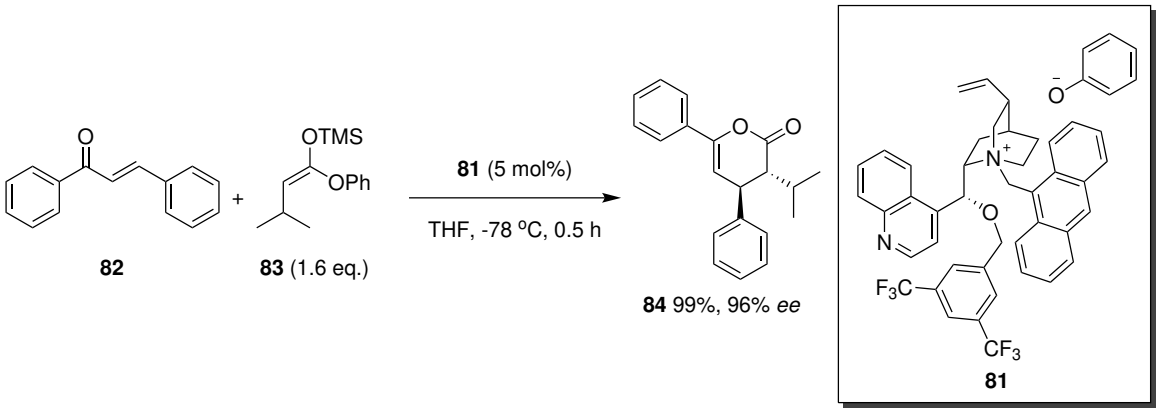

Scheme 1.31: One pot enantioselective Mukaiyama-Michael addition and lactonisation

The addition of hydrogen bonding *motifs* to the *cinchona* PTC core can stabilise the anion or activate the substrate.[98] Substituting the alcohol at *C*-9 is a common modification found in *cinchona* alkaloid catalysts to increase its hydrogen bonding capabilities (*vide supra*), however, it is possible to install *H*-bonding functionality in other parts of the catalyst core. In 2020 Jurczak *et al*. utilised bifunctional phase-transfer catalysis for the asymmetric α-chlorination of β-keto esters.[99] Catalyst synthesis was relatively facile; quinine **85** was alkylated with bromoacetamide **86** to form catalyst **87** (Scheme 1.32).[86]

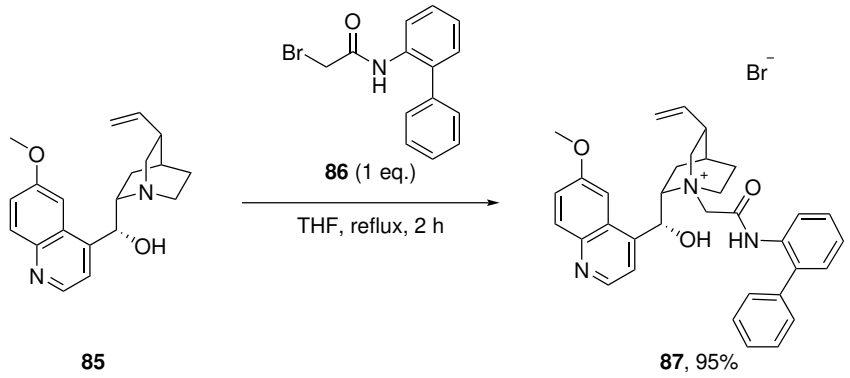

Scheme 1.32: Synthesis of quaternary ammonium bromide salt **87**

This catalyst features two hydrogen bond donors, an alcohol at the *C*-9 position and an *N*-aryl acetamide covalently linked to the cationic nitrogen. Catalyst **87** facilitated the active and enantioselective α-chlorination of various β-keto esters, such as **88** in the synthesis of **89**, using *N*-chlorosuccinimide (NCS) as a chlorinating reagent (Scheme 1.33).

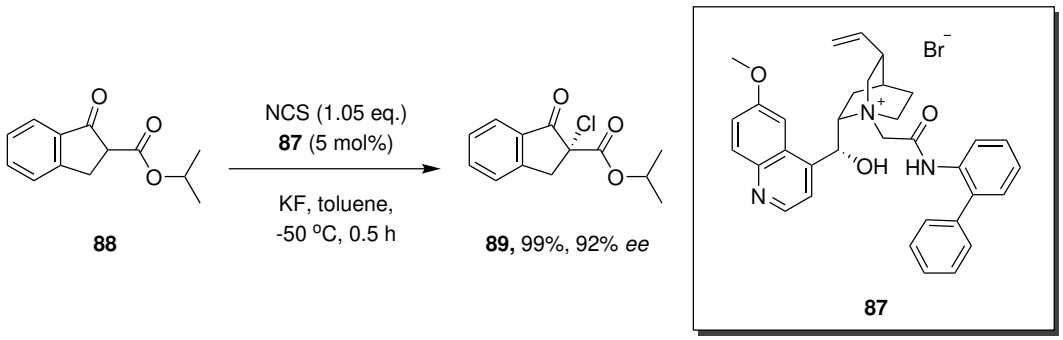

Scheme 1.33: Enantioselective α-chlorination of various β-keto esters

The installation of a hydrogen bond donor through the quaternisation of the quinuclidine nitrogen has been shown to be relatively facile and highly yielding; previous work by Jurczak *et al.* detailed the synthesis of over 20 catalysts using this methodology.[86]

1.4 Initial investigations into the indirect aminolysis of azlactones

The direct aminolysis of azlactones remains relatively unexplored and poses a significant challenge.[36] An attractive alternative to direct aminolysis of azlactones is indirect aminolysis; *i.e.* forming an enantiopure active ester through enantioselective alcoholysis and then displacing the active ester with an amine to form an amide bond, in one pot. This concept is depicted in Scheme 1.34; azlactone **90** and a pronucleophilic alcohol react to form enantioenriched amino acid ester **91** in the presence of a chiral catalyst; **91** then undergoes an *in situ* acyl transfer with amino acid ester **92** to form orthogonally protected dipeptide **93** in high *ee* and high yield.

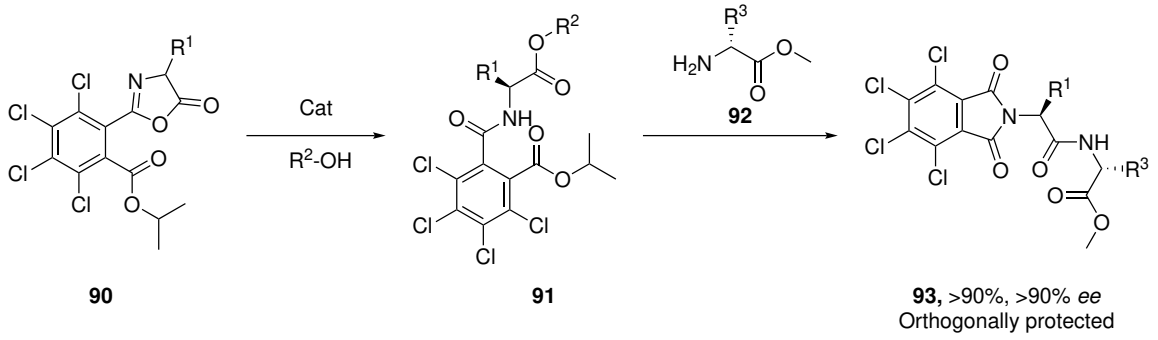

Scheme 1.34: Indirect aminolysis of theoretical azlactone **90** through **91** to form **93**

Initial work performed by Dr. Amy Maguire[100] aimed to develop a reproducible and enantioselective peptide ligation *via* indirect aminolysis of azlactone **41**. Preliminary studies focused on the use of bifunctional catalyst **40**, which had previously been used in the highly enantioselective

alcoholysis of **41** (Scheme 1.35).[27,35]

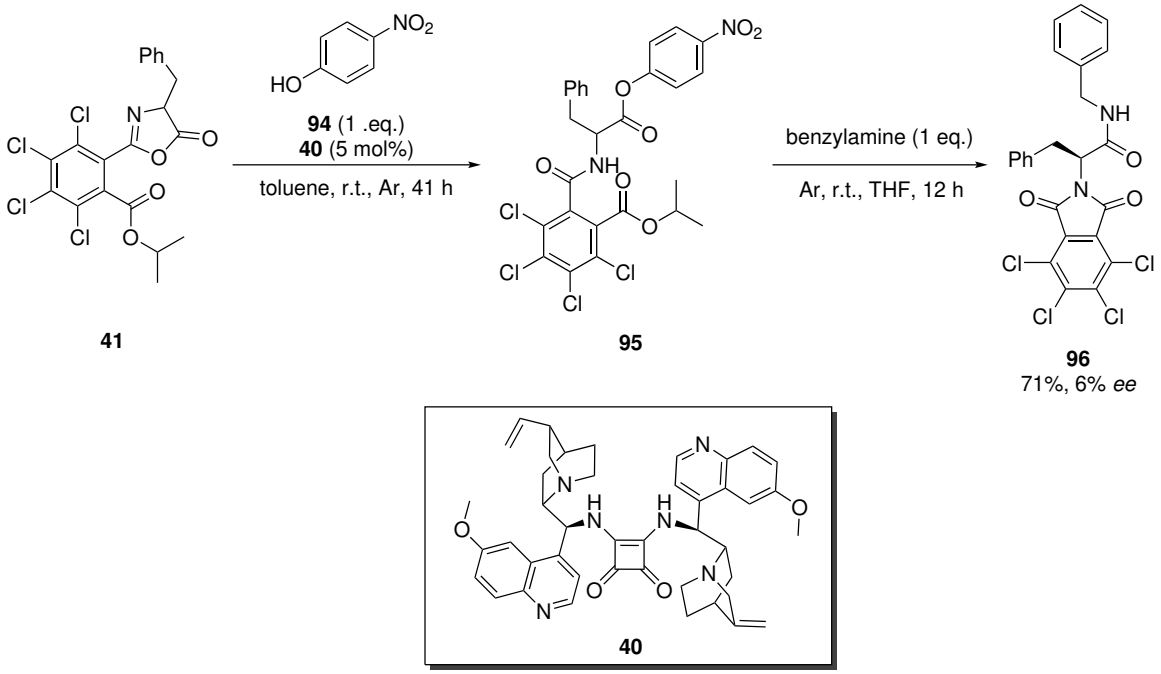

Scheme 1.35: Indirect aminolysis of azlactone **41** *via* bifunctional catalysis carried out by Dr. Amy Maguire

Using *p*-nitrophenol (**94**) as a nucleophile, the resulting hydrolytically unstable active ester **95** was successfully displaced *in situ* by benzylamine in moderate yield, however, the *ee* of the resulting diamide **96** was minimal. Later work by Dr. Maguire utilised solid-liquid phase-transfer catalysis to dynamically resolve **41**, mediated by the PTC **97** in conjunction with sodium *para*-nitrophenolate **98** to form the active catalyst (Scheme 1.36).[100]

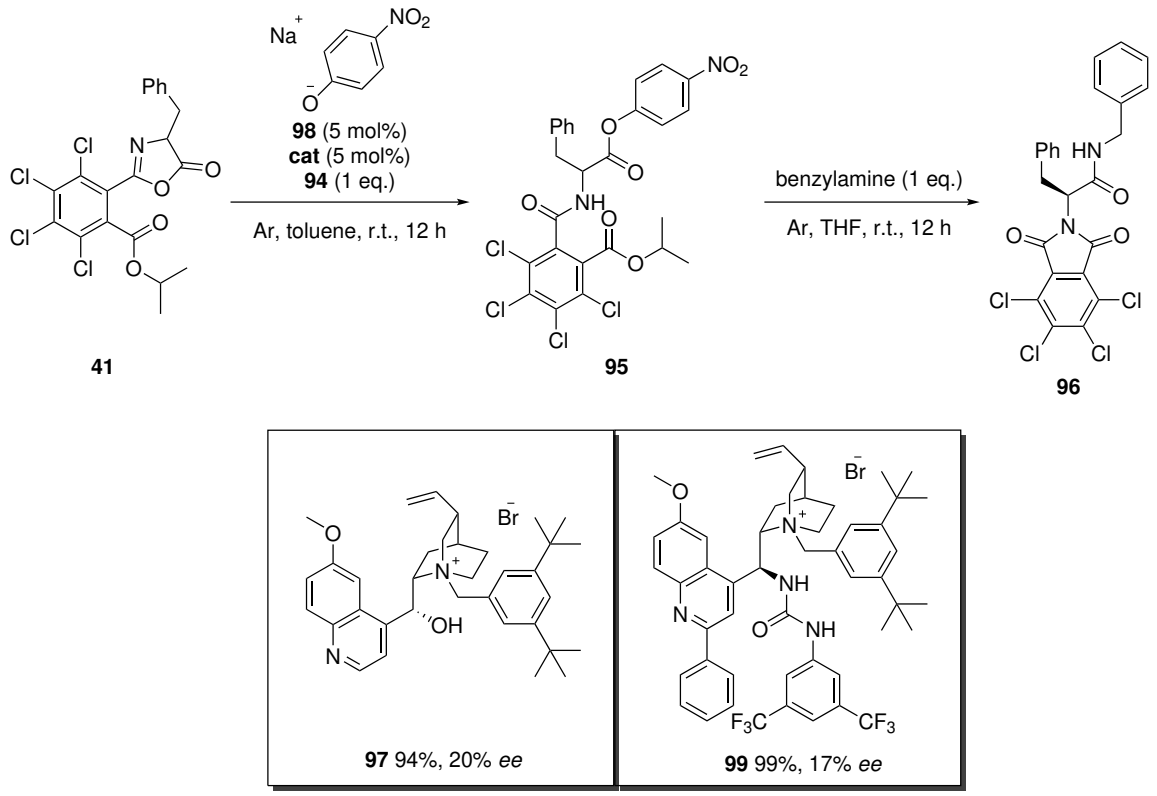

Scheme 1.36: Initial work into the indirect aminolysis of azlactone **41** carried out by Dr. Amy Maguire *via* phase-transfer catalysis

This method produced **96** in low *ee* and high yield. Increasing the hydrogen bonding capabilities of **97** by synthesising *C*-9 urea PTC **99** proved to be equally ineffective in inducing stereocontrol. Additionally, Dr. Maguire found that it was difficult to achieve reproducibility when using **97** and **99**. While enantiocontrol is short of what is required for synthetic utility, this process presents a proof of concept that enantioselective formation of a phenolate ester intermediate under phase-transfer conditions followed by an *in situ* amination, could serve as an attractive solution to an inherent difficulty associated with the nucleophilicity of amines in the presence of azlactones. Improvement and optimisation of this process are discussed in Chapter 2.1.

1.5 Ecological and health implications of plastic waste

Plastics have shaped the modern world since their inception in the early 20th century. In 2021, 390.7 million metric tonnes (Mt) of plastic were produced worldwide; more than 90% of this total was derived from fossil-based feedstock.[101] The primary industry that used plastic in 2021 was the packaging industry with 44% of the market share, with the remaining amount finding applications (*inter alia*) in the construction and automotive industries. Between 1950 and 2018, an estimated 6300 Mt of plastic was disposed of; only 14% of this quantity was recycled, another 14% was incinerated, and the remaining 72% were either put in landfills or polluted the environment.[102] The resilience and versatility of plastics that use petroleum as a feedstock[103] means that contamination in natural environments is long-lasting compared to their relatively ephemeral uses. For example, the half-life of a single-use plastic bottle made from poly(ethylene terephthalate) (PET) under accelerated biodegradation conditions (*i.e.* UV light and heat) is 2.3 years.[104] Additionally, the ingestion[105] and environmental dispersion[106] of plastic particles between 0.1 µm and 5 mm in size (microplastics) is a growing ecological concern.[107] The environmental impact of plastic waste accumulation in aquatic environments is undeniable;[108] a high level of plastic accumulation in waterways has been associated with the transport of disease in coral reefs[109] and fish.[110] Additionally, approximately 45% of marine mammals either have ingested or have been entrapped by plastic waste.[107,111] The dispersion of microplastics in soil has been reported,[106]; however, the ecological impact associated with this is not as readily understood when compared to the impact associated with aquatic environments.[112] Microplastic accumulation in rats is associated with reduced fertility[113] and has other potential health implications.[114] Microplastics have been introduced in humans through biomagnification[115] (*i.e.* the concentration of a substance in an organism higher up the food chain through their diet), among other things; however, the impact associated with microplastic bioaccumulation in humans remains uncertain.[116] A method to reduce the overall impact of plastic debris in the environment is through recycling.[103]

1.5.1 The uses and life cycle of poly(ethylene terephthalate)

PET is a thermoplastic polymer that is derived from terephthalic acid (TPA) and ethylene glycol (EG).[117] Around 35.2 Mt of PET was produced worldwide in 2021, the majority of which was found in single-use plastic bottles.[118] The high-tensile strength and chemical resistance of PET make it ideal for use in food packaging and also in textiles.[4] TPA **100** is derived from *p*-xylene, and EG **101** is derived from ethylene; both of these starting materials are found in a fraction of crude oil, a hydrocarbon mixture known as naphtha. The esterification of **100** and **101** is a contemporary method to form bis(2-hydroxyethyl) terephthalate (BHET, **102**); historically **100** was first converted to dimethyl terephthalate **103** to remove impurities, before being processed into **102**, but modern processes have removed this necessity. The polycondensation of **102** under reduced pressure and heat is the industrial method of synthesising PET **104**; a catalyst can be added to increase the efficiency of this reaction (Scheme 1.37).[119]

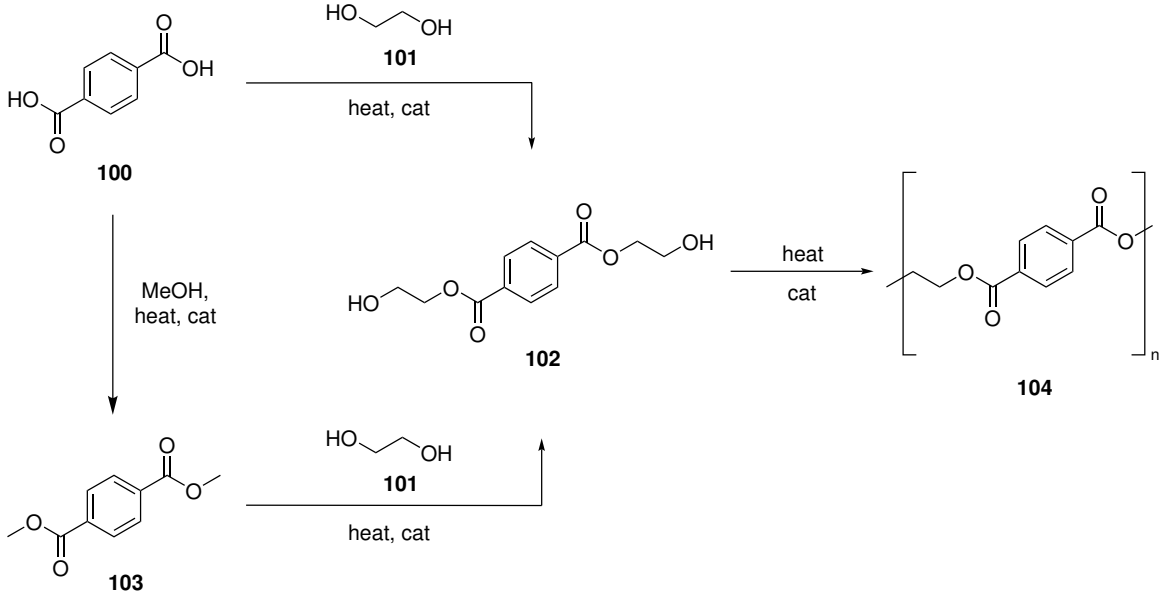

Scheme 1.37: The synthesis of PET in industry

There are dire ecological implications associated with the extraction[120] and refinement of crude oil[121] towards the manufacture of PET, such as greenhouse gas emissions and the disposal of contaminated waste products, among other things.[122] The environmental impact associated with the synthesis of new virgin PET from petroleum-based feedstocks can be mitigated through recycling. A general lifecycle of PET is presented in Figure 1.6 with statistics on the waste collected from Europe.[123]

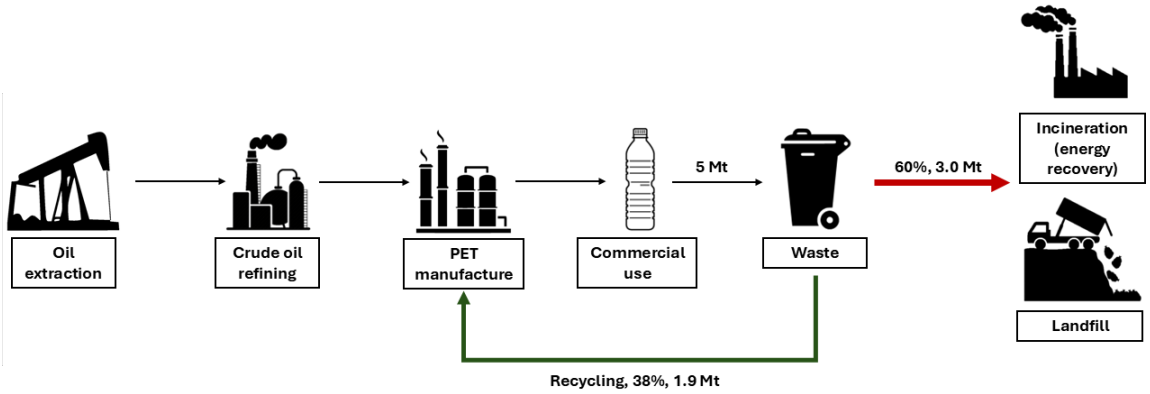

Figure 1.6: The general lifecycle of PET[123]

In Europe, in 2022, a total of 5 Mt of PET packaging was disposed of; from this, 2.7 Mt was processed into flakes, and only 1.9 Mt of flakes were processed back into PET-based packaging.[123] The waste not recycled was sent either to landfills,[124] incinerated for energy recovery[125] or exported out of Europe. Disposal of waste in landfills[126] and incineration[127] have significantly larger health and ecological burdens associated with them relative to recycling. Currently, PET single-use plastic bottles in Europe consist of 25% recycled PET,[123]; however, a recent decision by the European Commission demands that by 2030 all plastic bottles must consist of 30% recycled material.[128] From the PET that was recycled in 2022, the majority of it was mechanically recycled,[129], where the PET is melted and extruded for reuse. This process degrades the mechanical properties (*i.e.* tensile strength *etc.*) associated with PET after each extrusion,[130], resulting in an overall less valuable product relative to its feedstock (downcycling).[130] A solution to retain the value of PET is chemolytic recycling;[118] here the PET polymer is depolymerised through a chemical reaction so it can be repurposed either back into virgin quality PET[131] or into other high-value products (upcycling).[132] An alternative to chemolytic recycling is biocatalytic recycling, which is the use of an organism to depolymerise PET. The ester bonds in PET can undergo transesterification to other products, making PET an ideal candidate for large-scale chemical or biocatalytic recycling.

1.5.1.1 The chemical properties of PET

The glass-transition temperature (T_g) of a polymer is the temperature at which either an amorphous polymer or the amorphous region in a semi-crystalline polymer, transitions from being a hard, brittle material to a malleable solid; cooling the PET below the T_g restores its durable

properties.[133] PET used in consumer products is generally a semi-crystalline solid, meaning it is composed of both amorphous regions (*i.e.* disordered polymer chains) and crystalline regions (*i.e.* parallel and closely packed polymer chains).[134] Crystalline PET is generally brittle and harder than amorphous PET. The T_g ranges between 67 °C and 81 °C; the more crystalline the PET the higher T_g,.[135,136] The degree of crystallinity (X_C) associated with PET can be controlled by heating above the T_g and then either stretching the polymer or cooling the polymer at a controlled temperature. There are other intrinsic factors that can affect the X_C in PET, such as the polydispersity and the moisture content of the polymer.[137] The X_C of PET-based material can influence it's properties and it's use, for example the body of single-use PET bottles are highly crystalline (25.9-33.8%) while amorphous PET films can have an associated X_C below 5%.[138]

1.5.1.2 Biocatalytic recycling of PET

Biocatalysis of PET is the degradation of **104** using either enzymes or organisms that secrete enzymes to form various products. The products that can be produced through biodegradation are TPA **100**, BHET **102**, and mono(2-hydroxyethyl) terephthalate (MHET, **105**) (Scheme 1.38).[139]

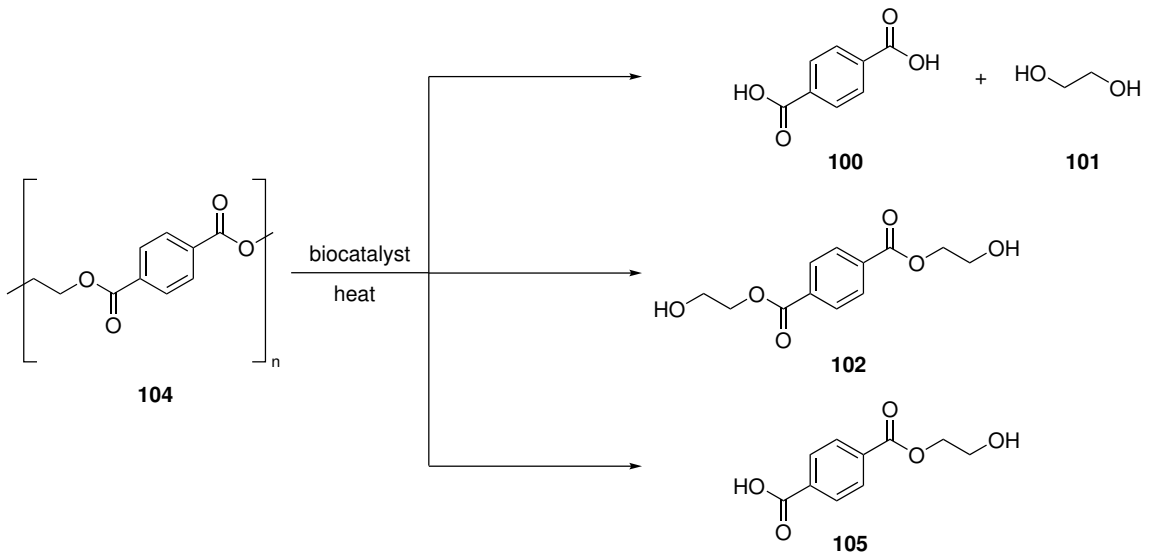

Scheme 1.38: General examples of the biocatalytic recycling of PET

A distinct advantage associated with biocatalysis is the relatively mild temperatures (25 - 90 °C) needed to facilitate catalysis; however, these processes can take multiple days to complete.[139] In some cases, a mix of products can be obtained, for example, Sonnendecker *et al.* isolated both **100** and **105** when using enzymes derived from *Thermobifida cellulosilytica DSM44535*.[140]

There are many examples of PETases that can depolymerise amorphous PET or PET with a low X_C (<5%); however, crystalline PET remains a challenge.[141]

A study conducted by Meyer *et al.* found that when the catalysis occurs below the T_g of PET, the effectiveness of enzymes such as LCC_{ICCG}, DuraPETase, and PHL7/PES-H1 is heavily dependent on the X_C; the enzymes are efficient at converting surface level amorphous PET, but struggle to consume the crystalline regions. Additionally, activity is negligible when the X_C is above 20%.[137] This same study found that, increasing the reaction temperature above 70 °C when using highly crystaline PET can decrease enzyme activity, because as the amorphous PET on the surface surpasses the T_g, it can begin to crystallise, therefore inhibiting PET biodegredation. To remedy this, pre-processing can be done before catalysis, for example, reducing the particle size using a ball-mill increased enzymatic activity,[142] as did processing the PET into a slurry.[143]

While biocatalysis of PET can operate at relatively mild temperatures, the non-negligible limitations (*vide supra*) restrict its applicability on an industrial scale. Chemolytic recycling is a potential alternative which can isolate singular products; however, higher temperatures are required.

1.5.1.3 Chemolytic recycling of PET

Chemolytic recycling generally operates at temperatures far above the T_g, and therefore is less dependent on the X_C of the PET. Processes to depolymerise PET by chemical means are defined by the nucleophile used *i.e.* aminolysis,[144], hydrolysis,[145], glycolysis[146] and methanolysis (Scheme 1.39).[147]

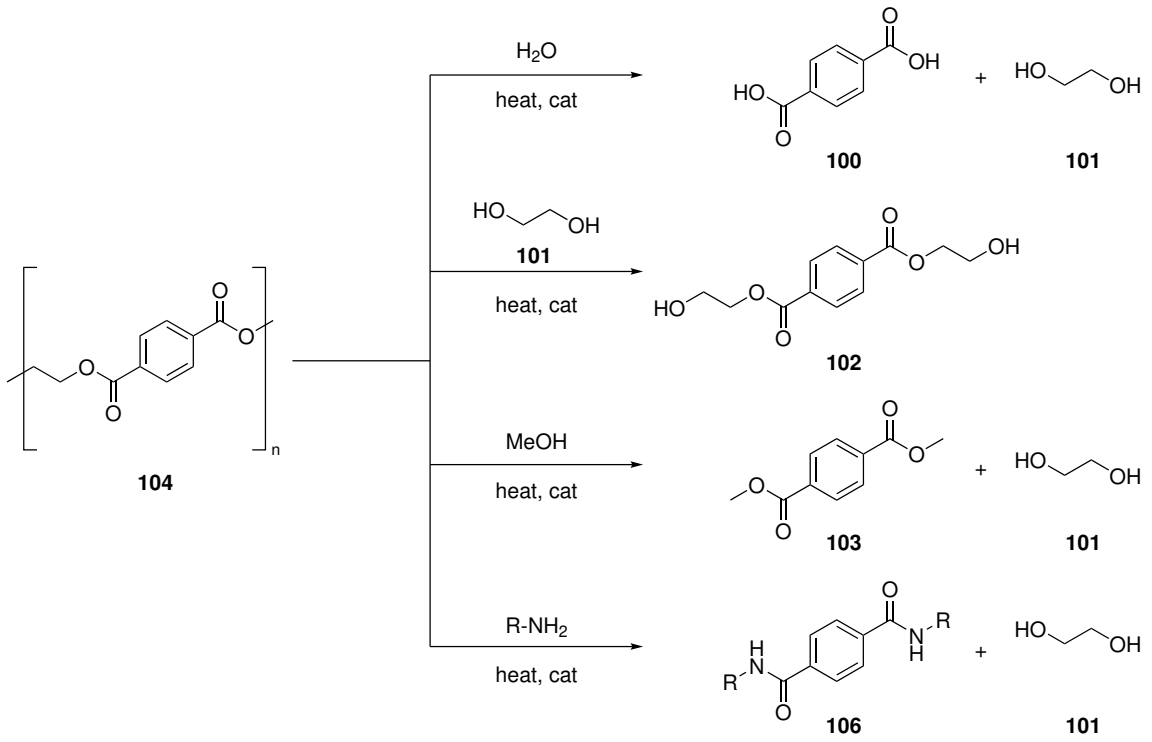

Scheme 1.39: General examples of the chemical recycling of PET

The products associated with hydrolysis **100**, glycolysis **102**, and methanolysis **103** can be reappropriated into virgin-like PET, among other things. The aminolysis of PET is the only process that generally repurposes the product terephthalamides **106** into something other than virgin-like PET, such as either epoxy resins[132] or other novel polyamide materials.[148,149] Despite chemolytic recycling of PET providing a product that is at least of equal value,[144] only 12,000 metric tonnes of PET was chemically recycled in 2022.[123] The chemical recycling of PET currently has a significantly higher associated cost compared to mechanical recycling,[144], and technologies on the market are currently in a pilot stage.[118] In 2022, the largest contributor to chemolytic PET recycling in Europe was glycolysis at 90%; however, by 2027, the European recycling landscape is expected to comprise 73% hydrolysis and methanolysis plants.[123] Reducing the cost associated with industrial-scale PET hydrolysis is therefore imperative to incentivise a circular PET economy and to ensure increased PET recycling capacity goals are met; this can be done by designing novel catalysts and optimising methods. Hydrolysis of PET is defined by the relative acidity/basicity associated with the aqueous medium used to form TPA **100**, *i.e.* neutral hydrolysis, acid hydrolysis and alkaline hydrolysis.[150]

1.5.1.4 Acidic hydrolysis of PET

The hydrolysis of PET in acidic environments has been the subject of numerous works since the mid-20th century.[151,152] A study comparing various acids and acidic catalysts in the depolymerisation of PET was performed by Pester *et al.*[153] There was a clear correlation between activity and medium acidity when using mineral acids and organic acids; the lower the pH of the aqueous solution, the higher the isolated yield of **100** from **104**. For example, when using an aqueous nitric acid solution at pH 0.6, the yield of **100** was 77% (Scheme 1.40); increasing the pH of the solution limited the formation of **100** (20 - 60% yield) under the same conditions. There are safety concerns when using mineral acids for the hydrolysis of PET because of the corrosive waste produced, coupled with the high heat (200 °C) needed to catalyse the reaction.[150]

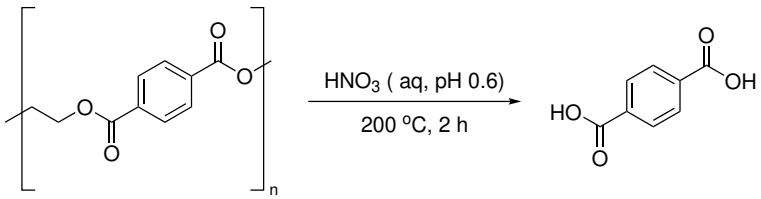

104 **100**, 77%

Scheme 1.40: Acid hydrolysis of PET using nitric acid

A shrinking core model is a representation of a solid particle being dissolved or consumed in a chemical reaction and therefore shrinking.[154] It is derived from kinetic experiments and is dependent on a few assumptions, such as that the particle is non-porous and that the particle is perfectly spherical. A modified shrinking core model can be used to represent the acidic hydrolysis when using different acids as catalytic media. From kinetic experiments performed by Okuwaki and coworkers in 1998 on the consumption of PET powder, it was found that in nitric acid, the initial consumption of PET was rapid, but the rate of consumption lessened over time.[155] The modified shrinking core model is seen in Figure 1.7A; due to the TPA deposition on the surface of the PET as it is being consumed, the particle size stays the same, and the PET becomes increasingly difficult to access.

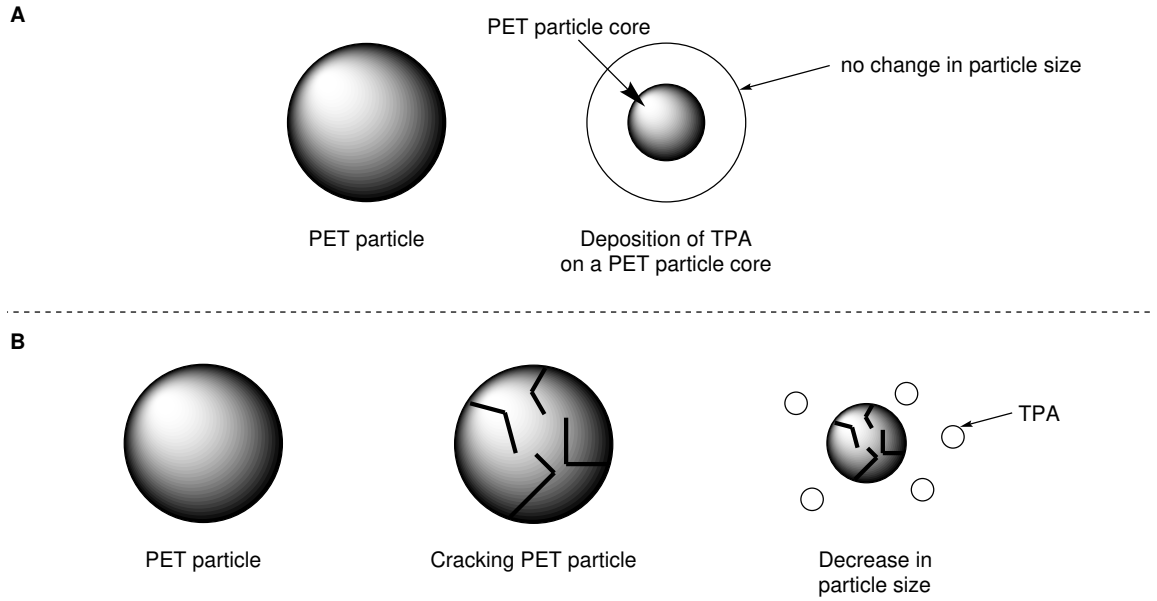

Figure 1.7: **A**: A depiction of the shrinking core model when using nitric acid to catalyse the depolymerisation of PET, **B**: A depiction of the shrinking particle size model when using sulfuric acid to catalyse the depolymerisation of PET

When using sulfuric acid as the catalytic medium, under the same conditions, the rate of reaction was initially far slower; however, the rate of formation of **100** rapidly increased as the reaction time increased. A modified shrinking core model is seen in Figure 1.7B; the unreacted PET would crack, increasing the effective surface area of the acid, and this would even rapidly decrease the particle size and produce TPA. This was reinforced using scanning electron microscopy (SEM), which clearly showed the formation of cracks on the surface of the partially reacted PET.[156]

1.5.1.5 Alkaline hydrolysis of PET

The hydrolysis of PET in sodium hydroxide solutions (4-20 *wt*%) to yield disodium terephthalate **107** has been studied for over two decades.[157] The post-reaction solution containing **107** can then be acidified to precipitate **100**; filtration of this supernatant allows for clean isolation of **100**.[158] In 2001 Karranyanidis *et al*. performed a study comparing various reaction conditions, such as NaOH concentrations, catalyst loadings and temperature when using trioctylmethylammonium bromide **108** as a PTC in the alkaline hydrolysis of **104** to form **107** (Scheme 1.41).[159]

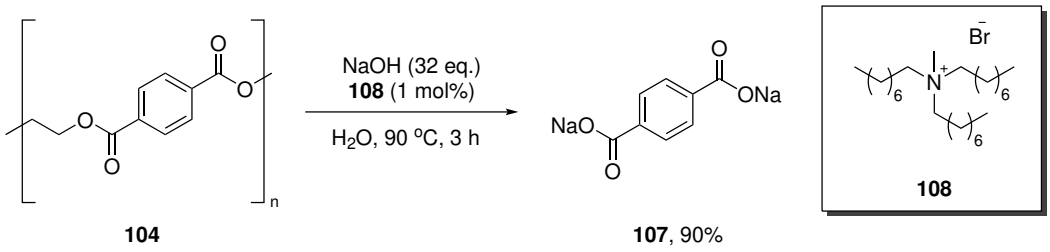

Scheme 1.41: Alkaline hydrolysis using catalyst **108**

This work found that the temperatures required for efficient catalysis using **109** were substantially lower than those needed for the same activity in the acid-catalysed hydrolysis of PET. Additionally, this study also found that reducing PET particle size correlated with faster catalysis. The core limitation of this study is the excessive amount of sodium hydroxide used (32 - 96 equivalents relative to **104**), which makes this process less industrially viable. A separate study in 2007 by Das *et al*. compared different alkyl ammonium salts in the depolymerisation of PET;[160] finding that increasing the lipophilicity of the quaternary ammonium cation enhanced the efficiency of the PTC; *i.e*. catalysts **110**, **111**, **112** were inferior to the lipophilic and benzylated catalyst **113** (Scheme 1.42).

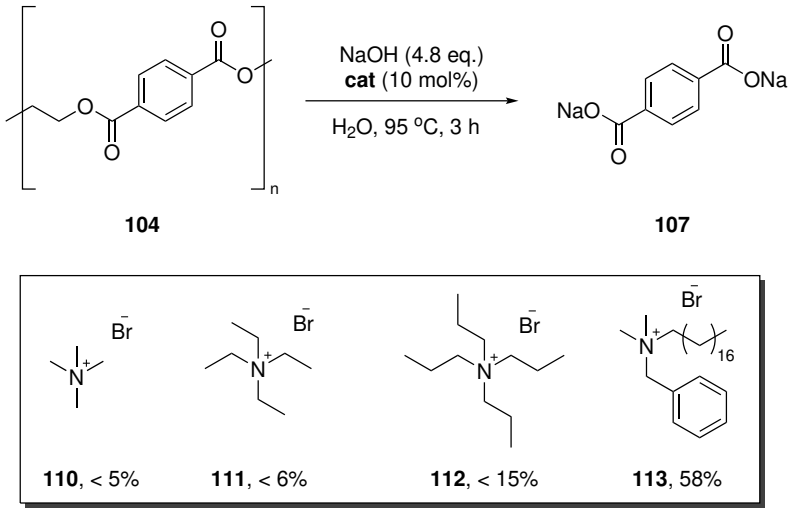

Scheme 1.42: Screening of various PTCs in the alkaline hydrolysis of PET by Das *et al*.[160]

Notably, this study used significantly less base, however, its scope was limited to commercial PET powder. There are other examples of PTC catalysed alkaline hydrolysis,[157,159] however, elucidating a relationship between activity and catalyst structure between studies is difficult due to the inconsistent conditions used such as; different sources of PET; different particle sizes of PET; different sodium hydroxide/water concentrations; varied temperatures; varied stirring speeds; being microwave-assisted[161] and being ultrasound-assisted.[162]

A modified shrinking core model was derived from experiments performed when using tributylhexadecylphosphonium bromide as a catalyst in the depolymerisation of PET powder.[163] The PET is consumed at a faster rate when there is an increased number of reactive hydroxide ions in the PET/water interface (Figure 1.8); this can be done by either increasing the amount of base in the reaction or increasing the amount of catalyst. This potential could justify why increasing lipophilicity is beneficial (*vide supra*) because the PTC will have a higher affinity to the lipophilic PET and therefore be more likely to shuttle hydroxide ions to the interface.

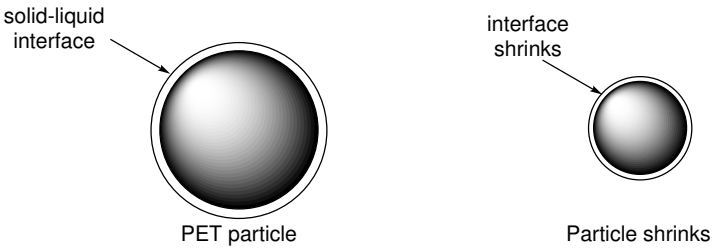

Figure 1.8: A depiction of an alkaline PET hydrolysis shrinking core model

1.5.1.6 Neutral hydrolysis of PET

The hydrolysis of PET to form TPA in aqueous media at a neutral pH is an attractive alternative compared to either acid or base-mediated hydrolysis, since process waste from the process may be less corrosive. The product **100** is insoluble in the reaction medium, meaning unlike alkaline hydrolysis post-processing, precipitating TPA from solution is not required. This reaction can be uncatalysed[164] requiring 200 °C and long reactions (24 h) to isolate **100** in high yields (77 - 97% yield, Scheme 1.43); this example was performed using post-consumer PET waste with a particle size of 5 mm x 5 mm.

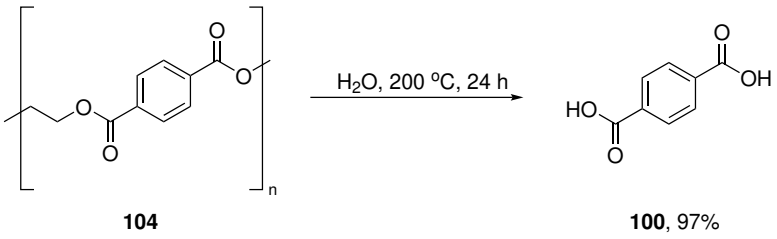

104 **100**, 97%

Scheme 1.43: Uncatalysed neutral hydrolysis of PET

Studies into the neutral hydrolysis of PET above the melting point of PET bottles (depending on the source, this can range between 247-251 °C) have shown that this can lead to the rapid

and high-yielding synthesis of **100**.[165] For example, Pester *et al*. conducted the hydrolysis of 3 mm x 5 mm post-consumer PET bottle flakes at 500 °C; only a one minute reaction time was required to achieve a >75% yield of **100** (Scheme 1.44).[165] Increasing the reaction time beyond one min reduced the yield of **100** considerably; in only 2 minutes yield of **100** was negligible (>5%) due to the rapid degradation of TPA to gaseous byproducts at high temperature.

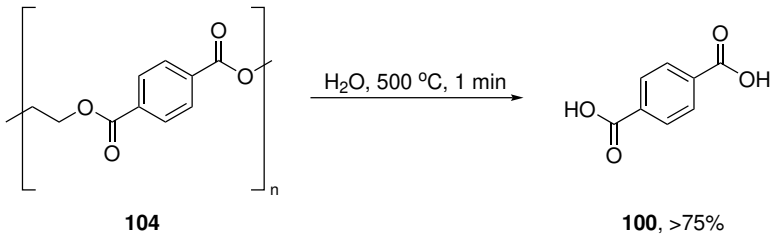

104 **100**, >75%

Scheme 1.44: Hydrolysis of molten PET

Marine water from both the Atlantic Ocean and the Black Sea has also been shown to catalyse the hydrolysis of PET at 205 °C and 195 °C respectively.[166] The percentage of dissolved salts in the Atlantic Ocean water (3.5%) is double that of the Black Sea water (1.6%), therefore, a direct comparison can indicate if the level of salinity affects catalysis. It was shown that the rate of depolymerisation is independent of salinity at approximately 200 °C for 2 hours, with the Atlantic Ocean water converting 87% of the PET, while the Black Sea water catalysed conversion of 86% of the PET (Scheme 1.45).

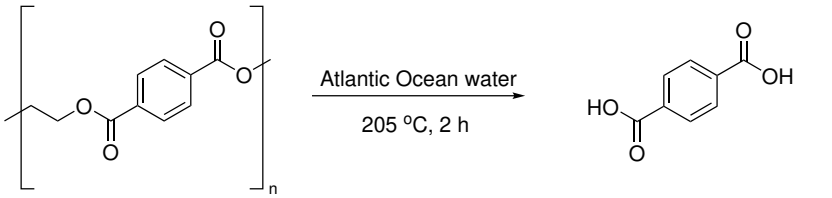

104 **100**, PET conversion 87.5%

Scheme 1.45: Hydrolysis of PET in Atlantic Ocean water

This showed that while the depolymerisation of **104** to **100** is possible using heated seawater, the **100** produced has a non-negligible amount of oligomers (*i.e*. short chain lengths of polymeric PET) present. The number of catalysts assessed in the neutral hydrolysis of PET is relatively limited.[150] Various phosphotungstinic acid-derived catalysts were assessed in the hydrolysis of **104** to **100** by Yi *et al*.[145] The most active PTC, **114**, catalysed the high-yielding conversion of **104** to **100** at 145 °C in 2 h (Scheme 1.46). A core limitation associated with this work was the need for a relatively small PET particle size (0.25 - 0.5 mm^2) to allow for efficient

catalysis. Increasing the particle size to something more comparable to flakes usually produced by industrial shredders (8-15 mm) reduced TPA yield to <60%.

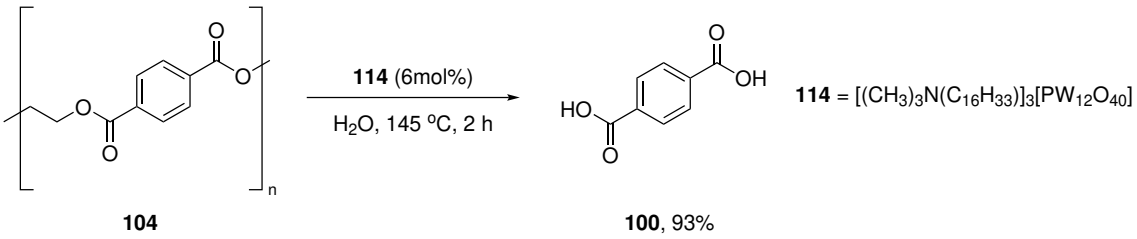

Scheme 1.46: Neutral hydrolysis of PET by Yi *et al*.

The product of the depolymersation of PET, **100**, can autocatalyse the reaction in a neutral aqueous medium, however, when using it as a catalyst, stoichiometric amounts of **100** were needed to obtain high yields of **100** in 3 h (Scheme 1.47).[151]

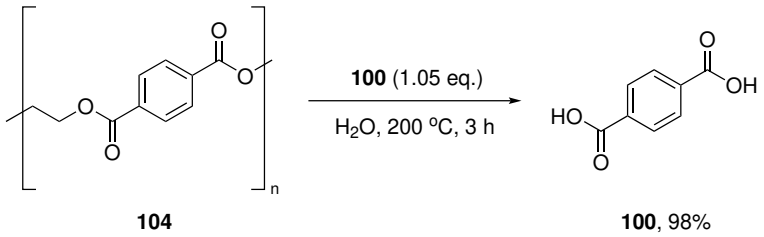

Scheme 1.47: Neutral hydrolysis of PET facilitated by **100**

Metal salts,[167] such as zinc acetate,[168] are well-established catalysts in the glycolysis of PET; zinc acetate (**115**) specifically was previously used in the hydrolysis PET at >250 °C.[169] Recently, Pester *et al*. conducted a screening of various metal salts in the neutral hydrolysis of PET;[170] these reactions were performed at 200 °C on 6 x 8 mm PET bottle flakes (Scheme 1.48). It is worth noting that many of the salts screened affected the pH of the resulting medium; for example, zinc acetate increased the pH to 9 when 10 mol% was used.

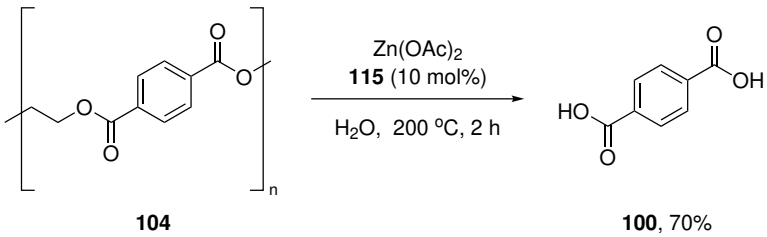

Scheme 1.48: Neutral hydrolysis of PET using zinc acetate as a catalyst

Use of **115** yielded **100** in 70% yield, and it could be recycled up to 6 times with a minimal change in **100** yield.

An ionic liquid (IL) is an ionic compound that is a liquid below 100 °C; ILs have found use as solvents but also have been used as catalysts.[171] In 2009 Liu *et al.* obtained **100** using IL **116** as a catalyst in tandem with IL **117** as both a co-catalyst and a solvent at 170 °C in 4.5 h, using commercial PET powder (Scheme 1.49).[172] Removal of **117** reduced catalyst efficiency and TPA was isolated in 73.6% yield. The effects of particle size in this system were significant; the use of commercial PET pellets (2 mm x 3 mm) led only to 10% isolated yield of **100**.

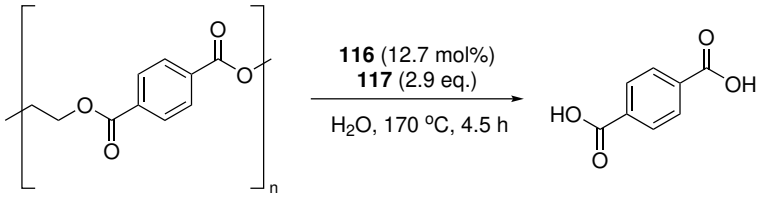

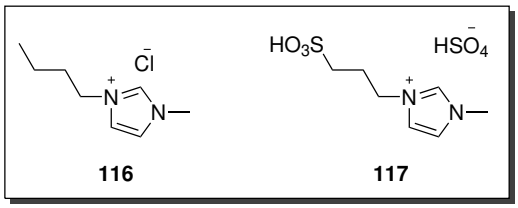

Scheme 1.49: Neutral hydrolysis of PET using ionic liquid catalysts **116** and **117**

Zeolites are crystalline aluminosilicate structures that can have complex porous architecture, comprised of channels which can contain *ad hoc* functionality to catalyse reactions, such as acidic or basic sites.[173–175] A series of ZSM-5-based zeolites, containing acidic functionality, were applied to the microwave-assisted hydrolysis of PET granules.[176] Cha *et al.* achieved high yields of **100** in 40 min at 240 °C (Scheme 1.50) using the acidified zeolite H^+@ZSM-5-25. The catalyst could be recycled up to 6 times with little change in yield.

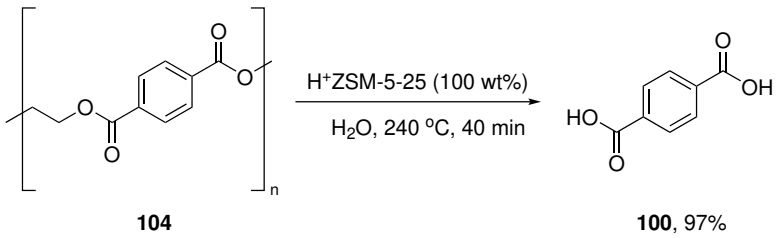

Scheme 1.50: Neutral hydrolysis of PET using H^+@ZSM-5-25

A low molecular weight polymer of poly(ethylene glycol) (PEG-400) is a viscous liquid with a variety of pharmaceutical applications, however, it has found use as a PTC.[177] In 2023, Nayaran

et al. used PEG-400 as a PTC in the neutral hydrolysis of post-consumer PET flakes (0.8 - 5mm) at 240 °C for 30 min (Scheme 1.51).[178] This study also included comparing the effects of time, stirring speed and temperature on the reaction; it was found that increasing each factor had a positive impact on the yield of **100**.

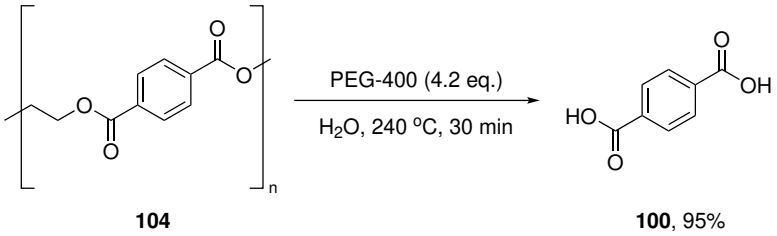

Scheme 1.51: Neutral hydrolysis of PET facilitated by PEG-400

A modified shrinking core model for the uncatalysed neutral hydrolysis of PET was derived from experiments performed by Mishra *et al.* in 2008.[179] In this model, the PET particle fragments and cracks into oligomers before being depolymerised into TPA (Figure 1.9). They postulated that the increase in rate when the particle size is smaller is due to the increased prevalence of cracks, increasing the overall active surface area. Additionally, it was postulated that the acidic PET end chains can catalyse the reaction.[180]

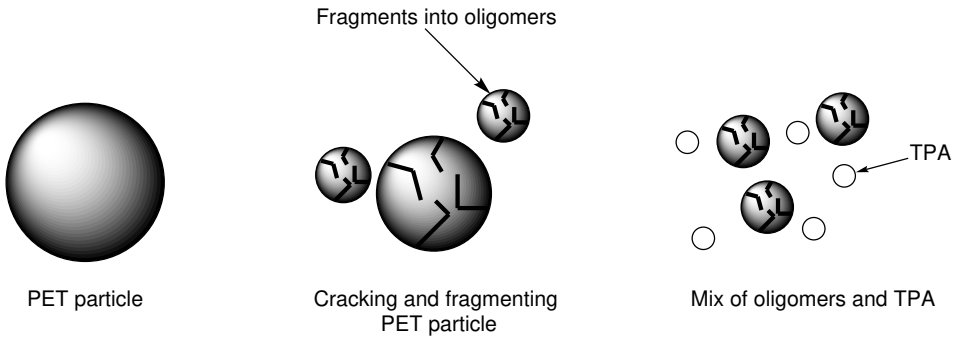

Figure 1.9: A depiction of an uncatalysed neutral PET hydrolysis shrinking core model

As mentioned in Section 1.5.1.5, the examination of literature to find the optimal catalyst for use in the alkaline hydrolysis of PET is difficult due to the varying conditions between studies. Additionally, a limited number of phase-transfer catalysts have been used in the neutral hydrolysis of PET (*vide supra*); therefore, screening various ammonium and phosphonium catalysts in both alkaline and neutral hydrolysis could be beneficial in developing a structure-activity relationship.

1.5.1.7 Investigating phase-transfer catalysts and ionic-liquids as a strategy towards the neutral hydrolysis of PET

The relative dearth of catalysts used in the neutral hydrolysis of PET, coupled with the inconsistent conditions between studies, makes it difficult to discern factors that affect catalyst efficiency. The synthesis and screening of various alkyl ammonium and phosphonium PTCs would be beneficial to distinguish not only a structure-activity relationship but also a potential mechanism of action.

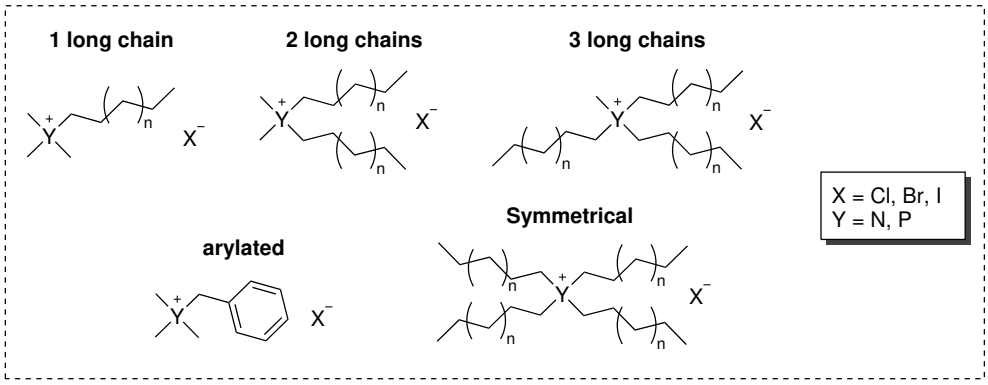

Figure 1.10: General examples of alkyl ammonium cations that will be examined in the neutral hydrolysis of PET

This will include comparing various quaternary ammonium and phosphonium PTCs that are either symmetrical (*i.e*. all four carbon chain lengths covalently bonded to the cation are identical), asymmetrical with varying chain lengths (*i.e*. the four carbon chains lengths covalently bonded to the cation are not identical), or arylated species (Figure 1.10).

The effect of the counterion should be investigated as it could provide mechanistic insight into the PTC-mediated neutral hydrolysis of PET. Alkyl ammonium PTCs could potentially facilitate catalysis in the hydrolysis of PET in two separate mechanisms; either by nucleophilic phase-transfer catalysis or *via* general base catalysis. In the nucleophilic phase-transfer catalysis mechanism, the PTC undergoes ion metathesis with hydroxide; enabling hydrolysis of PET at the interfacial region; however, this is incredibly unlikely given the ionisation constant of water (K_W) at 200 °C is 1 x 10^{-11}. (Scheme 1.52A). An alternative mechanism is general base catalysis; water is deprotonated at the interface by the catalyst's counterion, and the resulting hydroxide ion attacks the PET (Scheme 1.52B). In the general base mechanistic model, as the

concentration of the TPA rises, catalyst deactivation through protonation of the anion by **100** could be problematic if the counterion is moderately basic (*i.e.* pK_{aH} > 3.5); if the resulting salt is ultimately a solid, it could contaminate the desired TPA. To make the study comprehensive and as compatible with industrial applications as possible, consumer PET was used with similar dimensions to those outputted by industrial shredders.

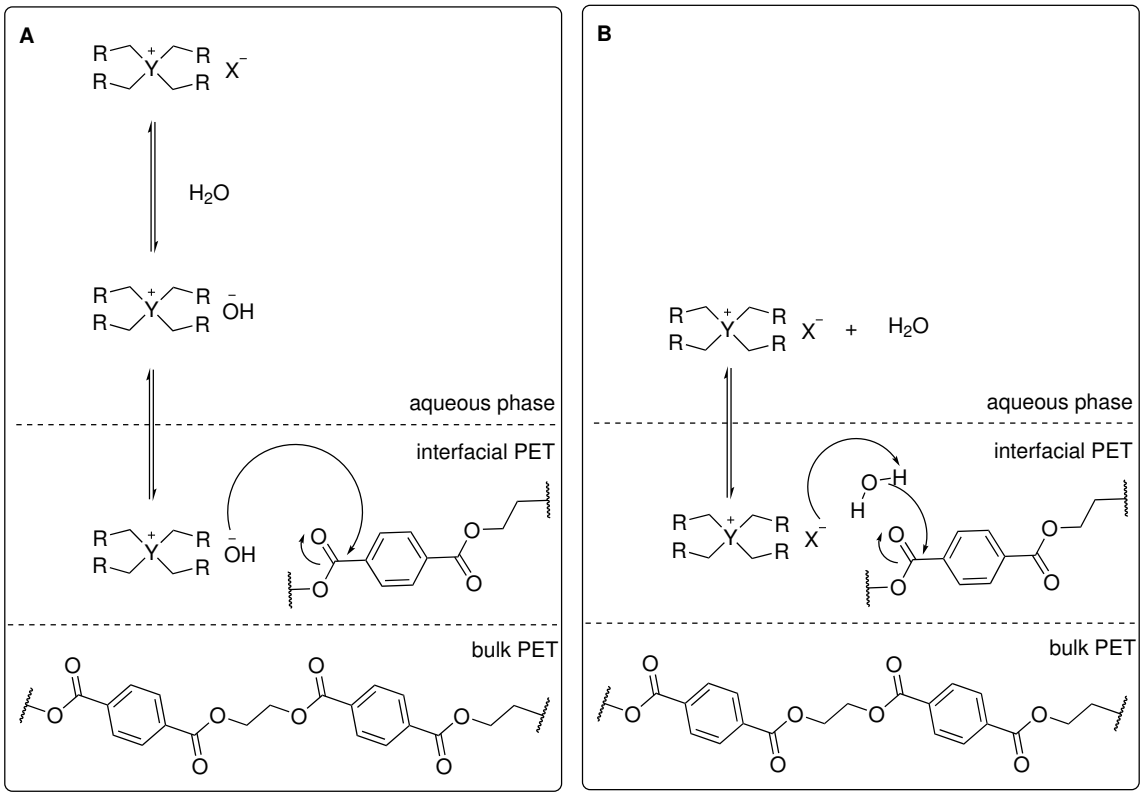

Scheme 1.52: **A**: A proposed nucleophilic catalysis mechanism for the neutral hydrolysis of PET, **B**: A proposed general base catalysis mechanism for the neutral hydrolysis of PET

A recent study by Holbey *et al.* demonstrated the effectiveness of imidazolium terephthalate ionic liquid catalysts in the production of **102** from **104** in ethylene glycol.[181] Catalyst **118** was highly active at the depolymerisation of PET powder at extremely low catalyst loadings (0.25 mol%) (Scheme 1.53). Anionic terephthalate-based catalysts have yet to be used in the neutral hydrolysis of PET, however, this could be a potential solution to the issue of catalyst deactivation (*vide supra*) outlined in the postulated base catalysis mechanism.

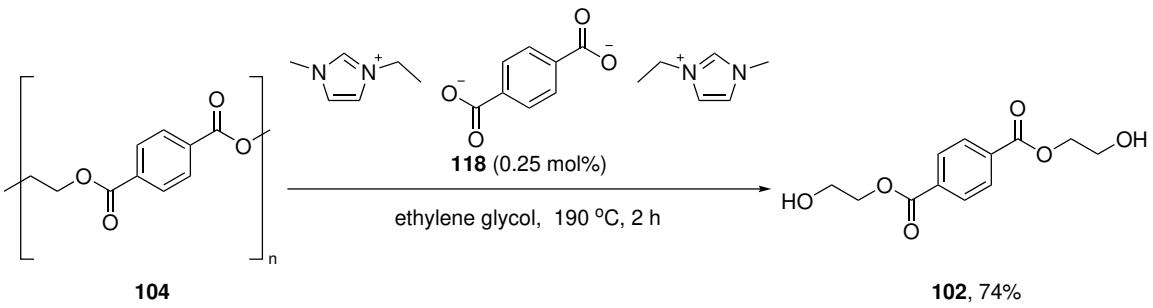

Scheme 1.53: Glycolysis of PET using imidazolium terephthalate catalyst **118**

1.5.1.8 The synthesis of alkyl-ammonium salts to investigate the alkaline hydrolysis of PET

It has been shown that increasing the lipophilicity of the PTC can be beneficial in increasing the activity, however, some factors were previously unexplored; such as the length of the carbon chains in the cation; the symmetry of the cation (*i.e.* whether the four carbon chain lengths are identical or not); the effect of the anion and catalyst solubility. Therefore, an extensive investigation into various alkyl ammonium salts towards the depolymerisation of PET would be beneficial to determine a catalyst's structure-activity relationship. Pyridinium salts **119** and dimethyl dialkyl ammonium salts **120** had previously not been investigated towards this end and gave useful insight into beneficial catalytic properties (Figure 1.11). This study ultimately had the goal of identifying beneficial catalyst properties and then optimising the process to reduce the sodium hydroxide concentration, to make it as industrially viable as possible.

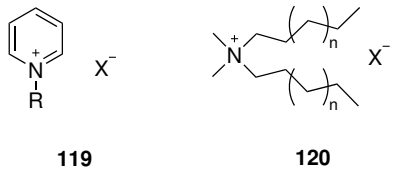

Figure 1.11: Examples of alkyl ammonium salts to be synthesised for the alkaline hydrolysis of PET

Results and Discussion

2 | The DKR of azlactones towards dipeptide formation *via* solid-liquid phase transfer catalysis

2.1 Phenylalanine-derived azlactone synthesis optimisation study

A significant limitation when conducting research into azlactone DKR is the relatively time-consuming and moderately yielding synthesis of **41**.[27] Tetrachlorophthalic anhydride (**121**) underwent an isopropoxide-mediated ring-opening to form **122** (Scheme 2.1). Previous research in our group by Dr. Lee Anderson[182] showed that *N*-(3-dimethylaminopropyl)-*N'*-ethylcarbodiimide hydrochloride (EDC·HCl) could be used as a substitute for *N*,*N'*-dicyclohexylcarbodiimide (DCC) for the amide coupling of hemiester **122** and *tert*-butyl ester **123** to form **124**.

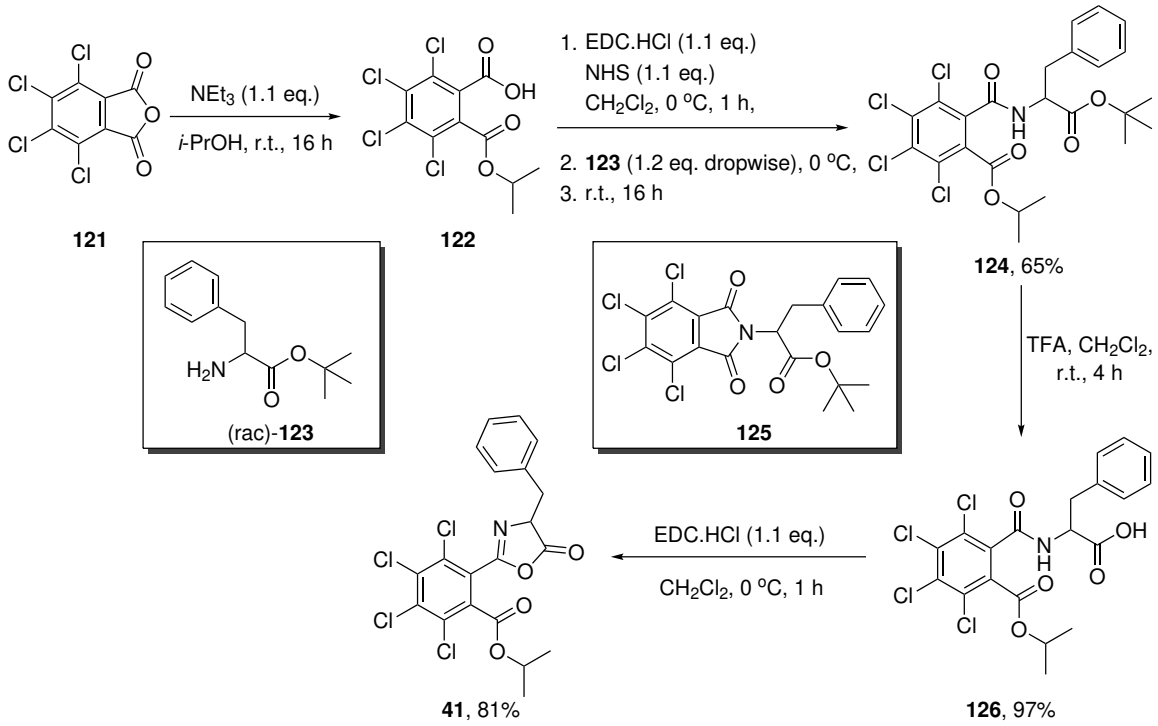

Scheme 2.1: Synthetic route towards azlactone **41**

This previously developed route[182] bypassed the requirement for column chromatography to

remove the urea by-product formed from the hydrolysis of DCC and purify **124**; however, the use of EDC·HCl significantly reduced product yield due to the *in situ* formation of phthalimide **125**. A simple yet effective improvement I developed involved cooling down the reaction mixture to 0 °C before and during the dropwise addition of **123**, yielding **124** in moderate yield. The literature reported protocol to fabricate **41** is through the trifluoroacetic anhydride (TFAA)-mediated cyclisation of **126**; however, TFAA and the byproduct of the reaction, trifluoroacetic acid (TFA), are challenging to remove without **41** decomposing. A solution devised to remedy this was the use of EDC·HCl to synthesise azlactone **41** (Scheme 2.1);[27] making purification significantly more facile.

2.2 Preliminary investigations into the DKR of azlactones using benzyl bromide derived PTCs

As mentioned in Section 1.4, Dr. Maguire evaluated various catalysts towards the indirect aminolysis of azlactones; however, reproducibility when using PTCs was challenging. One possible reason for this is that the aminolysis product **96** has limited solubility in common organic solvents, which can artificially inflate or deflate *ee via* recrystallisation (precipitation). Work performed by Dr. Lee Anderson[182] proved that piperidine-based phthalimide **127** was fully soluble in acetonitrile, a solvent compatible with HPLC analysis, and therefore, gave consistent *ee*. Figure 2.1

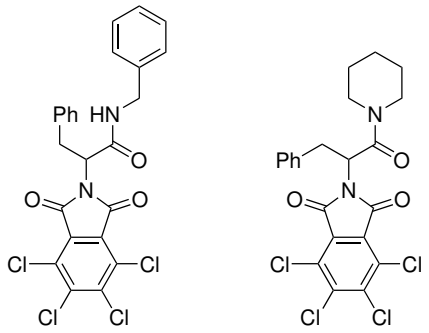

Figure 2.1: DKR products when using piperidine and benzyl amine

Before initiating the investigation into the DKR of azlactones *via* phase-transfer catalysis, a suite of benzylated quinine-based PTCs were synthesised; these catalysts proved to be uncomplicated to prepare, requiring a one-step synthesis from commercially available starting materials. An

example of this synthesis is depicted in Figure 2.2, quinine **85**, the 3,5-dimethoxy benzyl bromide **128** are heated to form **129** in moderate yield.

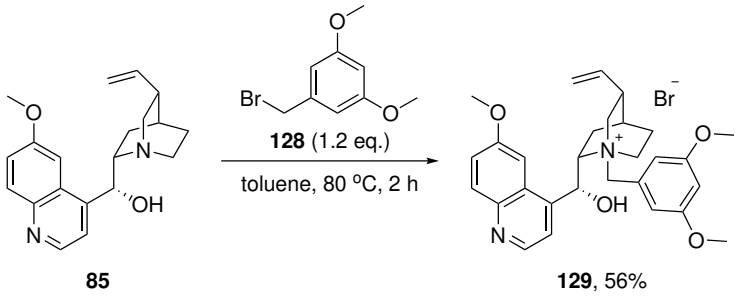

Figure 2.2: Synthesis of benzyl bromide-derived PTC **129**

To compare the activity of catalysts in the DKR of **41**, samples of the reaction mixture were taken for ^{1}H NMR spectroscopic analysis; this was used to quantify the conversion of **41** to **95**. Once **41** was fully consumed, aminolysis and *in situ* ring-closure by piperidine afforded amide **127**. It is important that in these reactions the nucleophilic anion **98** is insoluble in the reaction medium, this is to ensure that the reaction with **41** can only occur when the anion is chaperoned into the organic liquid phase by the chiral catalyst. If the reaction is in a solvent where **98** is soluble, rapid uncatalysed racemic addition occurs. The results of these experiments using benzyl bromide-derived PTCs are outlined in Table 2.1.

A control experiment was first performed, which proved that **98** does not react with **41** without a catalyst present in toluene (Table 2.1, entry 1). The simplest benzyl bromide salt **130** catalysed the slowest reaction of all the screened PTCs, and its use afforded no stereocontrol (entry 2). *Ortho*-substituted analogues **131** and **132** promoted the formation of the opposite enantiomer to that observed by Dr. Maguire in low *ee* (entries 3 and 4). Use of the *bis-meta*-substituted aryl analogue **129** yielded racemic **127** (entry 5). In contrast, **97** and **133** induced the highest *ee* of the assay and were the only catalysts soluble under the reaction conditions (entries 6 and 7). Although the screening of these catalysts only provided **127** with low enantioenrichment, two trends could be discerned from this study. Firstly, the solubility of the catalyst is crucial for preventing racemic formation of **95** (entries 2 and 5). Secondly, *ortho*-substitution provides the opposite enantiomer using this family of catalysts (entries 3 and 4). Structural variation of the *meta*-position, using either sterically large *tert*-butyl groups (entry 6) or electron withdrawing substituents (entry 7), did provide a marginal increase in enantioselectivity; however, it was

clear that a more extended set of modifications was required to achieve synthetic utility.

Table 2.1: Evaluation of benzyl bromide-derived catalysts in the enantioselective indirect aminolysis of **41**

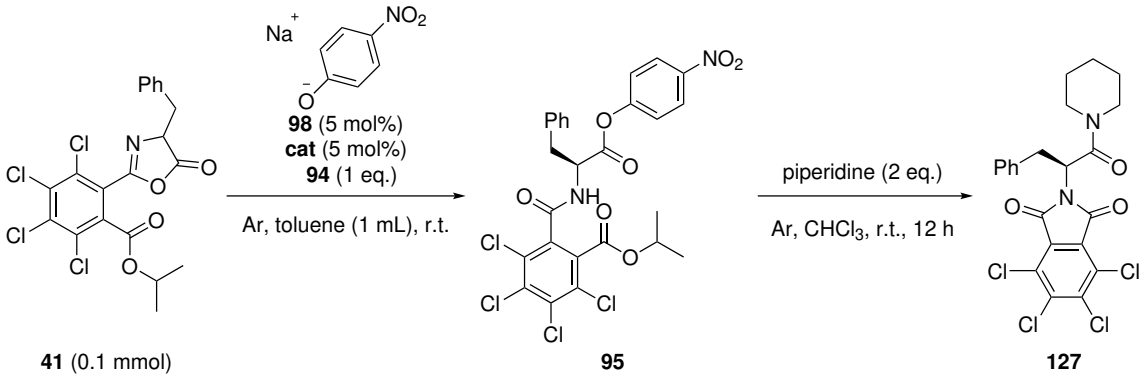

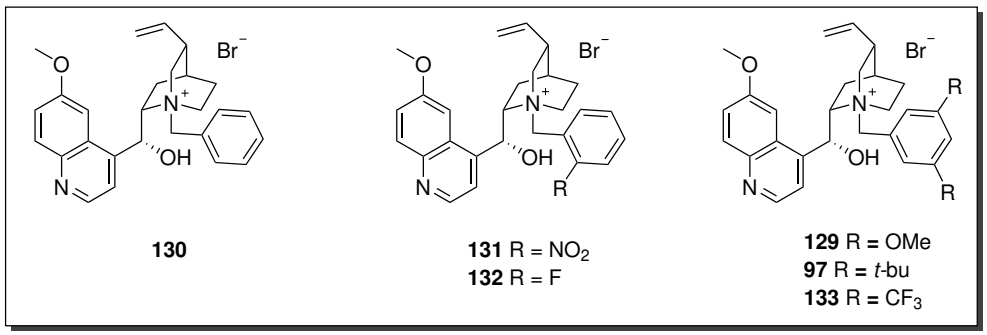

entry	catalyst	time[a] (h)	yield of 127 (%)	*ee*[b] of 127 (%)
1	-	-	0	0
2	**130**[c,d]	336	29	0
3	**131**[d]	16	41	-10
4	**132**[d]	16	40	-8
5	**129**[d]	16	45	0
6	**97**[e,f]	16	55	15
7	**133**[e]	16	54	20

[a]Time to 100% conversion to **95** determined by using ^{1}H NMR spectroscopy [b]Determined by CSP-HPLC. [c]Catalyst synthesised by Dr. Lee Anderson. [d]Catalyst partially soluble. [e] Catalyst synthesised by Dr. Mili Litvajova. [f]Repeat of an experiment initially carried out by Dr. Amy Maguire.

2.2.1 Computational insights into the origin of enantioselectivity when using benzyl bromide-derived catalysts

Through computational analysis, a deeper understanding of the origin of enantioselectivity can be obtained, which I hoped would influence future catalyst design. Computational transition

states were obtained through collaboration with Dr. Cristina Trujillo's research group. These models, and the resulting energies of the transition states, were calculated based on the interaction between the active form of catalyst **97** and azlactone **41**. These pre-transition state assemblies (binding modes), which lead to the transition states, are defined by the direction of approach associated with the phenolate anion, *i.e.* in the "left" binding pre-transition state model (Figure 2.3, as drawn), the phenolate approaches the azlactone from the "left" of the catalyst and underneath the quinoline ring, with which it can participate in π-stacking. While in the "right" binding mode, the phenolate approaches from open space to the right (as drawn); therefore, the benzyl group associated with **41** is oriented towards the quinoline ring (Figure 2.4). In both the "left" and "right" binding modes, it is shown that the phenolate approaches from the opposite direction to the benzyl group in **41**. Figure 2.3 is a diagrammatic representation of the "left" pre-transition state assemblies that result in the (*R*) and (*S*) enantiomers of **41**. The resulting transition states that form the (*R*) and (*S*) enantiomers were predicted to have lower energies than the "right" binding transition states (meaning they are more likely to occur) and the difference between them is minute ($\Delta\Delta G$ = 0.2 kcal/mol). In both "left" binding modes that lead to the (*R*) and (*S*) enantiomers, there is a steric clash between the aryl substituent on the catalyst and the benzyl unit in **41**. The hypothetical *ee* generated from the "left" binding modes was calculated to be 16% of the (*R*) enantiomer.

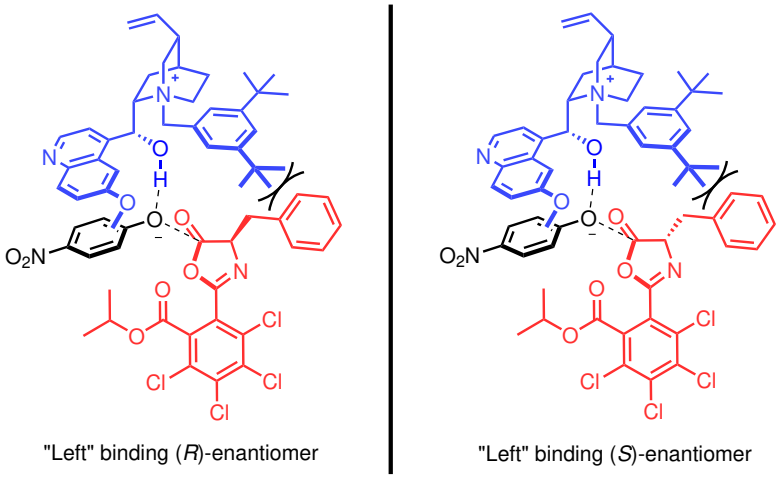

Figure 2.3: A diagrammatic representation of the "left" binding modes associated with the active form of catalyst **97** based on computational analysis

The predicted "right" binding transition states are shown in Figure 2.4. In the "right" binding pre-transition states, the differential in predicted energy between the transition states is greater

($\Delta\Delta G$ = 0.7 kcal/mol) because there is a steric clash between quinoline and the benzyl group in the transition state assembly that results in the (*R*) enantiomer; while, in the binding mode that leads to the (*S*) enantiomer, this steric clash is minimised.

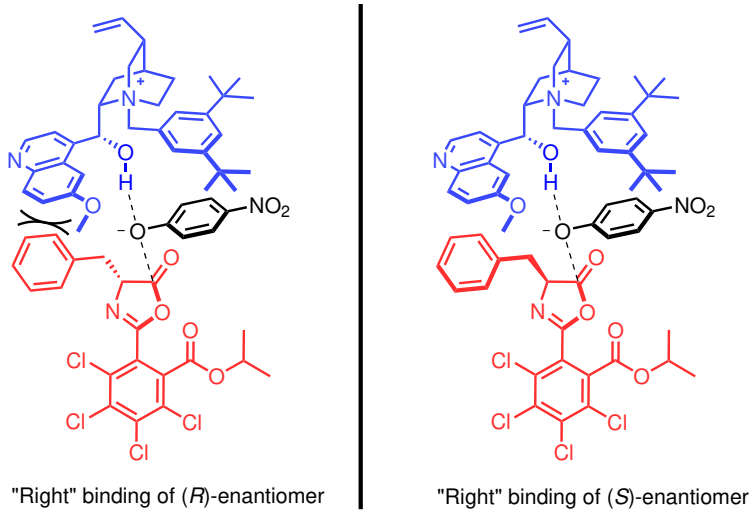

Figure 2.4: A diagrammatic representation of the "right" binding modes associated with the active form of catalyst **97** based on computational analysis

Although computational analysis can be useful in identifying the origin of enantioselectivity, in this case, the models are not representative of the experimental findings in Table 2.1. Computation transition states acquired for **130** predicted 99% of the (*R*) enantiomer would be formed. It is also important to note that Dr. Maguire performed a DKR of **41** and used L-alanine methyl ester to quench the reaction. The resulting imide **134** was deprotected to form **135** in a diastereomeric mixture (Scheme 2.2). By comparing the ^{1}H NMR spectrum of **135** to a literature ^{1}H NMR spectrum of L-phenylalanine L-alanine methyl ester; Dr. Maguire proved that the major enantiomer formed from the DKR of **41** is the (*S*) enantiomer, which was not predicted by the lowest energy calculated transition states.[100]

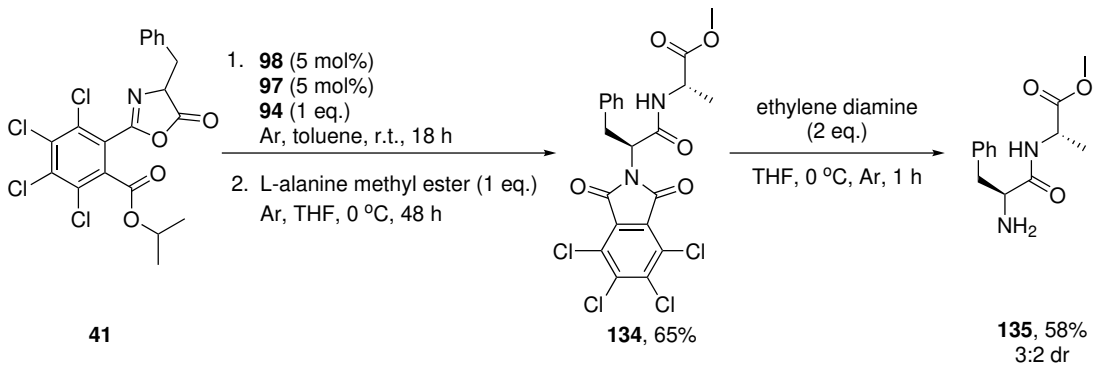

Scheme 2.2: Dipeptide coupling performed by Dr. Amy Maguire

The enantiocontrol observed in Table 2.1 is small compared to what is needed for synthetic utility; possibly due to a negligible amount of interaction between the catalyst and **41** (besides steric clashes). I theorised that if I implemented a second hydrogen-bond donor on the catalyst framework, this could provide an azlactone binding site. As mentioned in Section 1.4 Dr. Maguire[100] installed additional *H*-bond donors through modification of *C*-9 and this proved to be ineffective; therefore a solution could be installing a binding site covalently linked to the quaternary nitrogen in the catalyst as seen in Figure 2.5.

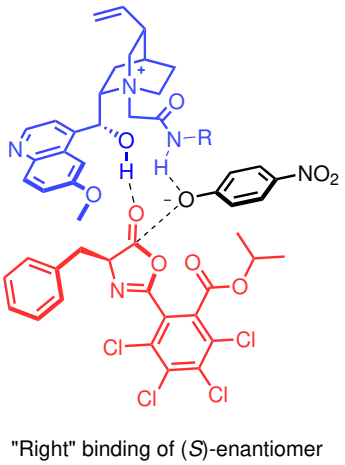

Figure 2.5: A diagrammatic representation of the "right" binding mode associated with a theoretical acetamide-based catalyst

2.3 Synthesis and use of acetamide-derived PTCs in the DKR of azlactone 41

As mentioned in Section 1.3, a contemporary solution to install additional *H*-bonding *motifs* to quinine-based catalysts is through quaternisation of the quinuclidine nitrogen.[86] The alkylating agents are typically made in the high-yielding selective aminolysis of bromoacetyl bromide **136** from commercially available anilines such as **137**; these are purified through a basic workup to yield products such as **138** (Scheme 2.3).

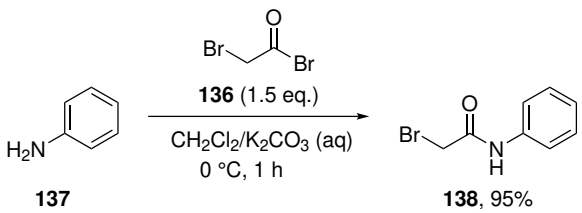

Scheme 2.3: Synthesis of a 2-bromoacetamide alkylating agent

The synthesis of the catalyst is facile, for example, the nucleophilic substitution reaction of quinine **85** with 2-bromoacetamide alkylating agents such as **138** to form **139** (Scheme 2.4).

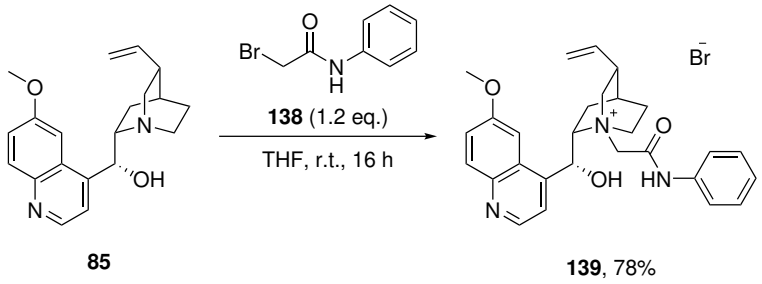

Scheme 2.4: Alkylation of quinine using **138**

A set of acetamide derivatives were synthesised and investigated (Table 2.2). The use of the simplest acetamide-derived promoter, **140**, facilitated formation of **127** in higher degrees of enantiocontrol relative to the PTCs in Table 2.1 (Table 2.2, entry 1). *N*-cyclohexyl substituted species **141** gave a significant increase in yield and generated low *ee* (entry 2). The sterically bulky benzhydryl-derived catalyst **142** was more enantioselective in the formation of **127** (entry 3) when compared to **141**. Interestingly, the simple *N*-phenyl acetamide derivative **139** gave the highest degree of enantiocontrol of any catalyst previously assayed (entry 4). All the acetamide-derived catalysts assessed were significantly more active than the previously examined benzyl bromide-derived catalysts, as seen in Table 2.1. Given this result, it is conceivable that hydrogen-bonding by the amide substituent could have a dominant role in enantiocontrol, and it significantly increases the rate of reaction when compared to the catalysts found in Table 2.1.

Table 2.2: Evaluation of acetamide-derived catalysts in the enantioselective indirect aminolysis of **41**

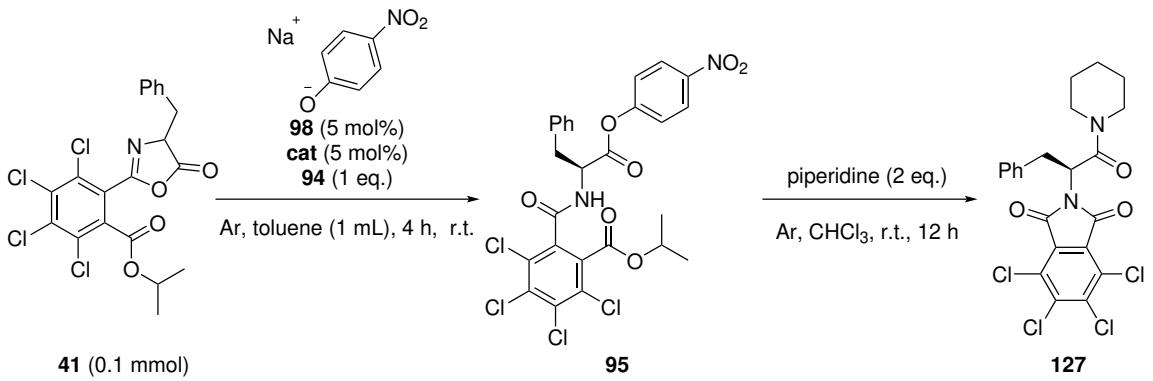

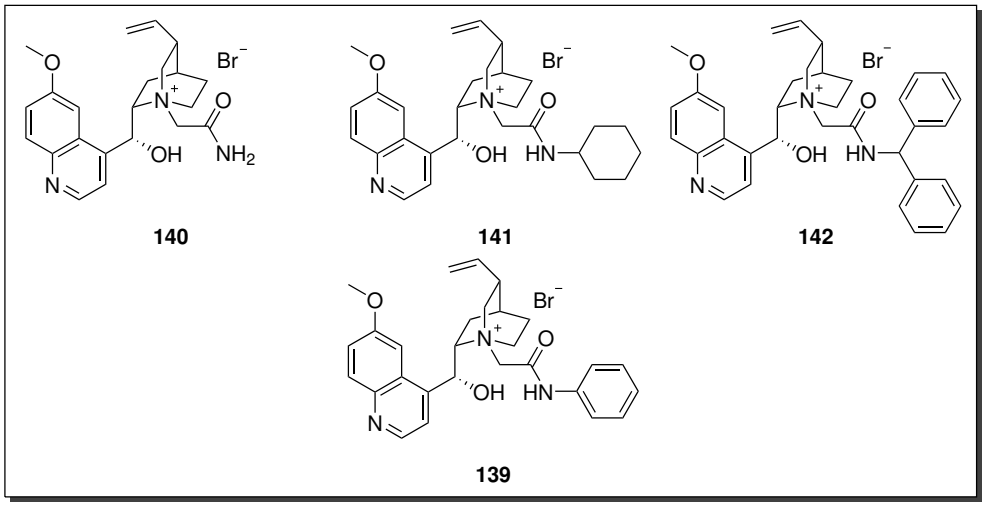

entry	catalyst	yield of 127 (%)	*ee*[a] of 127 (%)
1	**140**	70	25
2	**141**[b]	86	8
3	**142**[b]	63	17
4	**139**	94	38

[a]Determined by CSP-HPLC. [b]Catalyst synthesised by Mr. Hugh Etchingham Coll.

Product enantioselectivtiy increasing in the presence of **139** indicates that the associated amide acidity (relative to the others assayed in Table 2.2) could be a direct cause of enantiocontrol, and for this reason, a series of substituted *N*-phenyl acetamide-derived catalysts were screened to better understand the source of stereocontrol.

Table 2.3: Evaluation of substituted phenyl-acetamide derivatives in the enantioselective indirect aminolysis of **41**

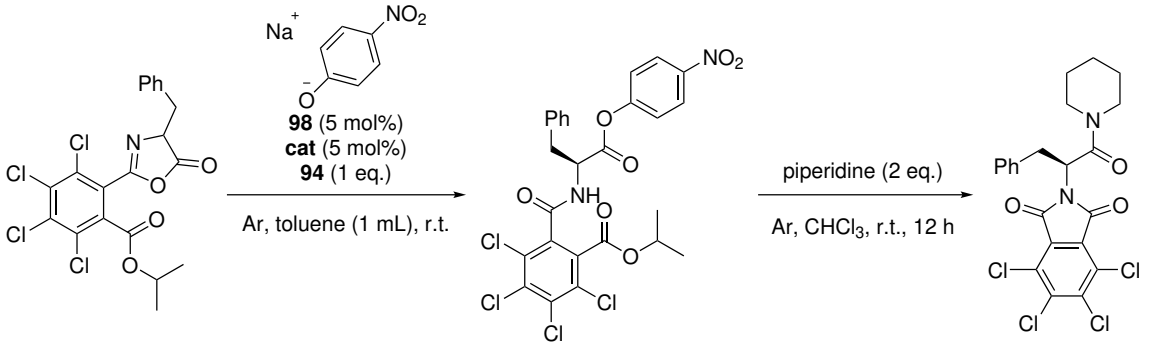

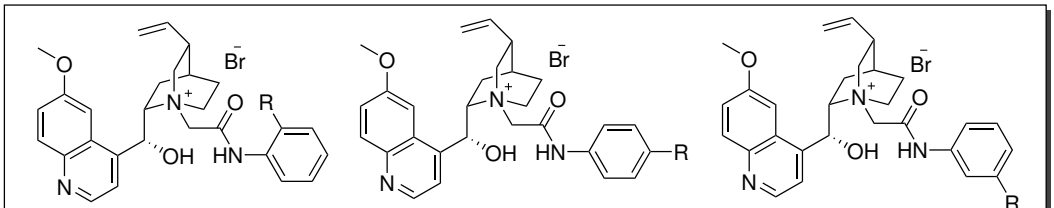

143 R = Me
144 R = Br
145 R = NO_2

146 R = Br
147 R = NO_2

148 R = Me
149 R = Br
150 R = NO_2

entry	catalyst	time[a] (h)	yield of 127 (%)	*ee*[b] of 127 (%)
1	**143**[c]	4	74	14
2	**144**[c]	48	75	14
3	**145**[d]	4	90	52
4	**146**[c]	4	94	47
5	**147**[d]	4	95	54
6	**148**[c]	4	96	32
7	**149**	4	90	64
8	**150**	4	81	58

[a]Time to 100% conversion to **95** determined by using ^{1}H NMR spectroscopy [b]Determined by CSP-HPLC. [c]Catalyst synthesised by Mr. Hugh Etchingham Coll. [d]Catalyst partially soluble

A series of second-generation *N*-phenyl acetamide derivatives were next evaluated (Table 2.3). Catalysts **143** and **144** performed poorly in promoting the stereoselective formation of **127**

(Table 2.3, entries 1 and 2), while use of the *o*-nitro substituted derivative **145** led to improved enantiocontrol (entry 3). *Para*-substitution with electron-withdrawing motifs (*i.e*. **146** and **147**) greatly increased enantiocontrol when compared to **144** (entries 4 and 5), while *meta*-substitution with a methyl group (*i.e*. **148**) afforded slightly decreased product enantioenrichment (entry 6). Catalysts characterised by electron-withdrawing groups at the 3-position of the aromatic amide substituent (*i.e*. **149** and **150**) promoted the most selective formation of **127** while also affording high yields (entries 7 and 8). It seems clear that increasing the acidity of the amide correlates with higher degrees of enantiocontrol, however, it is postulated that other factors might influence the stereoselectivity associated with the catalyst structure. For example, a possible reason for the 2-nitro substituted catalyst **145** being superior when compared to the other *ortho*-substituted catalysts is due to a possible hydrogen bond between the amide and the nitro substituent; this has been reported in other *N*-(2-nitrophenyl)-acetamide structures (Scheme 2.5).[183,184] Additionally, crystal structures found in the literature of *N*-(2-bromophenyl)-acetamide show that the phenyl ring rotates to be "out-of-plane" with the amide to avoid a steric clash between bromine and either the hydrogen or the carbonyl-*moeities*.[185] It is possible that ensuring the phenyl ring is "in-plane" with the amide (Scheme 2.5) could be a factor that facilitates enantioselective catalysis in the DKR of **41**. I predicted that, when using electron-withdrawing *meta*-substituents, there is an internal hydrogen bond between a proton in the *ortho*-position and the carbonyl; this, in tandem with the increased acidity of the amide, could provide better enantiodiscrimination.

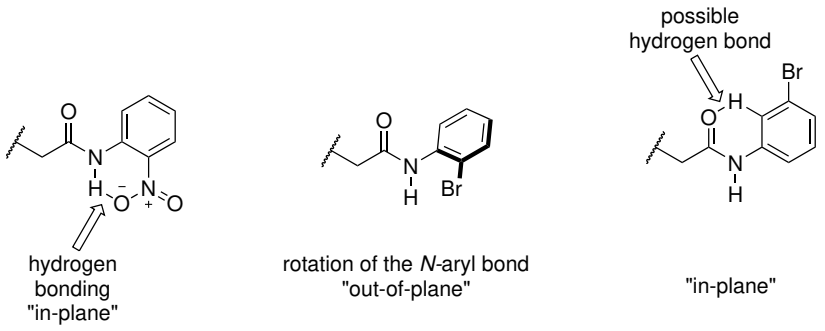

Scheme 2.5: Potential rigidity in acetamide-derived catalysts

Research conducted by Dr. Lee Anderson on the racemisation of **95** measured by deuterium labelling, demonstrated that after the addition of deuterated piperidine, substantial incorporation of deuterium in product **127** was observed (*i.e*. product **95** is racemising when using piperidine

before formation of **127**). To circumvent this, morpholine was found to be a suitable less basic substitute as a nucleophilic amine for forming protected *bis*-amide **151**, and I realised at this stage that the formation of product **127** was sub-optimal. A third generation of acetamide catalysts with increased NH acidity was assayed using this newly developed protocol, and the previous benchmarks were re-examined (Table 2.4).

Table 2.4: Evaluation of third-generation acetamide catalysts and benchmark catalyst re-evaluation in the enantioselective indirect aminolysis of **41**

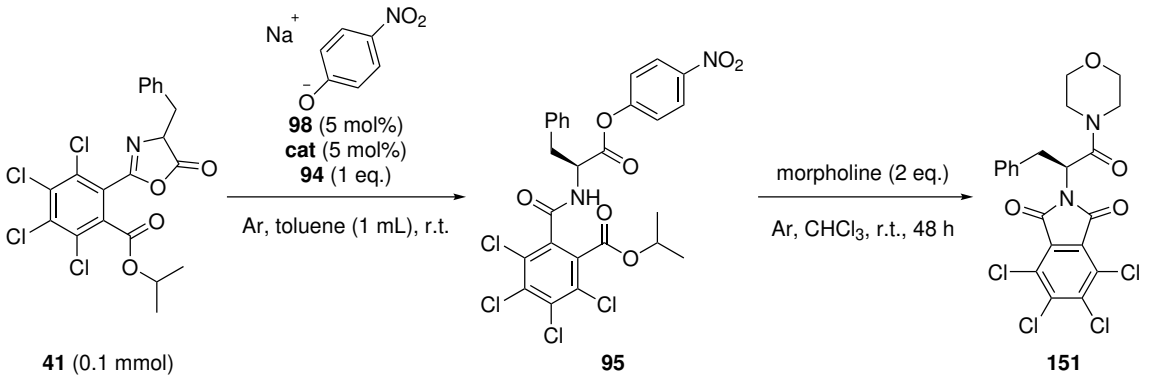

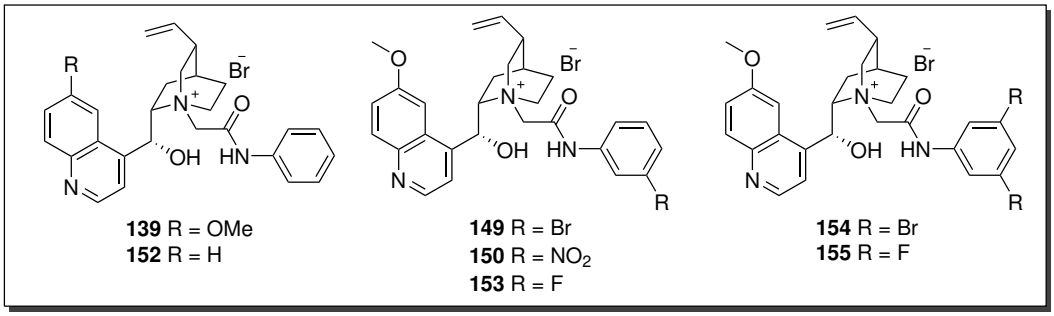

entry	catalyst	time[a] (h)	yield of 151 (%)	*ee*[b] of 151 (%)
1	**139**	4	94	45
2	**152**[c]	2	80	43
3	**149**	4	98	58
4	**150**[d]	4	97	50
5	**153**	4	90	58
6	**154**[d]	4	89	57
7	**155**[d,e]	4	91	57

[a]Time to 100% conversion to **95** determined by using ^{1}H NMR spectroscopy [b]Determined by CSP-HPLC. [c]Catalyst synthesised by Dr. Lee Anderson. [d]Catalyst partially soluble. [e]Catalyst synthesised by Mr. Hugh Etchingham Coll.

Using this new system, catalyst **139** induced a higher degree of stereocontrol in the synthesis of **151** when compared to the selective formation of **127** (Table 2.4, entry 1). Variation of the

alkaloid catalyst scaffold from a quininium to a cinchonidinium-based catalyst **152** led to faster but less selective catalysis (entry 2). The benchmark catalysts of Table 2.3 (*i.e.* **149** and **150**) facilitated the formation of **151** in lower *ee* (entries 3 and 4) relative to when they promoted the enantioselective formation of **127** (Table 2.3, entries 7 and 8). This was unexpected and could indicate that the previously isolated product (*i.e.* **127**) was precipitating in acetonitrile, despite best efforts to ensure it was homogenous. Given that modifications at the *meta*-positions of **149** and **150** are far larger than a hydrogen atom, catalyst **153** was developed to examine if the effects of a sterically simpler electron-withdrawing group would induce a higher degree of stereoselectivity (entry 5). *Bis-meta*-substitution using electron-withdrawing functionalities (*i.e.* **154**, **155**) afforded product **151** in moderate levels of enantiocontrol (entries 6 and 7). It is noteworthy that catalysis by *meta*-halogen analogues (*i.e.* **149** and **153**) and *bis-meta*-halogen substituted (*i.e.* **154**, **155**) PTCs afforded **151** with similar levels of enantiocontrol, meaning that increasing the relative acidity of the amide leads to diminishing returns, when it comes to increasing the stereopurity of **151**. Given these results, conditions were to be optimised in the attempt to develop a synthetically viable method and to achieve highly selective aminolysis. A potential limitation of this system is the rate of racemisation since if k_{rac} is slower than k_{slow}, a reduction in *ee* would be observed (Section 1.2.1). A potential way to increase k_{rac} could be to add *para*-nitrophenol portion-wise to the reaction mixture, promoting formation of the enolate tautomer of azlactone **41** (by increasing the proportionate amount of phenolate ion to phenol in solution), consequently increasing racemisation *in situ*. It would also be possible to maximise the relevance of k_{fast} relative to k_{slow} by reducing the temperature of the reaction. The effects of these two approaches are examined in Table 2.5 using catalyst **152** due to its relatively high activity.

2.3.1 Optimisation study into the effects of temperature and reactant loadings when using an acetamide-derived PTC

Table 2.5: Optimisation study for the formation of **151** using catalyst **152**

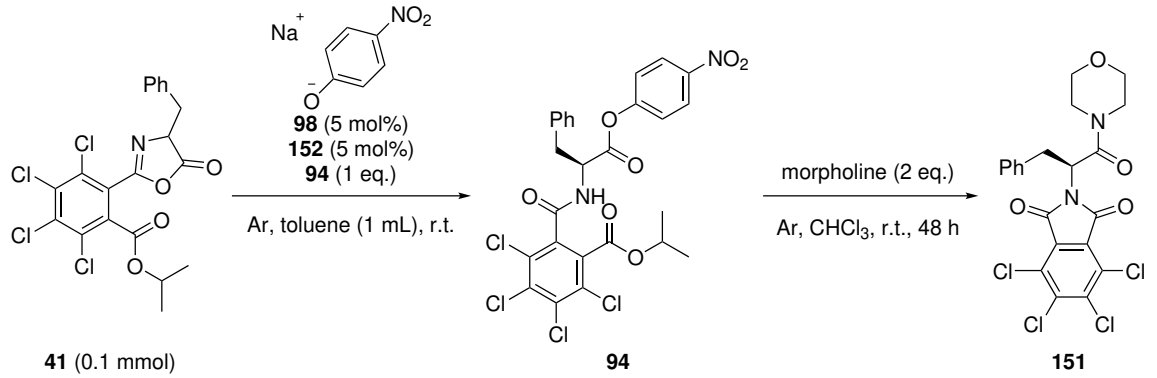

entry	time[a] (h)	temperature (°C)	yield of 151 (%)	*ee*[b] of 151 (%)
1[c]	12	20	79	52
2	24	0	81	53
3	48	-10	72	54
4[c]	24	0	82	53
5[c]	48	-10	75	55
6[d]	1	20	74	45

Catalyst **152** synthesised by Dr. Lee Anderson. [a]Time to 100% conversion to **95** determined by using ^{1}H NMR spectroscopy. [b]Determined by CSP-HPLC. [c]*Para*-nitrophenol added portion-wise at 10 mol% every hour. [d]Loading of catalyst **152** and **98** increased to 15 mol%.

The addition of 4-nitrophenol portion-wise proved to be a worthwhile method for increasing the *ee* of product **151** (Table 2.5, entry 1), which perhaps suggested that the rate of racemisation of **41** was increased. Similarly, a reduction in reaction temperature promoted the formation of **151** in higher degrees of selectivity; however, it significantly impacted reaction times (entries 2 and 3). Unfortunately, these effects were not cumulative, giving only a moderate degree of stereocontrol in the presence of catalyst **152** (entries 4 and 5). Increasing the loading of **152** and **98** was met with faster formation of **95** yet did not affect the *ee* when compared to 5% catalyst loading (entry 6). From this, I can conclude that a marginal increase in stereocontrol is possible by reducing temperature, however, this significantly increases the reaction times. Portion-wise addition of *para*-nitrophenol also generated conditions to form **151** in higher *ee* in the presence of a chiral catalyst; possibly due to an increased rate of racemisation. However, this

catalyst system has two significant limitations. Firstly, our group has previously found that more complex cinchona alkaloid-based chiral catalysts[100,182] are not soluble in toluene and changing the solvent is difficult without racemic addition of **98**. Secondly, it is difficult to ascertain the exact amount of active catalyst in solution (*i.e.* a phenoxide ion-pair). From these summarised studies in Table 2.1 - Table 2.5, it was obvious that a novel solution was required to circumvent these problems.

2.4 Synthesis and use of ion-pair catalysts for the DKR of azlactones

As mentioned in 1.3, the collective works of the groups led by Reetz[94] and Mukaiyama[95] outlined a novel class of catalyst that remedies the issues regarding phase-transfer catalysis; *i.e.* the formation of a nucleophilic ion-pair. Although they did not use this technology for the DKR of azlactones, I believed it could be applied to our reaction. It would remedy multiple limitations thanks to the removal of **98** from the system, allowing for a wide variety of solvents to be used, assuming the ion-pair catalyst is soluble. This is beneficial since **98** adds racemically to **41** in most solvents without the need of a phase-transfer catalyst (excluding toluene), and by removing this restriction with regards to solvent choice, I can guarantee the catalyst will be soluble in the reaction mixture. Furthermore, the nucleophilic anion is bound ionically to the chiral cation, meaning there is a known amount of active catalyst in solution. To elaborate on another potential benefit, each solvent has a different dielectric constant (ε) (*i.e.* a solvent's ability to stabilise charges) which greatly influences the behaviour of ion pairs in solution. The higher the polarity, the greater the ε and the more separated the ions are in solution. This effect can have a significant change associated with how the ionic catalyst interacts with the substrates, which could greatly influence *ee*.[186]

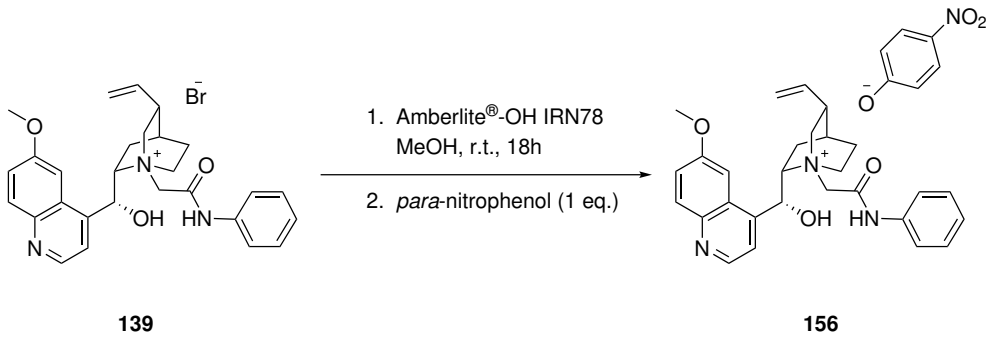

Scheme 2.6: Synthesis of *para*-nitrophenolate ion pair catalyst **156**

I began our investigation using catalyst **139** which can be used to form catalyst **156** using an ion-exchange resin (*i.e.* Amberlite®-OH IRN78) to form the hydroxide salt which, *in situ* can undergo a neutralisation reaction using the appropriate phenol to form a permanent ion pair (Scheme 2.6). The formation of **151** using **156** as the catalyst was investigated using various solvents. The result of this study is outlined in Table 2.6.

Table 2.6: Solvent screening using using ion-pair catalyst **156**

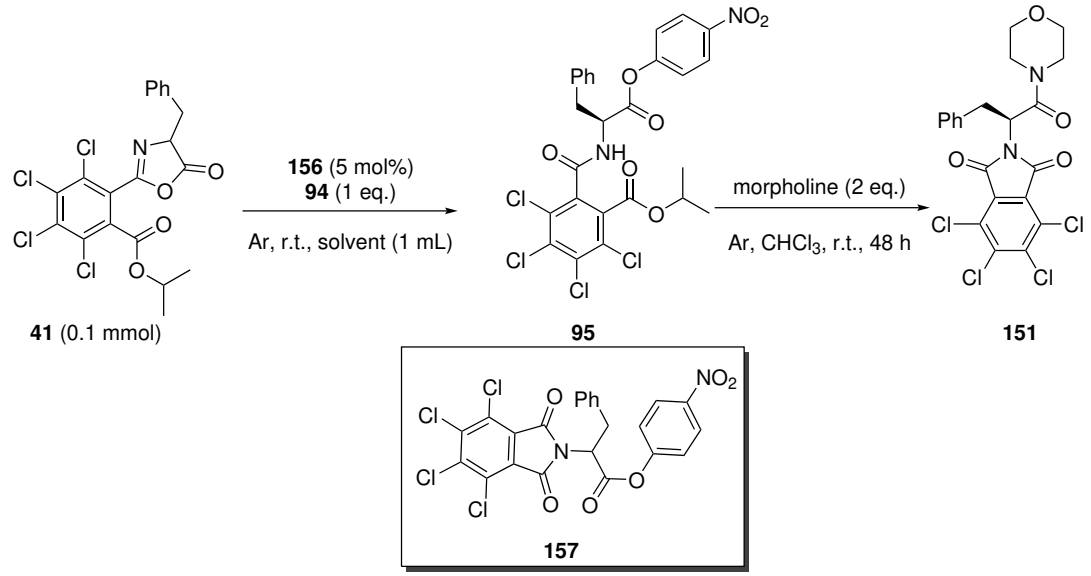

entry	time[a] (min)	solvent	conversion to **157**[b] (%)	yield of **151** (%)	*ee*[c] of **151** (%)
1	10	MeCN	100	92	0
2	10	THF	50	15	14
3	20	toluene	15	27	27
4[d]	10	MTBE	10	89	30
5[d,e]	10	Et_2O	0	93	30 (30)
6[e,f]	10	CH_2Cl_2	0	91 (92)	40 (40)
7[e,f]	10	$CHCl_3$	0	94 (97) [95]	35 (30) [25]
8[g]	10	$CHCl_3$	0	90	35

[a]Time to 100% conversion to **95** determined by using ^{1}H NMR spectroscopy. [b]Conversion to **157** determined by using ^{1}H NMR spectroscopy. [c]Determined by CSP-HPLC. [d]Catalyst partially soluble. [e]Results of duplicate experiment in parentheses. [f]Results of triplicate experiment in square brackets. [g]Solvent treated with an anhydrous potassium carbonate plug before use.

Catalyst **156** in acetonitrile promoted the rapid formation of the ring-closed imide **157**. After the addition of morpholine, **151** was isolated and was found to be racemic (Table 2.6, entry 1). Byproduct **157** was produced in tetrahydrofuran, toluene, and methyl *tert*-butyl ether (MTBE), but not to the same extent as in acetonitrile; regardless, enantiocontrol was still poor (entries

2-4). Interestingly, despite **41** not being fully soluble in diethyl ether, the catalysed formation of **151** was quantitative and with moderate *ee* (entry 5). Dichloromethane and chloroform performed similarly as reaction media, allowing formation of **151** in moderate *ee* and high yield. Repetition of catalytic reactions in chloroform led to successive reductions in the degree of stereocontrol, while the stereoselectivity in dichloromethane using **156** was maintained (entries 6 and 7). A possible reason for the erosion of *ee* is the acidification of $CHCl_3$ when exposed to UV irradiation. To test this theory, the solvent was passed through a flame-dried, anhydrous potassium carbonate plug, which restored enantioselectivity (entry 8). Overall, this solvent screening demonstrated there are two solvents (*i.e.* dichloromethane and diethyl ether) conducive to reproducible results using this class of catalyst. Formation of **157** in selected solvents proved to be detrimental to stereocontrol. For this reason, despite MTBE facilitating the formation of **151** when catalysed by **156**, with the same selectivity as Et_2O, the formation of **157** is an unfortunate and uncontrollable variable and so was ultimately deemed an unsuitable solvent for later experimentation. Similarly, the erosion of *ee* found when the reaction was performed in $CHCl_3$ gives cause for concern for the reproducibility and was eliminated as a candidate solvent.

It is interesting to note that the reactions outlined in Table 2.6 are substantially faster than those associated with the phase-transfer catalysts reported in Table 2.4; this is likely because the ion-pair catalyst system circumvents the need for mass transfer. I examined whether modifications to either the nucleophilic anion or the chiral cation affect the selective formation of **151**. Catalyst **158** incorporates the bulkier and more basic *ortho*-methylated *para*-nitro phenoxide salt, I postulated it should increase k_{rac} and decrease both k_{fast} and k_{slow}; this is to examine if k_{rac} is limiting *ee*. Catalyst **159** is derived from **149** (*i.e.* the catalyst that promoted the most enantioselective formation of **127** and **151** under phase-transfer conditions, outlined in Table 2.3). Evaluation of these catalysts in dichloromethane and diethyl ether is outlined in Table 2.7.

Table 2.7: Examination of second-generation phenoxide salt ion pair catalysts in the asymmetric aminolysis of **41**.

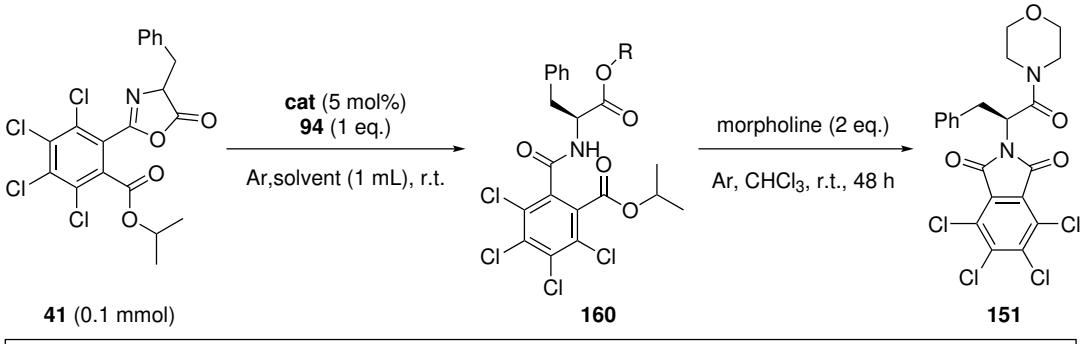

entry	catalyst	time[a] (h)	solvent	yield of 151 (%)	*ee*[c] of 151 (%)
1	-	-	CH_2Cl_2	0	0
2	-	-	Et_2O	0	0
3	**156**[c,d,e]	48	CH_2Cl_2	96	45
4	**156**[f]	10	CH_2Cl_2	90	15
5	**158**[d,g]	-	Et_2O	-	-
6	**159**	0.2	Et_2O	84	50
7	**158**[g]	0.2	CH_2Cl_2	71	35
8	**159**	0.2	CH_2Cl_2	93	51

[a]Time to 100% conversion to the active ester **160** determined by using ^{1}H NMR spectroscopy. [b]Determined by CSP-HPLC. [c]Experiment conducted at −50 °C. [d]Catalyst insoluble. [e]*Para*-nitrophenol partially soluble. [f]*Para*-nitrophenol added portionwise, at a rate of 10 mol% every hour. [g]Reaction performed with 2-methyl *para*-nitrophenol (1 eq.) instead of *para*-nitrophenol.

Control experiments demonstrated that 4-nitrophenol does not participate in nucleophilic attack on **41** without an initiator (Table 2.7, entries 1 and 2). When the reaction was exposed to a decrease in temperature and when the simplest phenoxide derivative **156** was used, a marginal increase in enantioselectivity was recorded (when compared to catalysis at room temperature (Table 2.6, entry 6)) along with a reduction in the formation of **151** (entry 3). I postulated that a method to simplify the reaction by reducing the number of possible hydrogen bonding interactions was to add 4-nitrophenol dropwise; however, formation of **151** after dropwise addition of *para*-nitrophenol significantly decreased enantiocontrol (entry 4). No reaction was observed in diethyl ether when using catalyst **158** since the salt is not soluble (entry 5), while catalyst **159** promoted the selective formation of **151** with a moderate *ee* (entry 6). Disappointingly, **158** induced less stereocontrol in dichloromethane when compared to catalyst **156** (entry 7); this implies that k_{rac} is likely not limiting. When the reaction was catalysed by **159**, the stereoselective formation of **151** was similar to that found in diethyl ether (entry 8). The results of this study proved that modifications to both ions are important for inducing selectivity and have a marginal effect on activity. Increasing the hydrogen-bond donating ability of the amide NH bond proved to be beneficial in the stereoselective formation of **151** catalysed by **159**. Augmentation of the bulk of the phenoxide nucleophile led to a further reduction in product *ee*.

To this point, the catalysts assessed only contained chiral hydrogen bond donor (*i.e.* the *C*-9 alcohol), I next examined if substituting the amide for a chiral hydrogen bond donor could be beneficial.

2.5 Synthesis and use of ion-pair *trans*-1,2-diaminocyclohexane-derived catalysts

As mentioned in Section 1.2.2.3.1, *trans*-1,2-diaminocyclohexane derivatives can be useful bifunctional catalysts in a wide variety of different transformations. I posited that replacing the installed amide close to the quaternary nitrogen with a chiral amide could potentially increase the stereocontrol associated with catalysts by allowing fine tuning of the catalyst's chiral *moieties* (Figure 2.6).

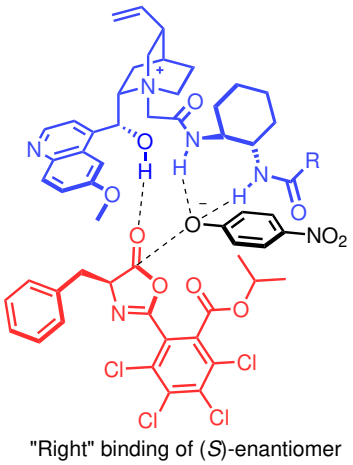

Figure 2.6: A proposed diagrammatic representation of the "right" binding mode associated with the active form of a theoretical *trans*-1,2-diaminocyclohexane diamine-derived catalyst

I aimed to synthesise catalysts derived from both enantiomers of *trans*-1,2-diaminocyclohexane, (1*R*, 2*R*, **161**) and (1*S*, 2*S*, **162**), to see if either of the chiral amides had a more significant effect on *ee*. I also designed catalyst **163** to examine if increasing the acidity of the newly installed amide would affect the associated stereocontrol brought about by the catalyst, as it could either associate with the phenol or the azlactone (Figure 2.7).

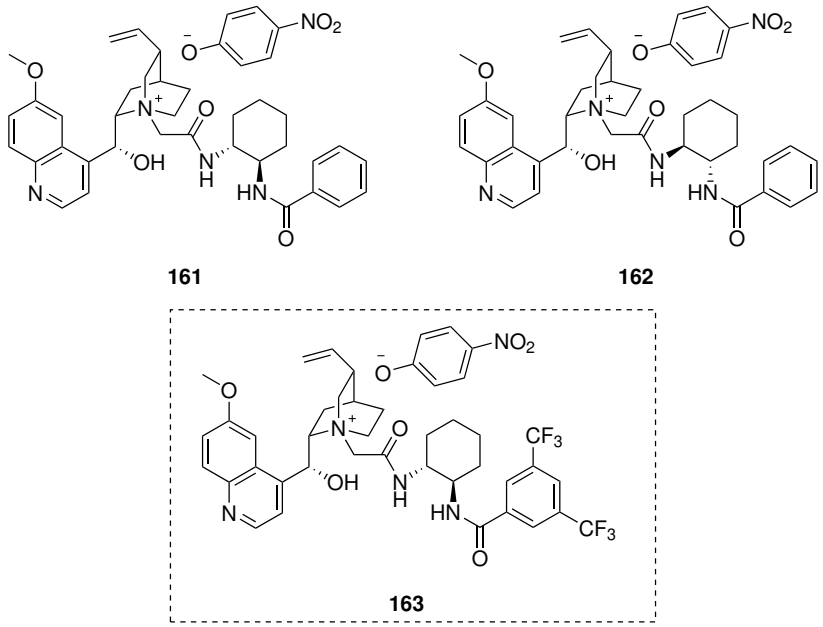

Figure 2.7: *Trans*-1,2-diaminocyclohexane-derived catalysts **161**, **162** and **163**

Both enantiomers of *trans*-1,2-diaminocyclohexane have two nucleophilic nitrogen atoms; regioselective functionalisation of one nitrogen is difficult, however, a protocol does exist to mono-benzoylate **164** using benzoyl chloride **165**.[187] Unfortunately, attempts to replicate this procedure yielded the mono-benzoylated product **166** in low yield, with the majority of the

starting material converting to the *bis*-benzoylated byproduct **167** (Scheme 2.7).

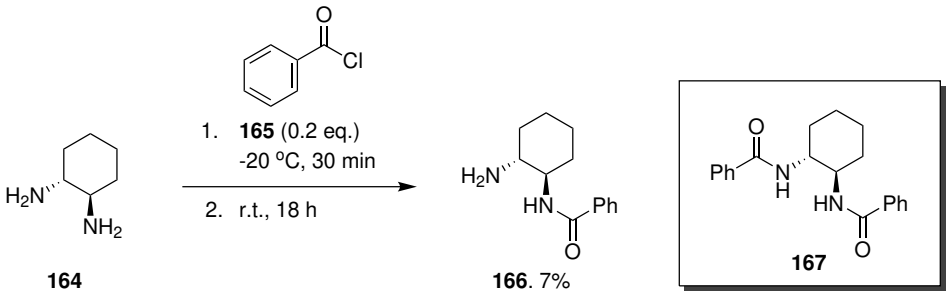

Scheme 2.7: The low yielding mono-benzoylation of **164**

I began to explore a protection strategy after failing to mono-benzoylate **164** directly in high yield. I attempted a literature procedure to singularly add a *tert*-butyloxycarbonyl (Boc) protecting group to one of the nitrogen atoms;[188] however, **168** was not isolated, instead the reaction resulted in total formation of **169** (Scheme 2.8). Additionally, both protocols outlined in Scheme 2.7 and Scheme 2.8 use a vast excess of **164** and are atom inefficient.

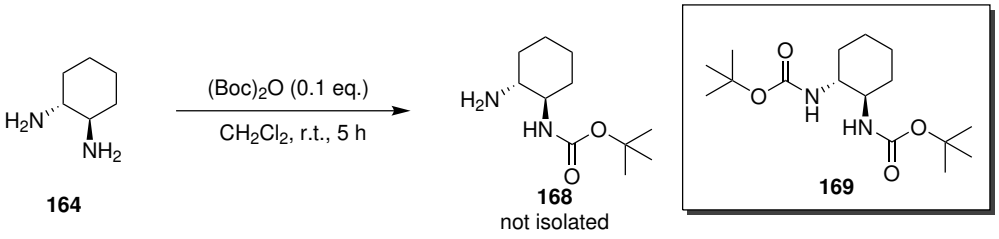

Scheme 2.8: The attempted mono-Boc protection of **164**

An alternative route to synthesise **166** is through a benzimidazole intermediate using commercially available ethyl benzimidate hydrochloride, which can ultimately undergo base-mediated hydrolysis.[189] A notable advantage associated with this synthesis is that it has far better atom economy. This method was successful in isolating benzimidazole **170**; which was subsequently hydrolysed to **166** in low/moderate yield (Scheme 2.9A). Compound **171** was amenable to this synthetic route and resulted in the synthesis of **172**, which was carried forward to synthesise **173** in low overall yield (Scheme 2.9B).

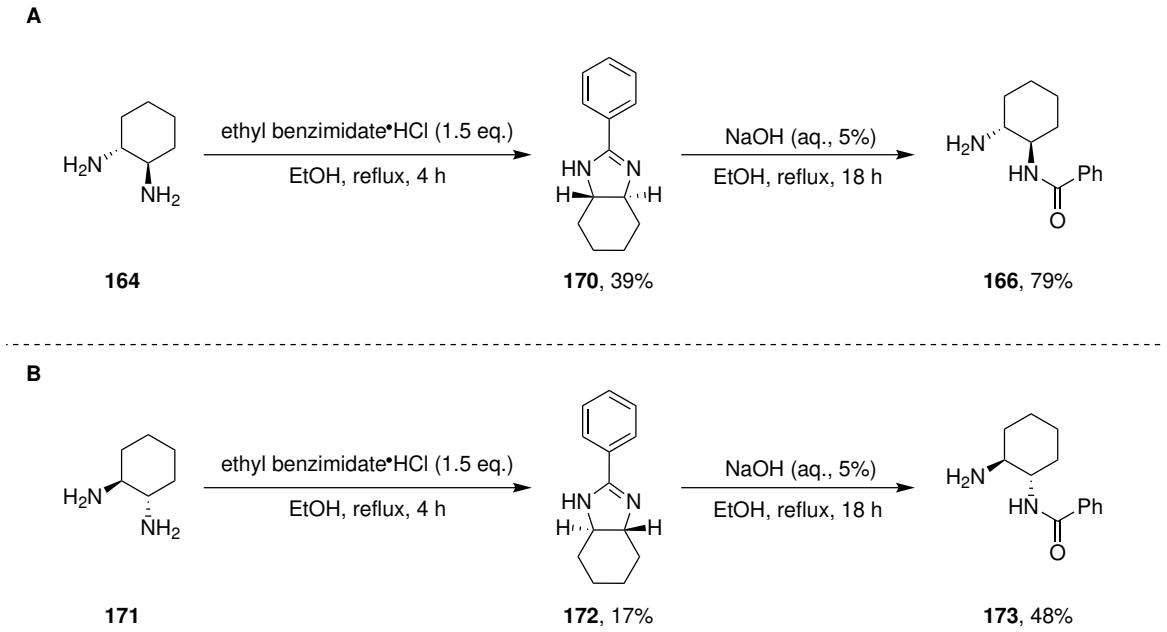

Scheme 2.9: **A**: The synthesis of **166** *via* **170**. **B**: The synthesis of **173** *via* **172**

An alternative strategy was needed to make the precursor for catalyst **163**; the required benzimidate was not commercially available. I used a modified literature procedure to synthesise **174** from **164** and tetrachlorophthalic anhydride[190] in low yield. The low yield is likely attributed to the base-catalysed formation of symmetrical byproduct **175**. The imide **174** was then alkylated using 3,5-*bis*-trifluoromethylbenzoyl chloride to obtain **176** (Scheme 2.10).

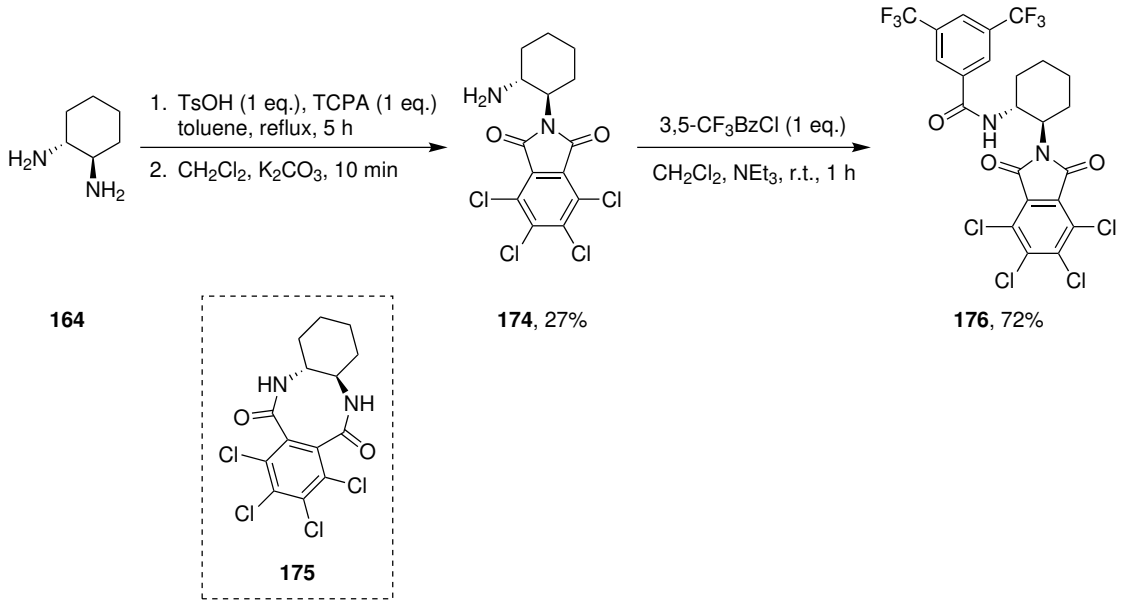

Scheme 2.10: The synthesis of **176**

Attempts to remove the imide protecting group in compound **176** using either hydrazine monohydrate or ammonia in methanol resulted in total deprotection and formation of **164**. Heating

the reaction to reflux in tetrahydrofuran and ethylene diamine produced product **177** in moderate yield (Scheme 2.11).

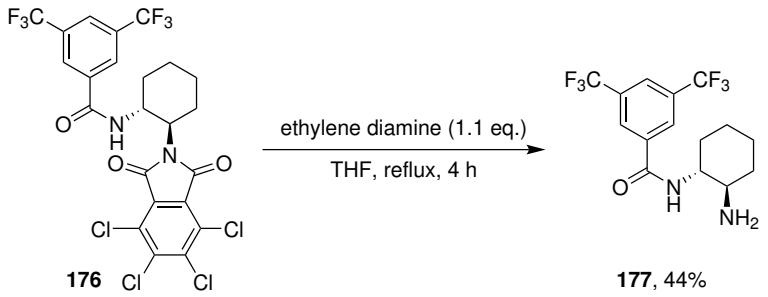

Scheme 2.11: Deprotection of **176** to form **177**

The synthesis of the respective alkylating agents using freshly distilled **136** was relatively facile, and resulted in the isolation of **178**, **179** and **180** in moderate to high yields (Scheme 2.12).

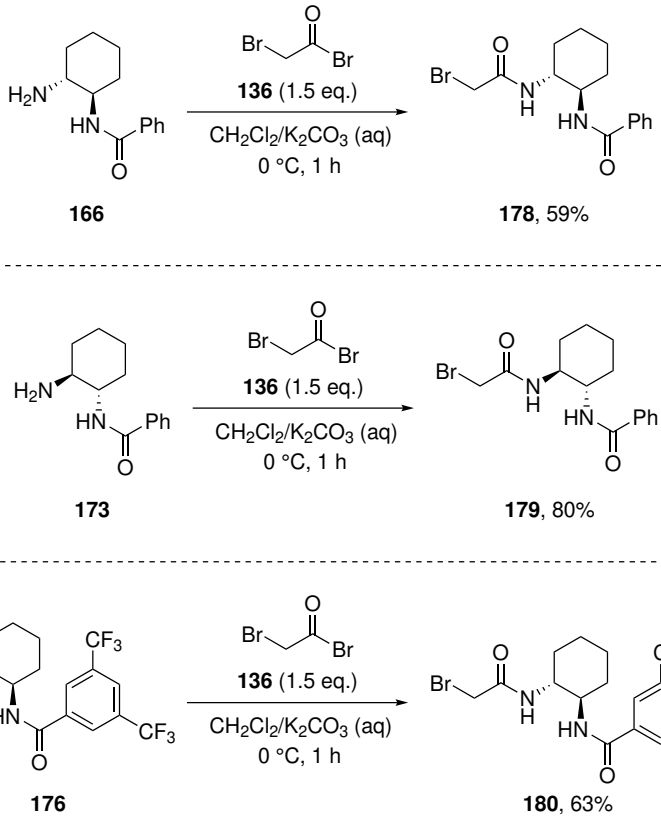

Scheme 2.12: Synthesis of alkylating agents **178**, **179** and **180**

Synthesis of the quinine analogues **181**, **182** and **183** was performed using 1 equivalent of the alkylating agent; further addition of the respective 2-bromoacetamide derivatives resulted in formation of unwanted byproducts which could not be removed (Scheme 2.13).

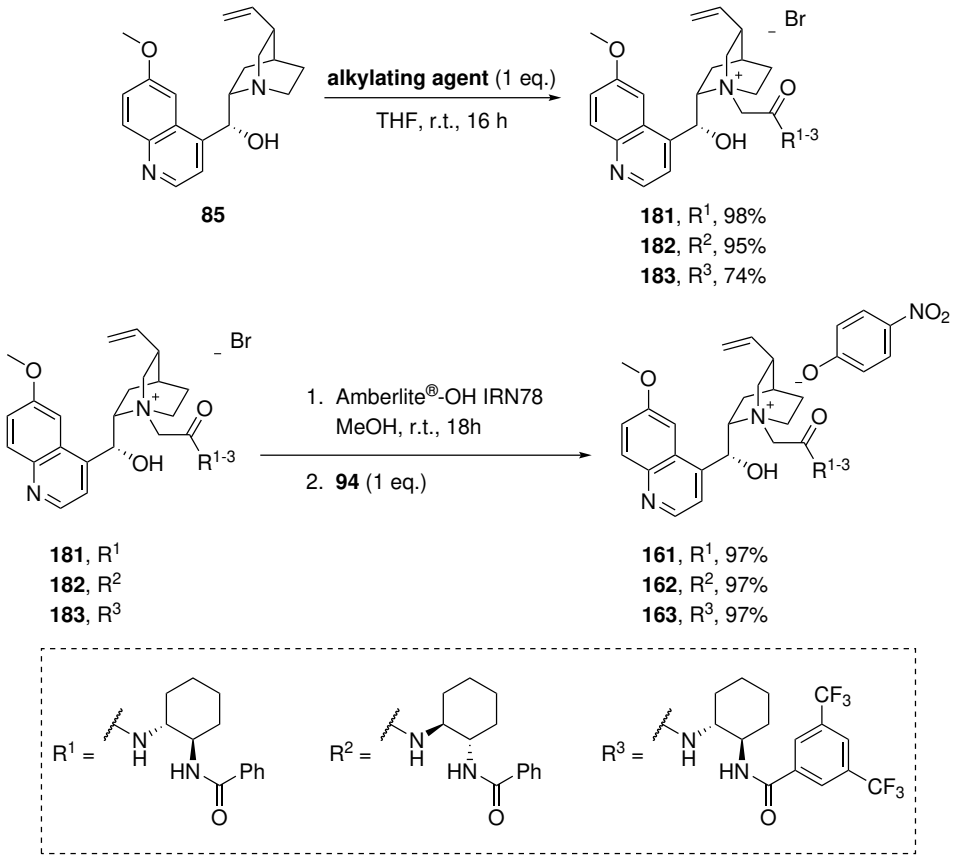

Scheme 2.13: The synthesis of catalysts **161**, **162** and **163**

The catalysts **161**, **162** and **163** were synthesised *via* ion-metathesis using a strongly basic hydroxide ion-exchange resin (Scheme 2.13) and were later applied in the DKR of **41** to **151** (Table 2.8).

All three *trans*-1,2-diaminocyclohexane-derived catalysts **161**-**163** were ineffective at facilitating high *ee* in the DKR of **41** (Table 2.8, entries 1-3). The catalysts performed marginally better than the cyclohexyl-derived PTC **141** (Table 2.2), meaning the second hydrogen bond donor did not influence stereocontrol significantly, and the facilitated enantioselectivity did not surpass the *ee* when employing electron-deficient anilide-derived catalysts. Therefore, additional catalyst development is required; heterocyclic anilide analogues would add functionality to the aryl ring, while also potentially maintaining amide acidity.

Table 2.8: Evaluation of third-generation acetamide catalysts and benchmark catalyst re-evaluation in the enantioselective indirect aminolysis of **41**

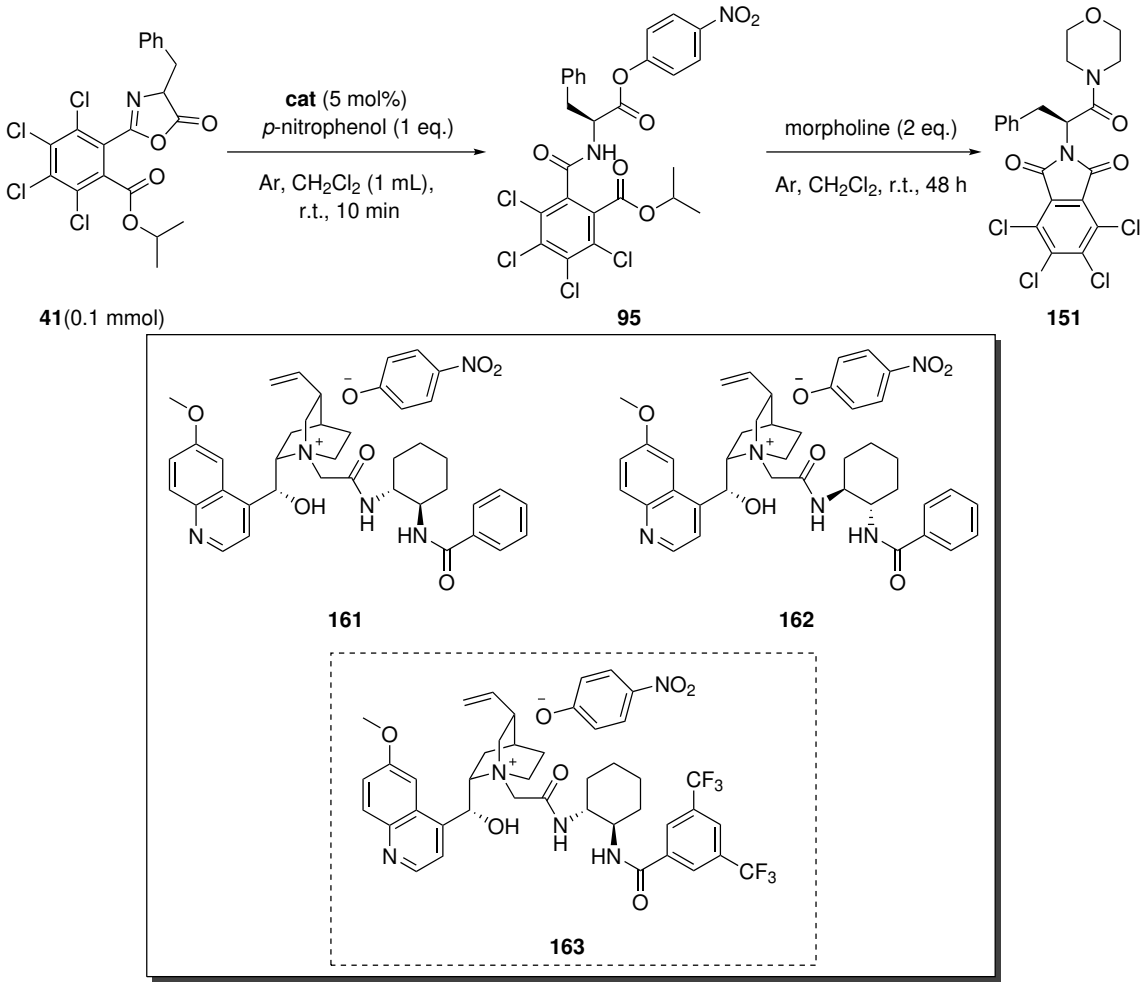

entry	catalyst	yield of 151 (%)	*ee*[a] of 151 (%)
1	**161**	77	15
2	**162**	92	14
3	**163**	98	15

[a] Determined by CSP-HPLC.

2.6 Synthesis of heterocyclic catalyst scaffolds

Considering that most of the catalyst modifications so far have affected both the acidity of the installed amide and the sterics of the aryl ring, I aimed to make catalysts that had sterics similar to the simplest *N*-phenyl acetamide (*i.e*. **139**) while making the amide more acidic.

The catalyst derived from 2-amino pyrazine (**184**), would increase the acidity of the amide while maintaining the *ortho*-proton (for potential *H*-bonding with the carbonyl); while the pyrimidine-derived catalyst **185** removes any potential *ortho*-proton interaction (Figure 2.8).

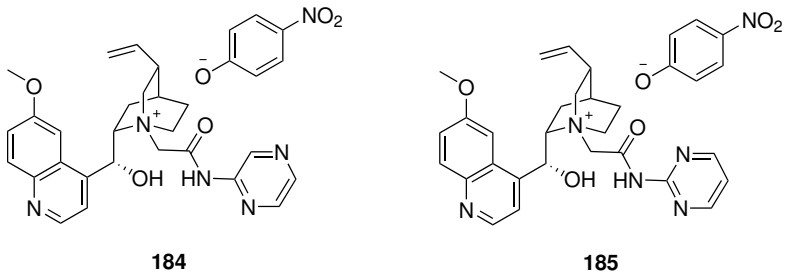

Figure 2.8: Proposed catalysts **184** and **185**

Attempts to use 2-aminopyrazine **186** to synthesise the respective 2-bromoacetamide alkylating agent **187** resulted in an intramolecular cyclisation to form **188**. Similarly, attempts to use 2-aminopyrimidine **189** to form **190** yielded bicyclic compound **191** (Scheme 2.14).

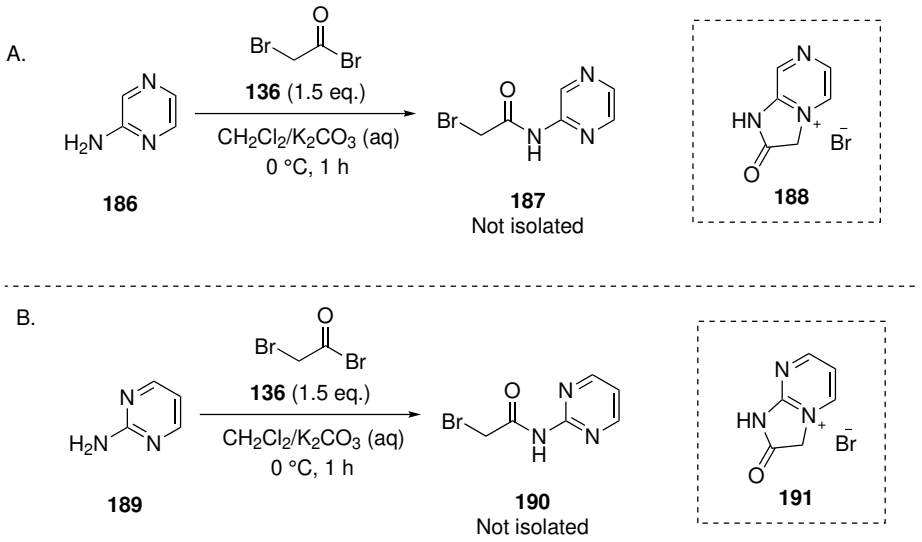

Scheme 2.14: **A**: Attempted bromoacetylation of **186** to form **187**. **B**: Attempted bromoacetylation of **189** to form **190**.

Proposed catalysts **192** and **193**, both derived from 2-aminothiazole **194** and **195**, respectively,

would be interesting substrates to examine if potential chalcogen-bonding (*i.e.* a non-covalent bond between the carbonyl oxygen and a σ-hole in the bivalent sulfur atom) could induce rigidity (Figure 2.9).

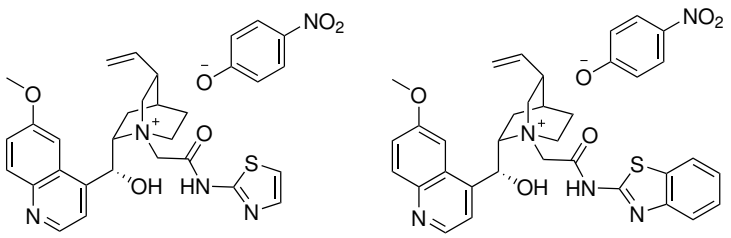

Figure 2.9: Proposed catalysts **192** and **193**.

Bromo-acetylating agents **196** and **197** were formed in the reaction mixture which was indicated through *in situ* ^{1}H NMR spectroscopic analysis, however, attempts to workup, purify or concentrate the products resulted in decomposition (Scheme 2.15).

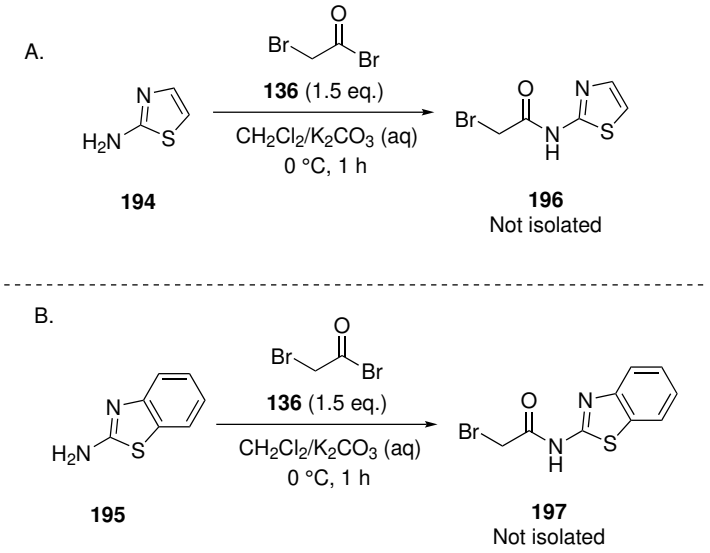

Scheme 2.15: **A**: Attempted synthesis of **196**. **B**: Attempted synthesis of **197**.

With the attempts to synthesise heterocyclic catalyst scaffolds being ultimately unsuccessful, our next goal was to optimise conditions when using anilide-derived catalysts. It was worth noting that work performed by Dr. Lee Anderson and Dr. Anshul Jain identified two phenyl acetamide-derived betaine catalysts that were promising candidates for further optimisation.

2.7 Optimisation study of phenyl acetamide-derived betaine catalysts

Dr. Lee Anderson continued working on electron-deficient actemaide-derived catalysts and identified catalyst **198** as the best from his screen;[182] he also recognised that it was possible to transform **198** into an air-stable betaine (**199**, Scheme 2.16). Dr. Anderson found this technology to be incredibly versatile; he could add this betaine directly to the DKR of **41** with **94** and obtain **151** with discernible no change in enantioselectivity, relative to when the respective phenolate salt was used.

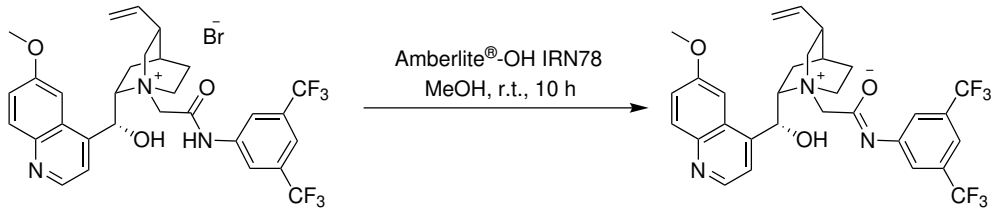

Scheme 2.16: The synthesis of **199** performed by Dr. Lee Anderson

The catalyst **199** was used by Dr. Anderson to screen a plethora of different nucleophilic phenols in the DKR of **41**; additionally, he optimised the synthesis of imide **151** by adding 1,8-diazabicyclo[5.4.0]undec-7-ene (DBU) to the reaction after initial formation of the morpholine amide.[182] To expand on this research, I took the pronucleophilic phenols that were congruent with the highest *ee* from his original assay, and attempted to improve the catalyst system by cooling the reaction and seeing if the *ee* of **151** increased; the results of these experiments are listed in Table 2.9.

Table 2.9: Optimisation study, examining the stereoselective synthesis of **151** when using different phenols and varying the temperature.

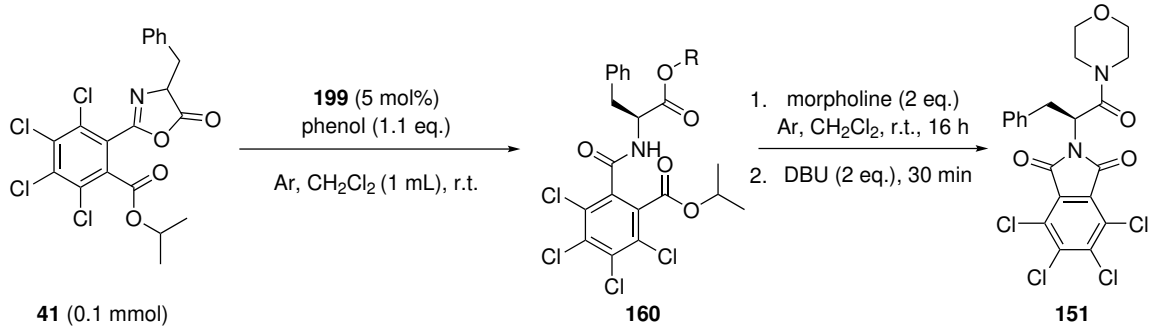

41 (0.1 mmol) **160** **151**

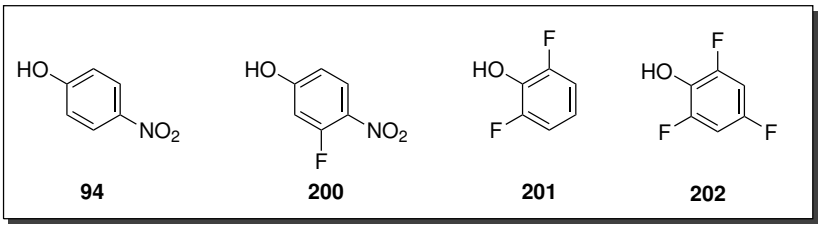

94 **200** **201** **202**

entry	phenol	time[a] (h)	temperature (°C)	yield of 151 (%)	*ee*[b] of 151 (%)
1[c]	**94**	0.2	20	93	58
2[d]	**94**	16	-25	96	77
3[e]	**94**	-	-30	-	-
4[c]	**200**	0.2	20	90	64
5[d]	**200**	16	-25	98	72
6[c]	**201**	2	20	96	66
7	**201**	16	-25	94	66
8	**201**	24	-30	88	66
9[c]	**202**	0.2	20	92	58
10	**202**	24	-30	92	64

Catalyst **199** synthesised by Dr. Lee Anderson. [a]Time to 100% conversion to active ester **160** determined by using ^{1}H NMR spectroscopy. [b]Determined by CSP-HPLC. [c]Repeat of an experiment initially carried out by Dr. Lee Anderson. [d]Phenol partially soluble. [e]Phenol insoluble.

Repeating Dr. Anderson's work using **94** as the pronucleophilic phenol and **199**, facilitated the moderately enantioselective formation of **151** in high yield (Table 2.9 entry 1), which was consistent with the results produced by Dr. Anderson. Cooling the system to −25 °C yields a significantly higher degree of enantiocontrol (entry 2), however, it is worth noting that when **94** was used at −30 °C no reaction occured (entry 3); this is due to **94** being insoluble in the reaction medium. Substituting **94** for 3-fluoro-4-nitrophenol (**200**) as the pronucleophile at room temperature, **151** was isolated in higher *ee* compared to when **94** was used (entry 4). When using **200** at −25 °C, **151** was isolated in higher enantiopurity (entry 5), yet the increase in enantiocontrol was not as substantial as when **94** was assayed under the same conditions; this may be because **200** has a lower pK_a (pK_a = 6.10, H_2O) than **94** (pK_a = 7.01, H_2O)[191]; therefore, k_{rac} may be lower when using more acidic phenols and when conducting the reaction at lower temperatures (*i.e.* <0 °C). When 2,6-fluorophenol (**201**) was used as the pronucleophilic phenol at room temperature, formation of **160** was far slower, but **151** was isolated in relatively high *ee* (entry 6). The reaction involving **201** produced the same *ee* regardless of the temperature change. Given that the pK_a of **201** (pK_a = 6.80, H_2O)[192] is higher than **200** (at least in water), I was expecting the *ee* to increase more considerably when the reaction was cooled. Additionally, the reaction being significantly slower when using **201** which could potentially be explained by the di-*ortho* fluoro substitution; however, the tri-fluoro-substituted pronucleophile **202** had a significantly faster reaction time under room temperature conditions (entry 9) and reducing reaction temperature correlated with an increase in *ee* (entry 10). Given the results found in Table 2.9, it was difficult to understand why **201** was slower at forming the associated active ester **160** at room temperature and why the associated enantiopurity of **151** did not change when lowering the temperature. To this point I have been designing catalysts based on the assumption that the induction of enantiocontrol is through a nucleophilic ion-pair catalysis mechanism (Figure 2.10A), however, I postulated that a general-base catalysis mechanism could also be feasible (Figure 2.10B) which could be favored when using select pronucelophiles such as **201**.

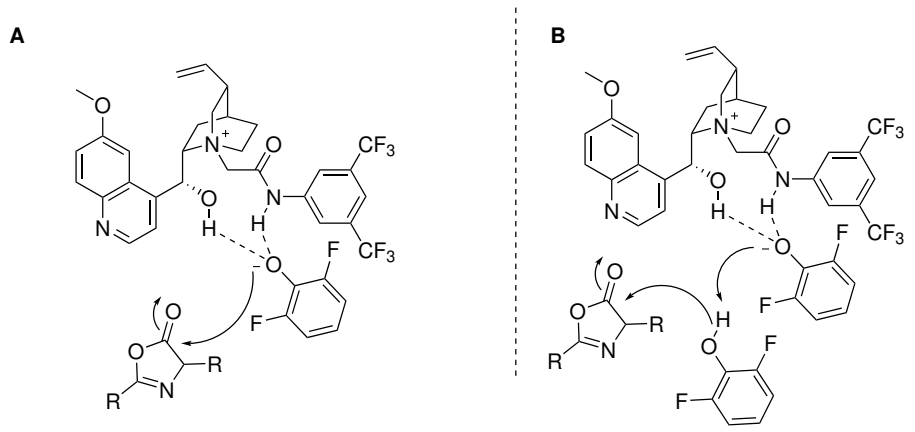

Figure 2.10: **A**: A proposed nucleophilic catalysis mechanism of azlactones **B**: A proposed general-base catalysis mechanism of azlactones

2.7.1 The addition of acidic additives using phenyl acetamide-derived betaine catalysts

To test the theory that when **201** is used, the reaction is undergoing a general-base catalysis mechanism, I added an acidic additive into the reaction that met certain criteria. The additive had to be more acidic than **94** and **201**, to ensure it coordinated with the catalyst and formed an ion-pair. It also had to be a non-nucleophilic anion to ensure it did not compete with the phenol as a nucleophile. I posited that 1,1'-binaphthyl-2,2'-diol (BINOL) derivatives substituted with electron withdrawing groups, such as **203** and **204** could be viable candidates given they have a lower pK_a (pK_a = 9.44, DMSO)[193] when compared to *p*-nitrophenol (pK_a = 10.8, DMSO).[194] It is worth noting that while the pK_a of a compound is a useful indicator of relative acidity, it is highly solvent dependent and the pK_a of compounds recorded in a specific solvent does not perfectly reflect interactions in all solvents.

Table 2.10: The addition of acidic additives to the DKR of **41**.

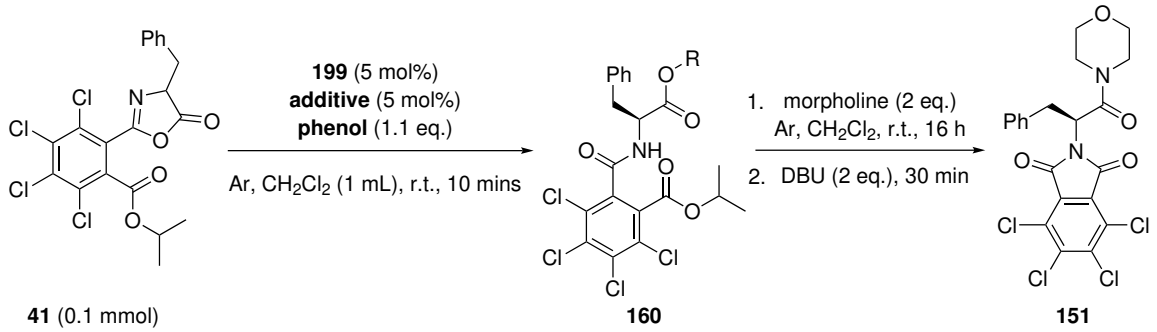

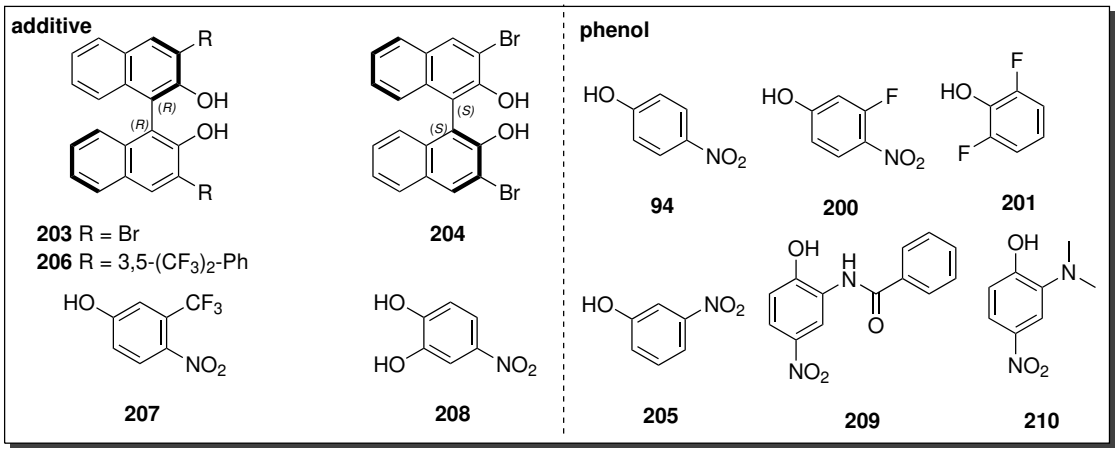

entry	phenol	additive	yield of 151 (%)	*ee*[a] of 151 (%)
1	-	**203**	0	0
2	**94**	**203**	92	70
3	**94**	**204**	98	66
4	**201**	**203**	88	66
5	**200**	**203**	84	67
6[b]	**205**	-	94	26
7	**205**	**203**	87	36
8[c]	**94**	**203**	95	76
9[c]	**94**	**206**	97	74
10	**94**	**207**	90	64
11	**94**	**208**	92	56
12	**209**	**206**	92	33
13	**210**	**206**	92	48

Catalyst **199** synthesised by Dr. Lee Anderson. [a]Determined by CSP-HPLC. [b]Experiment conducted by Dr. Lee Anderson. [c]**94** added *via* a syringe pump, at a rate of 11 mol% every 6 minutes

A control experiment where no phenol was added confirmed that **203** did not react with **41** (Table 2.10, entry 1). In experiments where **94** was added in one portion, there was a marked improved in the *ee* of **151** compared to when no BINOL was added (Table 2.9, entry 1); compound **203** provided a greater degree of enantiodiscrimination than its antipode **204**, meaning that the chirality of the binol is playing a role in enhancing the enantioselectivity (entries 2 and 3). It is noteworthy that the same major enantiomer of **151** is formed in both cases. When phenol **201** was used along with **199** and **203** in the DKR of **41**, it facilitated the same *ee* as if no acidic additive was added, however, formation of the respective active ester (**160**) was significantly more rapid (entry 4). I believe this adds validity to the aforementioned theory (*vide supra*) that **201** was participating in a general-base catalysed process. When using a more acidic phenol (*i.e.* **200**), the increase in *ee* was not as significant, potentially due to the phenol and BINOL-derived additive competing to be ionically bound to the catalyst. I next examined the use of 3-nitrophenol **205** (pK_a = 8.82, H_2O),[192] which is less acidic than **94**, in the hope that general base catalysis would be encouraged, however, **151** was isolated in low enantiopurity (entries 6 and 7). Despite previous experiments to add the phenol portion-wise (Table 2.5) only increasing the associated enantiopurity of **151** marginally, the DKR of **41** was notably more selective when using acidic additive **203** and slowly adding **94** (entry 8). BINOL **206** (pK_a = 9.68, DMSO), characterised by large electron-withdrawing substituted aryl rings, was utilised to understand if increasing the steric bulk associated with the BINOL additive would affect catalysis; however, the *ee* of the resulting **151** was ostensibly similar (entry 9). To investigate if a similar increase in *ee* could be garnered by using an achiral acidic counterion; I added 5 mol% of 3-CF_3-4-nitrophenol (**207**) (pK_a = 9.33, DMSO)[193] as the additive which resulted in the complete formation of the **94** active ester and **151** was isolated in 64% *ee* (entry 10). Given that a catalytic addition of **207** resulted in a minor improvement in enantiocontrol (relative to when the reaction was performed without acidic additive, *i.e.* Table 2.9, entry 1), 4-nitrocatechol (**208**) (pK_a = 6.61, H_2O)[195] was next examined as a catalytic additive, because it is more acidic than **94** and has a second *H*-bond donor; its use correlated with lower degrees of enantioselectivity (entry 11). *Ad hoc* nucleophiles **209** and **210** were synthesised and screened. This was to analyse if either adding additional hydrogen-bond donors (in the case of **209**) or a mildly basic tertiary nitrogen atom (in the case of **210**) was beneficial; yet, these modifications

were ineffective at facilitating high degrees of stereocontrol (entries 12 and 13).

From the results of Table 2.10; portion-wise addition of **94**, used in tandem with catalyst **199** and additive **203** were the optimal conditions for this assay. Given that the reaction environment is significantly different to previously evaluated conditions, I re-evaluated the choice of solvent (Table 2.11). Additionally, Dr. Anshul Jain had developed the *C*-9 *O*-acylated catalyst **211** derived from **199**, which facilitated the formation of **151** in high *ee* when using **94**.

Table 2.11: A screen of various solvents used in the DKR of **41** using catalysts **199** and **211** with **203**.

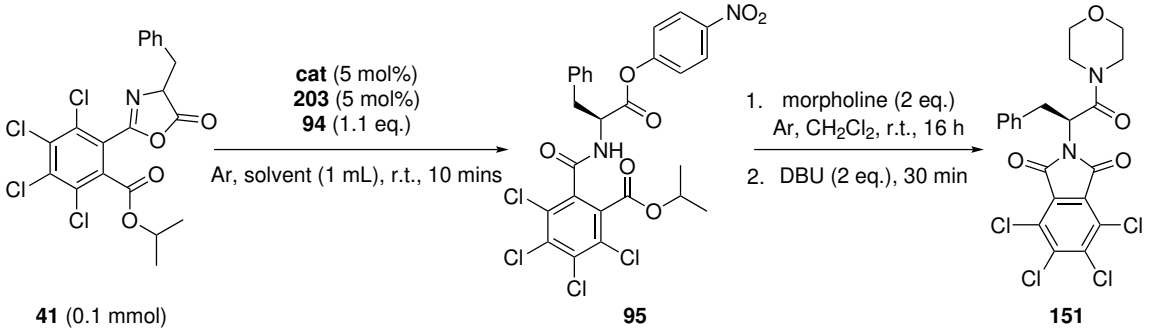

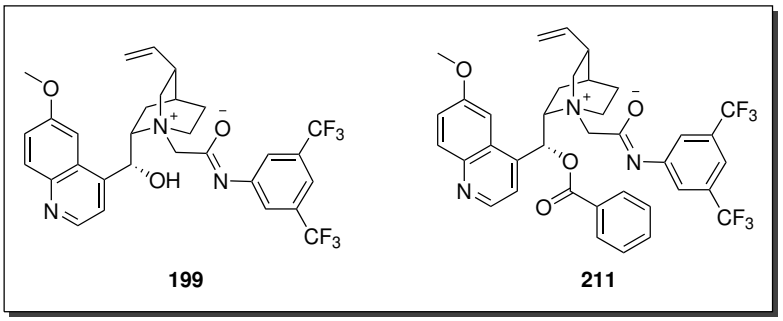

entry	catalyst	solvent	yield of 151 (%)	*ee*[a] of 151 (%)
1	**199**	DCE	91	72
2	**199**	THF	83	60
3	**199**	toluene/CH_2Cl_2 (8:2)	92	78
4	**199**	PhCl/CH_2Cl_2 (8:2)	87	77
5[b]	**211**	CH_2Cl_2	93	74
6	**211**	toluene/CH_2Cl_2 (8:2)	97	67

Catalyst **199** synthesised by Dr. Lee Anderson. Catalyst **211** synthesised by Dr. Anshul Jain. [a]Determined by CSP-HPLC. [b]Repeat of an experiment initially carried out by Dr. Anshul Jain; results presented are repeats of their work.

Using 1,2-dichloroethane (DCE) as a solvent in the DKR of **41** in conjunction with **199** and **203**

resulted in an enantioselectivity similar to when CH_2Cl_2 was used (Table 2.11, entry 1). The use of tetrahydrofuran under the same reaction conditions yielded **151** in moderate enantioselectivity (entry 2). Due to catalyst **199** being partially soluble in toluene and chlorobenzene (PhCl), they were mixed with CH_2Cl_2 in a ratio of 8:2 to ensure the reaction was homogenous. These reaction mixtures facilitated formation of **151** in high *ee* when using catalyst **199** and additive **203** at room temperature (entries 3 and 4); a potential explanation for the increase in *ee* is that both PhCl (ε = 5.6) and toluene (ε = 2.4) have lower dielectric constants than CH_2Cl_2 (ε = 8.9), leading to tighter ion-pair and a generally influence of the catalysts stereochemical information over the process.[196] Catalyst **211** proved to be capable of promoting highly a enantioselective reaction, and was active in the DKR of **41** in CH_2Cl_2; however, when the solvent was changed to a toluene/CH_2Cl_2 mixture, it facilitated formation of **151** in lower *ee* (entries 5 and 6).

2.7.1.1 Optimisation studies using phenyl acetamide-derived betaine catalysts

To advance the system outlined in Table 2.11, I wanted to try cooling it below −25 °C. As mentioned in Table 2.9, **94** is insoluble at −30 °C in CH_2Cl_2 which can affect activity. To ensure the reaction system was completely homogenous, I found two potential solutions to dissolve the reagents at lower temperatures. I could either increase the amount of solvent in the reaction or use tetrahydrofuran. Even though tetrahydrofuran did not facilitate a highly selective reaction environment, results from a solubility test showed that the reagents only began to precipitate below −50 °C. For this set of experiments, they were quenched with morpholine after a specific reaction time, as opposed to sampling during the reaction to ensure conversion to **95** was complete; this is due to concerns that the samples taken for ^{1}H NMR spectroscopic analysis could be inaccurate, due to the reaction potentially occurring during sampling.

Table 2.12: The effects of temperature and concentration in the DKR of **41** when using **199**, **203** and *p*-nitrophenol.

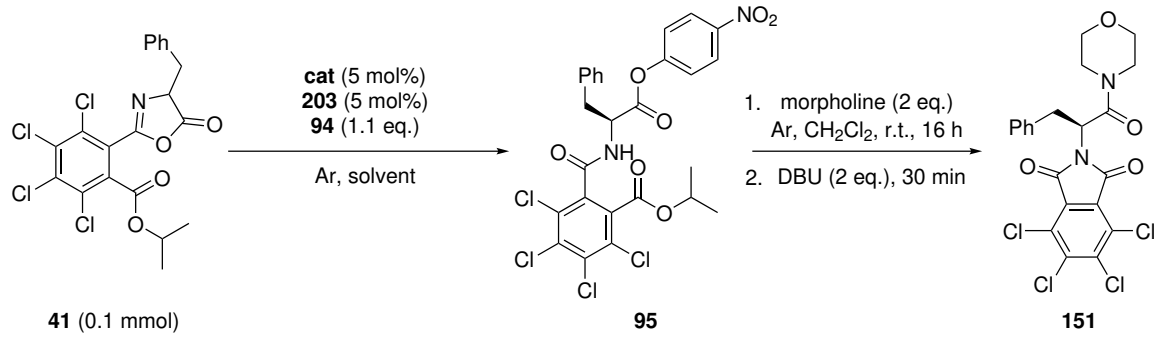

41 (0.1 mmol) **95** **151**

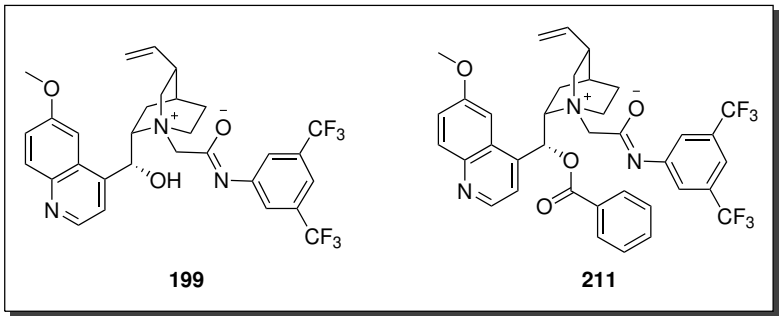

199 **211**

entry	catalyst	solvent [mL]	temperature (°C)	time (h)	yield of 151 (%)	*ee*[c] of 151 (%)
1	**199**	CH_2Cl_2 [1]	-10	18	92	77
2	**199**	PhCl/CH_2Cl_2 (8:2) [1]	-10	18	88	77
3	**199**	THF [1]	-10	18	97	46
4	**199**	CH_2Cl_2 [5]	-30	18	91	80
5	**199**	CH_2Cl_2 [10]	-30	18	88	83
6	**199**	CH_2Cl_2 [20]	-30	18	96	83
7	**199**	CH_2Cl_2 [10]	-30	48	93	83
8	**199**	CH_2Cl_2 [10]	-50	48	90	24
9	**199**	CH_2Cl_2 [10]	-50	96	95	25
10	**211**	CH_2Cl_2 [10]	-30	18	86	82
11	**211**	CH_2Cl_2 [10]	-50	48	93	65

Catalyst **199** synthesised by Dr. Lee Anderson. Catalyst **211** synthesised by Dr. Anshul Jain.
[a]Determined by CSP-HPLC.

Using **94**, **199** and **203** at −10 °C in CH_2Cl_2 was highly effective at facilitating enantiocontrol (Table 2.12, entry 1). A solvent mixture of PhCl/CH_2Cl_2 (8:2) under the same reaction conditions led to the discovery that the associated enantioselectivity was independent of the decrease in temperature in these solvents (entry 2); while in THF, **151** was isolated in moderate enantiopurity (entry 3). Since the use of CH_2Cl_2 as the reaction solvent led to an increase in *ee* at −10 °C, it was used as the solvent for the rest of the assay. When the volume of solvent was increased to 5 mL and the reaction was performed at −30 °C, it was far more stereoselective (entry 4). Doubling the volume of solvent to 10 mL led to another increment in **151** enantiopurity (entry 5); yet doubling the solvent to 20 mL led to a plateau in *ee* (entry 6). The enantiocontrol becoming more prominent at lower concentrations was unexpected and could indicate that the catalyst is aggregating in solution at low temperatures. A reaction with 10 mL of solvent was left for 48 h before being quenched by the amine, to see if the reaction was ending prematurely, which resulted in no change in enantiopurity compared to the 18 h reaction (entry 7). Decreasing the reaction temperature further to −50 °C under the best conditions resulted in a diminished enantiopurity (entry 8), and doubling the reaction time to confirm enantioselective formation of **95** was complete, afforded identical levels of enantiopurity (entry 9). Catalyst **211** under the current best performing conditions (*i.e.* entry 5) resulted in ostensibly similar results compared to when **199** was used as the catalyst (entry 10). Similar to **199**, catalyst **211** facilitated significantly less stereoselectivity when the temperature was reduced to −50 °C (entry 11). The enantiocontrol provided by catalysts **199** and **211** in conjunction with **203** increased in CH_2Cl_2 as a result of the drop in temperature. Catalysts **199** and **211** facilitated less stereocontrol when the temperature was reduced to −50 °C, which was difficult to rationalise. One potential reason for this is that either the catalyst or the BINOL is aggregating at low temperature, which could be detrimental to enantiocontrol.

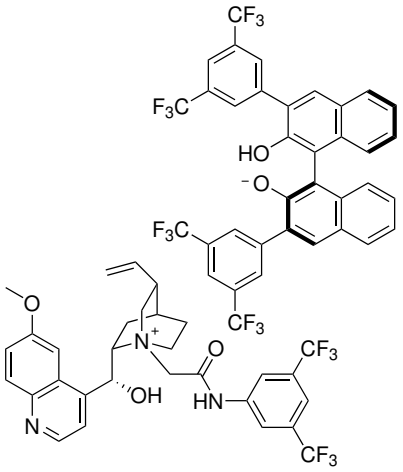

212

Figure 2.11: Catalyst **212**

Additionally, I have been assuming that the sole active catalyst in solution was a mono-cationic catalyst such as **212** (Figure 2.11); however, it is entirely possible that an active *bis*-quinine catalyst could also be present in solution. To understand more about the catalyst structure, **212** was synthesised and a X-ray crystal structure was obtained (Figure 2.12). I used **206** as the BINOL counter-ion because I believed the conformation of the large aryl rings in the BINOL could be more informative when obtaining the x-ray crystal structure. It is worth noting that solid-phase interactions found in an X-ray crystal structure are not a perfect representation of the interactions in the solution phase.

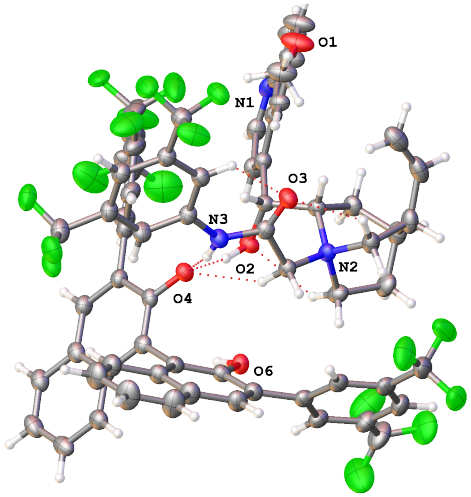

Figure 2.12: X-ray crystal structure of **212**

From the X-ray crystal structure, it was clear that a single quinine cation was present at room temperature in the solid phase; this also provided some useful insight, namely, a set of intramolecular

quinine hydrogen bonds, which rigidify the structure. This series of interactions includes the theorised intramolecular *ortho*-proton/carbonyl interaction, when electron-withdrawing substituents are present in the *meta*-position of the aryl ring (Figure 2.13). It was also unexpected that the phenolate binds to both *C*-9 OH unit and the amide NH bond; this may indicate there is an internal competition for binding sites available to the azlactone substrate.

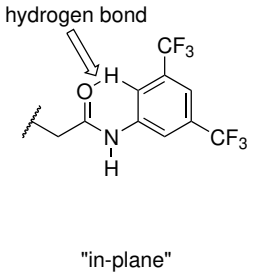

Figure 2.13: Intramolecular hydrogen-bonding interaction seen in the X-ray crystal structure of **212**

In order to understand if formation of a potentially *bis*-cationic system was detrimental to the DKR of **151**, I synthesised **213** for experimentation. To evaluate if the BINOL additive is responsible for the associated reduction in *ee* at cryogenic temperatures, an array of experiments will be performed where **203** is absent and all the reagents are in solution. The results of these experiments are outlined in Table 2.13.

Using catalyst **213** in the DKR of **41** at −30 °C resulted in the highly enantioselective formation of **151** (Table 2.13, entry 1); this indicates that the *bis*-cationic catalyst **213** is an equally active catalyst in solution and is conducive with high *ee*. An experiment with 10 mol% of **203** along with 5 mol% of **199** resulted in an overall decrease in enantioselectivity (entry 2); however, catalyst **211** under the same conditions was highly enantioselective (entry 3). The enantioselectivity associated with catalyst **199** must be significantly more affected by any potential BINOL aggregation. This could rationalise our findings in Table 2.12; catalyst **199** was more impacted than **211** in the experiments at −50 °C. To examine whether the **203** is the cause of the decrease in *ee* at low temperature, **199** was used in the DKR of **41** at −50 °C and **151** was isolated in high enantiomeric excess (entry 4); assaying **211** under the same conditions yielded ostensibly similar results. The results of Table 2.13 make it clear that in the DKR of **41** to **151**; **203** is beneficial in increasing the stereocontrol of the reaction when used in tandem with

an anilide-derived betaine catalyst, however, it is detrimental to stereocontrol below −30 °C, aggregation at low reaction temperatures is a possible reason. Given the enantiocontrol provided by **211**, I next wanted to examine if altering the functionality at *C*-9 could provide any additional enantiocontrol.

Table 2.13: An examination of potential aggregation in the DKR of **41** when using **199**, **211** and **213**.

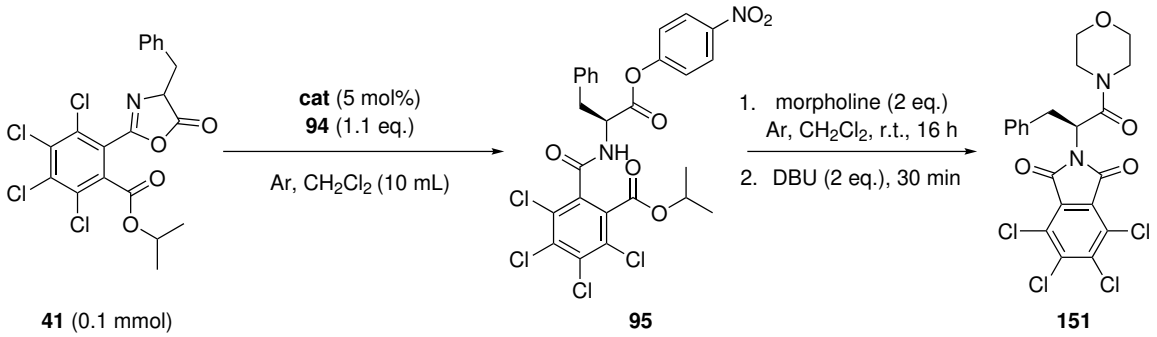

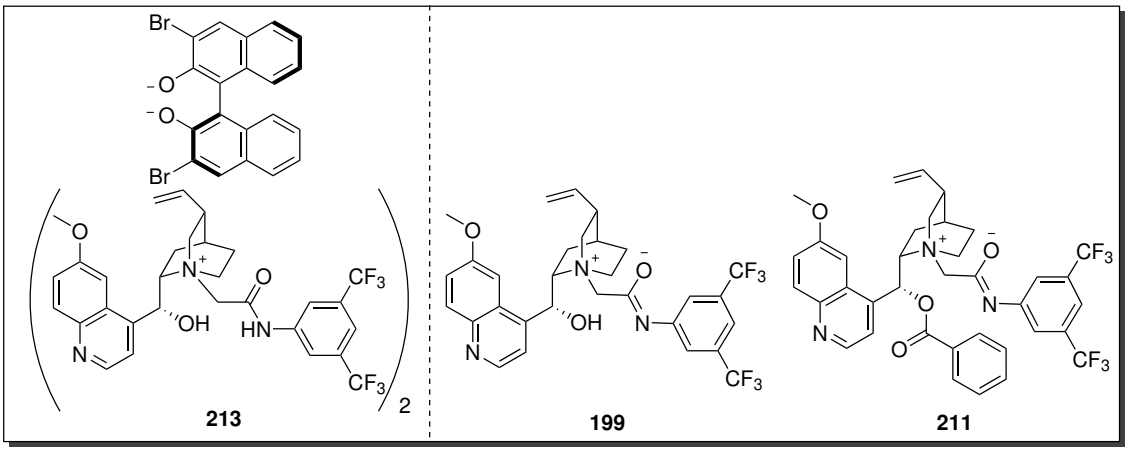

entry	catalyst	temperature (°C)	time (h)	yield of 151 (%)	*ee*[c] of 151 (%)
1	**213**	-30	18	94	81
2[b]	**199**	-30	18	89	70
3[b]	**211**	-30	18	91	82
4	**199**	-50	48	96	81
5	**211**	-50	46	96	80

Catalyst **199** synthesised by Dr. Lee Anderson. Catalyst **211** synthesised by Dr. Anshul Jain. [a]Determined by CSP-HPLC. [b]Experiment conducted with added **203** (10 mol%).

2.8 Synthesis of *cinchona*-alkaloid catalysts with modifications at *C*-9

As mentioned in Section 1.4, additional *H*-bond donors covalently bonded to *C*-9 and an epi-quinine derivative proved to be ineffective in providing **151** in higher degrees of stereocontrol. However, given the addition of acidic additives such as **203**, it is worth re-examining. I designed the epi-quinine-derived analogue of **211** (*i.e.* **214**) to examine if inverting the stereochemistry at *C*-9 and removing the hydrogen bonding capability will provide enantiodiscrimination (Figure 2.14).

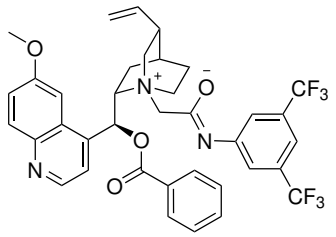

214

Figure 2.14: Proposed catalyst **214**

With regards to synthesising **214**, I initially intended to both invert the stereochemistry and install the benzoyl ester in one step, forming *via* a Mitsunobu reaction with benzoic acid. However, despite many attempts, **215** was inseparable from triphenylphosphine oxide (Scheme 2.17). Furthermore, **215** is hydrolytically unstable and will rapidly form **216** when in contact with air or water.

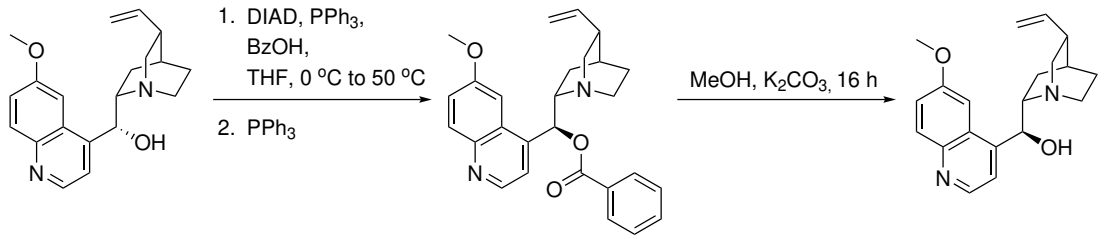

85 | **215** not isolated | **216**, 36%

Scheme 2.17: Initial synthesis towards **215**.

Therefore, to isolate pure **215**, I isolated **216** through hydrolysis of **215** and then subsequently alkylated it with benzoyl chloride. The alkylation with **217** to form bromide salt **218** was unsuccessful and resulted in a multitude of byproducts, and **218** was not successfully isolated (Scheme 2.18).

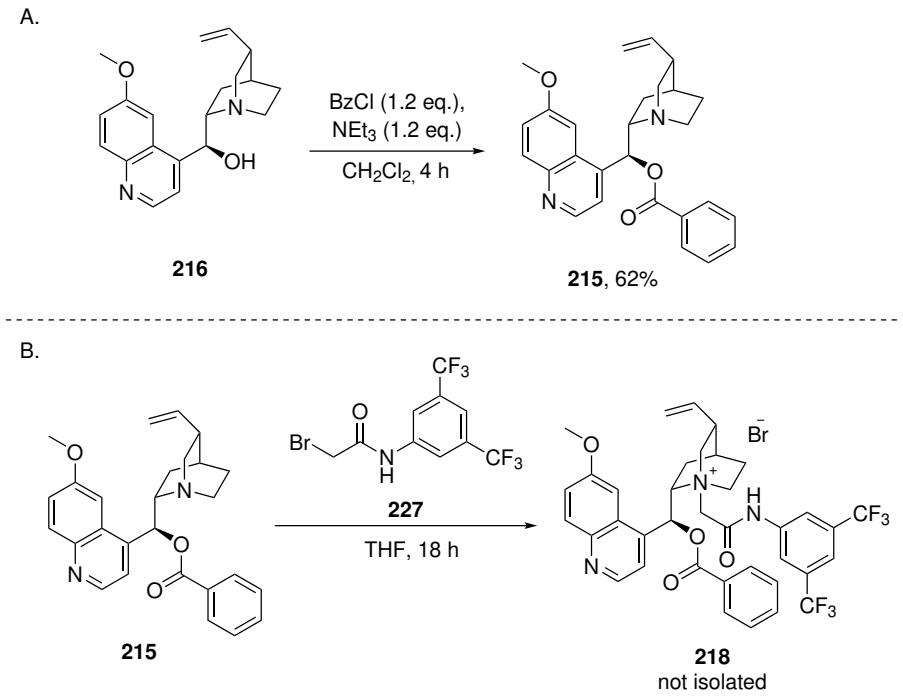

Scheme 2.18: **A**: Synthesis of **216**. **B**: Attempted synthesis of **218**.

With the synthesis of the epi-quinine-derived catalyst ultimately not being accomplished, its completion would be desirable to understand the structure-activity relationship of catalysts more profoundly. This, coupled with expanding the substrate scope to see if azlactones derived from other amino acids can be used to isolate enantiopure peptides in high yield, would be desirable.

2.9 Conclusions

The aminolysis of azlactones with synthetically-relevant amines has remained elusive in the literature due to the difficulty in controlling these active nucleophiles. This project aimed to use **41** and develop a reproducible and highly enantioselective methodology to form enantiopure and orthogonally protected dipeptides from **41**. A modification to the synthesis of **41** by using EDC·HCl proved worthwhile, maintaining the yield of the previously reported procedure while making the workup relatively facile.

Initial experiments using benzyl bromide-derived PTCs towards synthesising **127** provided low enantiocontrol. A series of *N*-phenyl acetamide nucleophilic PTCs provided greater stereocontrol; an increase in the acidity of the amide in the catalyst proved to have a positive correlation with regard to increasing the enantiopurity of **127**.

Later developments reduced the risk of racemisation and increased consistency of the system through the development of product **151**. Ion-pair nucleophilic catalysts proved to be highly active in the DKR of azlactone **41**, reducing reaction times to 10 minutes. The synthesis of *trans*-1,2-diaminocyclohexane-derived catalysts proved to be challenging and was unsuccessful in achieving high degrees of enantiocontrol in the DKR of **41**.

A further innovation by Dr. Lee Anderson was the development of catalyst **199**, which could be used in the efficient screening of many different nucleophiles in the DKR of **41**. This led to the discovery that a secondary general-base catalysis mechanism could lead to high degrees of enantiocontrol. When this theory was tested and a acidic additive was added (*i.e.* **203**) the formation of **151** was facilitated in significantly higher stereocontrol; this could be further optimised to achieve a maximum of 83% *ee* at −30 °C. It is noteworthy that this level would theoretically allow the coupling of the active ester **95** with a *C*-protected amino acid to form a dipeptide in 90:10 diastereomeric ratio; meaning 90% yield of a single dipeptide could potentially be isolated from a novel process involving the one-pot DKR and coupling of a phenylalanine-derived azlactone with an amino acid nucleophile. It is hoped that developing this methodology into a useful peptide-altering tool will be just a short distance away.

A series of experiments concluded that when using **199** in tandem with **203** in the KR of **41** their activity is highly temperature dependent likely due to aggregation when employing BINOL **203** at temperatures <-30 °C.

To develop this project further, computational studies could be performed to fully understand the catalyst / BINOL interaction; additionally, more azlactones should be tested to fully realise the potential of **199** and **203**.

3 | Neutral hydrolysis of poly(ethylene terephthalate) catalysed by terephthalate-based ionic liquids

3.1 Development of a standardised protocol in the neutral hydrolysis of PET

As mentioned in Section 1.5.1.6 the conditions used in studies to examine the neutral hydrolysis of **104** to form **100** are subject to a large amount of variance with regards to the catalyst loading, reaction conditions and the source of **104**. Furthermore, PTC and IL catalyst properties have not been adequately examined in the neutral hydrolysis of PET to develop a structure-activity relationship; therefore, standardised conditions and materials must be established.

With the help of Dr. Lee Anderson, we concentrated on making this system as commercially applicable as possible; for this reason, post-consumer PET bottle flakes (5x5 mm) were used as an initial starting point to begin the assay. For the experimentation itself, two stainless steel hydrothermal reactors containing Teflon® crucibles (23 mL) were used. Heating the hydrothermal reactors was performed in a high-temperature reaction oven (200 °C), which was provided by Prof. Peter Dunne. The reaction was cooled at room temperature after the desired time on a clay cooling block.

Post-reaction processing was performed using 550 mg of oven-dried NaOH (to ensure the addition of base was accurate), which was dissolved to form an aqueous solution (1 mL). To ensure equal dispersion of the NaOH solution and full dissolution of the product **100**, identical stir bars were used at 1300 RPM for 30 min. The remaining insoluble solids were filtered through a sintered glass funnel (pore size 3) and washed with water (3 x 10 mL) to ensure all the product was dissolved into the mother liquor. The remaining residue was washed with acetone (2 x 10 mL); this is to remove any potentially insoluble catalyst residues from the unreacted PET.

The remaining PET was dried in a vacuum oven at 60 °C for 16 h and its mass was measured (PET_c) which was used to determine the conversion of PET (*i.e.* the conversion (%) of PET is the consumption of PET relative to the starting material; a 0% conversion would imply all the PET is present after the reaction, while a 100% conversion implies none of the starting material remains).

The mother liquor was separated and placed into an ice bath for 5 minutes. To ensure reproducibility between experiments, exactly 5 mL of 2.5M HCl solution was added drop-wise to the mother liquor while in the ice bath. The product **100** was isolated by filtration through a sintered glass funnel (pore size 3) and washed with water (3 x 10 mL) before being dried in a vacuum oven at 60 °C for 16 h.

To measure the conversion of PET, the remaining PET and insoluble oligomers (PET_c) were weighed, and a percentage of the consumed material is calculated based on the initial quantity of PET (PET_i) (equation 1).

$$Conv.\,of\,PET\,(\%) = \frac{PET_i - PET_c}{PET_i}\,X\,100 \tag{1}$$

The "yield (%) of TPA" was calculated using ^{1}H NMR spectroscopic analysis (400 MHz); a known quantity of **100** (approximately 15 mg, (TPA_s)) and a known mass of 4-iodoanisole as an internal standard (15-25 mg) are sampled. The moles of 4-iodoanisole are calculated and recorded (I_m). The integrals associated with TPA (s, 8.02 ppm) (TPA_I) relative to 4-iodoanisole (d, 6.74 ppm, 2H) (Figure 3.1) were obtained and the moles of **100** in the sample (TPA_{smol}) were ascertained from the ^{1}H NMR spectrum as seen in equation 2.

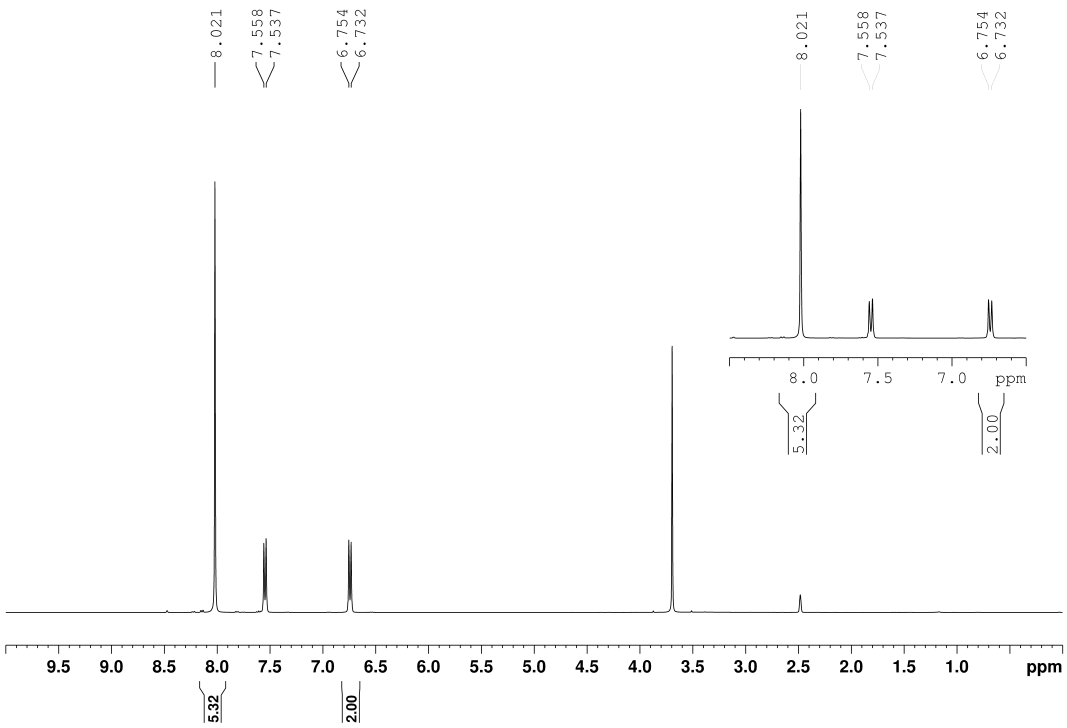

Figure 3.1: ^{1}H NMR spectroscopic data associated with product TPA and 4-iodoanisole used to determine the yield of TPA

$$TPA_m\,(mmol) = \frac{TPA_I}{4}\,X\,I_m \tag{2}$$

The number of moles of **100** in the sample (TPA_m) was then scaled to reflect the total number of moles in the product by calculating a ratio between the mass of the total solid product ($Product_{mass}$) and the mass taken for analysis (TPA_s). This was then multiplied by the molecular mass of **100** (166.13) to garner the total mass of pure **100** (TPA_t) in the product (3).

$$TPA_t\,(g) = (\frac{Product_{mass}}{TPA_s}\,X\,TPA_m)\,X\,166.13 \tag{3}$$

A percentage yield was obtained by dividing variable TPA_t by the total theoretical mass of monomeric units contained in the initial amount of PET, *i.e.* 1 g of PET contains up to 5.2 mmol of polymer monomeric units (Equation 4). Spectroscopically obtained yields agreed with those

derived from the mass of TPA within 1.1% in all cases.

$$Yield\ of\ BHET\ (\%) = \frac{TPA_t}{TPA_{theoretical}}\ X\ 100 \qquad (4)$$

With a suitable and repeatable method developed, work began on synthesising different PTCs for screening.

3.2 Synthesis of phosphonium halides

Conveniently, most of the catalysts required for the assay are commercially available; the only PTC synthesised *via* alkylation was **220**, which was synthesised by the methylation of a trioctylphosphine **219** (Scheme 3.1).

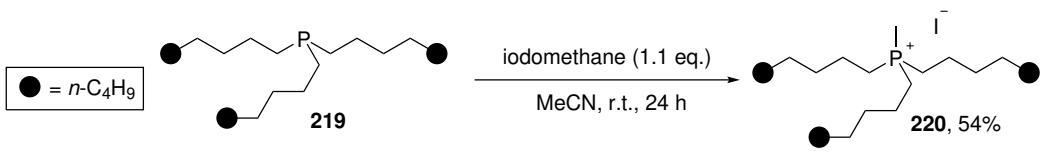

Scheme 3.1: Methylation of **219** to form **220**

The synthesis of phosphonium chlorides was through the facile ion-metathesis utilising chloride ion-exchange resin (*i.e.* Amberlite® IRA-900 chloride form). The synthesis of **221** from **220** was performed using this methodology (Scheme 3.2).

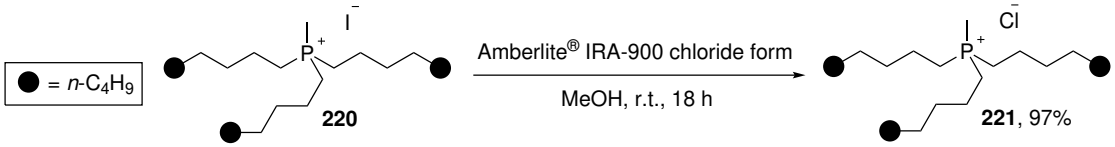

Scheme 3.2: Synthesis of catalyst **221**

With a range of alkyl phosphonium and ammonium PTCs of varying functionality, lipophilicity and geometry in hand, a thorough investigation was performed to discern desirable PTC qualities.

3.3 Initial catalyst screening

As mentioned in Section 1.5.1.7, catalyst inhibition could be detrimental to catalyst activity; therefore, I devised a method to sidestep product inhibition and contamination *via* the use of the conjugate base of **100** (*i.e.* **107**). Work in our group performed by Mr. Lorenzo Pedrini discovered that tetraalkylphosphonium ions are highly efficacious in the glycolytic depolymerisation of PET[146], thus I postulated they could be applicable in the neutral hydrolysis of **104**. The investigation began with the hydrolysis of PET from water bottles (cut into ≈ 5 x 5 mm flakes) under conditions at 200 °C for 3 h in the absence of a catalyst; which furnished only trace levels of the product **100** (Table 3.1, entry 1). To facilitate the rapid evaluation of catalyst structures, *bis*tetraalkylphosphonium terephthalate catalysts were generated *in situ* from phosphonium bromides and disodium terephthalate (**107**). Some catalysis by either **107** (2.5 mol%, entry 2) or tetrabutylphosphonium bromide (**222**, 5 mol%, entry 3) alone was discernible; however, when utilised together, markedly improved yields resulted (entry 4). Exchange of **222** for the larger, more lipophilic **223** led to a more active system (entry 5), while the corresponding chloride **224** proved inferior (entry 6). Use of a long chain isomer of **223** (*i.e.* **225**) delivered marginally improved performance (entry 7) and both catalysts could be employed at low levels of 1 mol% (based on **223**) without significantly impacting efficiency (entries 8 and 9). Catalysis by a smaller homologue of **225** (*i.e.* **226**, entry 10) provided **100** in similar yields at 1 mol% loading. To probe the influence of a less sterically encumbered cation 'head'[197], methyltrioctylphosphonium iodides and chlorides (**220** and **221** respectively) were synthesised and evaluated. The iodide salt **220** proved superior to either the chloride or **221**-**224** (entries 11–13).

Table 3.1: Neutral hydrolysis catalysed by a binary tetraalkylphosphonium salt-disodium terephthalate system.

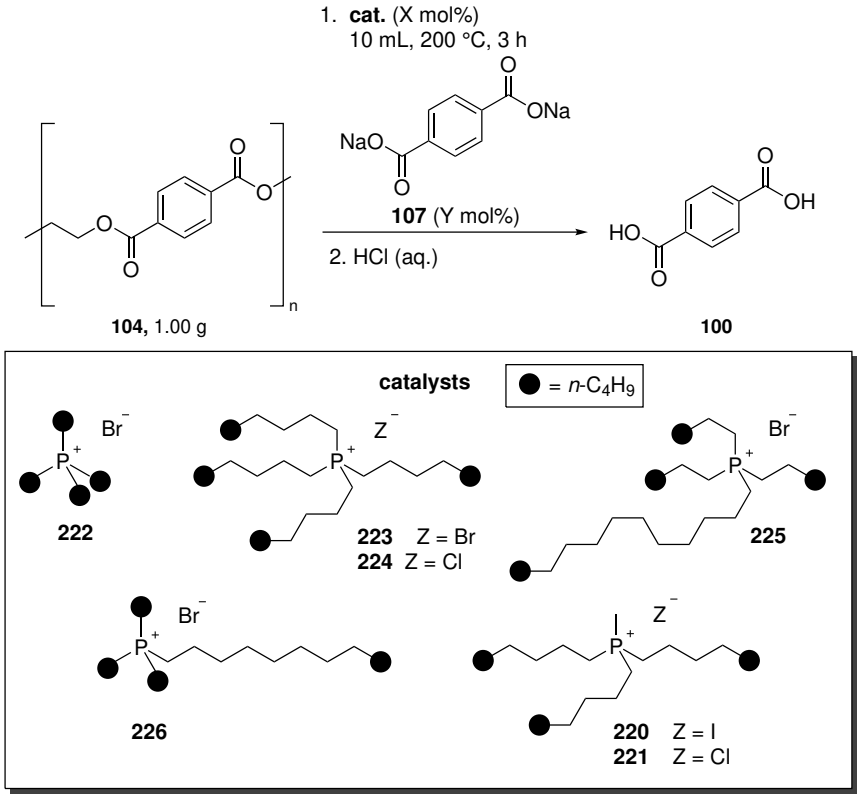

entry	catalyst	loading X (mol%)	loading Y (mol%)	conversion (%)	yield[a] (%)
1[b]	-	0	0	5	4
2[b]	-	0	2.5	10	9
3	**222**	5	0	17	17
4	**222**	5	2.5	48	47
5	**223**	5	2.5	79	59
6	**224**	5	2.5	72	51
7	**225**	5	2.5	80	63
8	**223**	2	1	65	62
9	**225**	2	1	60	58
10	**226**	2	1	67	60
11	**220**	5	2.5	79	68
12	**221**	5	2.5	70	52
13	**220**	2	1	74	71

[a]Isolated yield after precipitation corrected for additional TPA from the catalyst, confirmed by ^{1}H NMR spectroscopy using 4-iodoanisole as an internal standard (all agreeing within 1.1%). [b]Experiment performed by Dr. Lee Anderson

Analysing the results in Table 3.1, it would seem increasing the lipophilicity associated with the cation is beneficial towards increasing both the conversion of **104** and yield of **100**. Previous work in our group[197] discovered that substituting the anion can significantly affect the solubility of the PTC at 90 °C in the alkaline hydrolysis of PET. It is possible that the associated solubility of the catalyst can affect its hydrolytic activity in the neutral hydrolysis of **104** as well. Unusually increasing the loading of catalyst did not directly correlate with increased yield of **100** but did correlate with increased conversion of **104**. Catalyst auto-inhibition may occur at higher concentrations of catalyst loading, preventing it from converting the **104** oligomers into **100**. To better understand the structure-activity relationship, the corresponding systems using ammonium ions were also examined. At 2 mol% catalyst loading (in conjunction with 1 mol% of **107**), hydrolysis promoted by the tetrabutylammonium bromides and iodides **227** and **228** (Table 3.2, entries 1 and 2) proceeded in low yield. Catalysts that decomposed during the reaction, such as **227** and **228** leave a black residue on the remaining PET that is difficult to remove despite washing it with acetone; meaning the conversion is likely artificially reduced due to the mass of the residue remaining on the unreacted **104**. Here, catalyst lipophilicity is also important: the larger tetrahexyl analogue **229** is more active (entry 3). Higher homologues **230** and **231** offer little by way of improvement (entries 4 and 5). The influence of the size of cationic unit was interrogated through the evaluation of large, lipophilic cations incorporating either one (**232** and **233**, entries 6 and 7), two (**234** and **235**, entries 8 and 9) or three (**236**, entry 10) *N*-methyl moieties. The former two classes performed similarly to **229** regardless of size (indicating that while small polar catalysts are not effective in terms of delivery of the terephthalate ion to the PET surface, once a catalyst lipophilicity threshold has been reached, further reductions in polarity do not improve catalysis) while the latter class proved ineffectual and complicated product isolation due to it acting as a surfactant. Ammonium ions equipped with aromatic substituents (*i.e.* **237** and **238**, entries 11 and 12) decomposed and, interestingly, the polar, inner salt carboxylate bearing biomolecules carnitine (**239**) and betaine (**240**) performed similarly to catalysis by terephthalate **107** alone (entries 13 and 14).

Table 3.2: Neutral hydrolysis catalysed by binary ammonium salt-disodium terephthalate systems.

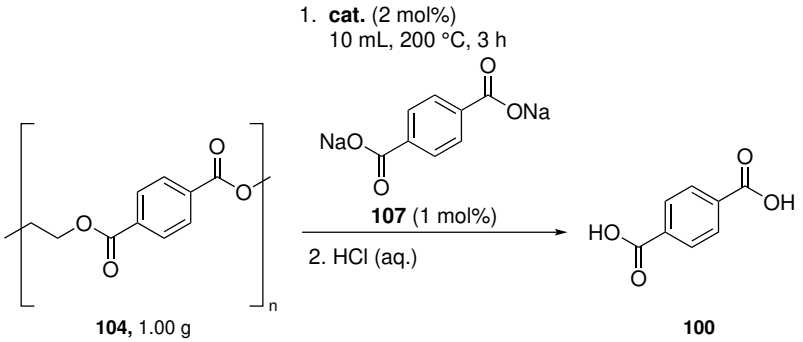

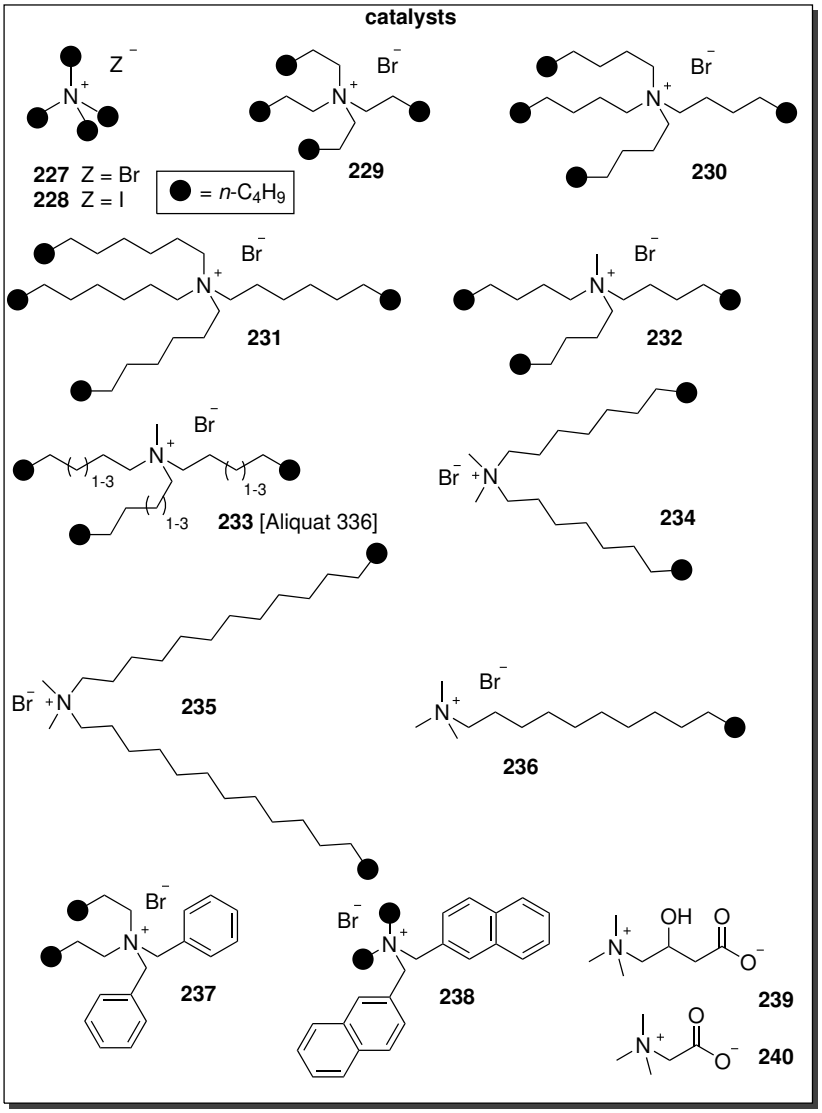

entry	catalyst	conversion (%)	yield[a] (%)
1	**227**[b]	12	17
2	**228**[b]	20	25
3	**229**	73	63
4	**230**	70	65
5	**231**[b]	49	51
6	**232**	65	60
7	**233**	66	62
8	**234**	69	64
9	**235**[c]	71	62
10	**236**	19	14
11	**237**[b]	28	34
12	**238**[b]	47	49
13	**239**[b]	6	10
14	**240**	7	10

[a]Isolated yield after precipitation corrected for additional TPA from the catalyst, confirmed by ^{1}H NMR spectroscopy using 4-iodoanisole as an internal standard (all agreeing within 1.1% [b]Catalyst decomposed. [c]Experiment performed by Dr. Lee Anderson.

Presumably, more lipophilic cations (entries 3–9) facilitate delivery of the anion to the PET surface. Given the results outlined in Table 3.2, it is clear that some of the selected alkyl ammonium salts examined are hydrolytically less stable and less active in the neutral hydrolysis of **104** than the alkyl phosphonium salts (Table 3.1). As mentioned in Section 1.5.1.7, ammonium terephthalate IL catalysts were found to be highly active in the glycolytic depolymersation of PET; so I applied this technology and fabricated novel terephthalate IL catalysts derived from the best catalysts from our assays (*i.e.* **220** and **223**, Table 3.1) to test their efficacy in the neutral hydrolysis of **104**.

3.4 Synthesis of terephthalate IL catalysts

Terephthalate catalysts were synthesised through ion-metathesis mediated by strongly basic hydroxide ion-exchange resin (*i.e.* Amberlite®-OH IRN78) which, *in situ*, can be neutralised using **100**. An example of this synthesis is seen in Scheme 3.3 for the synthesis of **241**.

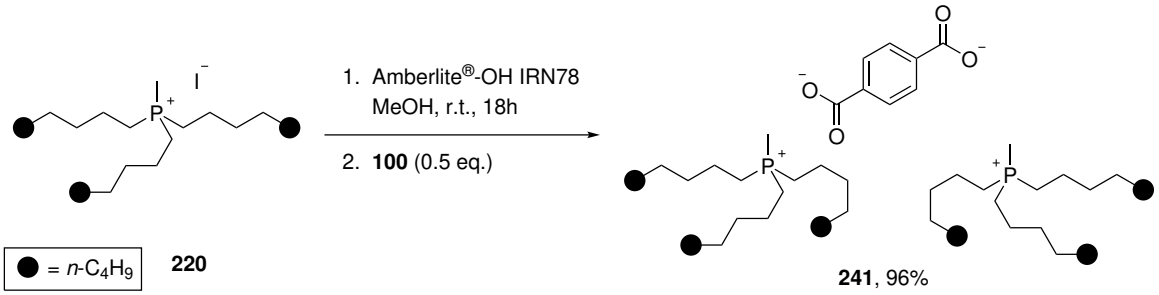

Scheme 3.3: Synthesis of IL catalyst **241**

To truly compare the terephthalate catalysts derived from **220** and **223** in the neutral hydrolysis of PET, literature benchmark catalyst **114** was synthesised using the literature procedure described *via* the direct neutralisation of ammonium salt **242** and phosphotungstic acid (Scheme 3.4).[145]

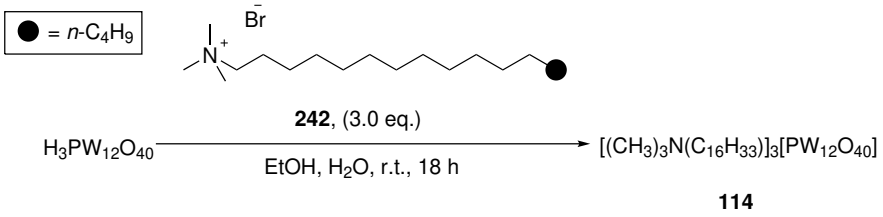

Scheme 3.4: Synthesis of catalyst **114**

Despite **114** only having one phosphorus atom in the catalyst structure, multiple phosphorus signals were detected in the ^{31}P NMR spectroscopic analysis (Figure 3.2). Substituting the solvent changed the ratio between the phosphorus signals considerably. Attempts to purify **114** *via* recrystalisation resulted in the signals changing in intensity. While best possible attempts were made to ensure **114** was pure, it is possible that the cause could be the reformation of the acid[198] or different catalyst architectures.[199]

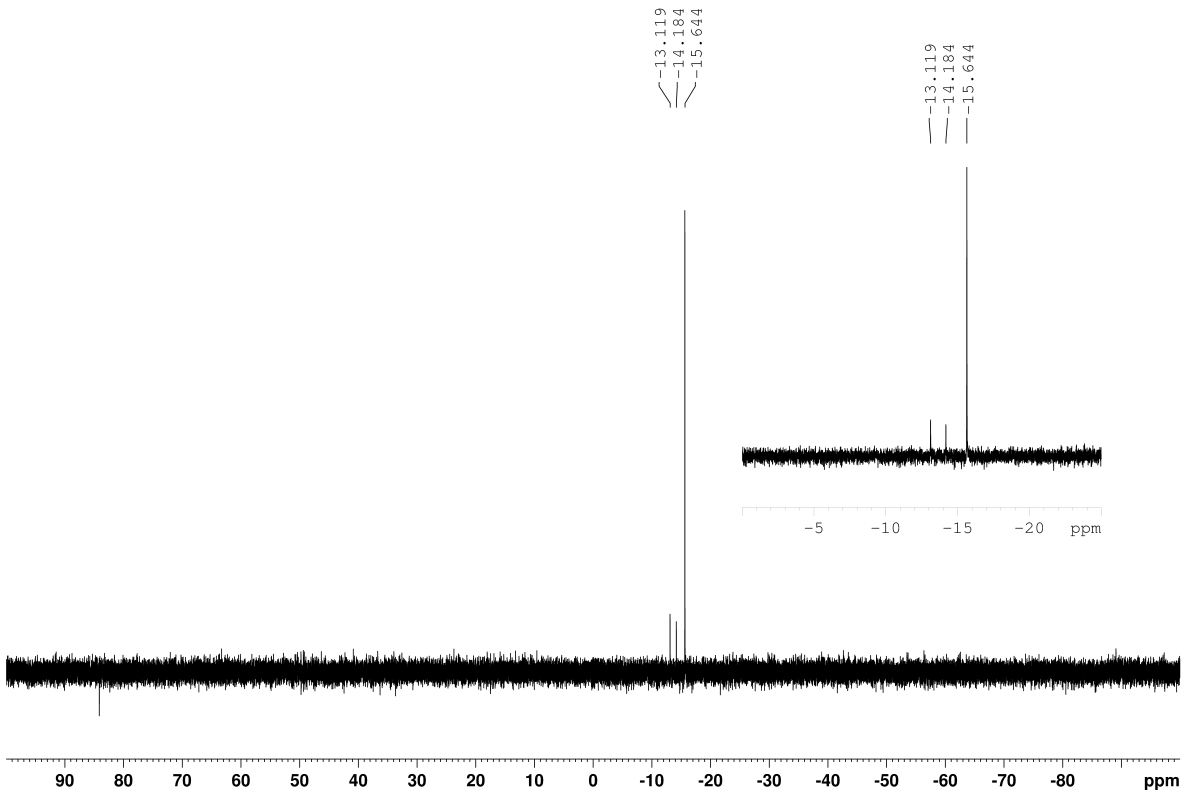

Figure 3.2: A ^{31}P NMR spectrum of **114**

With the novel terephthalate catalysts synthesised along with catalyst **114**, an assay of their performance under ostensibly similar conditions was performed; I also wanted to compare their efficacy relative to zinc acetate (**115**) in the hydrolysis of **104**.[170]

3.5 Terephthalate IL-derived catalyst screening

Next the novel *bis*-tetraalkylphosphonium terephthalate ILs **241** and **243** were prepared and evaluated. These incorporate lipophilic cations to associate with the PET surface, yet do not require ion metathesis to operate. Both exhibited strong activity (Table 3.3, entries 1 and 2) – with **243** proving marginally superior, possibly due to its increased lipophilicity. Either a two-fold increase or reduction in catalyst loading had little effect on yield (entries 3 and 4). At 0.5 mol% levels, these proved significantly superior to benchmark literature catalysts **115** and tungstophosphate **114** (entries 5 and 6). The discrepancy of the conversion (%) being lower than the yield (%) when using **114** is due to it being insoluble in acetone and could not be removed from the residual PET. Use of 50% less solvent (and hence less aqueous waste) was also tolerated (entries 7 and 8). Under optimised conditions involving 1:10 PET: H_2O and 4–5

h reaction times, the outstanding activity of the IL catalyst 30 is apparent: excellent yields of 2 were obtainable using 0.5 mol% catalyst loadings (entries 9 and 10). The effect of the flake size was also probed. Liu *et al*. reported that IL-catalysed PET hydrolysis was exquisitely sensitive to flake size; for instance, TPA yield improved from 10% using 2.5 x 3 mm flakes to 88% with 0.15 x 0.15 mm flakes.[181] I were interested in using larger flakes more commonly obtained from commercial mechanical recycling operations (8–15 mm). Accordingly, PET flakes of various sizes were hydrolysed, catalysed by **243** (0.5 mol%) for 3 h. Interestingly, only a marginal dependence on flake size in these ranges was apparent (entries 11-13) and a 90% yield of **100** could be obtained from 15 mm flakes in 4 h (entry 14). This relative lack of sensitivity to flake size in these ranges could be advantageous from both supply-chain and operational simplicity perspectives.

Table 3.3: Neutral hydrolysis catalysed by IL catalysts **241** and **243**.

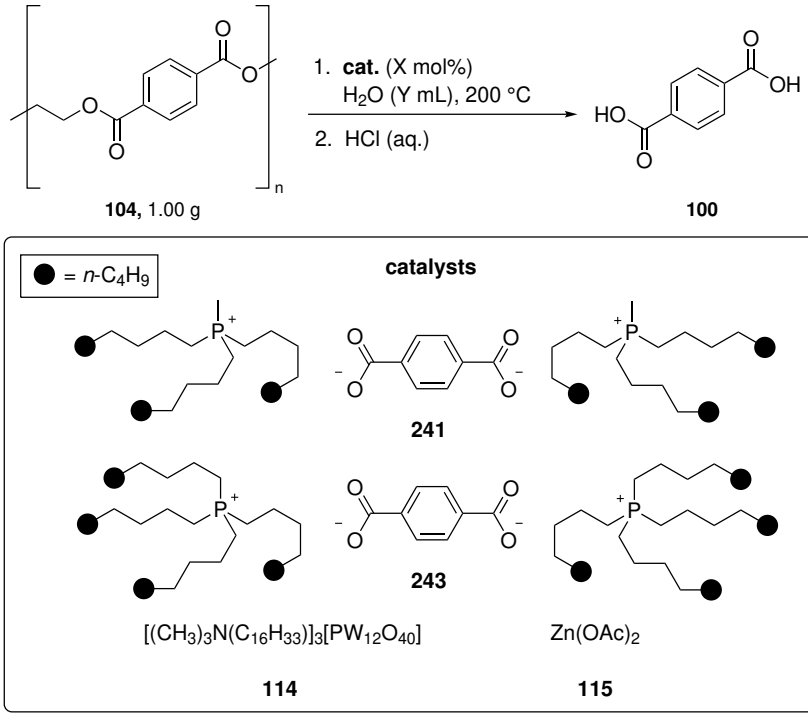

entry	catalyst	loading X (mol%)	Y (mL)	time (h)	flake size (mm x mm)	conversion (%)	yield[a] (%)
1	**241**	1	10	3	5	75	59
2	**243**	1	10	3	5	73	63
3	**243**	2	10	3	5	75	60
4	**243**	0.5	10	3	5	62	61
5	**115**	0.5	10	3	5	41	41
6	**114**	0.5	10	3	5	10	13
7	**243**	1	5	3	5	73	64
8	**243**	0.5	5	4	5	81	74
9	**243**	0.5	10	4	5	95	94
10	**243**	0.5	10	5	5	97	97
11	**243**	0.5	10	3	2.5	65	63
12	**243**	0.5	10	3	10	63	60
13	**243**	0.5	10	3	15	67	63
14	**243**	0.5	10	4	15	99	90

[a]Isolated yield after precipitation corrected for additional TPA from the catalyst, confirmed by ^{1}H NMR spectroscopy using 4-iodoanisole as an internal standard (all agreeing within 1.1%).

The discrepancy between literature results when using **114** under optimal conditions could potentially be due to a lack of agitation in the reaction mixture, meaning IL catalyst **243** may be more efficient in an oven where agitation is possible. A concern I had when conducting these experiments was the lack of knowledge regarding the exact reaction temperature inside the hydrothermal reactor. While I do set the oven to 200 °C, it was difficult to ascertain how quickly the reaction reaches the desired temperature. To remedy this, Prof. Peter Dunne manufactured a bespoke reactor, featuring internal temperature monitoring.

3.6 Temperature variation study method development

A new method was required to be developed for the *ad hoc* reactor. The reactor is significantly different as it is an 11 mL Teflon® coated stainless steel tube (internal diameter = 5 mm) attached with a thermocouple. The reactor was heated using a heating jacket. The hydrothermal batch reactor was 3 times larger in terms of volume and had an internal diameter of 15 mm, and the catalyst could be directly weighed into the Teflon® reactor. The awkward dimensions of the crucible in this setup made direct addition of the catalyst into the reactor untenable, therefore, a delivery method to introduce the catalyst into the reactor was required. Initial attempts to dissolve catalyst **243** in water were unsuccessful, and agitation of the sample resulted in an emulsion. Initial attempts to catalyse the neutral hydrolysis of PET were unsuccessful and resulted in incredibly low yields (Scheme 3.5).

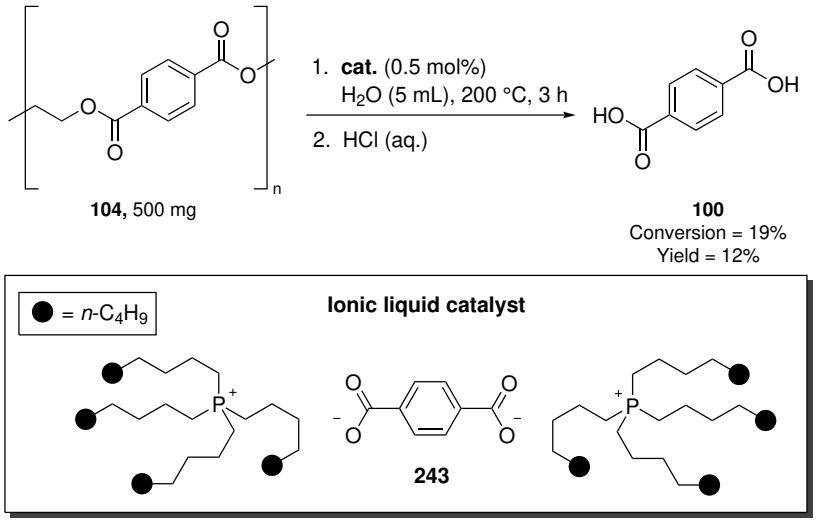

Scheme 3.5: Neutral hydrolysis of PET using a bespoke reactor and introducing the catalyst *via* emulsification

With the little amount of catalyst **243** required to catalyse the reaction and given it is quite viscid, I next attempted to directly weigh the required amount of catalyst onto a single **104** flake that could be dropped directly into the reactor; this method was exceptionally difficult to perform accurately and as a result was never used in the neutral hydrolysis of **104**.

The final attempt to introduce the catalyst was by unscrewing the bottom of the reactor and weighing the catalyst directly into the base plate; this has some associated risk and requires precision, if the catalyst is not directly in the centre of the plate it could extrude into the screw threads that attach the base plate to the reactor. This method was far more reproducible than the other methods of catalyst delivery, however, the associated conversion and yield were far below the values under optimal conditions (Scheme 3.6)

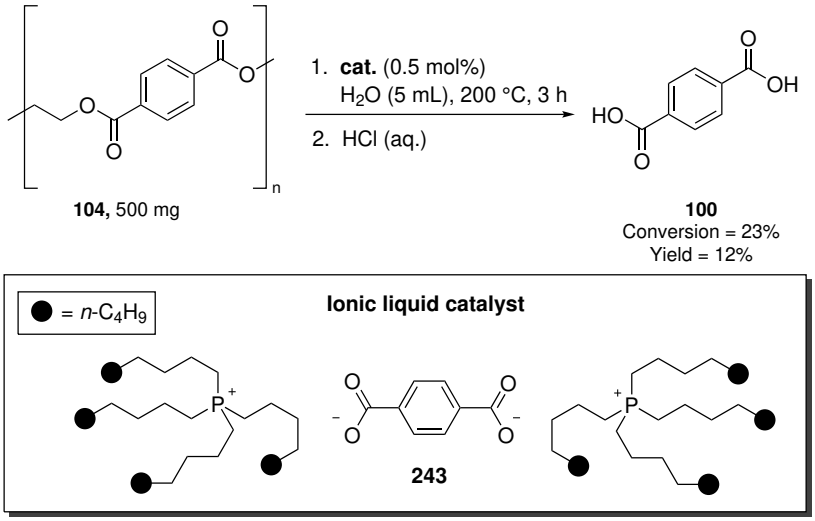

Scheme 3.6: Neutral hydrolysis of PET using a bespoke reactor and introducing the catalyst *via* direct loading

A method to deliver the catalyst into the *ad hoc*-designed reactor to attain conversion and yields ostensibly similar under optimal conditions was unsuccessful. I can still glean some useful information from these experiments, specifically, the only **104** flakes that were consumed were in contact with the catalyst on the bottom of the reactor. This further exemplifies that agitation may be beneficial when employing catalyst **243**. Additionally, the other useful piece of information was that the reaction temperature remained relatively consistent when using the bespoke reactor; while this is not a perfect representation of the hydrothermal reactor in the oven, it gives a certain amount of confidence internal temperature inside the reactor was 200 °C.

As mentioned in Section 1.5.1.6 some catalyst classes such as Zeolites[176] and zinc acetate[170]

could be recycled in the neutral hydrolysis of PET. Before a catalyst is deemed viable for recycling, I first examined if the catalyst decomposes after being used in the neutral hydrolysis of PET.

3.7 Catalyst recyclability

Given that I wash the unreacted solids with acetone to remove any catalyst remaining after the reaction, a sample of acetone used after the reaction (under optimal conditions using **243**) was concentrated *in vacuo* to a white solid. To ascertain if the catalyst decomposes after the neutral hydrolysis of **104** at 200 °C, 4-iodoanisole (15 mg) was added and the entire sample was dissolved in DMSO for ^{1}H NMR spectroscopic analysis. Comparing this to the original and pure spectrum of **243** (Figure 3.3) confirms that the catalyst does decompose after the reaction and therefore is not viable for a reproducibility study (Figure 3.4).

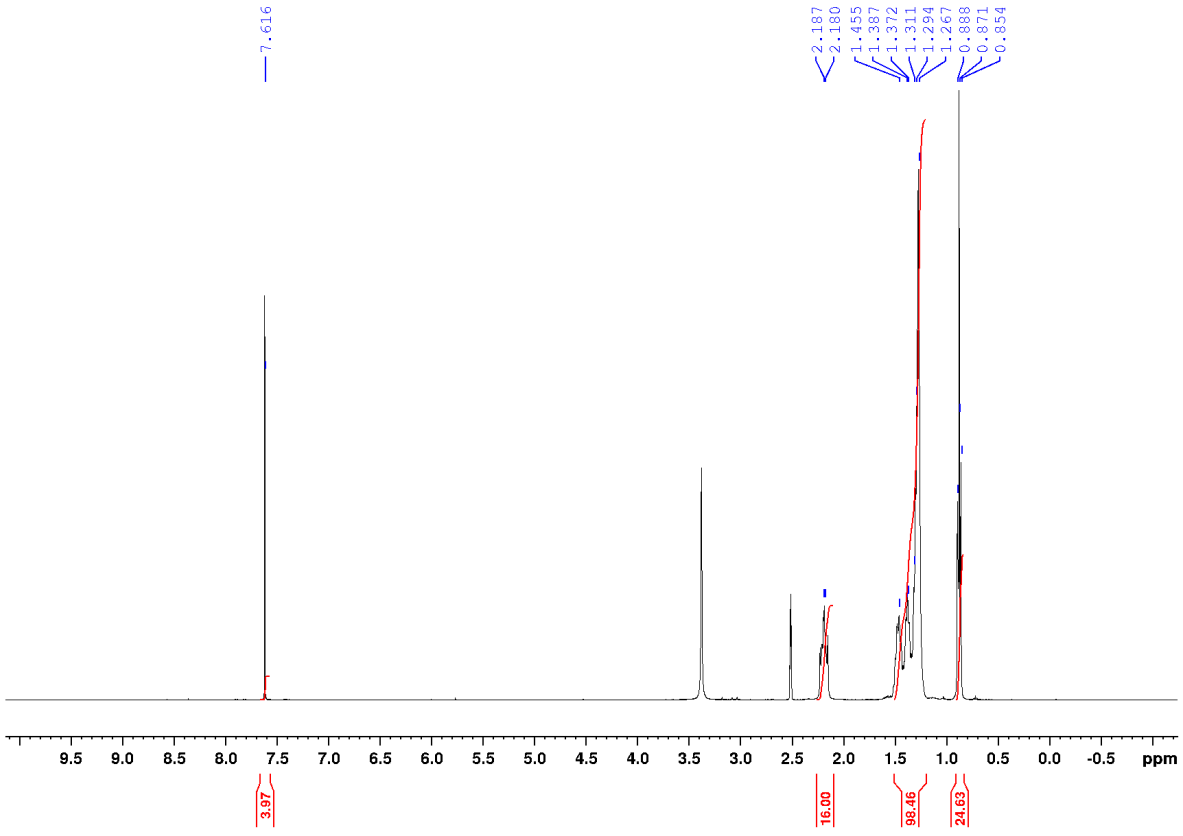

Figure 3.3: A ^{1}H NMR spectrum of **243**

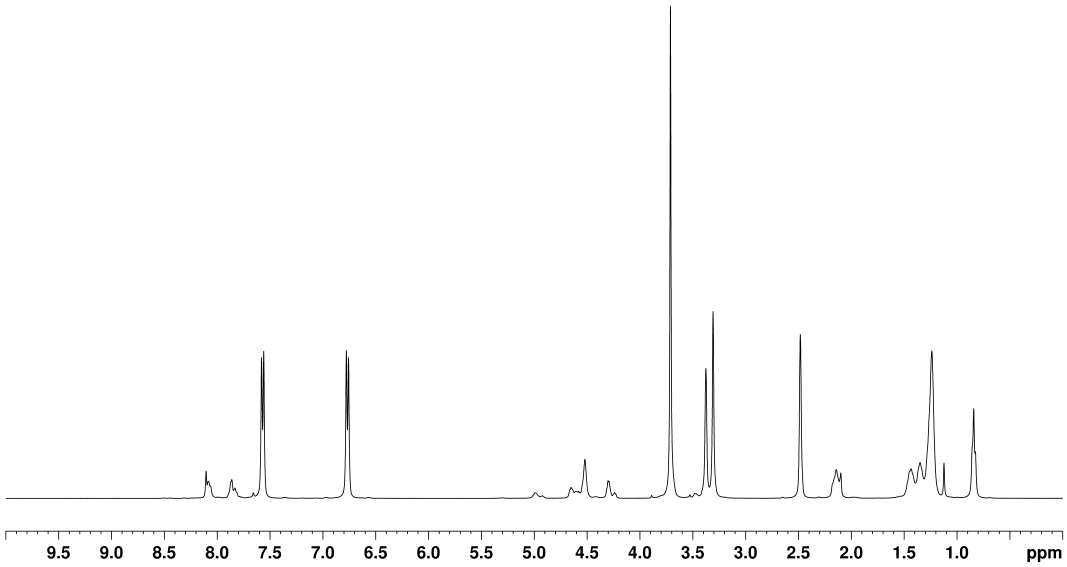

Figure 3.4: A ^{1}H NMR spectrum of **243** after the neutral hydrolysis of **104** at 200 °C

Most likely, the catalyst is undergoing ion-metathesis with oligomers of **104** during the reaction, such as BHET and MHET, among other things.

3.8 Potential mechanism of terephthalate-based ionic liquid catalysts

As mentioned in Section 1.5.1.7, part of the goal of this project was to assess a plausible mechanism for this reaction. I believe it is likely to facilitate the neutral hydrolysis of PET *via* general base catalysis. An example of this is seen in Figure 3.5 when using **243** as the active catalyst.

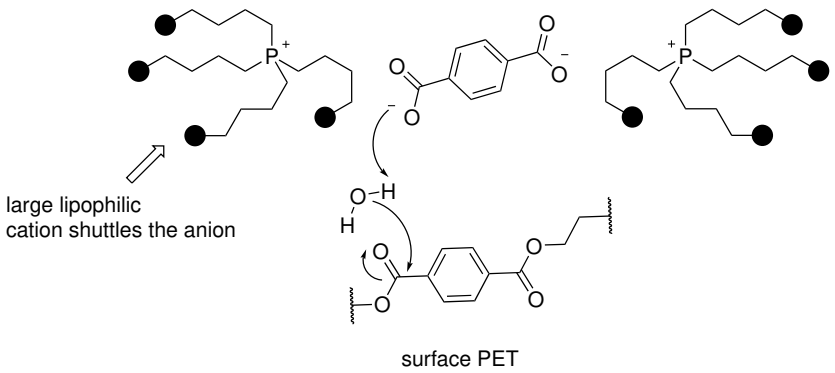

Figure 3.5: Proposed mechanism for the neutral hydrolysis of PET facilitated by **243**

The large lipophilic cations shuttle the terephthalate anion to the PET surface, water is deprotonated at the interface by terephthalate anion and the resulting hydroxide ion attacks the PET. It is worth noting that any generated terephthalic acid can then autocatalyse the reaction further as seen in Section 1.5.1.6.

3.9 Conclusions

In summary, novel *bis*-tetraalkylammonium and phosphonium terephthalate ILs serve as highly active catalysts for the neutral hydrolysis of PET. A structure–activity relationship study demonstrated that the lipophilicity of the cation is key; smaller cations are less able to associate with the PET surface, providing inferior results. The optimal catalyst **243** was highly active at unprecedented loadings (for an IL system) of 0.5 mol% and promoted the formation of TPA in 94% yield after 4 h at 200 °C–significantly outperforming a metal-carboxylate promoter. The use of the terephthalate-anion simultaneously solves the traditional twin problems of product-inhibition through catalyst protonation and contamination of **100** by the catalysts' conjugate acid, and it was found that **243** promoted the hydrolysis of large 15 mm flakes with similar efficiency to 5 mm analogues. Catalyst **243** was demonstrated not to be viable for recycling due to decomposition at 200 °C.

4 | The effect of a phase transfer catalyst structure on the alkaline hydrolysis of poly(ethylene terephthalate)

4.1 Catalyst synthesis

During the work to develop this thesis, Dr. Lee Anderson conducted a screen of various alkyl ammonium catalysts to establish a structure-activity relationship between catalyst structure and its effectiveness in the alkaline hydrolysis of PET. To aid with this investigation, a series of alkyl ammonium PTCs were synthesised with various properties.

The method development and the initial analysis were performed by Dr. Lee Anderson, however, a series of catalysts were synthesised to create a complete assay. The catalysts assessed will be of various architectures, including having dimethylated dialkyl ammonium halides. These catalysts were synthesised *via* the facile alkylation of dimethyl amine **244** with either heptyl bromide to form **245** or nonyl bromide to synthesise **246** (Scheme 4.1).

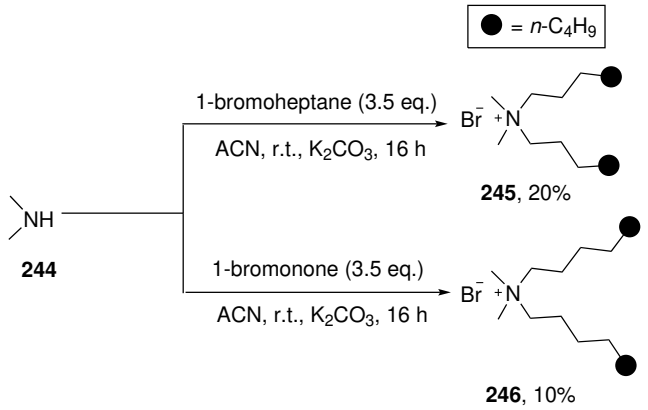

Scheme 4.1: The synthesis of catalysts **245** and **246** from dimethylamine.

The catalysts derived from pyridine **247** were alkylated either with methyl iodide to synthesise **248** or with 1-bromooctane to prepare **249** (Scheme 4.2A). Freshly distilled isoquinoline (**250**)

was reacted with 1-bromoheptane in the low-yielding synthesis of **251** (Scheme 4.2B)

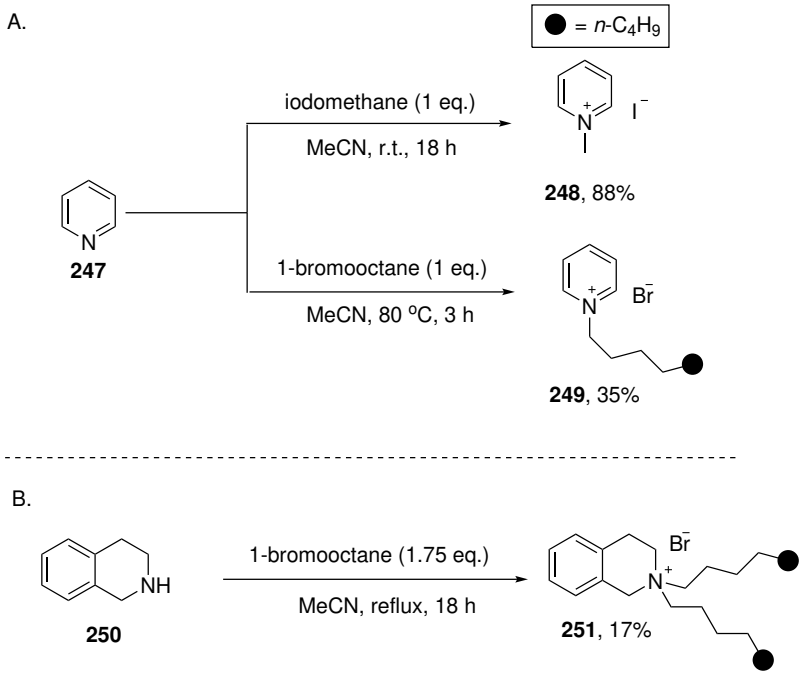

Scheme 4.2: **A**: The synthesis of catalysts **248** and **249**. **B**: The synthesis of PTC **251**.

With a range of catalysts synthesised, Dr. Anderson conducted a screen of various alkyl ammonium and phosphonium halides.

4.2 A summary of the catalyst screen in the alkaline hydrolysis of PET

Dr. Anderson first conducted a control experiment where no catalyst was added in the hydrolysis of **104**; **100** was attained in minimal yield (Table 4.1, entry 1). Catalyst **252** was the best performing symmetrical alkyl ammonium of the assay (entry 2); it also exhibited interesting behaviour, the catalyst was partially soluble, and the insoluble portion was very finely dispersed. Concerning The dimethyl-dialkyl catalysts, **253**, **245**, **254** and **246**, catalyst **245** was the best performing, due to it being the most lipophilic catalyst soluble in the reaction medium (entries 3-6). Pyridyl catalysts **248** and **249** were inefficient in the hydrolysis of PET (entries 7 and 8) as was the Tetrahydroisoquinoline-derived catalyst (entry 9).

Table 4.1: The alkaline hydrolysis of PET conducted by Dr. Lee Anderson

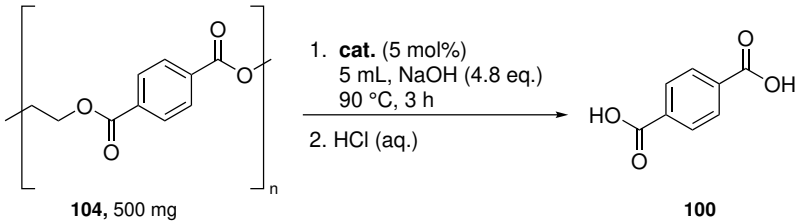

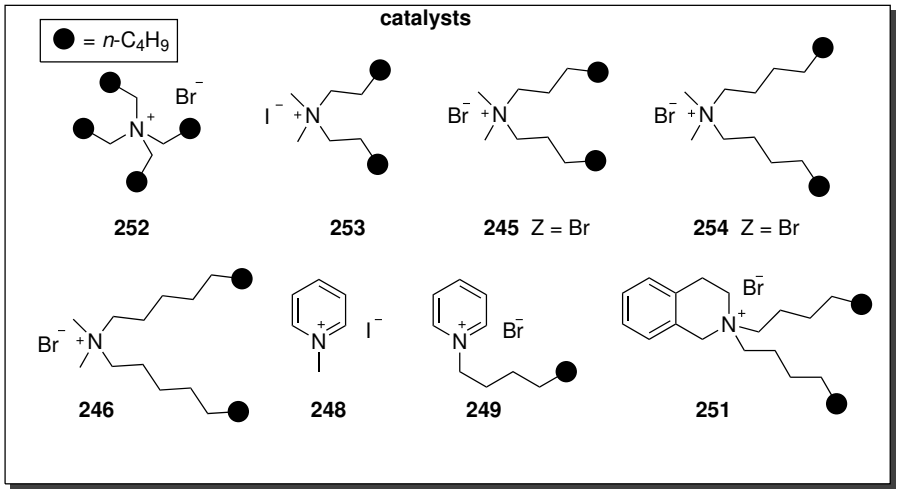

entry	catalyst	solubility under reaction conditions	yield[a] (%)
1	-	-	4
2	**252**	finely dispersed	68
3	**253**	soluble	41
4	**245**	soluble	82
5	**254**	finely dispersed	71
6	**246**	insoluble	58
7	**248**[b]	soluble	4
8	**249**[b]	insoluble	14
9	**251**	insoluble	41

Experiments performed by Dr. Lee Anderson. [a]Isolated yield after precipitation, confirmed by ^{1}H NMR spectroscopy using 4-iodoanisole as an internal standard. [b]Catalyst decomposed.

Dr. Anderson also discovered it was possible to fine-tune the solubility of select PTCs by substituting the halide anion. The iodide analogue of **245** (*i.e.* **255**) was insoluble in the reaction medium, which was ultimately harmful to its' activity; while the chloride derivative of **254** (*i.e.* **256**) performed considerably better in the alkaline hydrolysis of PET, due to an increase in catalyst solubility.

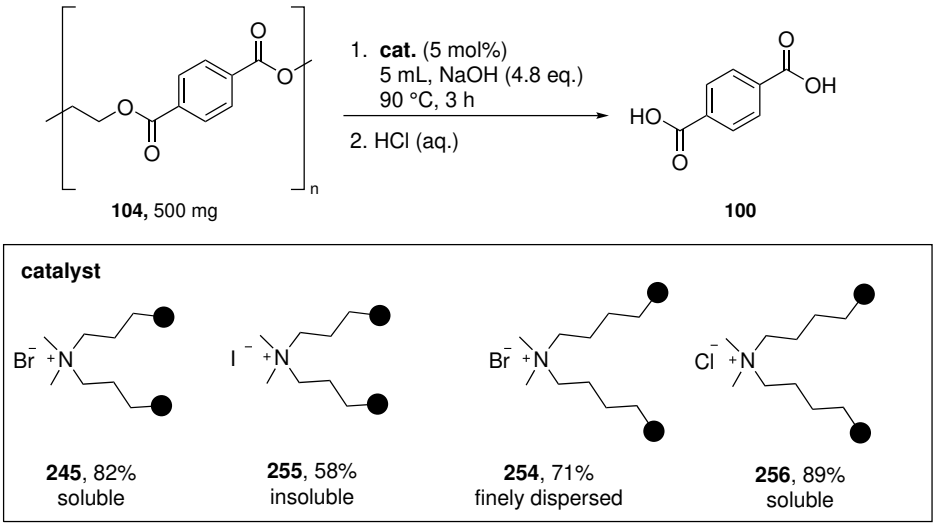

Scheme 4.3: The effect of changing the anion in the alkaline hydrolysis of PET, performed by Dr. Lee Anderson.

Dr. Anderson later optimised these conditions using **245**, by increasing the concentration of the reaction, he could achieve near quantitative yields of **100** using only 1 mol% of catalyst (Scheme 4.4)

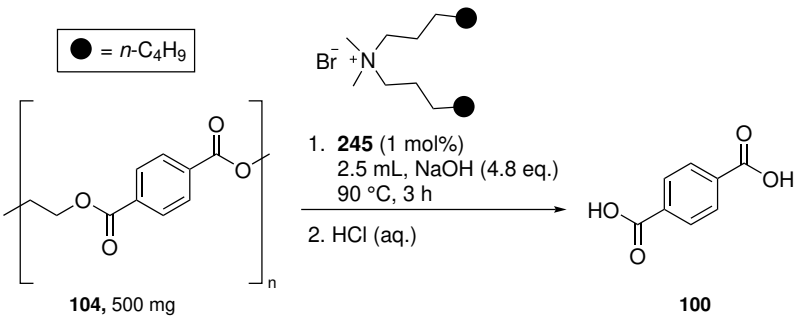

Scheme 4.4: Alkaline hydrolysis conducted by Dr. Lee Anderson under optimised conditions.

I wanted to examine the possibility of reducing the equivalents of sodium hydroxide used in the reaction, this could would be beneficial in making this methodology more economically viable and minimise waste. This would improve the industrial viability of this process significantly; since depolymerisation is performed on the scale of millions of metric tonnes, the cost of sodium hydroxide and post-processing would be significant.

4.3 Decreased sodium hydroxide loadings in the alkaline hydrolysis of PET

Catalyst **257** (*i.e*. the chloride analogue of the best performing symmetrical catalyst Table 4.1) and **256** were identified as optimal catalyst candidates for this assay because they are both soluble in the reaction medium and do not decompose. To assess both catalysts equally and to achieve maximum efficacy, I performed the experiments under the optimal conditions outlined in Scheme 4.4.[182,197] The yield of **100** was confirmed by ^{1}H NMR spectroscopy as per the protocol outlined in Section 3.1. To ensure reproducibility and accuracy, dried sodium hydroxide was used; conditions such as stirring speed and exact temperature were identical to those used by Dr. Lee Anderson. The initial experiment to hydrolyse **104** using half the concentration of sodium hydroxide, relative to amount initially used in Dr. Andersons' assay (Table 4.1), and using 1 mol% of catalyst **257** resulted in **100** being isolated in moderate yield (Table 4.2, entry 1). An increase in catalyst loading to 2.5 mol% resulted in a significant increase in yields of **100** (entry 2); however, further increasing catalyst loading up to 5 mol% furnished **100** similar yields to when 1 mol% catalyst loading was used (entry 3). It is possible that catalyst aggregation or loss of solubility can occur if the catalyst concentration is too high; this effect can be deleterious to the catalyst's activity. Increasing the reaction time led to an increase in the yield of **100** when **257** was used (entry 4). Similar to the results obtained when performing the experiments for 3 h (*i.e*. entries 1-3), increasing the catalyst loading to 2.5 mol% promoted formation of **100** in higher yields, while 5 mol% catalyst loading was detrimental to activity (entry 6). Attempting to substitute catalyst **257** for catalyst **256** resulted in significantly lower yields relative to when **257** was examined under the same conditions (entry 7).

Table 4.2: The alkaline hydrolysis of PET using a reduced concentration of sodium hydroxide

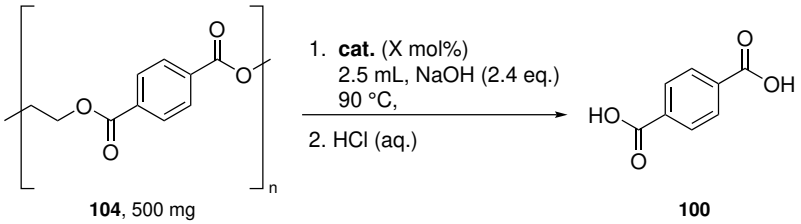

104, 500 mg

100

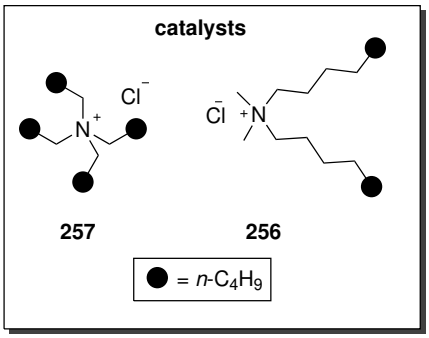

entry	catalyst	catalyst loading (mol%)	time (h)	yield[a] (%)
1	**257**	1	3	61
2	**257**	2.5	3	73
3	**257**	5	3	66
4	**257**	1	6	76
5	**257**	2.5	6	81
6	**257**	5	6	70
7	**256**	2.5	3	44

Catalysts synthesised by Dr. Lee Anderson [a]Isolated yield after precipitation confirmed by ^{1}H NMR spectroscopy using 4-iodoanisole as an internal standard.

With these results, it is clear that the alkaline hydrolysis of **104** using 2.4 equivalents of sodium hydroxide is possible, and the initial screen proved to be successful. Further development work will be required to achieve isolated yields of **100** >90%.

4.4 Conclusions

A series of catalysts were synthesised for the alkaline hydrolysis of PET. Dr. Lee Anderson conducted a thorough screen of various ammonium halides; this was used to develop an optimised method in which 1 mol% of catalyst can be used. Reducing the equivalents of sodium hydroxide under optimised conditions was congruent was moderate to high yields of **100**. Considering the results of this study, it is clear that additional catalyst development is required to further improve the yield of **100** when using 2.4 equivalents of sodium hydroxide. Additional examination of the effects when employing **104** flake of different sizes would also be needed to expand the current scope of alkaline hydrolysis.

5 | Experimental

General

Proton nuclear magnetic resonance spectra were recorded on a Bruker DPX (400 MHz)and Bruker Avance II (600 MHz) using $CDCl_3$ and DMSO-d_6, with chemical shift data referenced relative to residual resonances of the deuterated solvent (δ_H = 7.26, 2.50 ppm and 3.31 ppm respectively). Chemical shifts are reported in ppm, and coupling constants (J) are recorded in Hertz (Hz) and ^{13}C NMR (100.9 MHz, 150.9 MHz) spectra were recorded on the same instruments with total proton decoupling. Fluorine NMR spectra were recorded on the Bruker DPX400 machine (376.5 MHz). Phosphorous NMR spectra were recorded on the same instruments (162.0 MHz) HSQC, HMBC, TOCSY and NOE experiments were used to aid assignments of NMR peaks when required. Infrared spectra were obtained as neat solids on a Perkin-Elmer Spectrum100 FT-IR. All melting points are uncorrected. Column and flash chromatography were carried out using silica gel, particle size 0.04-0.063 mm. TLC analysis was performed using F254 silica gel plates and visualised by either UV irradiation, $KMnO_4$ or ninhydrin staining. Infrared spectra were obtained on a Perkin Elmer Spectrum 100 FT-IR spectrometer equipped with a universal ATR sampling accessory. ESI mass spectra were acquired using a Waters Micromass LCT-time of flight mass spectrometer (TOF), interfaced to a Waters 2690 HPLC. The instrument was operated in either positive or negative mode as required. Triethylamine, piperidine and morpholine were distilled from calcium hydride. Tetrachlorophthalic anhydride (TCPA) was recrystallised from acetic anhydride. *Para*-nitrophenol was recrystallised from toluene. Analytical CSP-HPLC was performed using Acquity UPC2 step 3 - Trefoil CEL2 (2.5 µm, 3.0 x 150 mm) with a gradient eluent. Anhydrous THF, CH_2Cl_2, MeCN and Et2O were acquired from a Pure Solv MD-4EN solvent purification system. Colourless poly(ethylene terephthalate) bottles were purchased from a local large supermarket chain and cut into flakes (*ca.* 5 mm square, Tesco® brand, Slievenamon, still Irish spring water). Anion exchange

resin Amberlite® OH IRN78 (Supelco, strongly basic, total exchange capacity (OH) 1.25 eq/L) was purchased from Sigma Aldrich. Anion exchange resin Amberlite® IRA-900 chloride form (Supelco, total exchange capacity (Cl) 1.0 eq/L) was purchased from Sigma Aldrich. Unless otherwise stated, all chemicals were obtained from commercial sources and used as received. For clarity, the numbering system associated with the assignment of the ^{1}H NMR peaks did not follow the IUPAC nomenclature system.

2,3,4,5-tetrachloro-6-(isopropoxycarbonyl)benzoic acid (122)

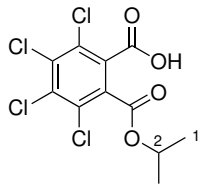

To a 100 mL round-bottomed flask (RBF) containing a stir bar and recrystalised TCPA (3.66 g, 12.8 mmol) was added *i*-PrOH (30 mL) and NEt_3 (1.6 mL, 11 mmol). The solution was stirred at room temperature for 16 h. HCl (2 N, 50 mL) was added, and the aqueous mixture was extracted with Et_2O (3 x 50 mL). The combined organic extracts were dried over $MgSO_4$, and the solvent was removed *in vacuo* to give product **122** as an off-white powder (3.90 g, 11.6 mmol, 91%).

Spectral data for this compound were consistent with those in the literature.[27]

δ_H (400 MHz, $CDCl_3$)	5.31 (sept, 1H, J = 6.2, H-2), 1.38 (d, 6H, J = 6.2, H-1) ppm
HRMS (m/z – ESI^-):	Found: 342.9103 (M^{-H}) $C_{11}H_7Cl_4O_4$ Requires: 342.9104

isopropyl 2-((1-(tert-butoxy)-1-oxo-3-phenylpropan-2-yl)carbamoyl)-3,4,5,6-tetrachlorobenzoate (124)

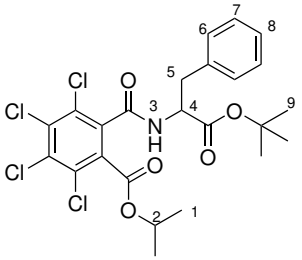

To a 250 mL RBF containing a magnetic stirrer and DL-phenylalanine (3.976 g, 24.0 mmol) was added *tert*-butylacetate (60 mL) *via* syringe under Ar atmosphere and the resulting suspension was cooled to 0 °C before concentrated $HClO_4$ (70%, aq, 3 mL, 32.58 mmol) was added dropwise *via* syringe. The reaction was allowed to warm to room temperature with stirring. After 16 h, aqueous HCl (1 N, 70 mL) was added, and the reaction mixture was adjusted to pH 9.0

using aqueous K_2CO_3 (10% w/v). The suspension was filtered, and the remaining salts were washed with CH_2Cl_2 (2 x 80 mL). The organic layer was separated, and the aqueous phase was extracted with CH_2Cl_2 (3 × 80 mL). The combined extracts were dried over anhydrous $MgSO_4$ and then concentrated *in vacuo*. Product **123** was obtained as a yellow oil and carried forward without further purification.[a] In a separate 250 mL RBF, **122** (3.90 g, 11.6 mmol), EDC·HCl (2.66 g, 13.92 mmol) and *N*-hydroxysuccinimide (1.60 g, 13.92 mmol) were stirred in CH_2Cl_2 (80 mL) under an Ar atmosphere for 1h. The reaction was cooled to 0 °C and **123** was dissolved in CH_2Cl_2 (20 mL) and added dropwise to the reaction mixture. The reaction was allowed to warm to room temperature after 16 h. H_2O (340 mL) was added, and the organic layer was separated. The aqueous phase was extracted with CH_2Cl_2 (3 x 100 mL), and the combined organic extracts were washed with K_2CO_3 (10% w/v, 340 mL) and brine (340 mL) before being dried with $MgSO_4$. The solvent was removed *in vacuo* and the resulting oil was triturated with Et_2O. Filtration of the resulting mixture obtained the product **124** as a white powder (4.02 g, 15.6 mmol, 65%). Spectral data for this compound were consistent with those in the literature.[27]

[a]Product too volatile to be exposed to the low pressure required to remove all solvent.

δ_H (400 MHz, $CDCl_3$) 7.30-7.21 (m, 5H, H-6, H-7, H-8), 6.48 (d, 1H, *J* = 7.6, H-3), 5.22 (sept, 1H, *J* = 6.0, H-2), 4.9 (m, 1H, H-4), 3.24 (dd, 1H, *J* = 6.5, 13.9, H-5a), 3.12 (dd, 1H, *J* = 6.5, 13.9, H-5b), 1.38 (s, 9H, H-9), 1.35 (d, 3H, *J* = 6.0, H-1), 1.33 (d, 3H, *J* = 6.0, H-1) ppm

HRMS (m/z – ESI+): Found: 570.0374 (M^{+Na}) $C_{24}H_{25}Cl_4NO_5Na$ Requires: 570.0379

(2,3,4,5-tetrachloro-6-(isopropoxycarbonyl)benzoyl)phenylalanine (126)

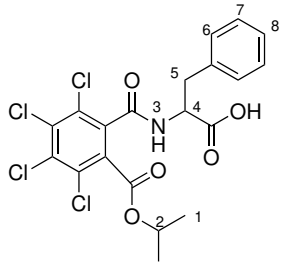

To a 250 mL RBF containing a magnetic stirrer and **124** (4.02 g, 7.5 mmol) was added CH_2Cl_2 (30 mL) and TFA (30 mL). The reaction mixture was stirred at room temperature. After 4 h, the solvent was removed *in vacuo* to yield **126** as a white solid (3.06 g, 7.3 mmol, 97%).

Spectral data for this compound were consistent with those in the literature.[27]

δ_H (400 MHz, $CDCl_3$) 9.14 (d, 1H, J = 8.1 Hz, H-3), 7.33-7.19 (m, 5H, H-6, H-7, H-8), 4.98 (sept, 1H, J = 6.3, H-2), 4.62 (ddd, 1H, J = 8.7, 8.1, 5.8, H-4), 3.04 (dd, 1H, J = 13.9, 5.8, H-5a), 2.92 (dd, 1H, J = 13.9, 8.7, H-5b), 1.22 (app t, 6H, H-1) ppm

HRMS (m/z – ESI+): Found: 513.9754 (M^{+Na}) $C_{20}H_{17}Cl_4NO_5Na$ Requires: 513.9753

(2,3,4,5-tetrachloro-6-(isopropoxycarbonyl)benzoyl)phenylalanine (41)

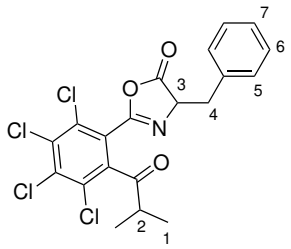

To a 100 mL RBF containing a magnetic stirrer and **126** (3.06 g, 7.3 mmol) was added anhydrous CH_2Cl_2 (30 mL) under Ar atmosphere. EDC·HCl (1.54 g, 8.0 mmol) was added in one portion, and the reaction was stirred for 1 h. The reaction was diluted with CH_2Cl_2 (30 mL) and washed with water (2 x 30 mL). The combined organic phase was collected and then removed *in vacuo*. The resulting residue was purified by passage through a plug of silica to yield **41** as a white powder (2.81 g, 5.9 mmol, 81%).

Spectral data for this compound were consistent with those in the literature.[27]

δ_H (400 MHz, $CDCl_3$) 7.32-7.22 (m, 5H. H-7, H-6, H-5), 5.20 (septet, 1H, J = 6.2, H-2), 4.61 (dd, 1H, J = 6.8, 5.1, H-3), 3.36 (dd, 1H, J = 14.3, 5.1, H-4a), 3.22 (dd, 1H, J = 14.3, 6.8. H-4b), 1.31 (d, 6H, J = 6.2, H-1) ppm

HRMS (m/z – ESI+): Found: 513.9754 (M^{+Na}) $C_{20}H_{17}Cl_4NO_5Na$ Requires: 513.9753

4,5,6,7-tetrachloro-2-(1-oxo-3-phenyl-1-(piperidin-1-yl)propan-2-yl)isoindoline-1,3-dione (127)

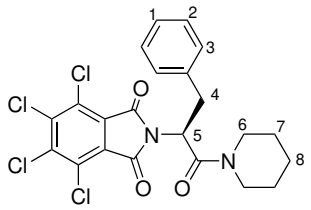

Under an atmosphere of Ar, **41** (47.5 mg, 0.1 mmol) and **149** (3.1 mg, 0.005 mmol) were dissolved in toluene (1 mL). *Para*-nitrophenol (13.9 mg, 0.1 mmol) and **98** (0.8 mg, 0.005 mmol) were added, and the mixture was stirred for 24 h. The reaction vessel was cooled to 0 °C before $CHCl_3$ (1 mL) was added. Piperidine (20 µL, 0.20 mmol) was added dropwise, and the mixture was stirred for 30 min. The solution was allowed to warm to room temperature and was stirred for 12 h. The solution was poured into HCl (1 M, 30 mL), and CH_2Cl_2 (20 mL), the aqueous phase was then extracted with CH_2Cl_2 (3 x 10 mL). The organic layers were combined before being washed with NaOH (aq, 1 M, 30 mL) and then brine (30 mL). The organic layer was separated and the solvent was removed *in vacuo*. The resulting oil was purified by column chromatography (8:2 *n*-hex/EtOAc) to afford product **127** as a white powder (47 mg, 0.094 mmol, 94%). Mp. 209-210 °C (CH_2Cl_2).

CSP-HPLC analysis. Acquity UPC^2 step 3 – Trefoil CEL2 (2.5 µm, 3.0 x 150 mm), gradient eluent A = CO_2, B = EtOH/CH_3CN (1:1, *v:v*); column temperature 30 °C, UV detection at 254 nm with PDA detector, retention times: 6.0 min and 4.5 min, 64% *ee*.

δ_H (400 MHz, $CDCl_3$) 7.26-7.18 (m, 5H, H-1, H-2, H-3), 5.39 (dd, 1H, *J* = 10.8, 5.5, H-5), 3.83 (dd, 1H, *J* = 14.4, 10.8, H-4a), 3.82-3.62 (m, 5H, H-4b, H-6), 1.65-1.46 (m, 6H, H-7, H-8) ppm

δ_C (101 MHz, $CDCl_3$) 166.3 (C=O), 163.6 (C=O), 140.3 (q), 136.8 (q), 129.9, 128.9,

128.9, 127.3, 127.2 (C=O), 54.1, 47.1, 44.0, 34.4, 26.6, 25.6, 24.5 ppm

HRMS (m/z – ESI+): Found: 520.9964 (M^{+Na}) $C_{22}H_{18}Cl_4N_2O_3Na$ Requires: 520.9960

ν_{max} (neat)/cm^{-1}: 2940, 2958, 1780, 1721, 1650, 1444, 1349, 1250, 1199, 1119, 1021, 911, 852, 737

4,5,6,7-tetrachloro-2-(1-morpholino-1-oxo-3-phenylpropan-2-yl)isoindoline-1,3-dione (151)

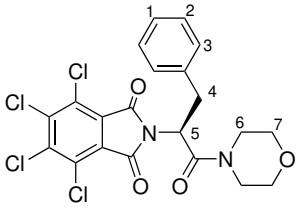

Method I: Using a phase-transfer catalyst

Under an atmosphere of Ar, **41** (47.5 mg, 0.1 mmol) and **149** (3.1 mg, 0.005 mmol) were dissolved in toluene (1 mL). *Para*-nitrophenol (13.9 mg, 0.1 mmol) and **98** (0.8 mg, 0.005 mmol) were added, and the mixture was stirred for 4 h. The reaction vessel was cooled to 0 °C and $CHCl_3$ (1 mL) was added. Morpholine (20 µL, 0.20 mmol) was added dropwise, and the mixture was stirred for 30 min. The solution was allowed to warm to room temperature and was stirred for 16 h. The solution was poured into HCl (1 M, 30 mL) and extracted with CH_2Cl_2 (20 mL). The aqueous phase was extracted with CH_2Cl_2 (3 × 10 mL). The organic layers were combined before being washed with NaOH (aq, 1 M, 30 mL) and brine (30 mL). The organic layer was separated and the solvent was removed *in vacuo*. The resulting oil was purified by column chromatography (8:2 *n*-hex/EtOAc) to afford product **151** as an off-white powder (47 mg, 0.094 mmol, 94%).

CSP-HPLC analysis. Acquity UPC^2 step 3 – Trefoil CEL2 (2.5 µm, 3.0 x 150 mm), gradient eluent A = CO_2, B = EtOH/CH_3CN (1:1, *v:v*); column temperature 30 °C, UV detection at 254 nm with PDA detector, retention times: 6.33 min and 4.69 min, 58% *ee*.

Method II: Using an ion-pair catalyst

Under an atmosphere of Ar, **41** (47.5 mg, 0.1 mmol) and *para*-nitrophenol (13.9 mg, 0.1 mmol) were dissolved in anhydrous CH_2Cl_2(1 mL). Catalyst **159** (3.4 mg, 0.005 mmol) was added, and the mixture was stirred for 10 min. The reaction vessel was cooled to 0 °C and $CHCl_3$ (1 mL) was added. Morpholine (20 µL, 0.20 mmol) was added dropwise, and the mixture was stirred for 30 min. The solution was allowed to warm to room temperature and was stirred for 48 h. The solution was poured into HCl (1 M, 30 mL) and CH_2Cl_2 (20 mL). The aqueous phase was extracted with CH_2Cl_2 (3 × 10 mL). The organic layers were combined before being washed with NaOH (aq, 1 M, 30 mL) and brine (30 mL). The organic layer was separated and the solvent was removed *in vacuo*. The resulting oil was purified by column chromatography (8:2 *n*-hex/EtOAc) to afford product **151** as an off-white powder (48 mg, 0.098 mmol, 98%).

CSP-HPLC analysis.	Acquity UPC^2 step 3 – Trefoil CEL2 (2.5 µm, 3.0 x 150 mm), gradient eluent A = CO_2, B = EtOH/CH_3CN (1:1, *v:v*); column temperature 30 °C, UV detection at 254 nm with PDA detector, retention times: 6.27 min and 4.66 min, 50% *ee*.

Method III: Using a betaine catalyst

Under an atmosphere of Ar, **41** (47.5 mg, 0.1 mmol) and *para*-nitrophenol (15.4 mg, 0.11 mmol) were dissolved in anhydrous CH_2Cl_2(1 mL). The solution was cooled to −25 °C before catalyst **199** (3.0 mg, 0.005 mmol) was added and the mixture was stirred for 1 h. CH_2Cl_2 (1 mL) and morpholine (20 µL, 0.20 mmol, dropwise) were added, and the mixture was stirred for 30 min. The solution was allowed to warm to room temperature and was stirred for 16 h. 1,8-Diazabicyclo[5.4.0]undec-7-ene (DBU) was added, and the reaction was stirred for 30 min before being poured into HCl (1 M, 30 mL) and CH_2Cl_2 (20 mL). The aqueous phase was extracted with CH_2Cl_2 (3 × 10 mL). The organic layers were combined before being washed with NaOH (aq, 1 M, 30 mL) and brine (30 mL). The organic layer was separated and the solvent was removed *in vacuo*. The resulting oil was purified by column chromatography (8:2 *n*-hex/EtOAc) to afford product **151** as an off-white powder (46 mg, 0.096 mmol, 96%).

CSP-HPLC analysis.	Acquity UPC^2 step 3 – Trefoil CEL2 (2.5 µm, 3.0 x 150 mm), gradient eluent A = CO_2, B = EtOH/CH_3CN (1:1, *v:v*); column temperature 30 °C, UV detection at 254 nm with PDA detector, retention times: 6.28 min and 4.65 min, 77% *ee*.

Method IV: Using a betaine catalyst with a BINOL-derived additive

Under an atmosphere of Ar, **41** (47.5 mg, 0.1 mmol) and *para*-nitrophenol (15.4 mg, 0.11 mmol) were dissolved in anhydrous CH_2Cl_2(9 mL). The solution was cooled to −30 °C before a stock solution of catalyst **199** (3.0 mg, 0.005 mmol) and **203** (2.2 mg, 0.005 mmol) in CH_2Cl_2 (1 mL) was added and the mixture was stirred for 16 h. CH_2Cl_2 (1 mL) and morpholine (20 µL, 0.20 mmol, dropwise) were added, and the mixture was stirred for 30 min. The solution was allowed to warm to room temperature and was stirred for 16 h. DBU was added, and the reaction was stirred for 30 min before being poured into HCl (1 M, 30 mL) and CH_2Cl_2 (10 mL). The aqueous phase was extracted with CH_2Cl_2 (3 × 10 mL). The organic layers were combined before being washed with NaOH (aq, 1 M, 30 mL) and brine (30 mL). The organic layer was separated and the solvent was removed *in vacuo*. The resulting oil was purified by column chromatography (8:2 *n*-hex/EtOAc) to afford product **151** as an off-white powder (48 mg, 0.096 mmol, 96%). Mp. 205-209 °C(CH_2Cl_2).

CSP-HPLC analysis.	Acquity UPC^2 step 3 – Trefoil CEL2 (2.5 µm, 3.0 x 150 mm), gradient eluent A = CO_2, B = EtOH/CH_3CN (1:1, *v:v*); column temperature 30 °C, UV detection at 254 nm with PDA detector, retention times: 6.26 min and 4.65 min, 83% *ee*.
δ_H (400 MHz, $CDCl_3$)	7.26-7.18 (m, 5H, H-1, H-2, H-3), 5.39 (dd, 1H, J = 10.8, 5.5, H-5), 3.79-3.33 (m, 10H, H-4, H-6, H7) ppm
δ_C (101 MHz, $CDCl_3$)	166.6 (C=O), 163.3 (C=O), 140.4 (q), 136.3 (q), 129.9, 129.6, 128.9, 128.8, 127.3, 127.0 (C=O), 125.3, 53.4, 34.6 ppm

HRMS (m/z – ESI+): Found: 522.9749 (M^{+Na}) $C_{21}H_{16}Cl_4N_2O_4Na$ Requires: 522.9762

ν_{max} (neat)/cm^{-1}: 3245, 2924, 2851, 1716, 1649, 1468, 1348, 1110, 1039, 838, 737

General procedure I: Synthesis of benzyl bromide derived catalysts

To a 50 mL round bottom flask containing a magnetic stirrer was added quinine **258** (324 mg, 1 mmol) and benzyl bromide (1.2 mmol). The apparatus was flushed with Ar before being fitted with a septum and balloon of Ar. Toluene (10 mL) was added *via* syringe and the solution was then heated to 80 °C for 2 h. The reaction mixture was allowed to cool to room temperature, Et_2O (20 mL) was added, and the resulting precipitate was filtered to give the product.

(1*S*,2*S*,4*S*,5*R*)-2-((*R*)-hydroxy(6-methoxyquinolin-4-yl)methyl)-1-(2-nitrobenzyl)-5-vinylquinuclidin-1-ium bromide (131)

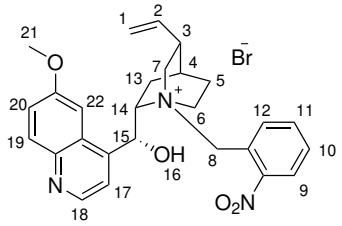

Synthesised using **General Procedure I** and 2-nitrobenzyl bromide (259 mg, 1.2 mmol). Product **131** was isolated as a yellow, amorphous solid (485 mg, 0.9 mmol, 90%). Mp. 174 °C *dec.* (Et_2O) $[\alpha]_D^{20}$ = -203.7 (*c* = 0.3, MeOH).

δ_H (400 MHz, $CDCl_3$) 8.84 (d, 1H, *J* = 4.6, H-18), 8.69 (app t, 1H, H-9), 8.22-8.16, (m, 1H, H-11), 8.13 (d, 1H, *J* = 9.2, H-19), 7.90 (m, 2H, H-10, H-17), 7.78-7.74 (m 1H, H-12), 7.45 (dd, 1H, *J* = 9.2, 2.6, H-20), 7.09 (d, 1H, *J* = 2.6, H-22), 6.85 (d, 1H, *J* = 10.2, H-8a), 6.71 (d, 1H, *J* = 7.0, H-16), 6.62 (d, 1H, *J* = 7.0, H-15), 5.63-5.51 (m, 2H, H-2, H-1a), 5.37-5.26 (m, 1H, H-7a), 5.11 (d, 1H, *J* = 10.2, H-8b), 5.01 (d, 1H, *J* = 17.1, H-1b), 4.05 (s, 3H, H-21), 3.82-3.73 (m, 1H, H-14), 3.24-3.09 (m, 3H, H-7b, H-6), 2.65-2.55 (m, 1H,

H-3), 2.54-2.43 (m, 1H, H-13a), 2.38-2.28 (m, 1H, H-5a), 2.12-2.07 (m, 1H, H-4), 1.92-1.81 (m, 1H, H-13b), 1.56-1.46 (m, 1H, H-5b) ppm

δ_C (101 MHz, $CDCl_3$) 164.9, 158.6 (q), 150.6 (q), 147.4, 143.9 (q), 143.0 (q), 137.9, 135.79, 134.9, 132.5, 132.2, 126.1, 125.5, 122.4, 121.5, 120.8, 118.4, 98.6, 72.3, 63.3, 60.7, 59.1, 55.8, 52.0, 38.0, 26.2, 24.9, 21.7 ppm

HRMS (m/z – ESI+): Found: 460.2240 (M^+) $C_{27}H_{30}N_3O_4$ Requires: 460.2231

ν_{max} (neat)/cm^{-1}: 3036, 2971, 1682, 1623, 1552, 1498, 1243, 971, 900, 758, 716, 692

((1*S*,2*S*,4*S*,5*R*)-1-(2-fluorobenzyl)-2-((*R*)-hydroxy(6-methoxyquinolin-4-yl)methyl)-5-vinyl-quinuclidin-1-ium bromide (132)

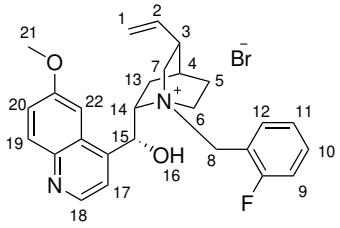

Synthesised using **General Procedure I** and 2-fluorobenzyl bromide (0.15 mL, 1.2 mmol). Product **132** was isolated as a yellow, amorphous solid (505 mg, 0.98 mmol, 98%). Mp. 160 °C *dec.* (Et_2O) $[\alpha]_D^{20}$ = -208.5 (*c* = 0.3, MeOH).

δ_H (400 MHz, $CDCl_3$) 8.81 (d, 1H, *J* = 4.6, H-18), 8.34-8.27 (m, 1H, H-9), 8.15 (d, 1H, *J* = 9.2, H-19), 7.88 (d, 1H, *J* = 4.6, H-17), 7.63-7.56 (m, 1H, H-10), 7.44 (dd, 1H, *J* = 9.2, 2.6, H-20), 7.41-7.34 (m, 1H, H-11), 7.26-7.19 (m, 2H, H-12, H-22), 6.81 (d, 1H, 6.8, H-16), 6.71 (d, 1H, *J* = 6.8, H-15), 6.54 (d 1H, *J* = 12.4, H-8a), 5.69-5.57 (m, 1H, H-2), 5.29-5.18 (m, 1H, H-7a), 5.16-5.04 (m, 2H, H-1), 4.61 (d, 1H, 12.4, H-8b), 4.00 (s, 3H, H-21), 3.83-3.74 (m,

1H, H-14), 3.38 (t, 1H, J = 11.2, H-6a), 3.25-3.09 (m, 2H H-7b, H-6b), 2.70-2.59 (m, 1H, H-3), 2.51-2.34 (m, 2H, H-5a, H-13a), 2.15-2.09 (m, 1H, H-4), 1.90-1.78 (m, 1H, H-13b), 1.65-1.52 (m, 1H, H-5b) ppm

δ_C (101 MHz, $CDCl_3$) 162.0 (d, $J_{C\text{-}F}$ = 248.5), 160.7 (q), 158.5 (q), 147.0, 143.9 (q), 143.4 (q), 136.2, 133.6 (d, $J_{C\text{-}F}$ = 9.1), 131.8, 125.9 (d, $J_{C\text{-}F}$ = 3.5), 122.0, 120.6, 118.3, 116.0 (d, $J_{C\text{-}F}$ = 22.2), 114.5 (d, $J_{C\text{-}F}$ = 12.8), 100.8, 71.3, 63.3, 61.3, 57.4, 56.0, 51.0, 30.2, 26.4, 25.6, 24.8, 21.4, 15.3 ppm

δ_F (377 MHz, $CDCl_3$) -113.3

HRMS (m/z – ESI+): Found: 433.2290 (M^+) $C_{27}H_{30}FN_2O_2$ Requires: 433.2286

ν_{max} (neat)/cm^{-1}: 3205, 2164, 1622, 1510, 1354, 1223, 1155, 1058, 898, 824, 772

(1*S*,2*S*,4*S*,5*R*)-1-(3,5-dimethoxybenzyl)-2-((*R*)-hydroxy(6-methoxyquinolin-4-yl)methyl)-5-vinylquinuclidin-1-ium bromide (129)

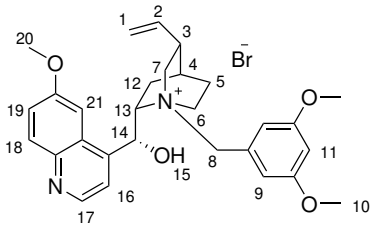

Synthesised using **General Procedure I** and 3-5 dimethoxybenzyl bromide (254 mg, 1.2 mmol). Product **129** was isolated as a red, amorphous solid (312 mg, 0.56 mmol, 56%). Mp. 202 °C *dec.* (Et_2O) $[\alpha]_D^{20}$ = -199.8 (c = 0.5, MeOH).

δ_H (400 MHz, $CDCl_3$) 8.74 (d, 1H, J = 4.6, H-17), 8.08 (d, 1H, J = 9.1, H-18), 7.79 (d, 1H, J = 4.6 H-16), 7.38 (dd, 1H, J = 9.1, 2.2, H-19), 7.35 (d, 1H, J = 2.2, H-21), 7.00 (d, 2H, J = 2.2, H-9), 6.70 (dd, 2H, J = 14.5, 7.7, H-15, H-14), 6.49 (t, 1H, J = 2.2, H-11), 6.10 (d, 1H 12.0, H-8a), 5.71-5.60 (m, 1H, H-2), 5.19-5.05 (m, 3H, H-7a, H-1),

	4.75 (d, 1H, J = 12.0, H-8b), 4.01 (s, 3H, H-20), 3.79 (s, 6H, H-10), 3.27-3.16 (m, 2H, H-6), 3.15-3.06 (m, 1H, H-7b), 2.68-2.58 (m, 1H, H-3), 2.45-2.29 (m, 2H, H-5a, H-12a), 2.10-2.05 (m, 1H, H-4), 1.90-1.78 (m, 1H, H-12b), 1.65-1.52 (m, 1H, H-5b) ppm
δ_C (101 MHz, $CDCl_3$)	161.2 (q), 158.4 (q), 146.7, 143.9 (q), 143.0 (q), 136.2, 131.4, 128.5, 126.2, 121.2, 120.5, 118.3, 111.7, 102.4, 102.1, 70.1, 63.9, 63.8, 61.5, 56.5, 55.9, 51.3, 38.3, 26.7, 24.9, 21.6 ppm
HRMS (m/z – ESI+):	Found: 475.2597 (M^+) $C_{29}H_{35}N_2O_4$ Requires: 475.2591
ν_{max} (neat)/cm^{-1}:	1596, 1510, 1457, 1229, 1200, 1152, 1035, 831

General procedure II: Synthesis of 2-bromoacetamides

To a 50 mL round bottom flask containing a magnetic stirrer, containing K_2CO_3 (10% aq, 5 mL) and CH_2Cl_2 (10 mL), was added the appropriate aniline (2 mmol). The apparatus was then cooled to 0 °C before bromoacetal bromide (0.23 mL, 2.5 mmol) in CH_2Cl_2 (10 mL) was added dropwise *via* syringe. After stirring for 1 h, the aqueous phase was separated, and the organic phase was washed with K_2CO_3 (10 mL) and brine (10 mL) before being dried over $MgSO_4$. The solvent was removed *in vacuo*, yielding the product.

2-bromo-*N*-phenylacetamide (138)

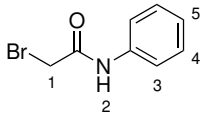

Synthesised using **General Procedure II** with aniline (1.86 mL, 2 mmol) to isolate product **138** as an off-white powder (406 mg, 1.9 mmol, 95%). Mp. 119-121 °C (CH_2Cl_2) (lit. 123-124 °C). Spectral data for this compound were consistent with those in the literature.[86]

δ_H (400 MHz, $CDCl_3$)	8.1 (br s, 1H, H-2), 7.53 (d, 2H, J = 7.9, H-3), 7.36 (m, 2H, H-4), 7.16 (t, 1H, J = 7.5, H-5), 4.03 (s, 2H, H-1) ppm

HRMS (m/z – ESI+): Found: 235.9685 (M^{+Na}) $C_8H_8BrNONa$ Requires: 235.9687

2-bromo-*N*-(2-nitrophenyl)acetamide (259)

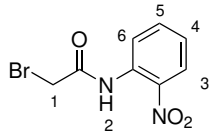

Synthesised using **General Procedure II** with 2-nitroaniline (276 mg, 2 mmol) to isolate product **259** as a yellow powder (439 mg, 1.9 mmol, 95%). Mp. 67-70 °C (CH_2Cl_2) (lit. 62-63 °C). Spectral data for this compound were consistent with those in the literature.[86]

δ_H (400 MHz, $CDCl_3$) 11.19 (br s, 1H, H-2), 8.74 (d, 1H, J = 8.8, H-3), 8.26 (d, 1H, J = 8.6, H-6), 7.69 (t, 1H, J = 8.6, H-5), 7.26 (t, 1H, J = 8.8, H-4), 4.07 (s, 2H, H-1) ppm

HRMS (m/z – ESI+): Found: 280.9539 (M^{+Na}) $C_8H_7BrN_2O_3Na$ Requires: 2380.9532

2-bromo-*N*-(3-bromophenyl)acetamide (260)

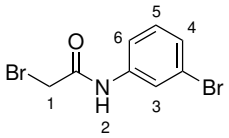

Synthesised using **General Procedure II** with 3-bromoaniline (2.17 mL, 2 mmol) to isolate product **260** as a white powder (564 mg, 1.9 mmol, 95%). Mp. 97-98 °C (CH_2Cl_2) (lit. 97-100 °C).

Spectral data for this compound were consistent with those in the literature.[200]

δ_H (400 MHz, $CDCl_3$) 8.09 (br s, 1H, H-2), 7.79 (s, 1H, H-3), 7.45 (d, 1H, J = 8.0, H-4), 7.32-7.18 (m, 2H, H-5, H-6), 4.03 (s, 2H, H-1) ppm

HRMS (m/z – ESI+): Found: 313.8793 (M^{+Na}) $C_8H_7Br_2NONa$ Requires: 313.8792

2-bromo-*N*-(3-nitrophenyl)acetamide (261)

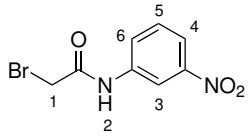

Synthesised using **General Procedure II** with 3-nitroaniline (286 mL, 2 mmol) to isolate product **260** as a yellow powder (356 mg, 1.4 mmol, 70%). Mp. 109-112 °C (CH_2Cl_2) (lit. 112-114 °C).

Product spectroscopic data correlated well with that in the literature.[200]

δ_H (400 MHz, $CDCl_3$)	8.42 (s, 1H, H-3), 8.33 (br s, 1H, H-2), 8.03 (d, 1H, *J* = 8.2, H-4), 7.95 (d, 1H, *J* = 8.2, H-6), 7.55 (t, 1H, *J* = 8.2, H-5), 4.07 (s, 2H, H-1) ppm
HRMS (m/z – ESI+):	Found: 280.9537 (M^{+Na}) $C_8H_7Br_2N_2O_3Na$ Requires: 280.9538

2-bromo-*N*-(3-fluorophenyl)acetamide (262)

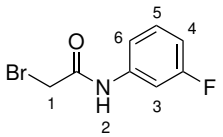

Synthesised using **General Procedure II** with 3-fluoroaniline (1.92 mL, 2 mmol) to isolate product **262** as an off-white powder (322 mg, 1.4 mmol, 70%). Mp. 105-107 °C (CH_2Cl_2) (lit. 109-110 °C).

Spectral data for this compound were consistent with those in the literature.[200]

δ_H (400 MHz, $CDCl_3$)	8.14 (br s, 1H, H-2), 7.50 (d, 1H, *J* = 8.0, H-3), 7.30 (dd, 1H, *J* = 14.6, *J* = 8.0, H-5), 7.18 (d, 1H, *J* = 8.0, H-6), 6.87 (m, 1H, H-4), 4.02 (s, 2H, H-1) ppm
HRMS (m/z – ESI+):	Found: 253.9588 (M^{+Na}) $C_8H_7BrFNONa$ Requires: 253.9593

2-bromo-*N*-(3-bromophenyl)acetamide (263)

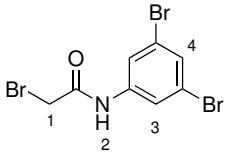

Synthesised using **General Procedure II** with 3,5-dibromoaniline (501.8 mg, 2 mmol) to isolate product **263** as a white powder (530 mg, 1.4 mmol, 71%). Mp. 68-69 °C (CH_2Cl_2).

δ_H (400 MHz, DMSO-d_6)	9.98 (br s, 1H, H-2), 7.94 (s, 2H, H-3), 7.45 (s, 1H, H-4), 3.97 (s, 2H, H-1) ppm
δ_C (101 MHz, DMSO-d_6)	172.3 (C=O), 141.5, 122.7, 121.4, 110.0, 62.2 ppm
ν_{max} (neat)/cm^{-1}:	3326, 1685, 1581, 1392, 1247, 1167, 1108, 909, 845, 751, 669

***N*-(3,5-*bis*(trifluoromethyl)phenyl)-2-bromoacetamide (264)**

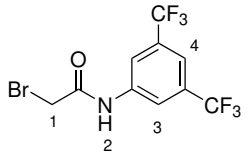

Synthesised using **General Procedure II** with 3,5-*bis*(trifluoromethyl)aniline (3.12 mL, 2 mmol) to isolate product **262** as an off-white powder (484 mg, 1.4 mmol, 69%). Mp. 94-96 °C (CH_2Cl_2) (lit. 95-96 °C).[200]

[2pt] Spectral data for this compound were consistent with those in literature[200]

δ_H (400 MHz, $CDCl_3$)	8.38 (br s, 1H, H-2), 8.08 (s, 2H, H-3), 7.70 (s, 1H, H-4), 4.09 (s, 2H, H-1) ppm

General procedure III: Synthesis of acetamide-derived phase transfer catalysts

A 50 mL round bottom flask containing a magnetic stirrer was added with **258** (324 mg, 1 mmol) and 2-bromoacetamide (1.2 mmol). The apparatus was flushed with Ar before being

fitted with a septum and a balloon of Ar. Anhydrous THF (10 mL) was added *via* syringe and the reaction mixture was stirred at room temperature for 16 h. Et_2O (20 mL) was added, and the resulting precipitate was filtered to give the product.

(1*S*,2*S*,4*S*,5*R*)-1-(2-amino-2-oxoethyl)-2-((*R*)-hydroxy(6-methoxyquinolin-4-yl)methyl)-5-vinylquinuclidin-1-ium bromide (140)

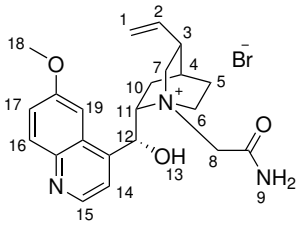

Synthesised using **General Procedure III** with 2-bromoacetamide (166 mg, 1.2 mmol) to isolate product **153** as an orange crystalline solid (322 mg, 0.66 mmol, 66%). Mp. 162 °C *dec.* (Et_2O) $[\alpha]_D^{20}$ = -255.8 (*c* = 0.2, MeOH).

δ_H (400 MHz, DMSO-d_6)	8.74 (d, *J* = 4.1 1H, H-15), 8.32 (s, 1H, H-9a), 7.99 (s, 1H, H-9b), 7.93 (d, 1H, *J* = 9.3, H-16), 7.72 (d, 1H, *J* = 4.3, H-14), 7.38 (d, 1H, *J* = 9.36, H-17), 7.29 (s, 1H, H-19), 6.75 (s, 1H, H-13), 5.83 (br s, 1H, H-12), 5.70-5.56 (m 1H, H-2), 5.15 (d, 1H, *J* = 17.3, H-1a), 4.92 (d, 1H, *J* = 10.6, H-1b), 4.65-4.53 (m, 1H, H-8a), 4.51-4.35 (m, 4H, H-8b, H-11, H-6a, H-7a), 3.99 (s, 3H, H-18), 3.82 (t, 1H, *J* = 10.6, H-7b), 3.57 (t, 1H, *J* = 10.6, H-6b), 2.85-2.75 (m, 1H, H-3), 2.14-1.78 (m, 4H, H-4, H-10, H-5a), 1.01-0.89 (m, 1H, H-5b) ppm
δ_C (101 MHz, DMSO-d_6)	167.1 (C=O), 158.5 (q), 147.7, 144.1 (q), 143.9 (q), 138.7, 132.6, 131.9, 125.9, 122.7, 120.8, 155.8, 101.2, 66.0, 62.8, 60.3, 58.7, 57.0, 37.1, 25.8, 25.2, 21.7 ppm
HRMS (m/z – ESI+):	Found: 382.2132 (M^+) $C_{22}H_{28}N_3O_3$ Requires: 382.2125
ν_{max} (neat)/cm^{-1}:	3247, 2941, 2858, 1689, 1621. 1538, 1510, 1433, 1363, 1300,

1240, 1228, 1100, 1081, 1027, 966, 918, 861, 801

(1*S*,2*S*,4*S*,5*R*)-2-((*R*)-hydroxy(6-methoxyquinolin-4-yl)methyl)-1-(2-oxo-2-(phenylamino)ethyl)-5-vinylquinuclidin-1-ium bromide (265)

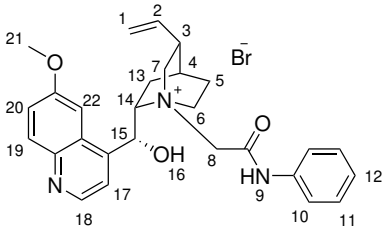

Synthesised using **General Procedure III** with **260** (257 mg, 1.2 mmol) to isolate product **265** as a white powder (435 mg, 0.94 mmol, 94%) Mp. 173 °C *dec.* (Et_2O) $[\alpha]_D^{20}$ = -48.8 (*c* = 0.2, MeOH).

δ_H (400 MHz, DMSO-d_6) 10.87 (s, 1H, H-9), 8.80 (d, 1H, *J* = 4.6, H-18), 7.97 (d, 1H, *J* = 9.1, H-19), 7.74 (d, 1H, *J* = 4.6, H-17), 7.61 (d, 1H, *J* = 7.7, H-10), 7.45-7.39 (m, 3H, H-20, H-11), 7.35 (d, 1H, *J* = 2.49, H-22), 7.21-7.14 (m, 1H, H-12), 6.78 (s, 1H, H-16), 5.99-5.95 (m, 1H, H-15), 5.77-5.65 (m, 1H, H-2), 5.23 (d, 1H, *J* = 17.4, H-1a), 5.01 (d, 1H, *J* = 17.4, H-1b), 4.77 (d, 1H, *J* = 16.4, H-8a), 4.57-4.45 (m, 3H, H-8b, H-6a, H-14), 4.40-4.33 (m, 1H, H-7a), 3.90 (s, 3H, H-21), 3.89-3.84 (m, 1H, H-7b), 3.60 (m, 1H, H-6b), 2.92-2.84 (m, 1H, H-3), 2.17-2.06 (m, 2H, H-4, H-13a), 2.04-1.85 (m, 2H, H-13b, H-5a), 1.07-0.97 (m, 1H, H-5b) ppm

δ_C (101 MHz, DMSO-d_6) 163.3 (C=O), 157.9 (q), 147.4, 143.7 (q), 143.4 (q), 137.0, 136.6, 131.6, 129.0, 125.9 (q), 125.4, 124.9, 122.0, 120.3, 120.3, 115.6, 101.0, 65.8, 63.0, 59.1, 57.0, 56.1, 36.7, 25.3, 24.9, 21.5 ppm

HRMS (m/z – ESI+): Found: 458.2445 (M^+) $C_{29}H_{35}N_2O_3$ Requires: 458.2438

ν_{max} (neat)/cm^{-1}: 1596, 1510, 1457, 1229, 1200, 1152, 1035, 831

(1*S*,2*S*,4*S*,5*R*)-2-((*R*)-hydroxy(6-methoxyquinolin-4-yl)methyl)-1-(2-((2-nitrophenyl)amino)-2-oxoethyl)-5-vinylquinuclidin-1-ium bromide (145)

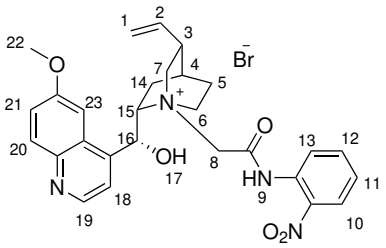

Synthesised using **General Procedure III** with **259** (311 mg, 1.2 mmol) to isolate product **145** as a yellow powder (431 mg, 0.74 mmol, 74%). Mp. 168 °C *dec.* (Et_2O) $[\alpha]_D^{20}$ = -84.1 (*c* = 0.4, MeOH).

δ_H (400 MHz, DMSO-d_6) 11.33 (s, 1H, H-9), 8.76 (d, 1H, *J* = 4.5, H-19), 8.05 (d, 1H, *J* = 8.0 H-10), 7.90 (d, 1H, *J* = 9.2, H-20), 7.88-7.80 (m, 1H, H-11), 7.72 (d, 1H, *J* = 4.5, H-18), 7.62 (d, 1H, *J* = 7.8, H-13), 7.61-7.54 (m, 1H, H-12), 7.32 (dd, 1H, *J* = 7.3, H-21), 7.14 (d, 1H, *J* = 7.1, H-23), 6.79 (d, 1H, *J* = 3.2, H-17), 6.01-5.89 (m, 1H, H-16), 5.73-5.62 (m 1H, H-2), 5.16 (d, 1H, *J* = 17.4, H-1a), 4.97 (d, 1H, *J* = 10.6, H-1b), 4.86 (d, 1H, *J* = 16.8, H-8a), 4.67 (d, 1H, *J* = 16.8, H-8b), 4.57-4.43 (m, 2H, H-7a, H-15), 4.19 (d, 1H, *J* = 12.6, H-6a), 3.85 (t, 1H, *J* = 11.2, H-6b), 3.63 (t, 1H, *J* = 11.2, H-7b), 3.53 (s, 3H, H-22), 2.91-2.81 (m, 1H, H-3), 2.16-2.05 (m, 2H, H-14a, H-4), 2.03-1.85 (m, 2H, H-14b, H-5a), 1.02-0.91 (m, 1H, H-5b) ppm

δ_C (101 MHz, DMSO-d_6) 164.8 (C=O), 158.2 (q), 147.6, 144.3 (q), 144.1 (q), 143.8 (q), 138.7, 134.8, 131.9, 129.4, 127.8, 127.4, 125.9, 125.6, 122.7, 120.7, 115.8, 101.1, 66.1, 63.4, 60.2, 59.2, 57.5, 56.0, 37.0, 25.7, 25.3, 21.9 ppm

HRMS (m/z – ESI+): Found: 503.2290 (M^+) $C_{28}H_{31}N_4O_5$ Requires: 503.2294

ν_{max} (neat)/cm^{-1}: 2996, 2941, 1698, 1594, 1524, 1505, 1434, 1355, 1238, 1108,

1080, 913, 856, 740, 720

((1*S*,2*S*,4*S*,5*R*)-2-((*R*)-hydroxy(6-methoxyquinolin-4-yl)methyl)-1-(2-((4-nitrophenyl)amino)-2-oxoethyl)-5-vinylquinuclidin-1-ium bromide (147)

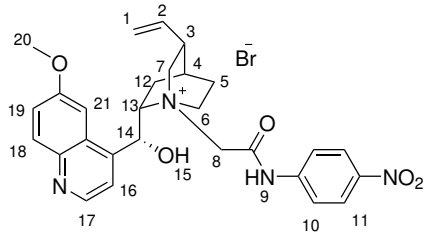

Synthesised using **General Procedure III** with 2-bromo-*N*-(4-nitrophenyl)acetamide (312 mg, 1.2 mmol) to isolate product **147** as a white powder (519 mg, 0.98 mmol, 98%). Mp. 181 °C *dec.* (Et_2O) $[\alpha]_D^{20}$ = -116.9 (*c* = 0.3, MeOH).

δ_H (600 MHz, $CDCl_3$) 11.48 (s, 1H, H-9), 8.76 (d, 1H, *J* = 4.3, H-17), 8.10 (d, 2H, *J* = 8.5, H-11), 8.00 (d, 1H, *J* = 9.2, H-18), 7.92 (d, 2H, *J* = 8.5, H-10), 7.77 (d, 1H, *J* = 4.3, H-16), 7.31 (d, 1H, *J* = 9.2, H-19), 6.97 (s, 1H, 1H, H-21), 6.14 (s, 1H, H-15), 5.79 (s, 1H, H-14), 5.67 (d, 1H, *J* = 16.3, H-1a), 5.62-5.50 (m, 1H, H-2), 5.26 (d, 1H, *J* = 17.2, H-1b), 5.10 (d, 1H, *J* = 10.6, H-8a), 5.05-4.92 (m, 1H, H-8b), 4.84-4.70 (m, 2H, H-7a, H-13), 4.52-4.41 (m, 1H, H-6a), 3.84-3.70 (m, 4H, H-20, H-6b), 3.63-3.51 (m, 1H, H-7b), 2.77-2.82 (m, 1H, H-3), 2.27-1.12 (m, 2H, H-4, H-12a), 2.07-1.87 (m, 2H, H-12b, H-5a), 1.17-1.07 (m, 1H, H-5b) ppm

δ_C (151 MHz, $CDCl_3$) 163.4 (C=O), 158.6 (q), 147.5, 144.3 (q), 144.2 (q), 142.6 (q), 142.1 (q), 136.3, 132.1, 125.5, 124.7, 121.8, 120.3, 120.2, 117.5, 100.6, 65.9, 63.9, 62.3, 60.0, 58.0, 56.3, 37.8, 26.0, 25.6, 22.1 ppm

HRMS (m/z – ESI+): Found: 503.2289 (M^+) $C_{28}H_{31}N_4O_5$ Requires: 503.2294

ν_{max} (neat)/cm^{-1}: 3475, 2999, 2945, 1699, 1620, 1599, 1564, 1507, 1409, 1348,

1210, 1176, 899, 853, 750, 688

(1*S*,2*S*,4*S*,5*R*)-1-(2-((3-bromophenyl)amino)-2-oxoethyl)-2-((*R*)-hydroxy(6-methoxyquinolin-4-yl)methyl)-5-vinylquinuclidin-1-ium bromide (149)

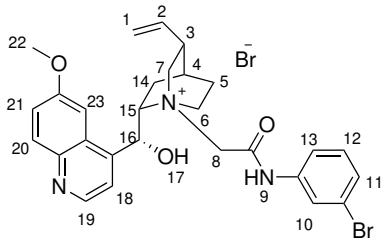

Synthesised using **General Procedure III** with **260** (352 mg, 1.2 mmol) to isolate product **149** as a white powder (435 mg, 0.8 mmol, 80%). Mp. 173 °C *dec.* (Et_2O) $[\alpha]_D^{20}$ = -126.0 (*c* = 0.2, MeOH)

δ_H (400 MHz, $CDCl_3$) 11.01 (s, 1H, H-9), 8.79 (d, 1H, *J* = 4.52, H-19), 8.04 (s, 1H, H-10), 7.97 (d, 1H, *J* = 9.20, H-20), 7.74 (d, 1H, *J* = 4.52 H-18), 7.45-7.39 (m, 5H, H-21, H-23 H-11, H-12, H-13), 6.73 (s, 1H, H-17), 5.98 (s, 1H, H-16), 5.73 (m 1H, H-2), 5.23 (d, 1H, *J* = 17.35, H-1a), 5.01 (d, 1H, *J* = 10.60, H-1b), 4.78 (d, 1H, *J* = 16.7 H-8a), 4.57-4.45 (m, 3H, H-8b, H-7a, H-15), 4.32 (d, 1H, *J* = 12.8, H-6a), 4.0 (s, 3H, H-22), 3.87-3.74 (m, 1H, H-6b), 3.60 (m, 1H, H-7b), 2.92-2.84 (m, 1H, H-3), 2.17-2.06 (m, 2H, H-4, H-14a), 2.04-1.85 (m, 2H, H-14b, H-5a), 1.07-0.97 (m, 1H, H-5b) ppm

δ_C (101 MHz, $CDCl_3$) 164.4 (C=O), 158.3 (q), 147.7, 144.2 (q), 144.0 (q), 143.8, 138.4, 132.8, 131.9, 130.1, 126.8, 126.7, 125.9, 125.6, 122.7, 120.8, 115.9, 101.3, 66.1, 63.7, 60.7, 59.9, 57.3, 56.3, 37.2, 25.8, 25.3, 21.9 ppm

HRMS (m/z – ESI+): Found: 536.1548 (M^+) $C_{28}H_{31}BrN_2O_3$ Requires: 536.1543

ν_{max} (neat)/cm^{-1}: 3065, 1686, 1592, 1480, 1238, 1188, 995, 913, 778, 676

(1*S*,2*S*,4*S*,5*R*)-2-((*R*)-hydroxy(6-methoxyquinolin-4-yl)methyl)-1-(2-((3-nitrophenyl)amino)-2-oxoethyl)-5-vinylquinuclidin-1-ium bromide (150)

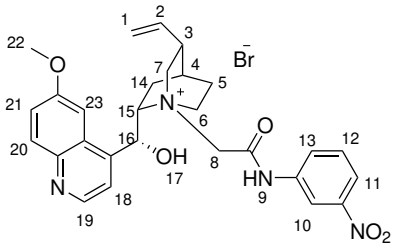

Synthesised using **General Procedure III** with **261** (312 mg, 1.2 mmol) to isolate product **150** as a white powder (332 mg, 0.63 mmol, 63%). Mp. 190 °C *dec.* (Et_2O) $[\alpha]_D^{20}$ = -138.6 (*c* = 0.3, MeOH)

δ_H (400 MHz, DMSO-d_6) 11.01 (s, 1H, H-9), 8.79 (m, 2H, H-19, H-10), 7.97 (d, 1H, *J* = 9.2, H-20), 7.89 (m, 1H, H-12), 7.78 (d, 1H, *J* = 4.5, H-18), 7.45-7.39 (m, 3H, H-13, H-11, H-21), 7.14 (d, 1H, *J* = 2.1, H-23), 6.18 (s, 1H, H-17), 5.86 (d, 1H, *J* = 5.3, H-16), 5.60 (d, 1H, *J* = 16.4, H-8a), 5.57-5.47 (m 1H, H-2), 5.22 (d, 1H, *J* = 17.1, H-1a), 5.07 (d, 1H, *J* = 10.6, H-1b), 4.94 (m, 2H, H-8b, H-15), 4.62-4.49 (m, 2H, H-6a, H-7a), 3.87 (s, 3H, H-22), 3.81 (t, 1H, *J* = 10.60, H-6b), 3.60 (t, 1H, *J* = 12.20, H-7b), 2.85-2.75 (m, 1H, H-3), 2.23-2.06 (m, 2H, H-5a, H-14a), 2.06-1.99 (m, 1H, H-4), 1.90-1.80 (m, 1H, H-14b), 1.07-0.97 (m, 1H, H-5b) ppm

δ_C (101 MHz, DMSO-d_6) 165.5, 163.3 (C=O), 158.7 (q), 148.2, 147.2, 144.4 (q), 138.6 (q), 136.3, 131.8, 129.7, 125.7, 125.6, 122.3, 120.2, 119.8, 117.4, 114.5, 100.6, 66.1, 63.7, 61.8, 60.1, 58.2, 56.4, 37.7, 26.1, 25.7, 22.2 ppm

HRMS (m/z – ESI+): Found: 503.2289 (M^+) $C_{28}H_{31}N_4O_5$ Requires: 503.2294

ν_{max} (neat)/cm^{-1}: 3243, 2936, 2858, 1661, 1630, 1605, 1544, 1451, 1251, 1075, 973, 893, 772

(1*S*,2*S*,4*S*,5*R*)-1-(2-((3-fluorophenyl)amino)-2-oxoethyl)-2-((*R*)-hydroxy(6-methoxyquinolin-4-yl)methyl)-5-vinylquinuclidin-1-ium bromide (153)

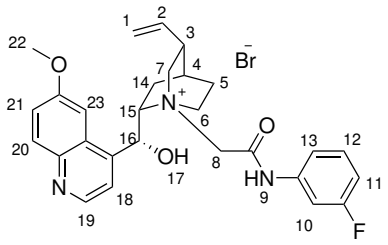

Synthesised using **General Procedure III** with **262** (278 mg, 1.2 mmol) to isolate product **153** as a white powder (451 mg, 0.81 mmol, 81%). Mp. 190 °C *dec.* (Et_2O) $[\alpha]_D^{20}$ = -55.2 (*c* = 0.3, MeOH)

δ_H (400 MHz, $CDCl_3$) 11.01 (s, 1H, H-9), 8.79 (m, 2H, H-19, H-10), 7.97 (d, 1H, *J* = 9.2, H-20), 7.89 (m, 1H, H-12), 7.78 (d, 1H, *J* = 4.5, H-18), 7.45-7.39 (m, 3H, H-13, H-11, H-21), 7.14 (d, 1H, *J* = 2.1, H-23), 6.18 (s, 1H, H-17), 5.86 (d, 1H, *J* = 5.3, H-16), 5.60 (d, 1H, *J* = 16.4, H-8a), 5.57-5.47 (m 1H, H-2), 5.22 (d, 1H, *J* = 17.1, H-1a), 5.07 (d, 1H, *J* = 10.6, H-1b), 4.94 (m, 2H, H-8b, H-15), 4.62-4.49 (m, 2H, H-6a, H-7a), 3.87 (s, 3H, H-22), 3.81 (t, 1H, *J* = 10.60, H-6b), 3.60 (t, 1H, *J* = 12.20, H-7b), 2.85-2.75 (m, 1H, H-3), 2.23-2.06 (m, 2H, H-4, H-14a), 2.06-1.99 (m, 1H, H-5a), 1.90-1.80 (m, 1H, H-14b), 1.07-0.97 (m, 1H, H-5b) ppm

δ_C (101 MHz, $CDCl_3$) 162.7 (C=O), 162.6 (d, $J_{C\text{-}F}$ = 245.4), 158.7 (q), 147.5, 144.3 (q), 142.3 (q), 138.3 (d, $J_{C\text{-}F}$ = 10.8), 136.3, 132.0, 130.2 (d, $J_{C\text{-}F}$ = 9.2), 125.6, 122.3, 120.4, 117.4, 116.0, 112.2 (d, $J_{C\text{-}F}$ = 21.01), 108.1 (d, $J_{C\text{-}F}$ = 27.01), 100.2, 65.8, 63.7, 62.3, 60.0, 58.1, 56.3, 37.9, 26.1, 25.6, 22.2 ppm

δ_F (377 MHz, $CDCl_3$) -111.1

HRMS (m/z – ESI+): Found: 476.2346 (M^+) $C_{28}H_{31}FN_2O_3$ Requires: 476.2346

ν_{max} (neat)/cm^{-1}: 2934, 2858, 1644, 1578, 1489, 1331,1270, 1105, 1035, 924, 820,

705

(1*S*,2*S*,4*S*,5*R*)-1-(2-((3,5-dibromophenyl)amino)-2-oxoethyl)-2-((*R*)-hydroxy(6-methoxyquinolin-4-yl)methyl)-5-vinylquinuclidin-1-ium bromide (154)

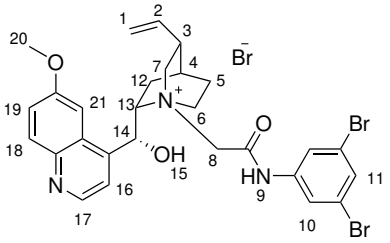

Synthesised using **General Procedure III** with **263** (427 mg, 1.2 mmol) to isolate product **154** as a yellow powder (599 mg, 0.86 mmol, 86%). Mp. 191 °C *dec.* (Et_2O) $[\alpha]_D^{20}$ = -162.4 (*c* = 0.3, MeOH)

δ_H (400 MHz, DMSO-d_6)	11.25 (s, 1H, H-9), 8.77 (d, 1H, *J* = 4.1, H-17), 8.01-7.91 (m, 2H, H-11, H-18), 7.87 (s, 2H, H-10), 7.72 (d, 1H, *J* = 4.3, H-16), 7.65 (d, 1H, *J* = 9.2, H-19), 7.43 (s, 1H, 1H, H-21), 6.73 (s, 1H, H-15), 5.99 (s, 1H, H-14), 5.77-5.63 (m, 1H, H-2), 5.18 (d, 1H, *J* = 18.0, H-1a), 5.00 (d, 1H, *J* = 9.7, H-8a), 4.84 (d, 1H, *J* = 17.2, H-1b), 4.65-4.42 (m, 3H, H-8b, H-7a, H-13), 4.30-4.19 (m, 1H, H-6a), 3.99 (s, 3H H-20), 3.90-3.80 (m, 1H, H-6b), 3.65-3.50 (m, 1H, H-7b), 2.89-2.79 (m, 1H, H-3), 2.16-1.77 (m, 3H, H-4, H-12a, H-5a), 1.50-1.36 (m, 1H, H-12b), 1.04-0.90 (m, 1H, H-5b) ppm
δ_C (101 MHz, DMSO-d_6)	164.3 (C=O), 158.2 (q), 147.9, 144.1 (q), 143.9 (q), 140.5, 138.6, 131.9, 129.7, 126.0, 122.9, 122.3, 122.0, 120.8, 116.1, 101.7, 67.4, 63.7, 60.7, 60.1, 57.4, 56.5, 37.2, 25.8, 25.3, 22.0 ppm
HRMS (m/z – ESI+):	Found: 616.0648 (M^+) $C_{28}H_{31}N_4O_5$ Requires: 616.0633
ν_{max} (neat)/cm^{-1}:	3217, 2946, 2162, 1689, 1619, 1581, 1509, 1435, 1404, 13566, 1240, 1228, 1204, 1137, 1084, 914, 833, 799, 719, 668

General procedure IV: Synthesis of ion-pair acetamide catalysts

To a 50 mL RBF was added phase-transfer catalyst (PTC) (1 mmol) and methanol (10 mL). Amberlite® OH IRN78 (1.59 g) in methanol (10 mL) was added in one portion. The apparatus was then flushed with Ar before being fitted with a septum and balloon of Ar. The vessel was then shaken at 450 rpm. After 16 h, the reaction was passed through a column containing Amberlite® OH IRN78 (1.59 g) with methanol and was collected into a 250 mL RBF. A stir bar was then added to the solution, and the apparatus was flushed with Ar before being fitted with a septum and balloon of Ar. Phenol (1 mmol) was then added in one portion. After 16 h of stirring, the reaction was concentrated *in vacuo*, yielding the product.

(1*S*,2*S*,4*S*,5*R*)-2-((*R*)-hydroxy(6-methoxyquinolin-4-yl)methyl)-1-(2-oxo-2-(phenylamino)ethyl)-5-vinylquinuclidin-1-ium 4-nitrophenolate (156)

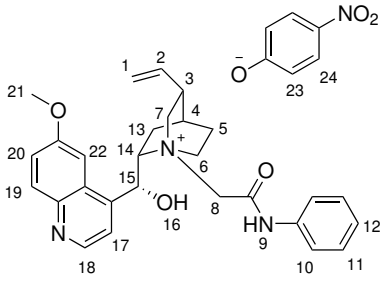

Synthesised using **General Procedure VI** with **265** (538 mg, 1 mmol) and 4-nitrophenol (139 mg, 1 mmol) to isolate product **156** as a yellow solid (317 mg, 0.8 mmol, 80%). Mp. 201 °C *dec.* (MeOH) $[\alpha]_D^{20}$ = -11.0 (*c* = 0.1, MeOH)

δ_H (600 MHz, DMSO-d_6) 10.91 (s, 1H, H-9), 8.80 (d, 1H, *J* = 4.5 H-18), 7.97 (d, 1H, *J* = 9.2 H-19), 7.74 (m, 3H, H-17, H-23), 7.65-7.59 (m, 1H, H-10), 7.45-7.39 (m, 3H, H-20, H-11), 7.35 (m, 1H, H-22), 7.20 (m, 1H, H-12), 6.78 (s, 1H, H-16), 6.00, (d, 2H, *J* = 8.7, H-24), 5.99-5.95 (m, 1H, H-15), 5.73 (m, 1H, H-2), 5.23 (d, 1H, *J* = 16.9 H-1a), 5.01 (d, 1H, *J* = 10.2, H-1b), 4.81 (d, 1H, *J* = 16.7 H-8a), 4.60 (d, 1H, *J* = 16.7 H-8b), 4.57-4.45 (m, 2H, H-6a, H-7a), 4.40-4.33 (m, 1H, H-14), 3.90 (s, 3H, H-21), 3.89-3.84 (m, 1H, H-6b), 3.6-3.5

(m, 1H, H-7b), 2.92-2.84 (m, 1H, H-3), 2.17-2.06 (m, 2H, H-4, H-13a), 2.04-1.85 (m, 2H, H-5a, H-13b), 1.07-0.97 (m, 1H, H-5b) ppm

δ_C (101 MHz, DMSO-d_6) 163.3 (C=O), 157.9 (q), 147.4, 143.7 (q), 143.4 (q), 138.3, 137.3, 131.6, 129.0, 127.3, 125.4, 124.9, 122.0, 120.3, 120.3, 118.9 115.6, 101.0, 65.8, 63.0, 60.3, 59.1, 57.0, 56.1, 36.7, 25.3, 24.9, 21.5, 18.6 ppm

HRMS (m/z – ESI+): Found: 458.2439 (M^+) $C_{29}H_{35}N_2O_3$ Requires: 458.2438

ν_{max} (neat)/cm^{-1}: 2639, 1588, 1565, 1490, 1447, 1268, 1235, 1127, 933, 822

(1*S*,2*S*,4*S*,5*R*)-2-((*R*)-hydroxy(6-methoxyquinolin-4-yl)methyl)-1-(2-oxo-2-(phenylamino)ethyl)-5-vinylquinuclidin-1-ium 4-nitrophenolate (158)

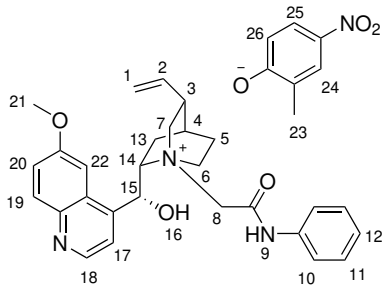

Synthesised using **General Procedure VI** with **265** (538 mg, 1 mmol) and 2-methoxy-4-nitrophenol (147 mg, 1 mmol) to isolate product **158** as an orange solid (582 mg, 0.96 mmol, 96%). Mp. 168 °C *dec.* (MeOH) $[\alpha]_D^{20}$ = -37.0 (*c* = 0.2, MeOH)

δ_H (600 MHz, DMSO-d_6) 10.9 (s, 1H, H-9), 8.81 (d, 1H, *J* = 4.7 H-18), 7.97 (d, 1H, *J* = 9.2 H-19), 7.76 (d, 1H, *J* = 4.4 H-17), 7.69 (m, 1H, H-24), 7.67 (dd, *J* = 9.8, 2.6,1H, H-25), 7.61 (d, 2 H, *J* = 8.0, H-10), 7.45-7.39 (m, 3H, H-20, H-11), 7.34 (m, 1H, H-22), 7.20 (t, 1H, *J* = 7.3 H-12), 6.78 (s, 1H, H-16), 5.99-5.95 (m, 1H, H-15), 5.90 (d, 1H, *J* = 9.8, H-26), 5.78-5.70 (m, 1H, H-2), 5.25 (d, 1H, *J* = 17.8 H-1a), 5.01 (d, 1H, *J* = 10.9, H-1b), 4.79 (d, 1H, 16.8, H-8a),

4.60-4.48 (m, 3H, H-8b, H-6a, H-7a), 4.40-4.33 (m, 1H, H-14), 3.90 (s, 3H, H-21), 3.87-3.80 (m, 1H, H-6b), 3.60-3.53 (m, 1H, H-7b), 2.92-2.85 (m, 1H, H-3), 2.16-2.11 (m, 2H, H-4, H-13a), 2.04-1.85 (m, 1H, H-13b), 1.93-1.89 (m, 1H, H-5a), 1.88 (s, 3H, H-23), 1.07-0.99 (m, 1H, H-5b) ppm

δ_C (151 MHz, DMSO-d_6) 163.3 (C=O), 157.9 (q), 147.4, 143.6 (q), 143.3 (q), 138.2, 131.5, 129.0, 126.6 (q), 126.2, 125.9, 125.3, 124.8, 121.9, 120.3, 120.2, 117.6, 115.5, 100.9, 65.8, 62.7, 60.2, 59.0, 57.0, 56.0, 36.7, 30.6, 25.2, 24.8, 21.4, 17.1 ppm

HRMS (m/z – ESI+): Found: 458.2439 (M^+) $C_{29}H_{35}N_2O_3$ Requires: 458.2438

ν_{max} (neat)/cm^{-1}: 2639, 1588, 1565, 1490, 1447, 1268, 1235, 1127, 933, 822

(1*S*,2*S*,4*S*,5*R*)-1-(2-((3-bromophenyl)amino)-2-oxoethyl)-2-((*R*)-hydroxy(6-methoxyquinolin-4-yl)methyl)-5-vinylquinuclidin-1-ium 4-nitrophenolate (159)

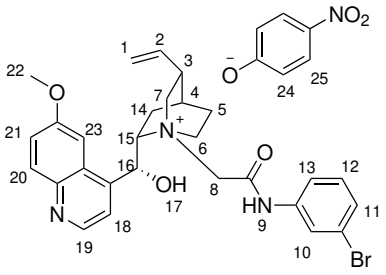

Synthesised using **General Procedure VI** with **149** (617 mg, 1 mmol) and 4-nitrophenol (139 mg, 1 mmol) to form **159** as an orange solid (662 mg, 0.98 mmol, 98%). Mp. 179 °C *dec.* (MeOH) $[\alpha]_D^{20}$ = -152.3 (*c* = 0.3, MeOH)

δ_H (400 MHz, DMSO-d_6) 11.0 (br s, 1H, H-9), 8.77 (d, 1H, *J* = 4.5 H-19), 8.03 (s, 1H, H-10), 7.95 (d, 1H, *J* = 9.2 H-20), 7.80-7.70 (m, 3H, H-24, H-18), 7.45-7.39 (m, 5H, H-21 , H-23 H-11, H-12, H-13), 7.01 (br s, 1H, H-17), 6.07 (d, 2H, *J* = 9.2, H-25), 5.99-5.95 (m, 1H, H-16), 5.74 (m, 1H, H-2), 5.23 (d, 1H, *J* = 16.9, H-1a), 5.01 (d, 1H, *J* = 10.2,

	H-1b), 4.78 (d, 1H, J = 16.9, H-8a), 4.57-4.45 (m, 3H, H-8b, H-6a, H-7a), 4.40-4.33 (m, 1H, H-15), 4.0 (s, 3H, H-22), 3.87-3.74 (m, 1H, H-6b), 3.64-3.58 (m, 1H, H-7b), 2.92-2.84 (m, 1H, H-3), 2.17-2.06 (m, 2H, H-4, H-14a), 2.04-1.85 (m, 2H, H-5a, H-14b), 1.07-0.97 (m, 1H, H-5b) ppm
δ_C (101 MHz, DMSO-d_6)	164.2 (C=O), 158.3 (q), 147.8, 144.2 (q), 143.9 (q), 138.3, 137.3, 132.0, 131.5, 127.7 (2 signals), 125.9, 123.2, 122.2, 122.1, 120.7, 119.6, 119.0 116.0, 101.6, 66.3, 63.3, 63.0, 60.7, 59.7, 37.2, 25.8, 25.3 22.0, 15.6 ppm
HRMS (m/z – ESI+):	Found: 536.1548 (M^+) $C_{28}H_{31}BrN_2O_3$ Requires: 536.1543
ν_{max} (neat)/cm^{-1}:	2994, 2539, 1588, 1480, 1447, 1238, 1188, 995, 913, 778, 676

(3a*R*,7a*R*)-2-phenyl-3a,4,5,6,7,7a-hexahydro-1H-benzo[d]imidazole (170)

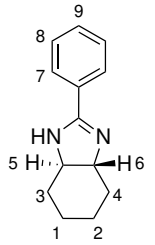

To a 50 mL RBF under Ar atmosphere containing a stir bar and equipped with a reflux condenser was added (*R*,*R*)-(-)-1,2-diaminocyclohexane (571 mg, 5 mmol), EtOH (7 mL) and ethyl benzimidate hydrochloride (1.1136 g, 6 mmol). The solution was refluxed for 4 h before being washed with NaOH (aq, 1 M, 10 mL). The aqueous phase was extracted with 95:5 CH_2Cl_2/MeOH (1:1, 3 × 10 mL). The combined organic phases were concentrated *in vacuo* to a brown solid before being purified by flash column chromatography (9:0.5:0.5 CH_2Cl_2/MeOH/NEt_3) (R_f=0.1) to afford **170** as a yellow crystalline solid (387 mg, 1.95 mmol, 39%). Mp. 162-165 °C (CH_2Cl_2) (lit. 159-162 °C). $[\alpha]_D^{20}$ = +98.3 (c = 0.3, MeOH)

Spectral data for this compound were consistent with those in the literature.[201]

δ_H (400 MHz, $CDCl_3$) 7.91 (d, J = 7.5, 2H, H-7), 7.50-7.42 (m, 1H, H-9), 7.38 (app.t, 2H, H-8), 3.21-3.14 (m, 2H, H-5, H-6), 2.33 (app.d, 2H, H-3), 1.84 (app.d, 2H, H-4), 1.64-1.41 (m, 2H, H-1), 1.40-1.40 (m, 2H, H-2) ppm

(3a*S*,7a*S*)-2-phenyl-3a,4,5,6,7,7a-hexahydro-1H-benzo[d]imidazole (172)

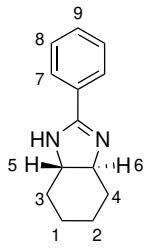

To a 50 mL RBF under Ar atmosphere containing a stir bar and equipped with a reflux condenser was added (*S*,*S*)-(+)-1,2-diaminocyclohexane (571 mg, 5 mmol), EtOH (7 mL) and ethyl benzimidate hydrochloride (1.1136 g, 6 mmol). The solution was refluxed for 4 h before being washed with NaOH (aq, 1 M, 10 mL). The aqueous phase was extracted with 95:5 CH_2Cl_2/MeOH (1:1, 3 × 10 mL). The combined organic phases were concentrated *in vacuo* to a brown solid before being purified by flash column chromatography (9:0.5:0.5 CH_2Cl_2/MeOH/NEt_3) (R_f=0.1) to afford **172** as a yellow crystalline solid (173 mg, 0.85 mmol, 17%). Mp. 159-164 °C (CH_2Cl_2) $[\alpha]_D^{20}$ = -121.6 (c = 0.3, MeOH)

Spectral data for this compound were consistent with those in the literature.[202]

δ_H (400 MHz, $CDCl_3$) 7.78 (d, J = 7.0, 2H, H-7), 7.48-7.34 (m, 3H, H-9, H-8), 3.20-3.06 (m, 2H, H-5, H-6), 2.31 (app.d, 2H, H-3), 1.85 (app.d, 2H, H-4), 1.63-1.49 (m, 2H, H-1), 1.44-1.28 (m, 2H, H-2) ppm

(*N*-((1*R*,2*R*)-2-aminocyclohexyl)benzamide (166)

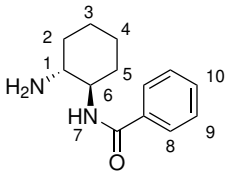

To a 50 mL RBF under Ar atmosphere containing a stir bar and equipped with a reflux condenser was added **170** (300 mg, 1.5 mmol), NaOH solution (5% aq, 3 mL) and a 2:1 EtOH/H_2O mixture (6 mL). The reaction was refluxed for 18 h before being extracted with CH_2Cl_2/MeOH (1:1, 3 x 10 mL). The combined organic phases were concentrated *in vacuo* to afford **166** as a brown amorphous solid (259 mg, 1.19 mmol, 79%). Mp. 165-168 °C (lit. 169-173 °C) (CH_2Cl_2).[203] $[\alpha]_D^{20}$ = +20.7 (c = 0.1, MeOH)

Spectral data for this compound were consistent with those in the literature.[189]

δ_H (400 MHz, $CDCl_3$) 7.80 (d, J = 7.7, 2H, H-8), 7.54-7.38 (m, 3H, H-9, H-10), 6.09 (br s, 1H, H-7), 3.78-3.66 (m, 1H, H-6), 2.54-2.44 (m, 1H, H-1), 2.19-2.09 (m, 1H, H-5a), 2.05-1.96 (m, 1H, H-5b), 1.81-1.70 (m 2H, H-2), 1.46-1.16 (m, 4H, H-3, H-4) ppm

(*N*-((1*S*,2*S*)-2-aminocyclohexyl)benzamide (173)

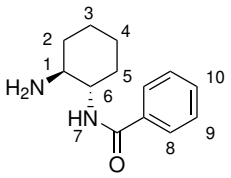

To a 50 mL RBF under Ar atmosphere containing a stir bar and equipped with a reflux condenser was added **172** (173 mg, 0.8 mmol), NaOH solution (5% aq, 1.7 mL) and a 2:1 EtOH/H_2O mixture (4 mL). The reaction was refluxed for 18 h before being extracted with CH_2Cl_2/MeOH (1:1, 3 x 10 mL). The combined organic phases were concentrated *in vacuo* to afford **173** as a brown amorphous solid (93 mg, 0.38 mmol, 48%). Mp. 169-174 °C (CH_2Cl_2) $[\alpha]_D^{20}$ = -16.2 (c = 0.1, MeOH)

Spectral data for this compound were consistent with those in literature.[202]

δ_H (400 MHz, $CDCl_3$) 7.80 (d, J = 7.2, 2H, H-8), 7.53-7.40 (m, 3H, H-9, H-10), 6.07 (br s, 1H, H-7), 3.77-3.66 (m, 1H, H-6), 2.54-2.45 (m, 1H, H-1), 2.19-2.10 (m, 1H, H-5a), 2.06-1.96 (m, 1H, H-5b), 1.83-1.71 (m 2H, H-2), 1.43-1.16 (m, 4H, H-3, H-4) ppm

2-((1*R*,2R)-2-aminocyclohexyl)-4,5,6,7-tetrachloroisoindoline-1,3-dione (174)

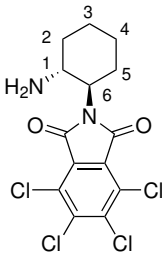

To a 250 mL RBF under Ar atmosphere containing a stir bar and equipped with a Dean-Stark apparatus was added (*R*,*R*)-(-)-1,2-diaminocyclohexane (2.28 g, 20 mmol), toluene (60 mL), *p*-toluenesulfonic acid (3.80 g, 20 mmol) and TCPA (5.72 g, 20 mmol). The solution was refluxed for 5 h before being filtered; the residue was washed with 1:1 toluene/hexane (3 x 60 mL). The white residue was dried *in vacuo* before being added into a 100 mL RBF containing a stir bar, CH_2Cl_2 and aqueous K_2CO_3 (10%, 60 mL). The mixture was stirred at room temperature for 10 min before being filtered; the resulting residue was recrystallised using EtOAc/hexane to obtain product **174** as an off-white crystalline solid (2.05 g, 5.4 mmol, 27%). Mp. 220 °C *dec.* (Hexane) $[\alpha]_D^{20}$ = +89.3 (c = 0.4, MeOH)

δ_H (600 MHz, $CDCl_3$) 3.68-3.61 (m, 1H, H-6), 3.21-3.14 (m, 1H, H-1), 2.05-1.95 (m, 1H, H-2a), 1.94-1.88 (m, 1H, H-5a), 1.79-1.64 (m, 3H, H-2b H-3a, H-4a), 1.33-1.10 (m, 3H, H-3b, H-4b, H-5b) ppm

δ_C (140 MHz, DMSO-d_6) 164.1 (C=O), 138.3, 128.9, 128.3, 59.5, 50.7, 35.8, 28.8, 25.7, 25.2 ppm

HRMS (m/z – ESI+): Found: 380.9731 (M^+) $C_{14}H_{13}Cl_4N_2O_2$ Requires: 380.9726

ν_{max} (neat)/cm^{-1}: 3383, 3286, 2930, 2856, 1773, 1702, 1642, 1551, 1447, 1396, 1366, 1351, 1327, 1288, 1198, 1174, 1078, 1038, 952, 862, 823, 793, 774, 735

_N_-((1_R_,2R)-2-(4,5,6,7-tetrachloro-1,3-dioxoisoindolin-2-yl)cyclohexyl)-3,5-_bis_(trifluoromethyl)benzamide (176)

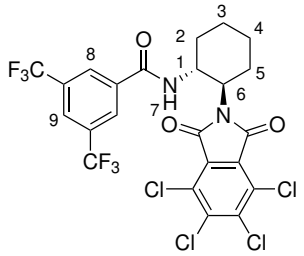

To a 50 mL RBF under Ar atmosphere containing a stir bar was added CH_2Cl_2 (20 mL), NEt_3 (139 µL, 1 mmol), 3,5-difluorobenzoyl chloride (181 µL, 1mmol) and **174** (380 mg, 1 mmol). The solution was stirred at room temperature for 1 h before being filtered. The resulting residue was washed with CH_2Cl_2 (3 x 20 mL) before being dried *in vacuo* to yield **176** as a white powder (445 mg, 0.72 mmol, 72%). Mp. 210 °C *dec.* (CH_2Cl_2) $[\alpha]_D^{20}$ = -49.2 (c = 0.2, MeOH)

δ_H (600 MHz, $CDCl_3$) 8.82 (d, J = 8.7, 1H, H-7), 8.26 (s, 1H, H-9), 8.06 (s, 2H, H-8), 4.51-4.43 (m, 1H, H-1), 4.08-4.01 (m, 1H, H-6), 2.45-2.34 (m, 1H, H-2a), 2.01-1.79 (m, 4H, H-2b, H-3a, H-4a, H-5a), 1.71-1.59 (m, 1H, H-5b), 1.43-1.28 (m, 2H, H-3b, H-4b) ppm

δ_C (140 MHz, $CDCl_3$) 163.9 (C=O), 163.4 (C=O), 138.3 (q), 136.7 (q), 130.3 (q, $J_{C\text{-}F}$ = 33.2), 128.0, 127.8-127.6 (2 signals), 124.7, 122.9 (q, $J_{C\text{-}F}$ = 273.5), 55.4, 49.7, 31.0, 27.6, 24.9, 24.4 ppm

δ_F (377 MHz, $CDCl_3$) -61.41

HRMS (m/z – ESI^{+Na}): Found: 642.9548 (M^+) $C_{23}H_{14}Cl_4F_6N_2O_3Na$ Requires: 642.9555

ν_{max} (neat)/cm^{-1}: 3252, 3089, 2942, 2859, 1738, 1644, 1552, 1451, 1364, 1274, 1289, 1176, 1161, 1126, 905, 484, 700, 681

_N_-((1_R_,2R)-2-aminocyclohexyl)-3,5-_bis_(trifluoromethyl)benzamide (177)

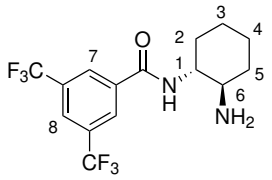

To a 50 mL RBF under Ar atmosphere containing a stir bar and equipped with a reflux condenser was added THF (25 mL), ethylenediamine (40 µL, 0.55 mmol) and **176** (270 mg, 0.5 mmol). The solution was refluxed for 4 h, before being concentrated *in vacuo*. The resulting yellow oil was dissolved in CH_2Cl_2 (10 mL) before being washed with H_2O (30 mL). The aqueous phase was extracted with CH_2Cl_2 (3 x 10 mL) and the combined organic phases were dried *in vacuo*. The product was purified *via* a silica plug to yield **177** as a yellow crystalline solid (78 mg, 0.22 mmol, 44%). Mp. 166-167 °C (CH_2Cl_2). $[\alpha]_D^{20}$ = +29.9 (c = 0.1, MeOH)

δ_H (600 MHz, $CDCl_3$) 7.91 (d, J = 7.5, 2H, H-7), 7.50-7.42 (m, 1H, H-9), 7.38 (app.t, 2H, H-8), 3.21-3.14 (m, 2H, H-1, H-6), 2.33 (app.d, 2H, H-2), 1.84 (app.d, 2H, H-3), 1.64-1.41 (m, 2H, H-3a, H-4a), 1.40-1.40 (m, 2H, H-3b, H-4b) ppm

δ_C (151 MHz, DMSO-d_6) 163.7 (C=O), 137.6, 130.8 (q, $J_{C\text{-}F}$ = 33.1), 128.7, 125.1, 123.7 (q, $J_{C\text{-}F}$ = 272.8), 56.7, 54.1, 49.0, 34.8, 32.2, 25.3 ppm

δ_F (377 MHz, $CDCl_3$) -61.41

ν_{max} (neat)/cm^{-1}: 3310, 3099, 2941, 2858, 1641, 1563, 1490, 1447, 1364, 1270, 1165, 1096, 904, 700, 672

(*N*-((1*R*,2*R*)-2-(2-bromoacetamido)cyclohexyl)benzamide (178)

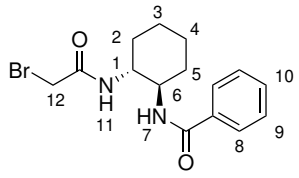

To a 50 mL round bottom flask containing a magnetic stirrer was added K_2CO_3 (10% aq, 5 mL) and CH_2Cl_2 (5 mL) was added **166** (130 mg, 0.6 mmol). The apparatus was then cooled to 0 °C before bromoacetal bromide (67 μL, 0.9 mmol) in CH_2Cl_2 (5 mL) was added dropwise *via* syringe. After stirring for 1 h, the aqueous phase was separated, and the organic phase was washed with K_2CO_3 (10 mL) and brine (10 mL) before being dried over $MgSO_4$. The solvent was removed *in vacuo* and the product was purified by passage through a plug of silica to yield **178** as a brown solid (119 mg, 0.35 mmol, 59%). Mp. 142 °C *dec.* (CH_2Cl_2) $[\alpha]_D^{20}$ = -70.6 (*c* = 0.3, MeOH).

δ_H (400 MHz, DMSO-d_6)	8.20 (d, *J* = 7.82, 1H, H-7), 8.11 (d, *J* = 8.05, 1H, H-11), 7.73 (d, *J* = 7.26, 2H, H-8), 7.52-7.35 (m, 3H, H-9, H-10), 3.81-3.61 (m, 4H, H-12, H-1, H-6), 1.91-1.77 (m, 2H, H-5), 1.73-1.59 (m, 2H, H-2), 1.45-1.15 (m, 4H, H-3, H-4) ppm
δ_C (101 MHz, DMSO-d_6)	167.6 (C=O), 166.8 (C=O), 134.1, 131.2, 128.1, 127.0, 54.4, 54.3, 32.4, 31.9, 29.4, 24.7, 24.6 ppm
HRMS (m/z – ESI+):	Found: 339.0700 (M^+) $C_{15}H_{20}BrN_2O_2$ Requires: 339.0703
ν_{max} (neat)/cm^{-1}:	3312, 3251, 3074, 2941, 2857, 1654, 1630, 1578, 1538, 1490, 1447, 1426, 1364, 1340, 1324, 1302, 1204, 1150, 942, 860, 703, 660

(*N*-((1*S*,2*S*)-2-(2-bromoacetamido)cyclohexyl)benzamide (179)

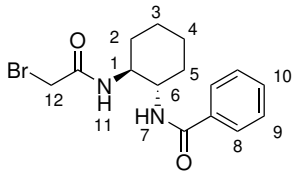

To a 50 mL round bottom flask containing a magnetic stirrer, containing K_2CO_3 (10% aq, 5 mL) and CH_2Cl_2 (5 mL) was added **173** (92 mg, 0.42 mmol). The apparatus was then cooled to 0 °C before bromoacetal bromide (45 μL, 0.6 mmol) in CH_2Cl_2 (10 mL) was added dropwise *via* syringe. After stirring for 1 h, the aqueous phase was separated, and the organic phase was washed with K_2CO_3 (10 mL) and brine (10 mL) before being dried over $MgSO_4$. The solvent was removed *in vacuo* and the product was purified by passage through a plug of silica to yield **179** as a brown solid (113 mg, 0.34 mmol, 80%). Mp. 139 °C *dec.* (CH_2Cl_2) $[\alpha]_D^{20}$ = +60.1 (c = 0.2, MeOH).

δ_H (400 MHz, DMSO-d_6)	8.20 (d, J = 7.82, 1H, H-7), 8.11 (d, J = 8.05, 1H, H-11), 7.73 (d, J = 7.26, 2H, H-8), 7.50-7.35 (m, 3H, H-9, H-10), 3.80-3.65 (m, 4H, H-12, H-1, H-6), 1.90-1.77 (m, 2H, H-5), 1.73-1.62 (m, 2H, H-2), 1.46-1.16 (m, 4H, H-3, H-4) ppm
δ_C (101 MHz, DMSO-d_6)	166.2 (C=O), 166.0 (C=O), 135.0 (q), 130.9, 128.1, 128.0, 127.3, 52.8, 52.5, 31.7, 31.6, 24.5-24.3 (2 signals) ppm
HRMS (m/z – ESI+):	Found: 339.0699 (M^+) $C_{15}H_{20}BrN_2O_2$ Requires: 339.0703
ν_{max} (neat)/cm^{-1}:	3250, 3073, 2934, 2858, 1661, 1629, 1605, 1555, 1490, 1433, 1339, 1323, 1278, 1226, 1150, 1098, 972, 920, 831, 683, 658

(*N*-((1*R*,2R)-2-(2-bromoacetamido)cyclohexyl)-3,5-*bis*(trifluoromethyl)benzamide (180)

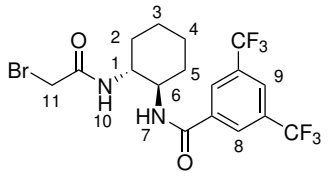

To a 50 mL round bottom flask containing a magnetic stirrer containing K_2CO_3 (10% aq, 5 mL) and CH_2Cl_2 (5 mL) was added **177** (100 mg, 0.3 mmol). The apparatus was then cooled to 0 °C before bromoacetal bromide (35 μL, 0.45 mmol) in CH_2Cl_2 (5 mL) was added dropwise *via* syringe. After stirring for 1 h, the aqueous phase was separated, and the organic phase was washed with K_2CO_3 (10 mL) and brine (10 mL) before being dried over $MgSO_4$. The solvent was removed *in vacuo* and the product was purified by passage through a plug of silica to yield **180** as a yellow solid (93 mg, 0.19 mmol, 63%). Mp. 156 °C *dec.* $(CH_2Cl_2)[\alpha]_D^{20}$ = -56.3 (*c* = 0.3, MeOH).

δ_H (400 MHz, DMSO-d_6)	8.70 (d, *J* = 9.1, 1H, H-7), 8.36 (s, 1H, H-8), 8.30-8.23 (m, 2H, H-9, H-10), 3.87-3.64 (m, 4H, H-1, H-6, H-11), 1.88-1.79 (m, 2H, H-5), 1.75-1.65 (m, 2H, H-2), 1.50-1.15 (m, 4H, H-3, H-4) ppm
δ_C (101 MHz, DMSO-d_6)	166.4 (C=O, 163.7 (C=O), 137.7 (q), 130.8 (q, $J_{C\text{-}F}$ = 33.2), 128.7, 125.0, 123.8 (q, $J_{C\text{-}F}$ = 275.1), 53.7, 52.7, 32.2-32.0 (2 signals), 29.9, 25.0, 24.9 ppm
δ_F (377 MHz, $CDCl_3$)	-61.25 ppm
HRMS (m/z – ESI+):	Found: 497.02668 (M^+) $C_{15}H_{20}BrN_2O_2$ Requires: 497.0270
ν_{max} (neat)/cm^{-1}:	3252, 3089, 2942, 2859, 1644, 1552, 1451, 1364, 1289, 1275, 1177, 1162, 1126, 905, 700, 681

(1*S*,2*S*,4*S*,5*R*)-1-(2-(((1*R*,2*R*)-2-benzamidocyclohexyl)amino)-2-oxoethyl)-2-((*R*)-hydroxy(6-methoxyquinolin-4-yl)methyl)-5-vinylquinuclidin-1-ium bromide (183)

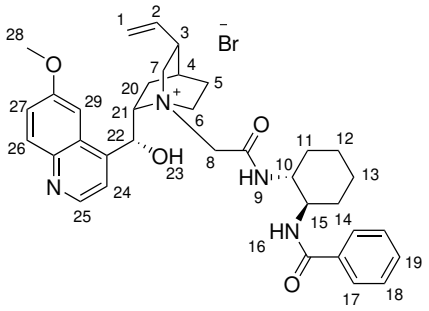

To a 10 mL round bottom flask containing a magnetic stirrer was added 13 (32 mg, 0.1 mmol) and **178** (41 mg, 0.1 mmol). The apparatus was flushed with Ar before being fitted with a septum and a balloon of Ar. Anhydrous THF (10 mL) was added *via* syringe and the reaction mixture was stirred at room temperature for 16 h. Et_2O (20 mL) was added, and the resulting precipitate was filtered to give product **181** as a white amorphous solid (65 mg, 0.12 mmol, 98%). Mp. 201 °C *dec.* (Et_2O) $[\alpha]_D^{20}$ = -52.1 (*c* = 0.2, MeOH).

δ_H (600 MHz, DMSO-d_6) 8.83 (d, 1H, *J* = 8.10, H-9), 8.77 (d, 1H, *J* = 4.5 H-25), 8.26 (d, 1H, *J* = 8.58, H-16), 7.97 (d, 1H, *J* = 9.72, H-26), 7.73 (dd, 2H, *J* = 9.48, 7.08, H-17), 7.65 (d, 1H, *J* = 4.5, H-24), 7.45-7.43 (m, 2H, H-27, H-29), 7.33 (t, 1H, *J* = 7.08, H-19), 7.19 (t, 2H, *J* = 9.48, H-18), 6.61 (d, 1H, *J* = 4.0, H-23), 5.99-5.95 (m, 1H, H-22), 5.68-5.60 (m, 1H, H-2), 5.06 (d, 1H, *J* = 17.4, H-1a), 4.96 (d, 1H, *J* = 10.4, H-1b), 4.37-4.26 (m, 3H, H-8, H-21), 4.22 (t, 1H, *J* = 8.6, H-7a), 4.03 (s, 3H, H-28), 3.98-3.91 (m, 1H, H-10), 3.82-3.67 (m, 3H, H-15, H-7b, H-6a), 3.54-3.47 (m, 1H, H-6b), 2.58-2.53 (m, 1H, H-3), 2.09-1.97 (m, 3H, H-20a, H-4, H-11a), 1.92-1.83 (m, 2H, H-14a, H-5a), 1.82-1.72 (m, 3H, H-14b, H-11b, H-20b), 1.55-1.38 (m, 2H, H-12), 1.37-1.24 (m, 2H, H-13), 1.07-1.01 (m, 1H, H-5b) ppm

δ_C (140 MHz, DMSO-d_6) 166.6 (C=O), 163.6 (C=O), 158.2 (q), 147.8, 144.2 (q), 144.0 (q), 138.3, 134.9 (q), 131.9, 131.4, 128.4, 127.7, 125.9, 122.4, 120.4, 116.3, 102.0, 35.9, 65.5, 60.6, 60.0, 56.5, 55.7, 53.3, 52.0, 37.3, 32.2, 32.1, 25.8, 25.1, 24.9, 24.8, 21.3 ppm

HRMS (m/z – ESI+): Found: 583.3279 (M^+) $C_{35}H_{43}N_4O_4$ Requires: 583.3278

ν_{max} (neat)/cm^{-1}: 3246, 3072, 2935, 1674, 1622, 1537, 1511, 1489, 1450, 1326, 1296, 1241, 1229, 1143, 1080, 1027, 916, 859, 832, 800, 713

(1*S*,2*S*,4*S*,5*R*)-1-(2-(((1*S*,2*S*)-2-benzamidocyclohexyl)amino)-2-oxoethyl)-2-((*R*)-hydroxy(6-methoxyquinolin-4-yl)methyl)-5-vinylquinuclidin-1-ium bromide (182)

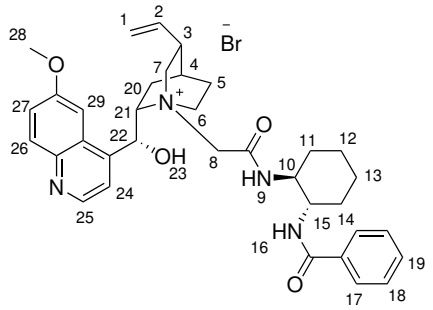

To a 10 mL round bottom flask containing a magnetic stirrer was added 13 (32 mg, 0.1 mmol) and **179** (41 mg, 0.1 mmol). The apparatus was flushed with Ar before being fitted with a septum and a balloon of Ar. Anhydrous THF (10 mL) was added *via* syringe and the reaction mixture was stirred at room temperature for 16 h. Et_2O (20 mL) was added, and the resulting precipitate was filtered to give product **182** as a white amorphous solid (63 mg, 0.11 mmol, 95%). Mp. 199 °C *dec.* (Et_2O) $[\alpha]_D^{20}$ = -10.0 (*c* = 0.2, MeOH).

δ_H (600 MHz, DMSO-d_6) 8.88 (d, 1H, *J* = 8.00, H-9), 8.79 (d, 1H, *J* = 4.5 H-25), 8.34 (d, 1H, *J* = 8.24, H-16), 7.98 (d, 1H, *J* = 9.17, H-26), 7.85 (dd, 2H, *J* = 9.45, 7.05, H-17), 7.70 (d, 1H, *J* = 4.5, H-24), 7.50 (t, 1H, *J* = 7.5, H-19), 7.47-7.41 (m, 4H, H-18, H-27, H-29), 6.72 (d, 1H, *J* = 3.7, H-23), 5.87-5.83 (m, 1H, H-22), 5.57-5.49 (m, 1H, H-2), 5.05 (d, 1H, *J* = 17.4, H-1a), 4.92 (d, 1H, *J* = 10.2, H-1b), 4.49 (d, 1H, *J* = 16.1, H-8a), 4.40 (t, 1H, *J* = 9.7, H-21), 4.36-4.29 (m, 1H, H-7a), 4.12-4.07 (m, 4H, H-8b, H-28), 4.04-3.99 (m, 1H, H-6a), 3.92-3.85 (m, 2H, H-10, H-15), 3.50-3.41 (m, 2H, H-6b, H-7b), 2.63-2.57 (m, 1H, H-3), 2.05-1.97 (m, 2H, H-4, H-11a),

1.97-1.84 (m, 3H, H-11b, H-5a, H-14a), 1.81-1.70 (m, 3H, H-12, H-14b), 1.55-1.46 (m, 1H, H-20a), 1.37-1.24 (m, 3H, H-20b, H-13), 1.07-1.01 (m, 1H, H-5b) ppm

δ_C (140 MHz, DMSO-d_6) 166.6 (C=O), 164.3 (C=O), 158.4 (q), 147.8, 144.2 (q), 143.9 (q), 138.3, 135.1, 132.0, 131.6, 128.7, 127.8, 125.9, 122.4, 120.7, 116.0, 101.8, 66.1, 63.6, 60.3, 59.22, 56.7, 56.6, 52.9, 52.6, 37.1, 32.4, 32.2, 25.7, 25.1, 24.9, 24.8, 21.6 ppm

HRMS (m/z – ESI+): Found: 583.3279 (M^+) $C_{35}H_{43}N_4O_4$ Requires: 583.3278

ν_{max} (neat)/cm^{-1}: 3217, 3060, 2936, 1673, 1621, 1537, 1510, 1489, 1451, 1327, 1241, 1229, 1142, 1081, 1026, 917, 859, 832, 801, 713

(1*S*,2*S*,4*S*,5*R*)-1-(2-(((1*R*,2*R*)-2-(3,5-*bis*(trifluoromethyl)-benzamido)cyclohexyl)amino)-2-oxoethyl)-2-((*R*)-hydroxy(6-methoxyquinolin-4-yl)methyl)-5-vinylquinuclidin-1-ium bromide (266)

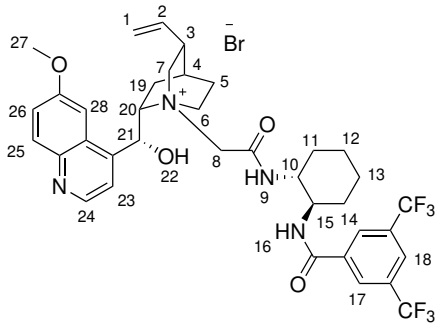

To a 10 mL round bottom flask containing a magnetic stirrer was added 13 (97 mg, 0.3 mmol) and **267** (143 mg, 0.3 mmol). The apparatus was flushed with Ar before being fitted with a septum and a balloon of Ar. Anhydrous THF (10 mL) was added *via* syringe and the reaction mixture was stirred at room temperature for 16 h. Et_2O (20 mL) was added, and the resulting precipitate was filtered. The product was purified by column chromatography 8:2, CH_2Cl_2/MeOH, Rf = 0.2) to yield **266** as a yellow amorphous solid (179 mg, 0.22 mmol, 74%). Mp. 157 °C *dec.* (CH_2Cl_2) $[\alpha]_D^{20}$ = -43.3 (c = 0.2, MeOH).

δ_H (600 MHz, DMSO-d_6) 8.81 (d, 1H, J = 7.8, H-9), 8.76 (d, 1H, J = 8.3, H-16), 8.71 (d,

1H, J = 4.4 H-25), 8.40 (s, 2H, H-17), 8.06 (s, 1H, H-18), 7.91 (d, 1H, J = 9.3, H-24), 7.58 (d, 1H, J = 4.5, H-23), 7.39 (dd, J = 9.3, 2.7, H-26), 7.31 (d, 1H, J = 2.7, H-28), 6.60 (d, 1H, J = 5.1, H-22), 5.83-5.80 (m, 1H, H-21), 5.62-5.55 (m, 1H, H-2), 5.01 (d, 1H, J = 17.5, H-1a), 4.91 (d, 1H, J = 10.9, H-1b), 4.32-4.22 (m, 3H, H-8, H-20), 4.18 (t, 1H, J = 8.6, H-7a), 4.05-3.96 (m, 4H, H-6a, H-27), 3.83-3.75 (m, 2H, H-10, H-15), 3.70 (t, 1H, J = 9.9, H-6b), 3.53-3.47 (m, 1H, H-7b), 2.59-2.55 (m, 1H, H-3), 2.11-1.95 (m, 3H, H-13a, H-14a, H-11a), 1.94-1.87 (m, 2H, H-20a, H-5a), 1.84-1.73 (m, 3H, H-14b, H-11b, H-4), 1.63-1.44 (m, 2H, H-12), 1.38-1.28 (m, 2H, H-20b, H-13b), 1.00-0.91 (m, 1H, H-5b) ppm

δ_C (140 MHz, DMSO-d_6) 163.6 (C=O), 163.3 (C=O), 158.2 (q), 147.6, 144.0 (q), 143.6 (q), 138.2, 136.5, 131.8, 130.6 (q, $J_{C\text{-}F}$ = 34.8), 128.4, 125.6, 125.1, 123.5 (q, $J_{C\text{-}F}$ = 275.5), 122.3, 120.2, 116.0, 101.3, 66.0, 65.3, 60.4, 59.8, 56.5, 55.8, 53.5, 52.7, 37.3, 32.0, 31.9, 25.8, 25.1, 24.8, 24.7, 21.2 ppm

HRMS (m/z – ESI+): Found: 719.3030 (M^+) $C_{37}H_{41}F_6N_4O_4$ Requires: 719.3027

ν_{max} (neat)/cm^{-1}: 3273, 3101, 2936, 1623, 1537, 1510, 1489, 1326, 1241, 1145, 1091, 1063, 907, 859, 832, 800, 714

(1*S*,2*S*,4*S*,5*R*)-1-(2-(((1*R*,2*R*)-2-benzamidocyclohexyl)amino)-2-oxoethyl)-2-((*R*)-hydroxy(6-methoxyquinolin-4-yl)methyl)-5-vinylquinuclidin-1-ium 4-nitrophenolate (161)

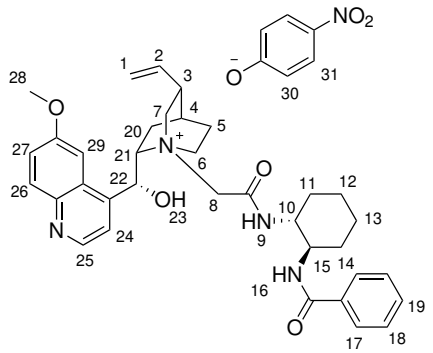

To a 50 mL RBF was added **181** (33 mg, 0.05 mmol) and methanol (5 mL). Amberlite® OH IRN78 (100 mg) in methanol (5 mL) was then added in one portion. The apparatus was flushed with Ar before being fitted with a septum and balloon of Ar. The vessel was then shaken at 450 rpm. After 16 h, the reaction was passed through a column containing. Amberlite® OH IRN78 (100 mg) with methanol and was collected into a 50 mL RBF. A stir bar was then added to the solution, and the apparatus was flushed with Ar. 4-Nitrophenol (7 mg, 0.05 mmol) was then added in one portion. After 16 h of stirring, the reaction was concentrated *in vacuo*, yielding product **161** as a yellow crystalline solid (35mg, 0.049 mmol, 97%). Mp. 192 °C *dec.* (MeOH) $[\alpha]_D^{20}$ = -62.1 (c = 0.2, MeOH).

δ_H (400 MHz, DMSO-d_6)	8.84 (d, 1H, J = 8.1, H-9), 8.76 (d, 1H, J = 4.4 H-25), 8.27 (d, 1H, J = 8.5, H-16), 7.97 (d, 1H, J = 10.1, H-27), 7.84 (d, 2H, J = 9.5, H-30), 7.71 (d, 2H, J = 7.1, H-17), 7.64 (d, 1H, J = 4.5, H-24), 7.63-7.41 (m, 2H, H-26, H-29), 7.30 (t, 1H, J = 7.3, H-19), 7.16 (t, 2H, J = 8.3, H-18), 6.23 (d, 2H, J = 9.5, H-31), 5.94-5.91 (m, 1H, H-22), 5.68-5.58 (m, 1H, H-2), 5.06 (d, 1H, J = 17.4, H-1a), 4.96 (d, 1H, J = 10.4, H-1b), 4.35-4.18 (m, 4H, H-6a, H-8, H-21), 4.03 (s, 3H, H-28), 3.99-3.88 (m, 1H, H-10), 3.83-3.74 (m, 2H, H-15, H-7a), 3.68 (t, 1H, J = 10.4, H-7b), 3.51-3.48 (m, 1H, H-6b), 2.59-2.53 (m, 1H, H-3), 2.10-1.95 (m, 3H, H-4, H-20a, H-11a), 1.92-1.68 (m, 5H, H-5a, H-14, H-11b, H-20b), 1.56-1.21 (m, 4H, H-12, H-13), 1.07-0.95 (m, 1H, H-5b) ppm
δ_C (101 MHz, DMSO-d_6)	166.6 (C=O), 163.7 (C=O), 158.2 (q), 147.7, 144.2 (q), 144.1 (q), 138.3, 134.9, 131.8, 131.3, 128.6 125.9, 125.8, 122.3, 120.4, 116.3, 102.0, 65.7, 65.6, 60.6, 59.9, 56.5, 55.5, 53.2, 52.2, 37.3, 32.1, 32.0, 29.5, 29.0, 25.8, 25.1, 24.9, 24.8, 22.6, 21.3, 19.7 ppm
HRMS (m/z – ESI+):	Found: 583.3280 (M^+) $C_{35}H_{43}N_4O_4$ Requires: 583.3278
ν_{max} (neat)/cm^{-1}:	3243, 2929, 2856, 1673, 1622, 1578, 1508, 1270, 1240, 1105, 1027, 986, 851, 704

(1*S*,2*S*,4*S*,5*R*)-1-(2-(((1*S*,2*S*)-2-benzamidocyclohexyl)amino)-2-oxoethyl)-2-((*R*)-hydroxy(6-methoxyquinolin-4-yl)methyl)-5-vinylquinuclidin-1-ium 4-nitrophenolate (162)

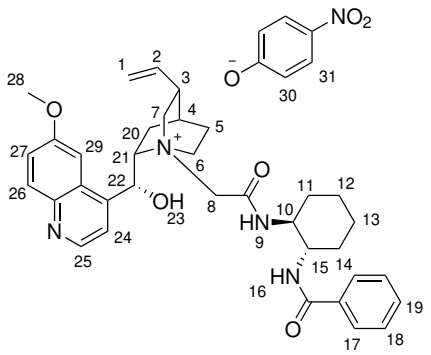

To a 50 mL RBF was added **182** (33 mg, 0.05 mmol) and methanol (5 mL). Amberlite® OH IRN78 (100 mg) in methanol (5 mL) was then added in one portion. The apparatus was flushed with Ar before being fitted with a septum and balloon of Ar. The vessel was then shaken at 450 rpm. After 16 h, the reaction was passed through a column containing. Amberlite® OH IRN78 (100 mg) with methanol and was collected into a 50 mL RBF. A stir bar was then added to the solution, and the apparatus was flushed with Ar. 4-Nitrophenol (7 mg, 0.05 mmol) was then added in one portion. After 16 h of stirring, the reaction was concentrated *in vacuo*, yielding product **162** as a yellow crystalline solid (32mg, 0.049 mmol, 97%). Mp. 192 °C *dec.* (MeOH) $[\alpha]_D^{20}$ = -9.5 (*c* = 0.2, MeOH).

δ_H (400 MHz, DMSO-d_6) 8.91 (d, 1H, *J* = 6.7, H-9), 8.78 (d, 1H, *J* = 4.5 H-25), 8.35 (d, 1H, *J* = 8.36, H-16), 7.98 (d, 1H, *J* = 9.0, H-26), 7.84 (d, 2H, *J* = 9.0, H-17), 7.75-7.68 (m, 3H, H-30, H-24), 7.54-7.38 (m, 5H, H-18, H-19, H-27, H-29), 5.96 (d, 2H, *J* = 9.4, H-31), 5.86-5.83 (m, 1H, H-22), 5.57-5.45 (m, 1H, H-2), 5.04 (d, 1H, *J* = 17.2, H-1a), 4.92 (d, 1H, *J* = 10.2, H-1b), 4.50 (d, *J* = 16.0, H-8a), 4.44-4.28 (m, 3H, H-7a, H-8b, H-21), 4.13-3.99 (m, 5H, H-6a, H-10, H-28), 3.82-3.67 (m, 3H, H-6b, H-7b, H-15), 2.64-2.56 (m, 1H, H-3), 2.08-1.97 (m, 2H, H-4, H-11a), 1.96-1.82 (m, 3H, H-11b, H-12a, H-14a), 1.82-1.67 (m, 3H, H-5a, H-14b, H-20a), 1.57-1.43 (m, 1H, H-12b), 1.37-1.24 (m, 3H, H-20b, H-13), 1.07-1.01 (m, 1H,

H-5b) ppm

δ_C (101 MHz, DMSO-d_6)	167.4 (C=O), 163.8 (C=O), 158.2, 147.7, 144.2 (q), 144.1 (q), 138.3, 131.7, 130.2, 127.6, 125.9, 124.0, 122.3, 120.5, 119.2, 116.3, 101.6, 66.4, 63.9, 60.3, 59.4, 57.0, 56.3, 51.3, 51.2, 37.0, 33.0, 32.3, 25.7, 25.2, 24.9, 24.8, 23.3, 21.9, 18.6 ppm
HRMS (m/z – ESI+):	Found: 583.3281 (M^+) $C_{35}H_{43}N_4O_4$ Requires: 583.3278
ν_{max} (neat)/cm^{-1}:	2923, 1739, 1665, 1622, 1579, 1496, 1459, 1359, 1273, 1240, 1168, 1108, 1027, 956, 987, 917, 845, 721, 786, 719, 703, 669

(1*S*,2*S*,4*S*,5*R*)-1-(2-(((1*R*,2*R*)-2-(3,5-*bis*(trifluoromethyl)-benzamido)cyclohexyl)amino)-2-oxoethyl)-2-((*R*)-hydroxy(6-methoxyquinolin-4-yl)methyl)-5-vinylquinuclidin-1-ium 4-nitrophenolate (163)

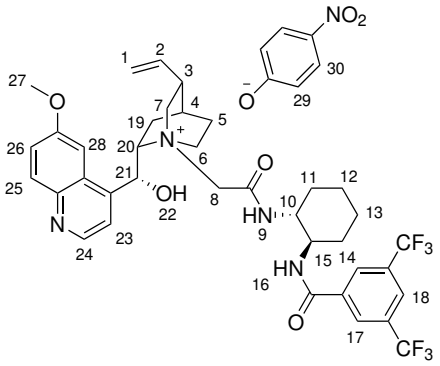

To a 50 mL RBF was added **266** (48 mg, 0.06 mmol) and methanol (5 mL). Amberlite® OH IRN78 (150 mg) in methanol (5 mL) was then added in one portion. The apparatus was flushed with Ar before being fitted with a septum and balloon of Ar. The vessel was then shaken at 450 rpm. After 16 h, the reaction was passed through a column containing. Amberlite® OH IRN78 (150 mg) with methanol and was collected into a 50 mL RBF. A stir bar was then added to the solution, and the apparatus was flushed with Ar. 4-Nitrophenol (8 mg, 0.06 mmol) was then added in one portion. After 16 h of stirring, the reaction was concentrated *in vacuo*, yielding product **163** as a yellow crystalline solid (50mg, 0.058 mmol, 97%). Mp. 173 °C *dec.* (MeOH)$[\alpha]_D^{20}$ = -58.2 (c = 0.2, MeOH).

δ_H (600 MHz, DMSO-d_6)	8.82 (d, 1H, J = 7.7, H-9), 8.77 (d, 1H, J = 8.3, H-16), 8.71 (d, 1H, J = 4.4 H-24), 8.40 (s, 2H, H-17), 8.06 (s, 1H, H-18), 7.91 (d, 1H, J = 9.1, H-25), 7.81 (d, 2H, J = 9.3, H-29), 7.58 (d, 1H, J = 4.5, H-23), 7.39 (dd, J = 9.3, 2.7, H-26), 7.31 (d, 1H, J = 2.7, H-28), 6.65 (d, 1H, J = 5.1, H-22), 6.14 (d, 2H, J = 9.3, H-30), 5.83-5.80 (m, 1H, H-21), 5.62-5.55 (m, 1H, H-2), 5.01 (d, 1H, J = 17.5, H-1a), 4.91 (d, 1H, J = 10.8, H-1b), 4.36-4.23 (m, 3H, H-8, H-20), 4.18 (t, 1H, J = 8.6, H-7a), 4.05-3.94 (m, 4H, H-6a, H-27) 3.83-3.75 (m, 2H, H-10, H-15), 3.70 (t, 1H, J = 9.9, H-7b), 3.53-3.47 (m, 1H, H-6b), 2.60-2.55 (m, 1H, H-3) 2.09-1.95 (m, 3H, H-5a, H-11a, H-19a), 1.94-1.86 (m, 2H, H-14a, H-19b), 1.84-1.74 (m, 3H, H-14b, H-11b, H-4) 1.63-1.43 (m, 2H, H-12), 1.37-1.28 (m, 2H, H-13), 0.98-0.90 (m, 1H, H-5b) ppm
δ_C (140 MHz, DMSO-d_6)	163.6 (C=O), 162.8 (C=O), 157.7 (q), 147.1, 143.6 (q), 143.2 (q), 137.7, 136.1, 130.2 (q, $J_{C\text{-}F}$ = 33.1), 127.8 (2 signals), 127.2, 125.1, 123.8, 122.0, 121.8, 119.7, 118.5, 116.0, 115.5, 101.2, 65.4, 64.8, 59.9, 59.3, 56.0, 55.3, 53.9, 52.2, 36.8, 31.5, 25.3, 24.6, 24.4, 24.3, 20.7 ppm
HRMS (m/z – ESI+):	Found: 719.3035 (M^+) $C_{37}H_{41}F_6N_4O_4$ Requires: 719.3027
ν_{max} (neat)/cm^{-1}:	2981, 1776, 1718, 1647, 1498, 1453, 1368, 1350, 1298, 1269, 1250, 1200, 1128, 1111, 1059, 1035, 953, 932, 868, 800, 738, 695

_N_-(2-hydroxy-5-nitrophenyl)benzamide (209)

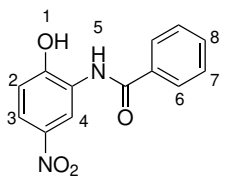

To a 25 mL RBF equipped with a stir bar was added 2-amino-4-nitrophenol (308.2 mg, 1 mmol),

Et_2O (20 mL), sat. $NaHCO_3$ (aq, 20 mL) and benzoyl chloride (116 µL, 1 mmol). The reaction was stirred at room temperature for 18 h before being filtered, and the residue was washed with H_2O (10 mL), 2M HCl (10 mL) and Et_2O before being dried *in vacuo*. Product was purified *via* recrystallization using hexane and CH_2Cl_2, yielding **209** as an orange solid (129.2 mg, 0.52 mmol, 52%).

Spectral data for this compound were consistent with those in the literature.[204]

δ_H (400 MHz, DMSO-d_6) 11.66 (s, 1H, H-1), 9.66 (s, 1H, H-5), 8.77 (d, J = 3.0, H-4), 8.04-7.97 (m, 3H, H-3, H-6), 7.63 (app.t, 1H, H-8), 7.56 (t, J = 7.9, H-7), 7.10 (d, J = 9.0, H-2) ppm

HRMS (m/z – ESI+): Found: 281.0537 (M^{+Na}) $C_{13}H_{10}N_2O_4Na$ Requires: 281.0538

2-(dimethylamino)-4-nitrophenol (210)

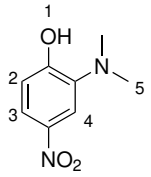

To a 25 mL RBF equipped with a stir bar was added 2-amino-4-nitrophenol (308.2 mg, 2 mmol), acetone (2 mL), NET_3 (417 µL, 3 mmol) and methyl iodide (250 µL, 4 mmol). The reaction was stirred at room temperature for 30 min before being refluxed for 4 h. CH_2Cl_2 (10 mL) was added, and the solution was washed with $NaHCO_3$ (30 mL) before being extracted with CH_2Cl_2 (3 x 20 mL). The combined organic extracts were washed with brine (30 mL) before being concentrated *in vacuo*, yielding a brown solid. Product was purified *via* recrystallization using hexane and CH_2Cl_2, yielding **210** as a red solid (206.2 mg, 1.14 mmol, 57%).

Spectral data for this compound were consistent with those in the literature.[205]

δ_H (400 MHz, $CDCl_3$) 8.12 (d, J = 2.7, H-4), 8.05 (dd, J = 2.7, 8.9, H-3), 7.03 (d, J = 7.03, H-2), 2.72 (s, H-5) ppm

HRMS (m/z – ESI+): Found: 429.2180 (M^{+Na}) $C_{27}H_{29}N_2O_3$ Requires: 429.2172

(1*S*,2*S*,4*S*,5*R*)-1-(2-((3,5-*bis*(trifluoromethyl)phenyl)amino)-2-oxoethyl)-2-((*R*)-hydroxy(6-methoxyquinolin-4-yl)methyl)-5-vinylquinuclidin-1-ium 3,3'-*bis*(3,5-*bis*(trifluoromethyl)phenyl)-2'-hydroxy-[1,1'-binaphthalen]-2-olate (212)

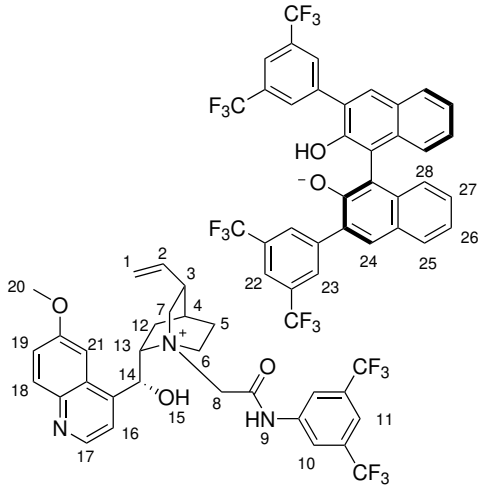

To a 50 mL RBF was added **199** (30 mg, 0.05 mmol) and methanol (5 mL). A stir bar was then added to the solution, and the apparatus was flushed with Ar before being fitted with a septum and a balloon of Ar. 3,3'-*Bis*(3,5-*bis*(trifluoromethyl)phenyl)-[1,1'-binaphthalene]-2,2'-diol (22 mg, 0.05 mmol) was then added in one portion. After 16 h of stirring, the reaction was concentrated *in vacuo*, yielding product **212** as a yellow crystalline solid (65 mg, 0.049 mmol, 97%). Mp. 180 °C *dec.* (MeOH)$[\alpha]_D^{20}$ = -15.8 (*c* = 0.2, MeOH).

δ_H (400 MHz, DMSO-d_6) 8.76 (d, 1H, *J* = 4.4, H-17), 8.48 (s, 4H, H-23), 8.17 (s, 2H, H-10), 8.06 (s, 2H, H-22), 8.00 (s, 2H, H-24), 7.97 (d, 1H, *J* = 9.2, H-18), 7.90-7.80 (m, 3H, H-11, H-25), 7.71 (d, 1H, *J* = 4.4, H-16), 7.39 (d, 1H, *J* = 9.2, H-19), 7.34 (s, 1H, H-21), 7.17-7.01 (m, 4H, H-26, H-27), 6.91 (d, 2H, *J* = 7.8, H-28), 6.01, (s, 1H, H-14), 5.76-5.64 (m, 1H, H-2), 5.20 (d, 1H, *J* = 17.5 H-1a), 5.00 (d, 1H, *J* = 10.7, H-1b), 4.78 (d, 1H, *J* = 15.7 H-8a), 4.56 (t, 1H, *J* = 8.7, H-7a), 4.51-4.40 (m, 2H, H-6a, H-8b), 4.33 (m, 1H, 6b), 3.91-5.73 (m, 5H, H-7b, H-13, H-20), 2.87-2.79 (m, 1H, H-3),

	2.17-2.01 (m, 2H, H-4, H-12a), 2.00-1.76 (m, 2H, H-5a, H-12b), 1.03-0.93 (m, 1H, H-5b) ppm
δ_C (101 MHz, DMSO-d_6)	165.0 (C=O), 158.2 (q), 147.9, 144.1 (q), 144.0 (q), 143.0 (q), 138.7, 135.2 (q), 132.0, 131.3 (q, $J_{C\text{-}F}$ = 32.6), 130.4, 130.1 (q, $J_{C\text{-}F}$ = 31.7), 129.0, 126.8 (q), 125.8 (q), 125.6 (q), 123.8 (q, $J_{C\text{-}F}$ = 277.3), 122.2, 122.0 (q, $J_{C\text{-}F}$ = 274.5), 121.0, 120.7, 120.2, 116.1, 101.8, 66.3, 65.4, 63.3, 60.8, 60.0, 57.6, 56.1, 37.2, 31.4, 25.8, 25.3, 22.5, 21.9, 15.6, 14.4, 11.8
δ_F (377 MHz, $CDCl_3$)	-61.17, -61.64
HRMS (m/z – ESI+):	Found: 594.2190 (M^+) $C_{30}H_{30}N_6N_3O_3$ Requires: 594.2186
ν_{max} (neat)/cm^{-1}:	3293, 3058, 2948, 1720, 1632, 1528, 1377, 1277, 1130, 1031, 844, 748, 682, 702

(1*S*,2*S*,4*S*,5*R*)-1-(2-((3,5-*bis*(trifluoromethyl)phenyl)amino)-2-oxoethyl)-2-((*R*)-hydroxy(6-methoxyquinolin-4-yl)methyl)-5-vinylquinuclidin-1-ium 3,3'-dibromo-[1,1'-binaphthalene]-2,2'-*bis*(olate) (213)

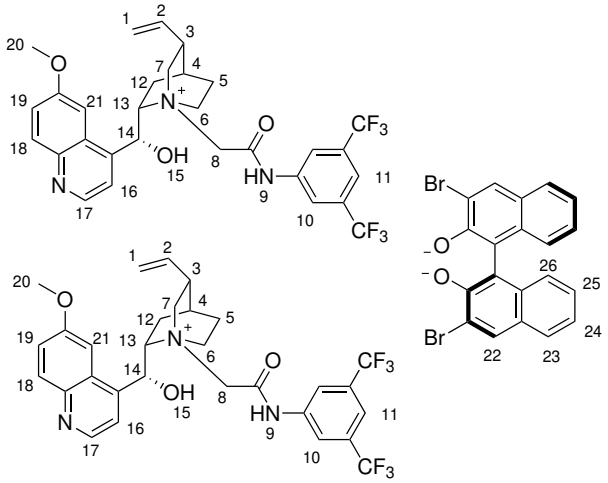

To a 50 mL RBF was added **199** (60 mg, 0.1 mmol) and methanol (5 mL). A stir bar was then added to the solution, and the apparatus was flushed with Ar before being fitted with a septum and a balloon of Ar. 3,3'-*Bis*(3,5-*bis*(trifluoromethyl)phenyl)-[1,1'-binaphthalene]-2,2'-diol (22 mg, 0.05 mmol) was then added in one portion. After 16 h of stirring, the reaction was

concentrated *in vacuo*, yielding product **212** as a yellow crystalline solid (80 mg, 0.049 mmol, 98%). Mp. 203 °C *dec.* (MeOH) $[\alpha]_D^{20}$ = -108.1 (*c* = 0.2, MeOH).

δ_H (400 MHz, DMSO-d_6)	8.79 (d, 2H, *J* = 4.3, H-17), 8.12-8.05 (m, 6H, H-10, H-18), 7.97 (s, 1H, H-22a), 7.95 (s, 1H, H-22b), 7.74 (d, 2H, *J* = 4.3, H-16), 7.69 (d, 2H, *J* = 8.1, H-23), 7.66-7.48 (m, 4H, H-21, H-11), 7.41 (dd, 2H, *J* = 2.4, 9.2, H-19), 7.05 (t, 2H, *J* = 8.1 H-24), 6.97 (t, 2H, *J* = 8.2, H-25), 6.81 (d, 2H, *J* = 8.1, H-26), 6.07 (d, 2H, *J* = 2.4, H-14), 5.79-5.67 (m, 2H, H-2), 5.27 (d, 1H, *J* = 17.3, H-1a), 5.02 (d, 1H, *J* = 10.6, H-1b), 4.76-4.43 (m, 6H, H-8, H-13), 4.38-4.24 (m, 4H, H-7a, H-6a), 3.91-3.85 (m, 8H, H-6b, H-20), 3.78-3.68 (m, 2H, H-7b), 2.89-2.81 (m, 2H, H-3), 2.14-2.04 (m, 4H, H-4, H-12a), 2.00-1.89 (m, 2H, H-5a), 1.88-1.78 (m, 2H, H-12b), 1.03-0.93 (m, 2H, H-5b) ppm
δ_C (101 MHz, DMSO-d_6)	165.9 (C=O), 158.3 (q), 147.8, 144.3 (q), 144.2 (q), 138.9 (2 signals), 134.1 (q), 131.9, 130.3, 127.4, 127.0 (q), 126.4 (q, $J_{C\text{-}F}$ = 55.9), 126.0, 125.5 (q), 125.0 (2 signals), 123.4 (q, $J_{C\text{-}F}$ = 269.7), 122.8 (q), 121.2, 120.6, 119.6 (q), 119.3 (q), 116.0, 112.4, 121.2, 120.9, 119.3, 116.0, 102.0, 66.4, 60.5, 56.3, 37.3, 25.9, 25.4, 21.9 ppm
HRMS (m/z – ESI+):	Found: 594.2184 (M^+) $C_{30}H_{30}F_6N_3O_3$ Requires: 594.2186
ν_{max} (neat)/cm^{-1}:	2948, 1750, 1643, 1520, 1358, 1273, 1130, 1031, 844, 748, 682, 702

((*S*)-(6-methoxyquinolin-4-yl)((1*S*,2*S*,4*S*,5*R*)-5-vinylquinuclidin-2-yl)methanol (216)

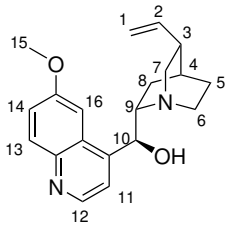

To a 100 mL RBF containing a stir bar and equipped with a reflux condenser was added quinine (1.63 g, 5 mmol), triphenylphosphine (1.84 g, 7 mmol). The flask was placed under an Ar atmosphere before being cooled to 0 °C. A solution of diisopropyl azodicarboxylate (DIAD, 1. mL, 7 mmol) in THF (10 mL) was added dropwise to the RBF and the resulting mixture was stirred for 15 min before a solution of benzoic acid (BzOH, 0.841 g, 7.5 mmol) in THF (20 mL) was added dropwise. The solution was stirred for 30 min at 0 °C before being stirred at room temperature for 20 h. Triphenylphosphine (1.84g, 7 mmol) was then added in one portion, and the reaction was heated to 50 °C for 4 h before being cooled to room temperature. Excess quinine was removed *via* column chromatography (8:2 CH_2Cl_2/MeOH). The fractions containing product and triphenylphosphine were concentrated under reduced pressure before being added to a solution of MeOH (10 mL) and K_2CO_3 (10% 10 mL). The aqueous phase was extracted with CH_2Cl_2 (3 × 10 mL). The organic extracts were combined before being concentrated under reduced pressure. The product was purified by flash column chromatography (8:2, CH_2Cl_2/MeOH, Rf = 0.3), resulting in **268** as a yellow oil (502 mg, 1.55 mmol, 31%). $[\alpha]_D^{20}$ = +38.2 (c = 0.2, MeOH)

Spectral data for this compound were consistent with those in the literature.[206]

δ_H (400 MHz, DMSO-d_6) 8.72 (d, 1H, J = 4.6, H-12), 7.95 (d, 1H, J = 9.1, H-13), 7.70 (d, 1H, J = 2.6, H-16), 7.55 (d, 1H, J = 4.6, H-11), 7.42 (dd, 1H, J = 2.6, 9.1, H-14), 5.89-5.78 (m, 1H, H-2), 5.28 (br s, 1H, OH), 5.20 (d, 1H, J = 9.4, H-9), 5.01 (d, 1H, J = 17.2, H-1a), 4.94 (d, 1H, J = 10.1, H-1b), 3.93 (s, 3H, H-15), 3.25-3.13 (m, 2H, H-6a, H-7a), 2.78-2.67 (m, 2H, H-6b, H-7b), 2.38-2.29 (m, 1H, H-3), 1.69-1.49 (m, 3H, H-8, H-4), 1.50-1.39 (m, 1H, H-5b), 0.77-0.67 (m, 1H, H-5b) ppm

HRMS (m/z – ESI+): Found: 325.1916 (M^+) $C_{20}H_{25}N_2O_2$ Requires: 325.1911.

(*S*)-(6-methoxyquinolin-4-yl)((1*S*,2*S*,4*S*,5*R*)-5-vinylquinuclidin-2-yl)methyl benzoate (215)

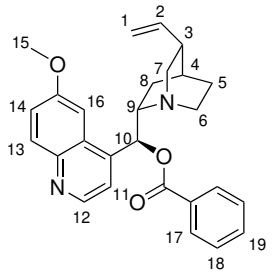

To a 25 mL RBF containing a stir bar was added **268** (108 mg, 0.33 mmol), CH_2Cl_2 (5 mL) and benzoyl chloride (61 µL, 0.5 mmol). The solution was stirred for 24 h before being concentrated under reduced pressure. The resulting brown solid was dissolved in CH_2Cl_2 (1 mL) before being triturated in Et_2O (10 mL). The resulting solid was filtered, isolating product **215** as a yellow solid (85 mg, 0.2 mmol, 62%). Mp. 185-195 °C (Et_2O).$[\alpha]_D^{20}$ = +61.4 (c = 0.3, MeOH)

δ_H (400 MHz, $CDCl_3$) 8.80 (d, 1H, J = 4.5, H-12), 8.09-8.04 (3, 3H, H-17, H-13), 7.71 (d, 1H, J = 2.8, H-16), 7.58-7.52 (m, 2H, H-19, H-11), 7.46-7.40 (m, 3H, H-14, H-18), 6.72 (d, 1H, J = 9.1, H-10), 5.90-5.80 (m, 1H, H-2), 5.08-5.00 (m, 2H, H-1), 4.04 (s, 3H, H-15), 3.68-3.58 (m, 1H, H-9), 3.47-3.36 (m, 1H, H-7a), 3.30-3.22 (m, 1H, H-6a), 2.82-2.76 (m, 2H, H-6b, 7b), 2.36-2.28 (m, 1H, H-3), 1.75-1.63 (m, 3H, H-4, H-8), 1.54-1.44 (m, 1H, H-5a), 1.00-0.90 (m, 1H, H-5b) ppm

δ_C (101 MHz, $CDCl_3$) 166.1 (C=O), 158.1(q), 147.5, 144.9 (q), 141.9 (q), 141.7 (q), 133.1, 131.9, 130.0, 129.9, 128.4, 127.8, 122.0, 120.5, 114.5, 101.7, 72.1, 59.3, 56.2, 55.6, 41.5, 39.6, 28.0, 27.4, 25.3 ppm

HRMS (m/z – ESI+): Found: 429.2173 (M^+) $C_{27}H_{29}N_2O_3$ Requires: 429.2180

ν_{max} (neat)/cm^{-1}: 2928, 1694, 1622, 1507, 1309, 1266, 1247, 1229, 1111, 1069,

1025, 961, 913, 848, 820, 712, 706

Neutral PET hydrolysis

Method I: using disodium terephthalate as a co-catalyst

To a 23 mL Teflon® cup was added water (10 mL), disodium terephthalate (0.0109 g, 1 mol%), a catalyst (2 mol%)[a] and poly(ethylene terephthalate) flakes (*ca.* 5 mm squares, 1.000g). The Teflon® cup was then sealed inside a batch hydrothermal autoclave before being placed for 3 h into an oven pre-heated at 200 °C. The batch hydrothermal autoclave was then placed on a ceramic tile for 16 h. To the reaction mixture was then added sodium hydroxide (0.550 g), HPLC-grade water (6 mL) and a stir bar. After 10 min of stirring, the reaction mixture was filtered, and the residue was washed with water (10 mL x 2).[b] The filtrate was adjusted, with cooling, to pH 2-3 using dilute hydrochloric acid and the precipitate was filtered. The residue was washed with water (10 mL) and the product was dried for 4 h in a vacuum oven at 60 °C[c]

[a]Mol% of catalyst is related to the number of moles of monomeric units (5.204 mmol) present in 1.000 g of polymer.

[b]To establish catalyst recyclability, the unreacted PET residue was subsequently washed with acetone (2 x 10 mL) and the washings concentrated *in vacuo*.

[c]Yield calculated based on the mass of recovered TPA after acidification. Correction is made for the additional TPA derived from protonation of the added disodium terephthalate upon workup. To evaluate purity and provide yield data based on an internal standard, samples of TPA post*in vacuo* drying were added to known amounts of 4-iodoanisole, and yield was calculated by ^{1}H NMR spectroscopy. Spectroscopically obtained yields agreed with those derived from the mass of TPA within 1.1% in all cases.

Method II: using an ionic liquid catalyst

To a 23 mL Teflon® cup was added water (10 mL), catalyst (0.5 - 1 mol%)[a] and poly(ethylene terephthalate) flakes (*ca.* 5 mm squares, 1.000g). The Teflon® cup was then sealed inside a batch hydrothermal autoclave before being placed for 3 h into an oven pre-heated at 200 °C.

The batch hydrothermal autoclave was then placed on a ceramic tile for 16 h. To the reaction mixture was then added sodium hydroxide (0.550 g), HPLC-grade water (6 mL) and a stir bar. After 10 min of stirring, the reaction mixture was filtered, and the residue was washed with water (10 mL x 2).[b] The filtrate was adjusted, with cooling, to pH 2-3 using dilute hydrochloric acid and the precipitate was filtered. The residue was washed with water (10 mL) and the product was dried for 4 h in a vacuum oven at 60 °C[c]

[a]Mol% of catalyst is related to the number of moles of monomeric units (5.204 mmol) present in 1.000 g of polymer.

[b]To establish catalyst recyclability, the unreacted PET residue was subsequently washed with acetone (2 x 10 mL) and the washings concentrated *in vacuo*.

[c]Yield calculated based on the mass of recovered TPA after acidification. Correction is made for the additional TPA derived from protonation of the added disodium terephthalate upon workup. To evaluate purity and provide yield data based on an internal standard, samples of TPA post*in vacuo* drying were added to known amounts of 4-iodoanisole and yield was calculated by ^{1}H NMR spectroscopy. Spectroscopically obtained yields agreed with those derived from the mass of TPA within 1.1% in all cases.

Terephthalic acid (100)

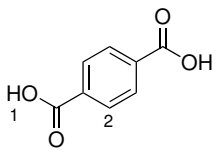

To a 23 mL Teflon® cup was added water (10 mL), **243** (0.0295 g, 0.026 mmol, 0.5 mol%).[a] and polyethylene terephthalate flakes (*ca.* 5 mm squares, 1.000 g). The Teflon® cup was then sealed inside a batch hydrothermal autoclave before being placed into an oven pre-heated at 200 °C for 5 h. The batch hydrothermal autoclave was then placed on a ceramic tile for 16 h. To the reaction mixture was then added sodium hydroxide (0.550 g) and water (6 mL). After 10 min, the reaction mixture was filtered and washed with water (10 mL x 2). The filtrate was adjusted, with cooling, to pH 2-3 using dilute HCl, and the precipitate was filtered. The residue was washed with water (10 mL) and the product was dried for 4 h in a vacuum oven at 60 °C.

100 was isolated as a white solid (0.8353g, 4.7 mmol, 97%). Mp. 299-301 °C (H_2O) (lit. Mp. 300 °C).[207].

[a]Mol% of catalyst is related to the number of moles of monomeric units (5.204 mmol) present in 1.000 g of polymer.

δ_H (400 MHz, DMSO-d_6) 13.29 (br s, 2H, H-1), 8.04 (s, 4H, H-2) ppm

Tetraoctylphosphonium chloride (224)

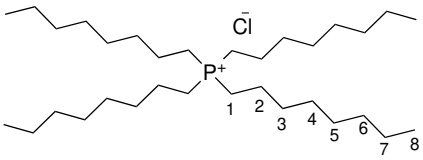

To a 25 mL RBF equipped was added tetraoctylphosphonium bromide (1.1276 g, 2 mmol), methanol (30 mL) and Amberlite® IRA-900 chloride form (6 g) and shaken for 18 h at room temperature The solution was then passed through a column containing Amberlite® IRA-900 chloride form (6 g) and the column was washed with methanol (3 x 30 mL). The solvent was removed under reduced pressure and the product dried *in vacuo*, yielding **224** as a yellow oil (1.096 g, 1.94 mmol, 97%).

Spectral data for this compound were consistent with those in the literature.[208]

δ_H (400 MHz, DMSO-d_6) 2.24-2.04 (m, 8H, H-1), 1.59-1.20 (m, 48H, H-2, H-3, H-4, H-5, H-6, H-7), 0.91-0.89 (m, 12H, H-8) ppm

δ_C (101 MHz, DMSO-d_6) 31.7, 30.5 (d, $J_{C\text{-}P}$ = 15.1), 28.6 (d, $J_{C\text{-}P}$ = 23.1), 22.5, 21.0, 21.0, 17.9 (d, $J_{C\text{-}P}$ = 47.0), 14.4 ppm

δ_P (162 MHz, DMSO-d_6) 33.8 ppm

HRMS (m/z – ESI+): Found: 483.5058 (M^+) $C_{32}H_{68}P^+$ Requires: 483.5053

ν_{max} (neat)/cm^{-1}: 2955, 2923, 2854, 1451, 1378, 1236, 1116, 1030, 720

Methyltrioctylphosphonium iodide (220)

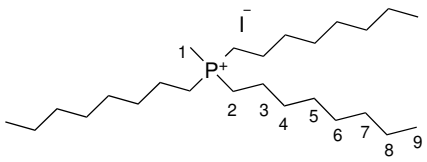

To a 25 mL RBF equipped with a stirring bar was added trioctylphosphine (2.52 mL, 10 mmol), acetonitrile (10 mL) and was cooled in an ice bath. Iodomethane (0.69 mL, 11 mmol) was added dropwise *via* syringe, and the heterogeneous mixture was stirred at room temperature for 24 h. The solvent was removed under reduced pressure, and the residue was washed with diethyl ether (2 x 5 mL). The resulting solid was dried *in vacuo*, yielding **220** as a colourless gum (3.12 g, 5.2 mmol, 52%).

δ_H (400 MHz, DMSO-d_6)	2.27–2.10 (m, 6H, H-2), 1.79 (d, J = 14.0, 3H, H-1), 1.56–1.17 (m, 36H, H-3, H-4, H-5, H-6, H-7, H-8), 0.93-0.80 (m, 9H, H-9) ppm
δ_C (101 MHz, DMSO-d_6)	31.2, 30.0 (d, $J_{C\text{-}P}$ = 15.1), 28.3 (d, $J_{C\text{-}P}$ = 18.8), 22.4, 22.0, 20.5, 19.1 (d, $J_{C\text{-}P}$ = 51.2), 13.9, 3.2 (d, $J_{C\text{-}P}$ = 51.2) ppm
δ_P (162 MHz, DMSO-d_6)	32.2 ppm
HRMS (m/z – ESI+):	Found: 385.3957 (M^+) $C_{25}H_{54}P^+$ Requires: 385.3958
ν_{max} (neat)/cm^{-1}:	2945, 2922, 2854, 1458, 1378, 1305, 1099, 1033, 943, 907, 770, 721

Methyltrioctylphosphonium chloride (221)

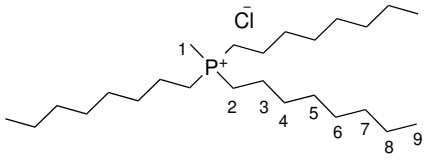

To a 25 mL RBF equipped with a stir bar was added 13 (0.5716 g, 1 mmol), methanol (40 mL) and Amberlite® IRA-900 chloride form (6 g) and shaken for 18 h at room temperature The solution was then passed through a column containing Amberlite® IRA-900 chloride form (6

g) and the column was washed with methanol (3 x 40 mL). The solvent was removed under reduced pressure, and the product was dried *in vacuo*, yielding **221** as a yellow oil (0.4070 g, 0.97 mmol, 97%).

Spectral data for this compound were consistent with those in the literature.[208]

δ_H (400 MHz, DMSO-d_6)	2.20–2.05 (m, 6H, H-2), 1.75 (d, J = 14.2, 3H, H-1), 1.51–1.20 (m, 36H, H-3, H-4, H-5, H-6, H-7, H-8), 0.87-0.82 (m, 9H, H-9) ppm
δ_C (101 MHz, DMSO-d_6)	31.7, 30.0 (d, $J_{C\text{-}P}$ = 15.1), 28.7 (d, $J_{C\text{-}P}$ = 18.8), 22.5, 21.0, 20.9, 19.5 (d, $J_{C\text{-}P}$ = 51.2), 14.4, 3.7 (d, $J_{C\text{-}P}$ = 51.2) ppm.
δ_P (162 MHz, DMSO-d_6)	32.2 ppm.
HRMS (m/z – ESI+):	Found: 385.3959 (M^+) $C_{25}H_{54}P^+$ Requires: 385.3958.
ν_{max} (neat)/cm^{-1}:	2923, 2855, 1727, 1452, 1377, 1305, 1100, 1033, 944, 721

Methyltrioctylphosphonium terephthalate (241)

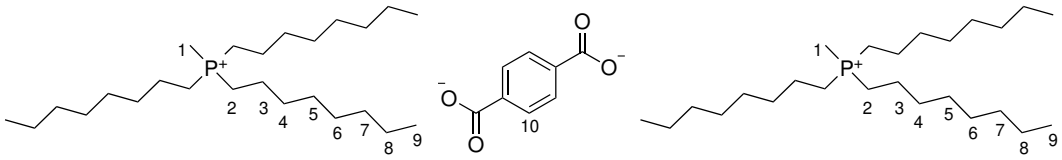

To a 25 mL RBF equipped was added catalyst **220** (1.0252 g, 2 mmol), methanol (30 mL) and Amberlite®-OH IRN78 (4.4 g) and shaken for 18 h at room temperature The solution was then passed through a column containing Amberlite®-OH IRN78 (4.4 g) and the column was washed with methanol (3 x 30 mL). The combined washes were placed in a 250 mL round-bottomed flask, and to the flask was added a stir bar and terephthalic acid (0.1661 g, 1 mmol) before being stirred at room temperature for 18 h. The solvent was removed under reduced pressure, and the product was dried *in vacuo*, yielding **241** as a white wax (0.897 g, 0.96 mmol, 96%).

δ_H (400 MHz, DMSO-d_6)	7.58 (s, 4H, H-10), 2.20–2.07 (m, 12H, H-2), 1.76 (d, J = 14.3,

6H, H-1), 1.46–1.25 (m, 72H, H-3, H-4, H-5, H-6, H-7, H-8), 0.87-0.82 (m, 18H, H-9) ppm.

δ_C (101 MHz, DMSO-d_6) 169.0, 142.2, 127.9, 31.7, 30.0 (d, $J_{C\text{-}P}$ = 15.5), 28.7 (d, $J_{C\text{-}P}$ = 18.3), 22.5, 21.0, 20.9, 19.5 (d, $J_{C\text{-}P}$ = 47.6), 14.4, 3.5 (d, $J_{C\text{-}P}$ = 53.4) ppm..

δ_P (162 MHz, DMSO-d_6) 32.3 ppm.

HRMS (m/z – ESI+): Found: 385.3957 (M^+) $C_{25}H_{54}P^+$ Requires: 385.3958.

ν_{max} (neat)/cm^{-1}: 2956, 2923, 2865, 1587, 1465, 1349, 1311, 1079, 1017, 945, 890, 801, 753, 721

Tetraoctylphosphonium terephthalate (243)

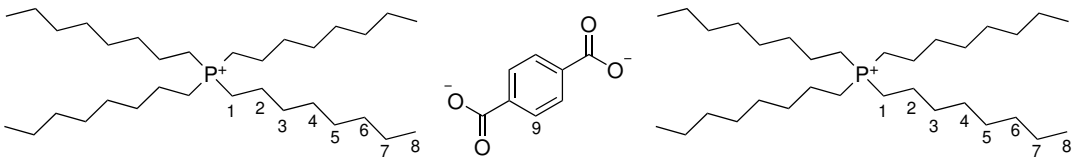

To a 25 mL round-bottomed flask equipped was added tetraoctylphosphonium bromide (1.1276 g, 2 mmol), methanol (30 mL) and Amberlite®-OH IRN78 (4.4 g) and shaken for 18 h at room temperature The solution was then passed through a column containing Amberlite®-OH IRN78 (4.4 g) and the column was washed with methanol (3 x 30 mL). The combined washes were placed in a 250 mL round-bottomed flask, and to the flask was added a stir bar and terephthalic acid (0.1661 g, 1 mmol) before being stirred at room temperature for 18 h. The solvent was removed under reduced pressure and the product was dried textit in vacuo, yielding **243** as a colourless gum (1.096 g, 0.97 mmol, 97%).

δ_H (400 MHz, DMSO-d_6) 7.62 (s, 4H, H-9), 2.34-2.04 (m, 16H, H-1), 1.59-1.14 (m, 96H, H-2, H-3, H-4, H-5, H-6, H-7), 0.99-0.74 (m, 24H, H-8) ppm.

δ_C (101 MHz, DMSO-d_6) 169.0, 142.2, 127.9, 31.7, 30.0 (d, $J_{C\text{-}P}$ = 15.5), 28.2 (d, $J_{C\text{-}P}$ = 21.2), 22.0, 21.0, 20.9, 17.4 (d, $J_{C\text{-}P}$ = 47.1), 14.4 ppm.

δ_P (162 MHz, DMSO-d_6)	33.8 ppm.
HRMS (m/z – ESI+):	Found: 483.5061 (M^+) $C_{32}H_{68}P^+$ Requires: 483.5053.
ν_{max} (neat)/cm^{-1}:	2923, 2854, 1581, 1464, 1350, 1116, 1017, 801, 754, 721

Basic PET hydrolysis procedure using a reduced concentration of sodium hydroxide

To an oven dried carousel flask was added water (5 mL), sodium hydroxide (0.250 g) and catalyst (X mol%).[a] The flask was placed under an atmosphere of nitrogen (balloon), and the reaction was stirred for 20 min at 90 °C. Polyethylene terephthalate flakes (*ca.* 5 mm squares, 0.500 g) were added, and the mixture was stirred (500 RPM) for 3 h. The flask was removed from the carousel and cooled in an ice bath for 10 min. The reaction mixture was then filtered, and the residue was washed with water (5 mL x 2). The filtrate was adjusted, with cooling, to pH 2-3 using dilute HCl, and the resulting precipitate was filtered. The solids were washed with water (5 mL) and the product was dried for 4 h in a vacuum oven at 60 °C. The yield of terephthalic acid was determined by ^{1}H NMR spectroscopy using 4-iodoanisole as an internal standard: known masses of product (> 15 mg) and 4-iodoanisole (> 15 mg) were weighed into a sample vial and dissolved in DMSO-d6. The integrals corresponding to both TPA and isophthalic acid (a common additive utilised in PET production) were used to determine yield.

[a]Mol% of catalyst is related to the number of moles of monomeric units (2.6 mmol) present in 0.500 g of polymer.

***N*,*N*-dimethyl, *N*,*N*-diheptyl ammonium bromide (269)**

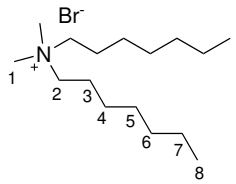

To a two-neck 25mL RBF containing a stir bar, under an Ar atmosphere and equipped with a reflux condenser, was added acetonitrile (4mL) and potassium carbonate (2.2g) and dimethyl amine (2M in THF, 2 mL, 4 mmol). 1-Bromoheptane (2.2 mL, 14 mmol) was added, and the solution was stirred at room temperature for 16 h before being filtered; the filtrate was dried under reduced pressure. The product was purified by flash column chromatography (CH_2Cl_2

to CH_2Cl_2/MeOH (95:5)) to afford **269** as a colourless gum (271 mg, 0.81mmol, 20%)

δ_H (400 MHz, DMSO-d_6)	3.26– 3.18 (m, 4H, H-2), 2.98 (s, 6H, H-1), 1.70 – 1.57 (m, 4H, H-3), 1.37 – 1.19 (m, 16H, H-4, H-5, H-6, H-7), 0.87 (t, J = 6.3 Hz, 6H, H-8) ppm
δ_C (101 MHz, DMSO-d_6)	62.9, 49.9, 31.0, 28.1, 25.7, 21.9, 21.6, 13.9 ppm
HRMS (m/z – ESI+):	Found: 242.2844 (M^+) $C_{16}H_{36}N^+$ Requires: 242.2842.
ν_{max} (neat)/cm^{-1}:	3011, 2925, 2858, 1467, 1275, 904, 729, 697

***N*,*N*-dimethyl, *N*,*N*-dinonyl ammonium bromide (270)**

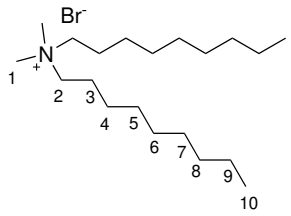

To a two-neck 25mL RBF containing a stir bar, under an Ar atmosphere and equipped with a reflux condenser, was added acetonitrile (4mL) and potassium carbonate (2.2g) and dimethyl amine (2M in THF, 2 mL, 4 mmol). 1-Bromonone (2.7 mL, 14 mmol) was added, and the solution was stirred at room temperature for 16 h before being filtered; the filtrate was dried under reduced pressure. The product was purified by flash column chromatography (CH_2Cl_2 to CH_2Cl_2/MeOH (95:5)) to afford **270** as a yellow oil (107 mg, 0.4mmol, 10%)

δ_H (400 MHz, $CDCl_3$)	3.56-3.47 (m, 4H, H-2), 3.40 (s, 6H, H-1), 1.77-1.63 (m, 4H, H-3), 1.48-1.18 (m, 24H, H-4, H-5, H-6, H-7, H-8, H-9), 0.88 (t, J = 7.0, 6H, H-10) ppm
δ_C (101 MHz, $CDCl_3$)	64.1, 51.4, 31.9, 29.4, 29.3, 29.2, 26.4, 22.9, 22.7, 14.2 ppm
HRMS (m/z – ESI+):	Found: 289.3468 (M^+) $C_{20}H_{44}N^+$ Requires: 289.3468.
ν_{max} (neat)/cm^{-1}:	2922, 2854, 1467, 927, 722

***N*,*N*-dioctyl tetrahydroisoquinolinium bromide (251)**

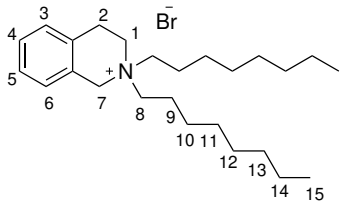

To a 25 mL RBF under Ar atmosphere, equipped with a stirring bar, was added acetonitrile (3 mL), potassium carbonate (0.70 g, 5.1 mmol) and tetrahydroisoquinoline (0.32 mL, 2.5 mmol). 1-Bromooctane (0.70 mL, 4.0 mmol) was added dropwise. The flask was equipped with a condenser, and the solution was heated under reflux for 16 h. After cooling to room temperature, the solution was filtered, and the filtrate was concentrated under reduced pressure. The resulting yellow oil was then dissolved in CH_2Cl_2 (1 mL) before being added dropwise to ice-cold diethyl ether (15 mL), yielding a yellow precipitate. The product was purified by flash column chromatography (CH_2Cl_2 to CH_2Cl_2/MeOH (95:5)) to afford **251** as a white solid (0.184 g, 0.43 mmol, 17% yield). Mp. 144-146 °C (CH_2Cl_2).

δ_H (400 MHz, $CDCl_3$)	7.29-7.14 (m, 4H, H-3, H-4, H-5, H-6), 4.90 (s, 2H, H-7), 4.10 (t, 2H, J = 6.5, H-1), 3.62-3.38 (m, 4H, H-8), 3.14 (t, 2H, J = 6.5, H-2), 1.84-1.64 (m, 4H, H-9), 1.38-1.12 (m, 20H, H-10, H-11, H-12, H-13, H-14), 0.83 (t, 6H, J = 6.8, H-15) ppm
δ_C (101 MHz, $CDCl_3$)	129.2, 128.9, 128.8, 127.8, 127.7, 126.2, 61.0, 58.5, 56.2, 31.6, 29.1, 29.0, 26.4, 23.9, 22.6, 22.2, 14.1 ppm
HRMS (m/z – ESI+):	Found: 358.3476 (M^+) $C_{20}H_{44}N^+$ Requires: 358.3478.
ν_{max} (neat)/cm^{-1}:	2955, 2923, 2854, 1494, 1453, 748, 724

***N*-methyl pyridinium iodide (248)**

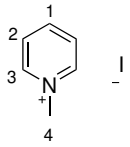

A 100mL RBF under Ar atmosphere, equipped with a stirring bar, was added anhydrous pyridine (0.40 mL, 5.0 mmol) and acetonitrile (50 mL). Methyl iodide (0.31 mL, 5.0 mmol) was added dropwise, and the mixture was refluxed for 18 h before being concentrated under reduced pressure. The resulting yellow solid was then dissolved in acetonitrile (7 mL) and was added to a stirring solution of diethyl ether (20 mL) before being filtered and washed with diethyl ether (3 x 10 mL) yielding **248** as a light-yellow solid (0.97 g, 4.4 mmol, 88% yield). Mp. 79-80 °C (Et_2O).

δ_H (400 MHz, DMSO-d_6)	8.99 (d, 2H, J = 5.6, H-3), 8.58 (t, 1H, J = 7.8, H-1), 8.14 (app. t, 2H, H-2), 4.36 (s, 3H, H-4) ppm
δ_C (101 MHz, $CDCl_3$)	145.5, 145.04, 127.7, 47.9 ppm
HRMS (m/z – ESI+):	Found: 94.0651 (M^+) $C_6H_8N^+$ Requires: 94.0651.
ν_{max} (neat)/cm^{-1}:	3033, 2989, 1629, 1497, 1482, 1284, 766, 673

_N_-octyl pyridinium bromide (249)

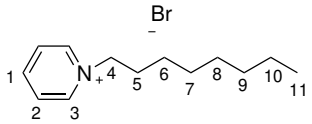

To a 25 mL RBF under Ar atmosphere, equipped with a stirring bar, was added anhydrous pyridine (1.05 mL, 13.0 mmol). 1-Bromooctane (2.25 mL, 13.0 mmol) was added, and the mixture was heated to 80 °C for 3 h. The mixture was concentrated under reduced pressure. The resulting yellow oil was triturated in diethyl ether (3 x 10 mL), yielding **249** as a light-yellow oil (1.23 g, 4.6 mmol, 35%).

δ_H (600 MHz, DMSO-d_6)	9.12 (d, 2H, J = 5.3, H-3), 8.61 (t, 1H, J = 7.8, H-1), 8.14 (app. t, 2H, H-2), 4.60 (t, 2H, J = 7.2, H-4), 1.99-1.83 (m, 2H, H-5), 1.38-1.14 (m, 10H, H-6, H-7, H-8, H-9, H-10), 0.85 (t, 3H, J = 8.3 Hz, H-11) ppm

δ_C (140 MHz, $CDCl_3$)	145.5, 144.7, 128.1, 60.7, 31.1, 30.7, 28.4, 28.3, 25.4, 22.0, 13.9 ppm
HRMS (m/z – ESI+):	Found: 192.1750 (M^+) $C_6H_8N^+$ Requires: 192.1747.
ν_{max} (neat)/cm^{-1}:	3028, 2955, 2925, 2855, 1633, 1486, 1170, 774, 683

5.1 X-ray crystallography data

Small Molecule X-ray Facility
School Of Chemistry

Trinity College Dublin
The University of Dublin

Structure Report

Filename: TCD2301

Submitted by: Ian Martin

Reference: IM_5E718

Group: Connon

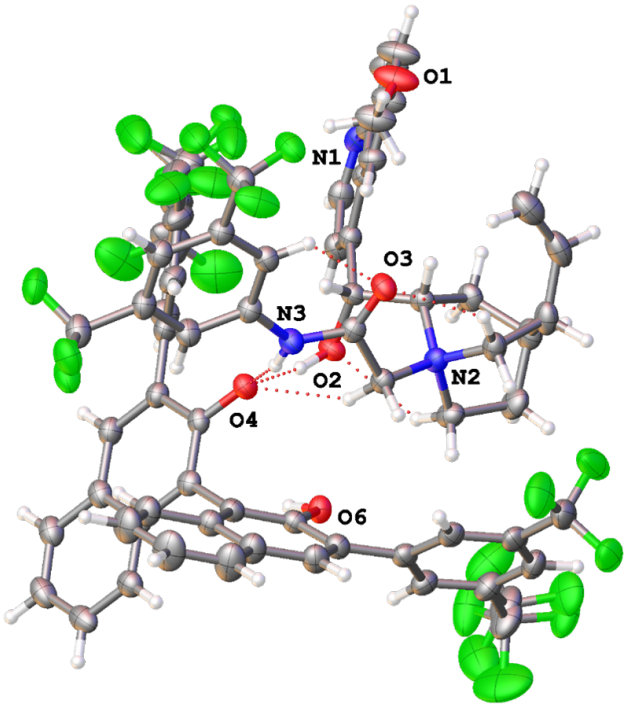

Fig. 1. Molecular structure of TCD2301 with partially occupied solvent molecules omitted for clarity. Displacement parameters shown at 50% probability and selected heteroatoms labelled only. Dotted lines indicate hydrogen bonding interactions.

06/06/2024

Author: Brendan Twamley

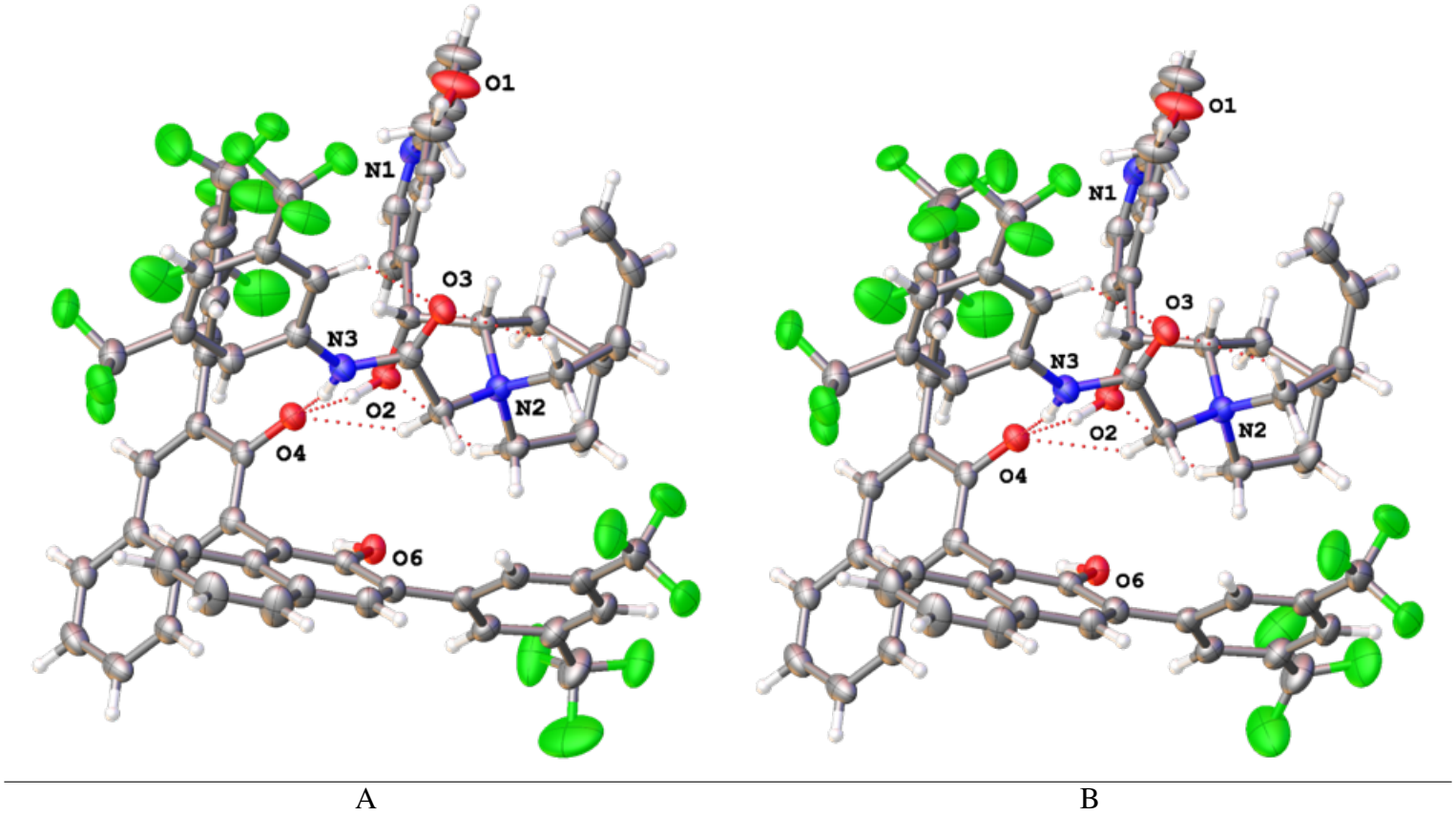

Fig. 2. Individual images of each disordered moiety in TCD2301 with (A) the majority occupied moiety with C65, 60% and C74, 69% occupied (disordered CF3 groups) and (B) minority occupied with C65, 40% and C74, 13%. Partially occupied solvent molecules omitted for clarity. Displacement parameters shown at 50% probability and selected heteroatoms labelled only. Dotted lines indicate hydrogen bonding interactions.

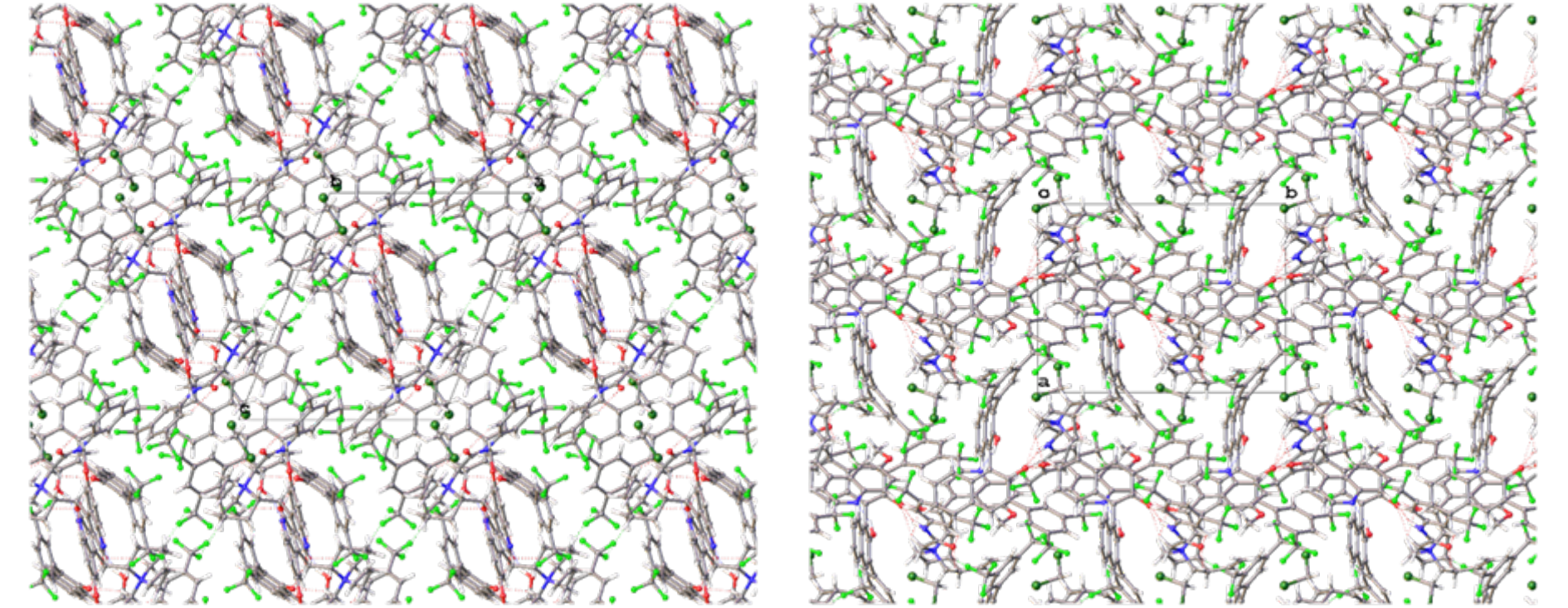

A B

Fig. 3. Schematic packing diagram of the majority occupied moiety and partially occupied CH_2Cl_2 TCD2301, with (A) viewed normal to the b-axis and (B) viewed normal to the c-axis. Dotted lines represent hydrogen bonding.

Crystal Structure Report for TCD2301

A specimen of $C_{70.17}H_{56.83}Cl_{0.51}F_{18}N_3O_{5.28}$, approximate dimensions 0.074 mm x 0.090 mm x 0.564 mm, was used for the X-ray crystallographic analysis. The X-ray intensity data were measured (λ = 1.54178 Å) on a Bruker APEX DUO with an Oxford Cobra Cryosystem low temperature device using a MiTeGen micromount. See Table 1 for collection parameters and exposure time.

A total of 5600 frames were collected. The total exposure time was 80.46 hours. The integration of the data using a monoclinic unit cell yielded a total of 63574 reflections to a maximum θ angle of 70.06° (0.82 Å resolution), of which 12204 were independent (average redundancy 5.209, completeness = 99.4%, R_{int} = 5.17%, R_{sig} = 3.54%) and 11587 (94.94%) were greater than $2\sigma(F_2)$. The final cell constants of a = 13.4278(4) Å, b = 16.3684(5) Å, c = 16.1941(5) Å, β = 111.9364(16)°, volume = 3301.63(18) $Å^3$, are based upon the refinement of the XYZ-centroids of 9886 reflections above 20 σ(I) with 5.883° < 2θ < 139.2°. Data were corrected for absorption effects using the Multi-Scan method (SADABS). The ratio of minimum to maximum apparent transmission was 0.735. The calculated minimum and maximum transmission coefficients (based on crystal size) are 0.5390 and 0.9130.

The structure was solved with the SHELXT structure solution program using Intrinsic Phasing and refined with the SHELXL refinement program with Least Squares minimisation within the OLEX2 Software Package, using the space group $P2_1$, with Z = 2 for the formula unit, $C_{70.17}H_{56.83}Cl_{0.51}F_{18}N_3O_{5.28}$. The final anisotropic full-matrix least-squares refinement on F2 with 1037 variables converged at R1 = 5.46%, for the observed data and wR2 = 15.50% for all data. The goodness-of-fit was 1.047. The largest peak in the final difference electron density synthesis was 0.902 $e^-/Å^3$ and the largest hole was -0.303 $e^-/Å^3$ with an RMS deviation of 0.062 $e^-/Å^3$. On the basis of the final model, the calculated density was 1.395 g/cm^3 and F(000), 1424 e^-.

Refinement details: Donor N-H and O-H hydrogen atoms located on the difference map and refined with restraints (DFIX). Two CF3 groups on the anion are disordered and modelled with restraints (DANG, SIMU, ISOR, RIGU, SADI) and constraints (EADP, C74A/B) over two locations with C65, 60:40% and C74, 69:13% occupied. There are several partially occupied

solvent molecules in the void, DCM (25%), hexane (47%) and diethyl ether (28%). Restraints (DFIX, DANG, RIGU, SIMU, SADI) and constraints (EADP, SUMP) used.

References:

Bruker (2016). SAINT v8.38A, Bruker AXS Inc., Madison, WI, USA.

Bruker (2021). APEX4, Bruker AXS Inc., Madison, WI, USA.

SADABS: Krause, L., Herbst-Irmer, R., Sheldrick, G. M., Stalke, D. (2015).

J. Appl. Cryst. 48, 3-10.

OLEX2: Dolomanov, O.V., Bourhis, L.J., Gildea, R.J, Howard, J.A.K. & Puschmann, H. (2009), J. Appl. Cryst. 42, 339-341.

SHELXL: Sheldrick, G. M. (2015). Acta Cryst. C71, 3-8.

SHELXT: Sheldrick, G. M. (2015). Acta Cryst. A71, 3-8.

References

[1] B. Marglin and R. Merrifield, *J. Am. Chem. Soc.*, 1966, **88**, 5051–5052.

[2] F. G. Banting, W. R. Campbell and A. A. Fletcher, *Br. Med. J.*, 1923, **1**, 8–12.

[3] H. Keen, J. Pickup, R. Bilous, A. Glynne, G. Viberti, R. Jarrett and R. Marsden, *The Lancet*, 1980, **316**, 398–401.

[4] K. Sharma, K. K. Sharma, A. Sharma and R. Jain, *Drug Discovery Today*, 2023, **28**, 103464.

[5] E. Fisher, K. Pavlenko, A. Vlasov and G. Ramenskaya, *Pharm. Med.*, 2019, **33**, 9–20.

[6] A. N. Zaykov, J. P. Mayer and R. D. DiMarchi, *Nat. Rev. Drug Discov.*, 2016, **15**, 425–439.

[7] L. Wang, N. Wang, W. Zhang, X. Cheng, Z. Yan, G. Shao, X. Wang, R. Wang and C. Fu, *Signal Transduction and Targeted Ther.*, 2022, **7**, 48.

[8] D. J. Craik, D. P. Fairlie, S. Liras and D. Price, *Chem. Biol. Drug Des.*, 2013, **81**, 136–147.

[9] G. A. Christou, N. Katsiki, J. Blundell, G. Fruhbeck and D. N. Kiortsis, *Obes. Rev.*, 2019, **20**, 805–815.

[10] G. Truccolo, *The 2023 Top-Selling Drugs | CCDC — ccdc.cam.ac.uk*, `https://www.ccdc.cam.ac.uk/discover/blog/the-2023-top-selling-drugs/`, 2024, [Accessed 08-01-2025].

[11] K. Fosgerau and T. Hoffmann, *Drug Discov. Today*, 2015, **20**, 122–128.

[12] L. Di, *The AAPS Journal*, 2015, **17**, 134–143.

[13] J. Lu, H. Xu, J. Xia, J. Ma, J. Xu, Y. Li and J. Feng, *Front. Microbiol.*, 2020, **11**, 3389.

[14] T. W. Greene, P. G. Wuts *et al.*, *Prot. Groups Org. Chem.*, Wiley New York, 1999.

[15] G. Barany and F. Albericio, *J. Am. Chem. Soc.*, 1985, **107**, 4936–4942.

[16] A. Isidro-Llobet, M. Álvarez and F. Albericio, *Chem. Rev.*, 2009, **109**, 2455–2504.

[17] M. Williams and G. Young, *J. Chem. Soc. (Resumed)*, 1963, 881–889.

[18] M. Bodanszky and V. du Vigneaud, *J. Am. Chem. Soc.*, 1959, **81**, 5688–5691.

[19] C. A. Montalbetti and V. Falque, *Tetrahedron*, 2005, **61**, 10827–10852.

[20] M. Bodanszky, in *Principles of peptide synthesis*, Springer Science & Business Media,

2012, vol. 16.

[21] R. B. Merrifield, *J. Am. Chem. Soc.*, 1963, **85**, 2149–2154.

[22] A. Di Fenza, M. Tancredi, C. Galoppini and P. Rovero, *Tetrahedron Lett.*, 1998, **39**, 8529–8532.

[23] A. Isidro-Llobet, M. N. Kenworthy, S. Mukherjee, M. E. Kopach, K. Wegner, F. Gallou, A. G. Smith and F. Roschangar, *J. Org. Chem.*, 2019, **84**, 4615–4628.

[24] A. Perdih, *Curr. Org. Chem.*, 2007, **11**, 801–832.

[25] D. V. Johnson, U. Felfer and H. Griengl, *Tetrahedron*, 2000, **56**, 781–790.

[26] S. J. Zuend, M. P. Coughlin, M. P. Lalonde and E. N. Jacobsen, *Nature*, 2009, **461**, 968–970.

[27] S. Tallon, F. Manoni and S. J. Connon, *Angew. Chem. Int. Ed. Engl.*, 2015, **54**, 813–7.

[28] I. F. S. Marra, P. P. De Castro and G. W. Amarante, *Eur. J. Org. Chem.*, 2019, **2019**, 5830–5855.

[29] Y. S. Rao, *J. Org. Chem.*, 1976, **41**, 722–725.

[30] P. P. De Castro, A. G. Carpanez and G. W. Amarante, *Chem. - Eur. J.*, 2016, **22**, 10294–10318.

[31] P. P De Castro, I. F Dos Santos and G. W Amarante, *Curr. Org. Synth.*, 2016, **13**, 440–444.

[32] M. Weber, W. Frey and R. Peters, *Adv. Synth. Catal.*, 2012, **354**, 1443–1449.

[33] S. Dong, X. Liu, X. Chen, F. Mei, Y. Zhang, B. Gao, L. Lin and X. Feng, *J. Am. Chem. Soc.*, 2010, **132**, 10650–10651.

[34] X. Yang, G. Lu and V. B. Birman, *Org. Lett.*, 2010, **12**, 892–895.

[35] A. Peschiulli, C. Quigley, S. Tallon, Y. K. Gun'Ko and S. J. Connon, *J. Org. Chem.*, 2008, **73**, 6409–6412.

[36] Y.-C. Zhang, Q. Yang, X. Yang, Q.-N. Zhu and F. Shi, *Asian J. Org. Chem.*, 2016, **5**, 914–919.

[37] H. Kagan and J. Fiaud, *Top. Stereochem.*, 1988, **18**, 249–330.

[38] G. P. Moss, *Pure and applied chemistry*, 1996, **68**, 2193–2222.

[39] E. Vedejs and M. Jure, *Angew. Chem., Int. Ed.*, 2005, **44**, 3974–4001.

[40] R. Noyori, *Angew. Chem., Int. Ed.*, 2002, **41**, 2008–2022.

[41] S. A. Brown, M.-C. Parker and N. J. Turner, *Tetrahedron: Asymmetry*, 2000, **11**, 1687–1690.

[42] P. P. De Castro, G. M. F. Batista, H. F. Dos Santos and G. W. Amarante, *ACS Omega*, 2018, **3**, 3507–3512.

[43] J. De Jersey and B. Zerner, *Biochemistry*, 1969, **8**, 1967–1974.

[44] H. S. Bevinakatti, R. V. Newadkar and A. A. Banerji, *J. Chem. Soc., Chem. Commun.*, 1990, 1091.

[45] G. Lu and V. B. Birman, *Org. Lett.*, 2011, **13**, 356–358.

[46] A. Berkessel, F. Cleemann, S. Mukherjee, T. N. Müller and J. Lex, *Angew. Chem., Int. Ed.*, 2005, **44**, 807–811.

[47] K. Wakafuji, S. Iwasa, K. N. Ouchida, H. Cho, H. Dohi, E. Yamamoto, T. Kamachi and M. Tokunaga, *ACS Catal.*, 2021, **11**, 14067–14075.

[48] D. Seebach, G. Jaeschke, K. Gottwald, K. Matsuda, R. Formisano, D. A. Chaplin, M. Breuning and G. Bringmann, *Tetrahedron*, 1997, **53**, 7539–7556.

[49] J. Geller, *Food and Foodways*, 1993, **5**, 255–267.

[50] D. A. Chaplin, M. E. Fox and S. H. Kroll, *Chem. Commun.*, 2014, **50**, 5858–5860.

[51] M. D. Cummings, J. Lindberg, T.-I. Lin, H. de Kock, O. Lenz, E. Lilja, S. Felländer, V. Baraznenok, S. Nyström, M. Nilsson, L. Vrang, M. Edlund, A. Rosenquist, B. Samuelsson, P. Raboisson and K. Simmen, *Angew. Chem., Int. Ed.*, 2010, **49**, 1652–1655.

[52] S. Wu, R. Snajdrova, J. C. Moore, K. Baldenius and U. T. Bornscheuer, *Angew. Chem., Int. Ed.*, 2021, **60**, 88–119.

[53] *Biocatalysis*, John Wiley & Sons, Ltd, 2015, ch. 4, pp. 81–98.

[54] S. France, D. J. Guerin, S. J. Miller and T. Lectka, *Chem. Rev.*, 2003, **103**, 2985–3012.

[55] L. Litvinenko, Dokl. Akad. Nauk. SSSR, 1967, p. 97.

[56] G. Höfle, W. Steglich and H. Vorbrüggen, *Angew. Chem., Int. Ed. Engl.*, 1978, **17**, 569–583.

[57] J. C. Ruble and G. C. Fu, *J. Am. Chem. Soc.*, 1998, **120**, 11532–11533.

[58] J. C. Ruble, H. A. Latham and G. C. Fu, *J. Am. Chem. Soc.*, 1997, **119**, 1492–1493.

[59] R. P. Wurz, *Chem. Rev.*, 2007, **107**, 5570–5595.

[60] C. O. Dalaigh, S. J. Hynes, J. E. O'Brien, T. McCabe, D. J. Maher, G. W. Watson and S. J. Connon, *Org. Biomol. Chem.*, 2006, **4**, 2785–2793.

[61] E. Larionov, M. Mahesh, A. C. Spivey, Y. Wei and H. Zipse, *J. Am. Chem. Soc.*, 2012, **134**, 9390–9399.

[62] H. Mandai, K. Fujii, H. Yasuhara, K. Abe, K. Mitsudo, T. Korenaga and S. Suga, *Nat. Commun.*, 2016, **7**, 11297.

[63] H. Mandai, K. Hongo, T. Fujiwara, K. Fujii, K. Mitsudo and S. Suga, *Org. Lett.*, 2018, **20**, 4811–4814.

[64] J. C. Ruble and G. C. Fu, *J. Org. Chem.*, 1996, **61**, 7230–7231.

[65] M. Xie, Y. Zhang, M. Shan, X. Wu, G. Qu and H. Guo, *Angew. Chem.*, 2019, **131**,

2865–2869.

[66] M.-S. Xie, M. Shan, N. Li, Y.-G. Chen, X.-B. Wang, X. Cheng, Y. Tian, X.-X. Wu, Y. Deng, G.-R. Qu and H.-M. Guo, *ACS Catal.*, 2022, **12**, 877–891.

[67] M.-S. Xie, B. Huang, N. Li, Y. Tian, X.-X. Wu, Y. Deng, G.-R. Qu and H.-M. Guo, *J. Am. Chem. Soc.*, 2020, **142**, 19226–19238.

[68] V. B. Birman, E. W. Uffman, H. Jiang, X. Li and C. J. Kilbane, *J. Am. Chem. Soc.*, 2004, **126**, 12226–12227.

[69] V. B. Birman and X. Li, *Org. Lett.*, 2006, **8**, 1351–1354.

[70] S. J. Connon, *Chem. Commun.*, 2008, 2499–2510.

[71] T. Okino, S. Nakamura, T. Furukawa and Y. Takemoto, *Org. Lett.*, 2004, **6**, 625–627.

[72] A. Berkessel, S. Mukherjee, T. N. Müller, F. Cleemann, K. Roland, M. Brandenburg, J.-M. Neudörfl and J. Lex, *Org. Biomol. Chem.*, 2006, **4**, 4319–4330.

[73] P. J. Boratyński, M. Zielińska-Błajet and J. Skarżewski, *The Alkaloids: Chemistry and Biology*, 2019, **82**, 29–145.

[74] H. Wynberg and R. Helder, *Tetrahedron Lett.*, 1975, **16**, 4057–4060.

[75] S.-K. Tian, Y. Chen, J. Hang, L. Tang, P. McDaid and L. Deng, *Accounts of Chemical Research*, 2004, **37**, 621–631.

[76] G. Tárkányi, P. Király, S. Varga, B. Vakulya and T. Soós, *Chem. - Eur. J.*, 2008, **14**, 6078–6086.

[77] H. B. Jang, H. S. Rho, J. S. Oh, E. H. Nam, S. E. Park, H. Y. Bae and C. E. Song, *Org. Biomol. Chem.*, 2010, **8**, 3918–3922.

[78] J. Woong Lee, T. Hi Ryu, J. Suk Oh, H. Yong Bae, H. Bin Jang and C. Eui Song, *Chem. Commun.*, 2009, 7224.

[79] J.-S. Oh, K. I. Kim and C. E. Song, *Org. Biomol. Chem.*, 2011, **9**, 7983.

[80] K. Yu, X. Liu, X. Lin, L. Lin and X. Feng, *Chem. Commun.*, 2015, **51**, 14897–14900.

[81] A. J. Metrano, A. J. Chinn, C. R. Shugrue, E. A. Stone, B. Kim and S. J. Miller, *Chem. Rev.*, 2020, **120**, 11479–11615.

[82] R. Kastl and H. Wennemers, *Angew. Chem.*, 2013, **125**, 7369–7373.

[83] A. J. Metrano and S. J. Miller, *J. Org. Chem.*, 2014, **79**, 1542–1554.

[84] C. M. Starks and M. Halper, *Phase-transfer catalysis: fundamentals, applications, and industrial perspectives*, Springer Science & Business Media, 2012.

[85] U. H. Dolling, P. Davis and E. J. J. Grabowski, *J. Am. Chem. Soc.*, 1984, **106**, 446–447.

[86] M. Majdecki, P. Niedbala and J. Jurczak, *Org. Lett.*, 2019, **21**, 8085–8090.

[87] P. E. Dawson, T. W. Muir, I. Clark-Lewis and S. B. H. Kent, *Science*, 1994, **266**, 776–779.

[88] Z. Rodríguez-Docampo, C. Quigley, S. Tallon and S. J. Connon, *J Org Chem*, 2012, **77**, 2407–14.

[89] P. P. De Castro, G. M. F. Batista, G. W. Amarante and H. F. Dos Santos, *J Org Chem*, 2021, **86**, 13169–13174.

[90] C. Palacio and S. J. Connon, *Eur. J. Org. Chem.*, 2013, **2013**, 5398–5413.

[91] R. Craig, M. Litvajova, S. A. Cronin and S. J. Connon, *Chem. Commun.*, 2018, **54**, 10108–10111.

[92] H. M. R. Hoffmann and J. Frackenpohl, *Eur. J. Org. Chem.*, 2004, **2004**, 4293–4312.

[93] J.-F. Brière, S. Oudeyer, V. Dalla and V. Levacher, *Chem. Soc. Rev.*, 2012, **41**, 1696–1707.

[94] R. Goddard, H. M. Herzog and M. T. Reetz, *Tetrahedron*, 2002, **58**, 7847–7850.

[95] T. Tozawa, H. Nagao, Y. Yamane and T. Mukaiyama, *Chem. - Asian J.*, 2007, **2**, 123–134.

[96] E. J. Corey, F. Xu and M. C. Noe, *J. Am. Chem. Soc.*, 1997, **119**, 12414–12415.

[97] D. Destro, C. Bottinelli, L. Ferrari, D. C. M. Albanese, G. Bencivenni, M. W. Gillick-Healy, B. G. Kelly and M. F. A. Adamo, *J. Org. Chem.*, 2020, **85**, 5183–5192.

[98] J. Tan and N. Yasuda, *Org. Process Res. Dev.*, 2015, **19**, 1731–1746.

[99] M. Majdecki, A. Tyszka-Gumkowska and J. Jurczak, *Org. Lett.*, 2020, **22**, 8687–8691.

[100] A. Maguire, *Thesis*, 2020.

[101] `https://plasticseurope.org/knowledge-hub/plastics-the-facts-2022/`, [Accessed 08-01-2025].

[102] S. S. Ali, T. Elsamahy, E. Koutra, M. Kornaros, M. El-Sheekh, E. A. Abdelkarim, D. Zhu and J. Sun, *Sci. Total Environ.*, 2021, **771**, 144719.

[103] H. Li, H. A. Aguirre-Villegas, R. D. Allen, X. Bai, C. H. Benson, G. T. Beckham, S. L. Bradshaw, J. L. Brown, R. C. Brown, V. S. Cecon, J. B. Curley, G. W. Curtzwiler, S. Dong, S. Gaddameedi, J. E. García, I. Hermans, M. S. Kim, J. Ma, L. O. Mark, M. Mavrikakis, O. O. Olafasakin, T. A. Osswald, K. G. Papanikolaou, H. Radhakrishnan, M. A. Sanchez Castillo, K. L. Sánchez-Rivera, K. N. Tumu, R. C. Van Lehn, K. L. Vorst, M. M. Wright, J. Wu, V. M. Zavala, P. Zhou and G. W. Huber, *Green Chem.*, 2022, **24**, 8899–9002.

[104] A. Chamas, H. Moon, J. Zheng, Y. Qiu, T. Tabassum, J. H. Jang, M. Abu-Omar, S. L. Scott and S. Suh, *ACS Sustainable Chem. Eng.*, 2020, **8**, 3494–3511.

[105] P. Pannetier, B. Morin, C. Clérandeau, J. Laurent, C. Chapelle and J. Cachot, *Environ. Pollut.*, 2019, **248**, 1098–1107.

[106] M. Scheurer and M. Bigalke, *Environ. Sci. Technol.*, 2018, **52**, 3591–3598.

[107] C. M. Rochman, M. A. Browne, B. S. Halpern, B. T. Hentschel, E. Hoh, H. K. Karapanagioti, L. M. Rios-Mendoza, H. Takada, S. Teh and R. C. Thompson, *Nature*, 2013, **494**, 169–171.

[108] C. R. Cook and R. U. Halden, *Plast. Waste Recycl.*, Academic Press, 2020, pp. 513–527.

[109] J. B. Lamb, B. L. Willis, E. A. Fiorenza, C. S. Couch, R. Howard, D. N. Rader, J. D. True, L. A. Kelly, A. Ahmad, J. Jompa and C. D. Harvell, *Science*, 2018, **359**, 460–462.

[110] M. K. Viršek, M. N. Lovšin, Š. Koren, A. Kržan and M. Peterlin, *Mar. Pollut. Bull.*, 2017, **125**, 301–309.

[111] J. G. Derraik, *Mar. Pollut. Bull.*, 2002, **44**, 842–852.

[112] A. A. Horton, A. Walton, D. J. Spurgeon, E. Lahive and C. Svendsen, *Sci. Total Environ.*, 2017, **586**, 127–141.

[113] R. An, X. Wang, L. Yang, J. Zhang, N. Wang, F. Xu, Y. Hou, H. Zhang and L. Zhang, *Toxicology*, 2021, **449**, 152665.

[114] Y. Deng, Y. Zhang, B. Lemos and H. Ren, *Sci. Rep.*, 2017, **7**, 46687.

[115] C. M. Rochman, A. Tahir, S. L. Williams, D. V. Baxa, R. Lam, J. T. Miller, F.-C. Teh, S. Werorilangi and S. J. Teh, *Sci. Rep.*, 2015, **5**, 1–10.

[116] S. L. Wright and F. J. Kelly, *Environ. Sci. Technol.*, 2017, **51**, 6634–6647.

[117] R. Geyer, J. R. Jambeck and K. L. Law, *Science Advances*, 2017, **3**, e1700782.

[118] E. Barnard, J. J. Rubio Arias and W. Thielemans, *Green Chem.*, 2021, **23**, 3765–3789.

[119] S. M. Aharoni, in *Industrial-Scale Production of Polyesters, Especially Poly(Ethylene Terephthalate)*, John Wiley & Sons, Ltd, 2002, ch. 2, pp. 59–103.

[120] J. E. Johnston, E. Lim and H. Roh, *Sci. Total Environ.*, 2019, **657**, 187–199.

[121] M. I. Ramirez, A. P. Arevalo, S. Sotomayor and N. Bailon-Moscoso, *Environ. Pollut.*, 2017, **231**, 415–425.

[122] N. Rustagi, S. Pradhan and R. Singh, *Indian J. Occup. Health*, 2011, **15**, 100–103.

[123] P.-C. Europe, *PET market in Europe: State of play*, 2022, `https://petcore-europe.org/news-events/582-pet-market-in-europe-state-of-play.html` [Accessed: (04/02/2025)].

[124] M. D. Vaverková, *Geosciences*, 2019, **9**, 431.

[125] H. K. Jeswani and A. Azapagic, *Waste Manage.*, 2016, **50**, 346–363.

[126] I. Wojnowska-Baryła, K. Bernat and M. Zaborowska, *Int. J. Environ. Res. Public Health*, 2022, **19**, 13223.

[127] J. Morris, *Int. J. Life Cycle Assess.*, 2005, **10**, 273–284.

[128] T. E. COMMISSION, *Commission Implementing Decision (EU) 2023/2683 of 30 November 2023 laying down rules for the application of Directive (EU) 2019/904 of the European Parliament and of the Council as regards the calculation, verification and reporting of data on recycled plastic content in single-use plastic beverage bottles*, 2023, `https://eur-lex.europa.eu/eli/dec_impl/2023/2683/oj` [Accessed: (05/02/2025)].

[129] Z. O. G. Schyns and M. P. Shaver, *Macromol. Rapid Commun.*, 2021, **42**, 2000415.

[130] F. P. La Mantia and M. Vinci, *Polym. Degrad. Stab.*, 1994, **45**, 121–125.

[131] P. Benyathiar, P. Kumar, G. Carpenter, J. Brace and D. K. Mishra, *Polymers*, 2022, **14**, 2366.

[132] S. Shukla and A. M. Harad, *Polym. Degrad. Stab.*, 2006, **91**, 1850–1854.

[133] N. Alves, J. Mano, E. Balaguer, J. Meseguer Dueñas and J. Gómez Ribelles, *Polymer*, 2002, **43**, 4111–4122.

[134] S. A. Jabarin, *Polym. Eng. Sci.*, 1984, **24**, 376–384.

[135] B. Demirel, A. Yaraş and H. Elcicek, 2011.

[136] E. Gorlier, J. Haudin and N. Billon, *Polymer*, 2001, **42**, 9541–9549.

[137] T. B. Thomsen, K. Almdal and A. S. Meyer, *New Biotechnol.*, 2023, **78**, 162–172.

[138] H. Lu, D. J. Diaz, N. J. Czarnecki, C. Zhu, W. Kim, R. Shroff, D. J. Acosta, B. R. Alexander, H. O. Cole, Y. Zhang *et al.*, *Nature*, 2022, **604**, 662–667.

[139] J. Qiu, Y. Chen, L. Zhang, J. Wu, X. Zeng, X. Shi, L. Liu and J. Chen, *Environ. Res*, 2024, **240**, 117427.

[140] C. Sonnendecker, J. Oeser, P. K. Richter, P. Hille, Z. Zhao, C. Fischer, H. Lippold, P. Blázquez-Sánchez, F. Engelberger, C. A. Ramírez-Sarmiento, T. Oeser, Y. Lihanova, R. Frank, H.-G. Jahnke, S. Billig, B. Abel, N. Sträter, J. Matysik and W. Zimmermann, *ChemSusChem*, 2022, **15**, e202101062.

[141] F. Kawai, *ChemSusChem*, 2021, **14**, 4115–4122.

[142] R. K. Brizendine, E. Erickson, S. J. Haugen, K. J. Ramirez, J. Miscall, D. Salvachúa, A. R. Pickford, M. J. Sobkowicz, J. E. McGeehan and G. T. Beckham, *ACS Sustainable Chem. Eng.*, 2022, **10**, 9131–9140.

[143] S. Kaabel, J. D. Therien, C. E. Deschênes, D. Duncan, T. Friščić and K. Auclair, *Proc. Natl. Acad. Sci.*, 2021, **118**, e2026452118.

[144] F. Awaja and D. Pavel, *Eur. Polym. J.*, 2005, **41**, 1453–1477.

[145] L. Zhang, J. Gao, J. Zou and F. Yi, *J. Appl. Polym. Sci.*, 2013, **130**, 2790–2795.

[146] L. Pedrini, C. Zappelli and S. J. Connon, *ACS Sustainable Chem. Eng.*, 2025.

[147] Z. Laldinpuii, V. Khiangte, S. Lalhmangaihzuala, C. Lalmuanpuia, Z. Pachuau, C. Lalhriatpuia and K. Vanlaldinpuia, *J. Polym. Environ.*, 2022, 1–15.

[148] A. Issam, *Res. Chem. Intermed.*, 2014, **40**, 3033–3044.

[149] L. Cosimbescu, D. Malhotra, M. R. Pallaka and M. S. Swita, *ACS omega*, 2022, **7**, 32026–32037.

[150] H. Abedsoltan, *Polym. Eng. Sci.*, 2023, **63**, 2651–2674.

[151] S. D. Mancini and M. Zanin, *Polym.-Plast. Technol. Eng.*, 2007, **46**, 135–144.

[152] W. McMahon, H. Birdsall, G. Johnson and C. Camilli, *J. Chem. Eng. Data*, 1959, **4**, 57–79.

[153] P. Pereira, P. E. Savage and C. W. Pester, *Green Chem.*, 2024, **26**, 1964–1974.

[154] V. Safari, G. Arzpeyma, F. Rashchi and N. Mostoufi, *Int. J. Miner. Process.*, 2009, **93**, 79–83.

[155] T. Yoshioka, N. Okayama and A. Okuwaki, *Ind. Eng. Chem. Res.*, 1998, **37**, 336–340.

[156] T. Yoshioka, T. Motoki and A. Okuwaki, *Ind. Eng. Chem. Res.*, 2001, **40**, 75–79.

[157] J. Payne and M. D. Jones, *ChemSusChem*, 2021, **14**, 4041–4070.

[158] S. Ügdüler, K. M. Van Geem, R. Denolf, M. Roosen, N. Mys, K. Ragaert and S. De Meester, *Green Chem.*, 2020, **22**, 5376–5394.

[159] V. A. Kosmidis, D. S. Achilias and G. P. Karayannidis, *Macromol. Mater. Eng.*, 2001, **286**, 640–647.

[160] J. Das, A. Halgeri, V. Sahu and P. Parikh, 2007.

[161] H. I. Khalaf and O. A. Hasan, *Chem. Eng. J.*, 2012, **192**, 45–48.

[162] N. R. Paliwal and A. K. Mungray, *Polym. Degrad. Stab.*, 2013, **98**, 2094–2101.

[163] R. López-Fonseca, J. González-Velasco and J. Gutiérrez-Ortiz, *Chem. Eng. J.*, 2009, **146**, 287–294.

[164] C. N. Onwucha, C. O. Ehi-Eromosele, S. O. Ajayi, M. Schaefer, S. Indris and H. Ehrenberg, *Ind. Eng. Chem. Res.*, 2023, **62**, 6378–6385.

[165] P. Pereira, P. E. Savage and C. W. Pester, *ACS Sustainable Chem. Eng.*, 2023, **11**, 7203–7209.

[166] D. Stanica-Ezeanu and D. Matei, *Sci. Rep.*, 2021, **11**, 4431.

[167] R. López-Fonseca, I. Duque-Ingunza, B. De Rivas, S. Arnaiz and J. I. Gutierrez-Ortiz, *Polym. Degrad. Stab.*, 2010, **95**, 1022–1028.

[168] J.-W. Chen, L.-W. Chen and W.-H. Cheng, *Polym. Int.*, 1999, **48**, 885–888.

[169] J. Campanelli, D. Cooper and M. Kamal, *J. Appl. Polym. Sci.*, 1994, **53**, 985–991.

[170] P. Pereira, W. Slear, P. M. Guirguis, P. E. Savage and C. W. Pester, *ACS ES&T Eng.*, 2025.

[171] Z. Lei, B. Chen, Y.-M. Koo and D. R. MacFarlane, *Introduction: ionic liquids*, 2017.

[172] F. Liu, X. Cui, S. Yu, Z. Li and X. Ge, *J. Appl. Polym. Sci.*, 2009, **114**, 3561–3565.

[173] S. Bhatia, *Zeolite catalysts: principles and applications*, CRC press, 2020.

[174] S. M. Auerbach, K. A. Carrado and P. K. Dutta, *Handbook of zeolite science and technology*, CRC press, 2003.

[175] S. Van Donk, A. H. Janssen, J. H. Bitter and K. P. de Jong, *Cat. Rev.*, 2003, **45**, 297–319.

[176] M. J. Kang, H. J. Yu, J. Jegal, H. S. Kim and H. G. Cha, *Chem. Eng. J.*, 2020, **398**, 125655.

[177] G. D. Yadav and B. G. Motirale, *Org. Process Res. Dev.*, 2009, **13**, 341–348.

[178] S. Sabde, G. D. Yadav and R. Narayan, *Journal of Cleaner Production*, 2023, **420**, 138312.

[179] V. S. Zope and S. Mishra, *J. Appl. Polym. Sci.*, 2008, **110**, 2179–2183.

[180] S. Conroy and X. Zhang, *Polym. Degrad. Stab.*, 2024, 110729.

[181] R. Zhang, X. Zheng, X. Yao, K. Song, Q. Zhou, C. Shi, J. Xu, Y. Li, J. Xin, I. E.-T. El Sayed *et al.*, *Ind. Eng. Chem. Res.*, 2023, **62**, 11851–11861.

[182] L. B. Anderson, *Thesis*, 2024.

[183] S. Darvesh, R. S. McDonald, K. V. Darvesh, D. Mataija, S. Mothana, H. Cook, K. M. Carneiro, N. Richard, R. Walsh and E. Martin, *Bioorg. Med. Chem.*, 2006, **14**, 4586–4599.

[184] B. T. Gowda, S. Foro and H. Fuess, *Acta Crystallogr., Sect. E:Struct. Rep. Online*, 2007, **63**, o1975–o1976.

[185] V. Ronaldson, J. M. Storey and W. T. Harrison, *Acta Crystallogr., Sect. E:Struct. Rep. Online*, 2005, **61**, o3156–o3158.

[186] K. Brak and E. N. Jacobsen, *Angew. Chem., Int. Ed.*, 2013, **52**, 534–561.

[187] J. hua Lao, X. jing Zhang, J. jia Wang, X. ming Li, M. Yan and H. bin Luo, *Tetrahedron: Asymmetry*, 2009, **20**, 2818–2822.

[188] L. Yan, G. Huang, H. Wang, F. Xiong, H. Peng and F. Chen, *Eur. J. Org. Chem.*, 2018, **2018**, 99–103.

[189] G. Suez, V. Bloch, G. Nisnevich and M. Gandelman, *Eur. J. Org. Chem.*, 2012, **2012**, 2118–2122.

[190] J. Wang, Z.-X. Deng, C.-M. Wang, P.-J. Xia, J.-A. Xiao, H.-Y. Xiang, X.-Q. Chen and H. Yang, *Org. Lett.*, 2018, **20**, 7535–7538.

[191] C. McWhirter, E. A. Lund, E. A. Tanifum, G. Feng, Q. I. Sheikh, A. C. Hengge and N. H. Williams, *J. Am. Chem. Soc.*, 2008, **130**, 13673–13682.

[192] S. R. Banks, S. R. Pygall, G. S. Bajwa, S. W. Doughty, P. Timmins and C. D. Melia, *Carbohydrate Polymers*, 2014, **101**, 1198–1204.

[193] X. Ni, X. Li, Z. Li and J.-P. Cheng, *Org. Chem. Front.*, 2016, **3**, 1154–1158.

[194] L. M. Huffman, A. Casitas, M. Font, M. Canta, M. Costas, X. Ribas and S. S. Stahl, *Chem. - Eur. J.*, 2011, **17**, 10643–10650.

[195] L. Novaroli, G. Bouchard Doulakas, M. Reist, B. Rolando, R. Fruttero, A. Gasco and P.-A. Carrupt, *Helv. Chim. Acta*, 2006, **89**, 144–152.

[196] R. Schmid, *J. Solution Chem.*, 1983, **12**, 135–152.

[197] L. B. Anderson, C. Molloy, L. Pedrini, I. L. Martin and S. J. Connon, *Green Chem.*, 2024, **26**, 11125–11131.

[198] R. I. Maksimovskaya and G. M. Maksimov, *Coord. Chem. Rev.*, 2019, **385**, 81–99.

[199] R. Massart, R. Contant, J. M. Fruchart, J. P. Ciabrini and M. Fournier, *Inorg. Chem.*, 1977, **16**, 2916–2921.

[200] E. Leung, L. I. Pilkington, M. van Rensburg, C. Y. Jeon, M. Song, H. J. Arabshahi, G. H. De Zoysa, V. Sarojini, W. A. Denny, J. Reynisson and D. Barker, *Bioorg. Med. Chem.*, 2016, **24**, 1142–1154.

[201] J. Tydlitat, F. Burevs, J. Kulhanek and A. Ruuvzivcka, *Synthesis*, 2010, **2010**, 3934–3940.

[202] L. Buzzetti, M. Puriņš, P. D. G. Greenwood and J. Waser, *J. Am. Chem. Soc.*, 2020, **142**, 17334–17339.

[203] M. Kaasik, S. Kaabel, K. Kriis, I. Järving and T. Kanger, *Synthesis*, 2019, **51**, 2128–2135.

[204] T. Ertan, I. Yildiz, S. Ozkan, O. Temiz-Arpaci, F. Kaynak, I. Yalcin, E. Aki-Sener and U. Abbasoglu, *Bioorg. Med. Chem.*, 2007, **15**, 2032–2044.

[205] Y. Taguchi and Y. Mushika, *J. Org. Chem.*, 1975, **40**, 2310–2313.

[206] S. Debarge, S. Thibaudeau, B. Violeau, A. Martin-Mingot, M.-P. Jouannetaud, J.-C. Jacquesy and A. Cousson, *Tetrahedron*, 2005, **61**, 2065–2073.

[207] X. Wang, C. Wang, Y. Liu and J. Xiao, *Green Chem.*, 2016, **18**, 4605–4610.

[208] G. Adamová, R. L. Gardas, L. P. N. Rebelo, A. J. Robertson and K. R. Seddon, *Dalton Trans.*, 2011, **40**, 12750–12764.